Explorative Investigation into the Thermal and Mechanical Properties of 2D Tubular Braided Composites with an outlook on the future of Green Composites

by

Ahmed Samir Ead

A thesis submitted in partial fulfilment of the requirements for the degree of

Doctor of Philosophy

Department of Mechanical Engineering

University of Alberta

ABSTRACT

Due to their tailorable mechanical and physical properties, 2D tubular braided composites (TBCs) have many potential applications in fields including aerospace, construction and medicine. Over the past 70 years, many studies have thoroughly investigated several aspects of braided composites including their manufacturing processes, the geometrical features and patterns of braided composites and the resulting mechanical properties. Although extensive literature exists on these materials, some gaps remain that present an obstacle to introducing these materials in their applications. The thermal expansion behaviour of TBCs has been sparsely experimentally and analytically investigated. Further, although mechanical properties are well documented, large variability is often seen between different studies for identical samples. Lastly, green composites have been proposed as more environmentally friendly alternatives to traditional synethic composites, however, remain largely unexplored. These specific gaps were addressed in this thesis.

In the first part of the thesis, the lack of research on the coefficient of thermal expansion is addressed. A literature review is presented, summarizing the experimental, analytical and numerical studies looking into thermal expansion behaviour of textile composites. The gaps from this literature review highlight the need to investigate the thermal expansion behaviour of 2D tubular braided composites. To do this, a novel non-contact experimental method is proposed and a classical laminate plate theory (CLPT) based analytical model is developed. Kevlar®/epoxy TBC samples were manufactured at three braid angles (35, 45 and 55 degrees) and heated to 150 °C. To measure the deformation of the samples, two-dimensional digital image correlation (DIC) was used. A CLPT-based model was then developed to calculate the longitudinal CTE and compare it to the existing available data on Kevlar®/epoxy composites and the collected experimental data. Results showed the ability of DIC to measure the coefficient of thermal expansion of 2D TBCs and the ability of the model to predict the thermal expansion behaviour of these materials.

In the second part of the thesis, the variability in documented tensile properties of TBCs is addressed. Two hypotheses are proposed as potential explanations to this variation. The first is the displacement rate defined as the rate at which the sample is loaded during tensile tests. ASTM standards do not specify this rate, but rather specify a timespan under which the sample should fail. To test this hypothesis, an experimental study was conducted. Kevlar®/epoxy TBC samples were manufactured at three braid angles (35, 45 and 55 degrees) and tested at three displacement

rates (1, 2 and 6 mm/min). DIC was used to measure the strain of the samples. The collected data was used to calculate the elastic moduli of the tested samples. Results showed that the higher strain rate (6 mm/min) resulted in larger deviations in the elastic moduli, particularly for the larger braid angles tested (45 and 55 degrees). These results suggest that to reduce variability in recorded mechanical properties, lower displacement rates in the range of 1 mm/min to 2 mm/min should be used. The second proposed hypothesis is stress-free aging time defined as the time between sample manufacture and testing. Literature has shown that the epoxy can fully set after the curing process is complete, altering the mechanical properties. To test this hypothesis, an experimental study was conducted. Kevlar®/epoxy TBC samples were manufactured at three braid angles (35, 45 and 55 degrees) and tested at three stress-free aging times (0, 2 and 6 weeks). DIC was used to measure the strain of the samples. The collected data was used to calculate the elastic moduli and the strength of the tested samples. Results of the work showed that longer stress-free aging times resulted in increased modulus and strength of the samples, providing a potential explanation to the variation documented in the mechanical properties of TBCs between different studies.

In the third and final part of the thesis, the potential of green composites as viable alternatives to synthetic composites is addressed. A literature review is conducted to assess the environmental impact of green composites using a life cycle analysis approach. The literature review discusses the relative differences between green composites and synthetic composites from procurement to use to end-of-life. Results of the literature review qualitatively strongly suggest that green composites are superior in terms of their environmental impact. Further studies should characterize the properties of green braided composites.

PREFACE

This thesis is a combination of traditional and paper-based format. Several sections of this thesis were submitted and/or accepted as journal papers and conference papers. Although chapter 2 provides a general overarching background to the thesis, following chapters contain elements from this chapter due to these chapters being previously submitted and/or published.

Chapter 3 was submitted as an article to the Journal of Engineered Fibres and Fabrics under the title "Textile Braided Composites: A Review of Thermal Expansion Literature", written by me and edited by Dr. Jason Carey and Dr. Cagri Ayranci. Chapter 4 was submitted as two articles to the Journal of Engineered Fibres and Fabrics under the titles "Thermal Expansion Coefficient of 2D Braided Composites, Part 1: Development of non-contact experimental measurement technique based on optical methods" and "Thermal Expansion Coefficient of 2D Braided Composites, Part 2: Classical Laminate Plate Theory analytical model development and verification", both written by me and edited by Dr. Jason Carey and Dr. Cagri Ayranci. Chapter 5 has been submitted as a conference paper to CANCOM 2024, planned for August 2024, under the title "Influence of Displacement Rate on Elastic Modulus and Strength of 2d Kevlar®/epoxy Tubular Braided Composites". This chapter was written by me and edited by Dr. Jason Carey and Dr. Cagri Ayranci. Chapter 6 has been submitted, accepted and published in the proceedings of CSME 2023 under the title "Influence of Stress-free Aging on Modulus and Strength of 2d Kevlar® Tubular Braided Composites", written by me and edited by Dr. Jason Carey and Dr. Cagri Ayranci. Finally, Chapter 7 was written in collaboration with Raelynn Appel and Nibin Alex and edited by Dr. Jason Carey and Dr. Cagri Ayranci. This chapter was published as an article in the Journal of Engineered Fibres and Fabrics under the title "Life cycle analysis for green composites – a review of literature including considerations for local and global agricultural use".

DEDICATION

I would like to dedicate this thesis to the people of Palestine. Your strength, courage and resilience have taught me how to be a better person, something we should all strive for. When I feel my humanity is at risk, I will always remember how despite all that has and is going on, you have held on to your humanity. I have learnt so much from you and it is only fitting to dedicate this Doctorate to you. Thank you Palestine.

ACKNOWLEDGEMENTS

It's a weird feeling being at the end of such a long journey and trying to find words of gratitude to the many people who were instrumental in me finally getting to this point. The language I use here will probably not be as well articulated as the rest of the thesis, but if you're reading this thesis specifically, I'm pretty sure you would understand why. This is the part of the thesis where I get to speak from the heart. This is a reflection of the author in a very unpolished form rather than an off-the-shelf acknowledgement you might expect from someone holding a Doctorate of Philosophy.

I think back to the decision to become a University Professor and how the path, partly represented in the many pages of this work, challenged me. As someone with an unsubtle obsession with giving back and trying to be a "light in the darkness", I can confirm that going down this path was certainly worth it. If you, dearest reader, feel like you want to add to the world through teaching and conducting research, I implore you to continue down the path of a PhD. It won't be easy, and you'll probably regret the decision on many occasions, but the minute you make it over to this side you'll understand how much it was worth it. We need more people who want to give back and use their gifts for teaching others and showing them how our beautiful universe works. That could be you if you want it to be. All it takes is a little belief, a lot of coffee and a touch of passion to get you through the many challenges that a PhD life will throw at you.

While I was writing this thesis, I was trying to think of who to thank and how laborious my acknowledgements will need to be, but right now I cannot help but smile at the thought that this thesis is more than just "another document for the internet archive". This work is the culmination of the effort of so many people. It is a living legacy document, containing years and months of genuinely wholesome individuals who were an instrumental part of the journey. In the case that I will ever need to remember these people, I am comforted by the fact that I can open this document and just by going through the pages, "see" memories of the people who made this PhD possible. By the least I can do is thank them, so let's get to it.

To my parents, Samir and Shazy, thank you. When I was a little kid, you always used to praise how intelligent I was. Ever since I could talk, you believed that I could change the world. You somehow knew that I would try and do just that and have always been pushing me to reach higher and explore my full potential. I have not reached said potential yet, but I hope that what I've

accomplished up to this point is a partial way to thank you for everything you've done for me. I must've been terribly challenging to deal with at times, so thank you for never giving up on me. To Reem, Maha, Rana, Hady and Hana, a sincere heartfelt thank you is more than overdue. When I think of what you've done, all I can see are memories of times we've travelled the world together, visited restaurants and complained that the food was too cold, watched movies together and all the hugs we have shared as family. You are my warmth, and I will never be able to thank you enough for always being there for me. And to Reem in particular, thank you for being my light. It got dark many times along the way, but you were always there to remind me that things will be okay.

To the lab and the many souls that have come and gone during my graduate experience, this work is not just mine, but ours. I think to my defence and the comment that was made by a professor that "this must be some kind of record [attendance at a defence]" but as I write this acknowledgement, I feel it was a very fitting end to this chapter of my life. I think of my years in the lab and can honestly say they were some of the best in my life. I think to the birthdays, the video game hangouts, the sushi outings, the late-night work sessions, the candid photos, the slack quotes and so much more and feel immense gratitude to you all. I have grown as a friend, a brother, a colleague, an engineer and a person and you all had a part in that growth. You all know that my slogan for how we do things is "better people and better engineers", but that only came about after getting to work with all of you, learn from you and teach you what I could. You will always be my "avengers", and I hope that no matter where life takes us, you will always reach out to me for help, for laughs, for advice or for lifting tips. I promise to do my best to see you all become better than I ever could.

I would also like to thank my supervisors, Jason Carey and Cagri Ayranci for their support and guidance. They've both been incredibly patient and understanding over the many years we've worked together. A special thank you to J for always being more than a supervisor, but also a true friend and amazing mentor. May our friendship grow stronger as we grow older and more wrinkly.

Lastly, my wholehearted gratitude is to Allah for granting me so many gifts and giving me the strength, courage, wisdom and the moral compass to always fight the good fight.

Thank you for reading this, and I hope the rest of this document doesn't put you to sleep (unless you're trying to get to sleep).

TABLE OF CONTENTS

List of Tables

List of Figures

CHAPTER 1 - Introduction

1.1 Motivation

Textile composites are combinations of a resin system with a textile fibre, yarn or fabric system. Braided composites are a type of textile composites that have gained popularity in recent years due to their tailorable mechanical and physical properties. Braided composites consist of continuous yarns interlocked together into a patterned preform that is impregnated with a supporting matrix and cured. Tubular braided composites (TBCs) are textile composites formed by interlacing yarns over a cylindrical mandrel. Due to their desirable properties, TBCs are used in several fields including medicine, aerospace and construction[1]. These applications require high-end properties of the selected materials. For aerospace and construction, materials are often used in environments with large ranges of temperatures. The thermal response is important for correct selection of materials that meet the temperature needs of these applications. Mechanical properties, and in particular tensile stiffness, strength and rigidity, are necessary for reinforcement structures, beams, tubing and medicine. Finally, an important aspect of choosing materials for these applications is the environmental impact these materials might have. Data collected by NASA's Goddard Institute for Space Studies shows that the temperature of Earth has increased by 1.1 °C over the past 150 years[2]. The results of these increases in temperature include flooding due to rising sea levels, drought due to warmer weather and increased risks of natural disasters due to the affected ecosystem[3]. One solution to combat climate change is replacing traditional materials with alternative materials that have lower environmental impact. Evidently, many different criteria interlace in the selection of composite materials and their use in their intended applications. Accordingly, much research has studied the mechanical and physical properties of TBCs.

A wealth of literature is available on these materials. These studies have examined many aspects of the manufacture and use of TBCs in their intended applications. Some research has looked into the kinematics of the braiding process. These studies have focused on relating the parameters of the different components of manufacturing to the resulting architecture of the produced braids[4–7]. In addition to the manufacturing process, several studies have also looked into studying the mechanical properties of TBCs. These works have experimentally, analytically and numerically characterized these materials. The results of these numerous studies have identified the tensile strength and modulus, compressive strength, creep response and fatigue behaviour of TBC[8–13].

In terms of characterizing studies, some areas of TBCs still remain unexplored. The thermal behaviour of TBCs has sparsely been looked into[14]. This is defined as the response of the material when exposed to temperatures outside the typical room temperature used in most characterization studies. Due to the complexity of accurately modelling the combined thermal behaviour of the fibres and the matrix in TBCs, the majority of work conducted has been numerical. If these materials are expected to be used in applications involving higher temperatures, the gaps in experimental and analytical thermal characterization must also be addressed[14].

Unlike thermal properties, many studies have looked into the tensile properties. the existing research into the properties of TBCs has shown variation between samples. Although many studies have experimentally tested for the mechanical properties of TBCs, the discrepancy between documented values remains unaddressed. These variations are not trivial; often exceeding 10% for a given measured property [8–13].

The multitude of studies conducted on TBCs have shown promise for the potential fields that these materials can be used in. One area that has been sparsely addressed is the use of natural fibres and resins to manufacture TBCs[13]. Although synthetic fibres have typically been selected in composite reinforcement due to their high strength and stiffness, natural fibres are emerging as alternatives. Some studies have begun characterizing "green" TBCs manufactured with natural fibres as well[13]. One aspect that has not been investigated is the environmental impact of greener TBCs.

With these gaps in understanding and predicting the behaviour of TBCs, using them into their intended applications is more difficult. Further research needs to be conducted on these materials to justify their use. Accordingly, this thesis sought to explore TBCs and address some of the gaps in the current literature. As the relative importance of these various issues to future research remains unknown, this thesis broadly explores a number of gaps to better appreciate where future research in the area should go. The main gaps addressed in this work are:

- The thermal behaviour of TBCs and the influence of braiding parameters on the resulting response. A novel method for experimentally measuring the thermal coefficient of expansion of TBCs is introduced and validated. A model is also devised to predict this behaviour and compared to experimental data. Addressing this expands the potential

applications of TBCs into industries where thermal behaviour must be well research experimentally and analytically.

- The discrepancy in documented mechanical properties. Two different hypotheses are put forth as potential reasons for the variation in measured mechanical properties. Experimental validation of these hypotheses is conducted and results reported. By attempting to address the variations in mechanical properties, introducing TBCs in stiffness-sensitive applications becomes easier due to their more reliable properties.
- The environmental impact of braided TBCs and the influence of greener materials on this environmental impact in terms of procurement, processing, and recycling. Addressing this gap will provide qualitative support for green composites and identify their potential as more environmentally friendly alternatives worth further investigation and characterization.

1.2 Thesis Scope

This thesis sought to investigate three principal gaps in TBC literature presented in section 1.1. Although studies have shown promising properties of TBCs, the current gaps present an obstacle for them to be utilized in a broader range of potential applications.

To investigate the thermal behaviour of braided composites, a literature review followed by a combined experimental-analytical study were conducted. All available research conducted on the thermal behaviour of laminates and textile composites are presented to the reader. The thermal behaviour is limited to expansion for brevity and to address the specific gap highlighted in 1.1. For the experimental-analytical study, Kevlar®/Epoxy TBCs were manufactured at three braid angles (35-, 45- and 55-degrees) following a process highlighted in previous work. Once manufactured, samples were exposed to elevated temperatures for a duration of two hours and their response measured using stereo digital image correlation (DIC). This experimental study focused on these materials and braid angles due to availability and the presence of data on the tensile properties of TBCs manufactured allowing for potential comparison. To supplement the experimental data, a classical laminate plate theory-based model was devised to predict the longitudinal coefficient of thermal expansion, and the results of the model compared to the collected experimental data.

To study the discrepancy in mechanical properties, stress-free aging time and loading rate were proposed as possible reasons. Kevlar®/Epoxy TBCs were manufactured at three different braid angles (35-, 45- and 55-degrees) and tested in tension at different aging times (0, 2 and 6 weeks) and displacement rates (1, 2 and 6 mm/min). Materials and configurations of TBCs were selected due to data availability. The elastic moduli and strength data were analysed to identify the influence of these factors on the properties and the variation between the properties measured in these studies.

A literature review was conducted to perform a Life Cycle Analysis (LCA) on TBCs. Natural fibres in Canada were presented as alternatives to typical synthetic materials. An entire LCA literature review analysis was performed using information extracted from research pertaining to fibres including hemp, wheat and flax. The results of this study are used to provide suggestions for future material trends in TBC research conducted in Canada and worldwide.

Through these studies, this work further expands on the studied properties of TBCs. Understanding the influence of material selection, testing parameters and operating conditions on the response of TBCs is paramount for their introduction into applications while attempting to reduce the environmental impact of materials. This work adds to the existing wealth of literature on TBCs by addressing the identified gaps through experimental and analytical work, presenting potential avenues for further TBC investigations and development.

1.3 Thesis Outline

In chapter two, a background of composite research with a focus on TBCs is presented to the reader. Through this chapter available literature is concisely presented on the thermal and mechanical properties and the use of natural fibres in TBCs. This is meant to highlight the importance of further characterization of TBCs in the areas of thermal expansion, variation in mechanical properties and use of natural fibres and resin for TBC manufacture. The chapter concludes with a full elaboration of the gaps addressed and the intended outcomes of the work.

In chapters three and four, we address the lack of characterization studies on the thermal behaviour of TBCs. A literature review on TBCs for temperature sensitive applications is presented in chapter three. This literature review identifies the existing experimental, analytical

and numerical research on the thermal response of braided composites. This is then used to specify the current gaps in the research which are addressed in chapter four. Chapter four details the experimental and analytical approach behind measuring the coefficient of thermal expansion of Kevlar®/Epoxy TBCs. The details of the manufacturing procedure, pilot testing, final experimental setup and data collection and processing are highlighted in this chapter. This chapter also presents a new CLPT-based model developed in this thesis. The fundamental mathematical formulae, analytical modelling approach, and results are presented and compared to the experimental data collected.

In chapters five and six, we address the second gap highlighted in the thesis motivation with regards to the variation seen in measured mechanical properties of TBCs. Chapter five proposes displacement rate as an important manufacturing parameter that influences tensile strength and modulus. ASTM standards provide a large range of displacement rates that can be used in tensile testing of polymer composites. Experimental testing is conducted and the results of these tests are presented in this chapter. Chapter six proposes stress-free aging as the parameter that results in variability between the elastic moduli of TBCs. This is hypothesized to influence the deviation between samples. Chapter six presents the experimental study used to investigate this hypothesis. Chapter six was accepted and published as a conference paper in CSME 2022.

In chapter seven, a literature review on the use of green composites in Canada is presented to the reader. Current material selection practices for TBCs and the overall trend towards materials with smaller environmental impact is introduced. To adequately approach this subject, the literature review is presented from the viewpoint of an LCA. In this chapter, the viability that green materials have in terms of their reusability is highlighted along with current applications that they are suitable for, encouraging further investigation into TBCs, particularly green TBCs. This chapter was submitted and accepted as a journal article in the Journal of Engineered Fibres and Fabric.

Finally, conclusions of the explorative studies conducted in this thesis are presented in chapter eight. This chapter also presents the limitations of the studies and recommendations for future work. A bibliography is presented at the end of the thesis with all the references used in this dissertation.

CHAPTER 2 - Thesis Background

2.1 Composite Materials

Composite materials consist of two or more constituents joined together macroscopically to form a new material that combines the properties of its constituents. When combined, the constituents maintain their individual phases and do not dissolve or chemically react. Many different techniques can be used to manufacture composites, offering highly tailorable mechanical and physical properties. Careful selection of the constituent materials can result in a composite material with superior stiffness, strength, resilience, and toughness to the raw materials. Composites consist of a matrix phase and one (or more) reinforcement phases. The reinforcement phase(s) is primarily responsible for the load bearing aspect of composite design. The matrix phase maintains the structural integrity of the composite and helps in load transfer and protection of the reinforcement phase(s). Figure 2.1a shows a schematic representing the distinction between the reinforcement and the matrix phase in a generic composite material. Figure 2.1b represents the resulting stress-strain properties in a composite based on the properties of the phases. Due to the innumerable combinations of materials that can be achieved, composites are used in a plethora of applications ranging from sports and construction to aerospace and medicine[15].

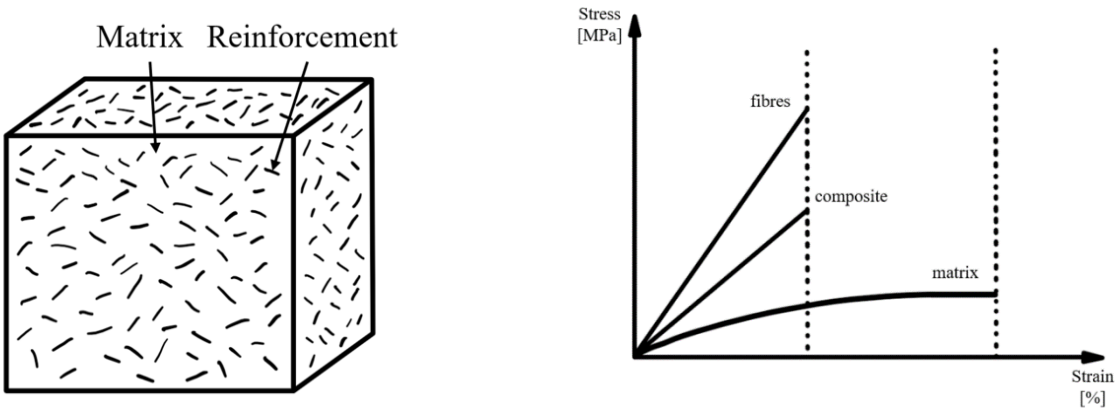

(a) (b)

Figure 2.1. Schematics representing (a) a generic composite material composed of a matrix and reinforcement and (b) a representative stress-strain plot for the relationship between the fibres, matrix and the overall properties of the composite

Composite materials are classified in several ways. The most common composite classifications are by the type of matrix and the geometry of the reinforcement. Composites can be classified according to the type of matrix into metal matrix composites (MMC), ceramic matrix composites (CMC) and polymer matrix composites (PMC). In this method of classification, the material classification of the matrix phase determines the type of composite[15].

Composites, however, are more typically classified according to the geometry and size of the reinforcement phase due to the role the reinforcement phase has in the overall properties of the composite. Particulate reinforced composites (PRC) consist of spherical-shaped (or more generally elliptical- or oblate-shaped) particle reinforcement randomly and uniformly dispersed in a matrix phase. Flake reinforced composites consist of relatively flatter reinforcements dispersed in a matrix phase. Finally, fibre reinforced composites (FRC) consist of matrices reinforced by short (discontinuous) fibres or long (continuous) fibres. Figure 2.2 shows schematics of the different types of composite classifications based on the geometry and size of the reinforcement phase[15].

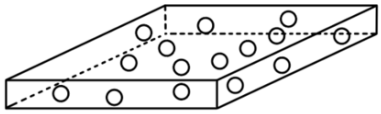

(a)

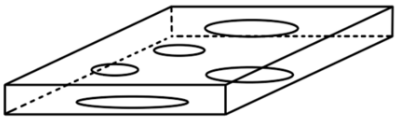

(b)

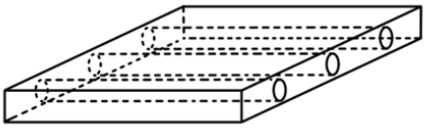

(c)

Figure 2.2. Schematic representations of composites classified according to the geometry and size of the reinforcement into (a) PRCs, (b) Flake Reinforced Composites and (c) FRCs.

Of the many types of composites, fibre reinforced polymer matrix composites (FRP composites or FRPC) are most common. These materials consist of continuous or discontinuous small diameter fibres reinforcing a polymer matrix composite. The small diameter of fibres minimizes material flaws and improves the overall bond between the matrix and reinforcement, resulting in improved overall properties of FRPCs. Due to the low cost, high specific strength, high specific toughness and diverse manufacturing methods, these composites are preferentially selected for applications. The typical properties of some FRPCs are presented in Table 2.1. Despite these merits, drawbacks of FRPCs include relatively low operating temperatures and moisture degradation (due to the polymeric nature of the fibres and matrix). Fibre and matrix developments, however, have allowed for material selection that mitigates these problems[15].

TABLE 2.1. PROPERTIES OF FRPCS COMPARED TO SOME COMMON METALS[15]

Properties	Graphite/Epoxy (V^*=0.7)		Glass/Epoxy (V^*=0.7)		Steel	Aluminium
	Axial	Transverse	Axial	Transverse		
Density (g/cm3)	1.6		1.8		7.8	2.6
Elastic Modulus (GPa)	181	10.3	38.6	8.27	206	68.9
Tensile Strength (MPa)	1500	40	1062	31	648	276
Coefficient of thermal expansion (strain/°C)	0.02	22.5	8.6	22.1	11.7	23

*where V=volume fraction

Fibres are the strong, stiff and lightweight reinforcement phase of FRPCs and fibre selection can drastically change the resulting properties of the composites due to their larger volume fraction. Consequently, fibres are typically chosen depending on the loading of the composite component or structure and the intended manufacturing method. At a higher level, fibres may be classified into synthetic (man-made) fibres or natural (green) fibres. Synthetic fibres include carbon, aramid

and glass. Natural fibres include cellulose, cotton and hemp. A general comparison of some of the properties of synthetic and natural fibres is presented in Table 2.2[15].

TABLE 2.2 PHYSICAL AND MECHANICAL PROPERTIES OF SOME COMMON FIBRES[15]

Properties	Graphite	E-Glass	Aramid	Basalt	Hemp
Density (g/cm^3)	1.8	2.5	1.4	2.8-2.8	1.4
Longitudinal Modulus (GPa)	230	85	124	79-93	30-70
Tensile Strength (MPa)	3500-5500	3500	3000-3600	3000-4800	690
Failure Strain (%)	0.8-2.0	4.4-4.8	1.9-4.4	3.1	1.6

Although fibres are primarily responsible for the overall strength and stiffness of the composite, matrix selection is also important. FRPC matrices can be categorized into thermosets and thermoplastics. Thermosets are cross-networked covalently bonded polymers. These strong bonds result in stiffer polymers that are thermally resistant. On heating, thermosets char rather than soften. Thermoplastics, on the other hand, are covalently bonded polymers with weak Van der Waal intermolecular forces. Accordingly, thermoplastics melt when heated due to the breaking of the weak bonds and movement of the molecular layers. For FRPCs, epoxy thermoset resins are the most common matrices used due to their high strength, lower viscosity and low shrink rates.

FRPCs have traditionally been comprised of laminate structures in which two-dimensional laminae are stacked until the required thickness and shape are achieved. Altering the materials used in the laminates as well as the fiber reinforcement can alter the properties of the composite to tailor the composites for specific applications. Such applications include maritime, aircraft, aerospace, automobiles and infrastructure [16–18]. Despite the simplicity involved in these laminate composites, manufacture is labour intensive and there is difficulty in manufacturing complex shapes. Accordingly, many components consist of several laminated parts joined together using an adhesion bonding method, which further limits the use of these composites [16].

In addition to manufacturing issues, laminate structures are not suitable in critical structures due to their inferior impact damage resistance and low through-thickness properties. These properties include elastic modulus, tensile strength and fatigue resistance. Furthermore, laminate composites suffer from delamination under impact loading due to their poor interlaminar properties. Although methods can be used to improve these issues, they are often impractical [19]. To overcome these problems, textile composites have gained increasing interest in recent years.

Textile composites are combinations of a resin system with a textile fiber, yarn or fabric system [20]. Textile composites may be classified using different criteria including yarn orientation, the manufacturing process used to manufacture the textile composites or the geometric features of the preform. Scardino categorized textile composites into four levels with each defined by the textile construction, the type of fiber reinforcement, the orientation of the fibers and the fiber entanglement[21]. This categorization is shown in Table 2.3.

TABLE 2.3. SCARDINO'S CLASSIFICATION SYSTEM FOR TEXTILE COMPOSITES[21]

Level	Reinforcement System	Textile Construction	Reinforcement Type	Fiber Orientation	Fiber Entanglement
I	Discrete	Chopped Fiber	Discontinuous	Random	None
II	Linear	Filament Yarn	Continuous	Linear	None
III	Laminar	Simple Fabric	Continuous	Planar	Planar
IV	Integrated	Advanced Fabric	Continuous	3D	3D

In addition to Scardino's method of classification, Fukuta and Aoki considered in their classification the methods of manufacturing along with the textile structure dimensions, the fabric architecture, yarn dimensions and directions in the preform [22]. This classification system can be seen in Table 2.4. Their classification for textile composites separates them into one-dimension, two-dimensional and three-dimensional textile composites. This work will focus on biaxial 2D tubular braided composites.

TABLE 2.4 CLASSIFICATIONS OF TEXTILE FABRICS ACCORDING TO DIMENSIONALITY AND NUMBER OF AXES OF MANUFACTURING

	Non-axial	Mono-axial	Biaxial	Triaxial
1D	Roving Yarn			
2D	Chopped Yarns	Pre-impregnation Sheet	Plane Weave 2D Braid	Triaxial Weave Triaxial 2D Braid
3D	Strand mat	3D Braid	Multi-ply weave	Triaxial 3D weave

2.2 2D Tubular Braided Composite Materials

2.2.1 Braided Composite Manufacture

Many different manufacturing techniques can be used to combine the fibres and epoxy for FRPC manufacture. Braiding is a continuous FRPC manufacturing method in which three or more parallel strands of fibre are intertwined together. The resulting interwoven braided structure distinguishes braiding from other composite manufacturing techniques. To create this braided structure, two motions happen concurrently, one rotational and the other translational. The rotation of the yarns about a common axis allows for the braided pattern to be formed circumferentially around a mandrel. The translational component of motion ensures that this pattern is repeated along a length. By combining these two motions, yarns are interlaced and a braided preform is created.

The rotational motion of the yarns is provided by the braiding machine (or braider). Several classifications of braiding machines exist; however, this work focuses on the maypole braider. Figure 2.3 shows an example of this machine. In these machines, yarns of the fibre that is desired for the final product are first spooled on carriers. Spooling is either a manual, semi-automatic or automatic process. In this work, semi-automatic spooling is used to add specified lengths of fibres to the carriers.

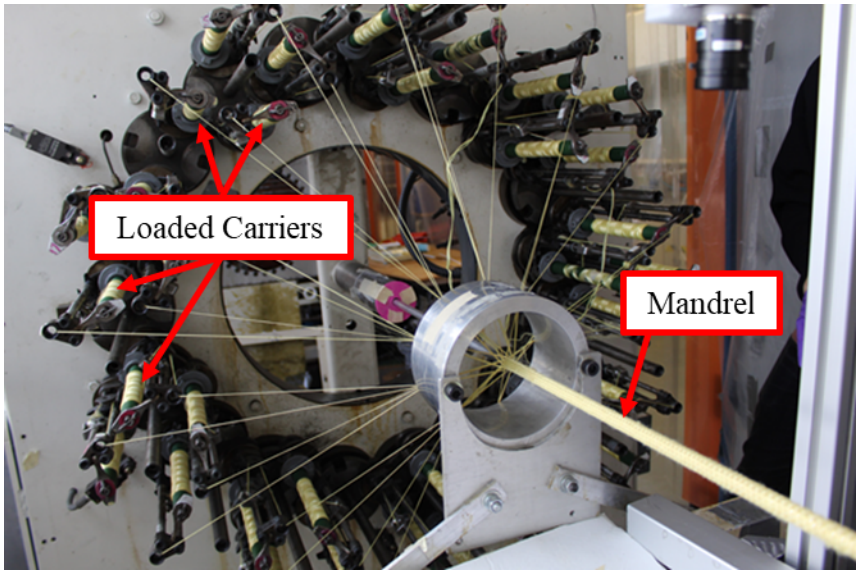

Figure 2.3 Image of a maypole braider highlighting the carriers spooled with Kevlar ® 49 fibres interlacing on the mandrel.

Once spooled, carriers are then loaded onto the braider. The carriers move along predetermined serpentine paths to create the interlacing pattern on a mandrel of the desired shape of the final component. To ensure that the final braided pattern is produced, each set of carriers move in opposite clockwise and counter-clockwise directions. Figure 2.4 shows a schematic of the motion of the carriers on a maypole braider. Horngears control the motion of the carriers relative to the machine. These components work synergistically to create a braided cross-section at the fell point. This is the point at which the yarns first interlace with the mandrel, just before displacement, shown in Figure 2.5. To ensure that the yarns are not constantly intertwining at a single point, a take-up mechanism provides the translational motion of the mandrel. This mechanism moves the formed braided preformed further down the production line, allowing new parts of the yarns to interlace at the fell point. This process is repeated until the desired length of the braided pattern is produced. Figure 2.6 shows a schematic of the entire braiding and take-up process combined.

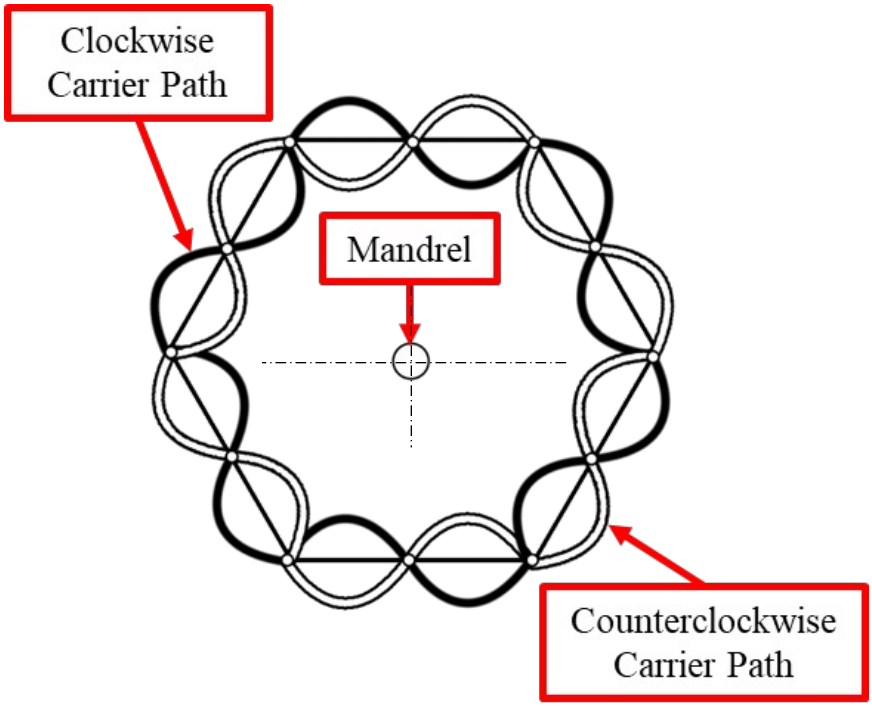

Figure 2.4. Schematic showing the front cross-sectional view of a maypole braider centered at the mandrel. Clockwise and counter clockwise paths represented the direction of motion of carriers along those paths.

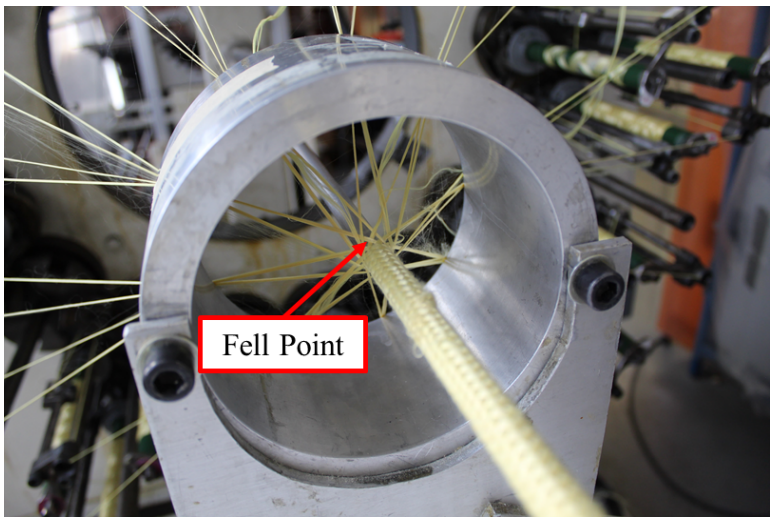

Figure 2.5. Zoomed image showing the interlacing of Kevlar® yarns at the fell point – the first point of contact between the deposited yarns and the mandrel.

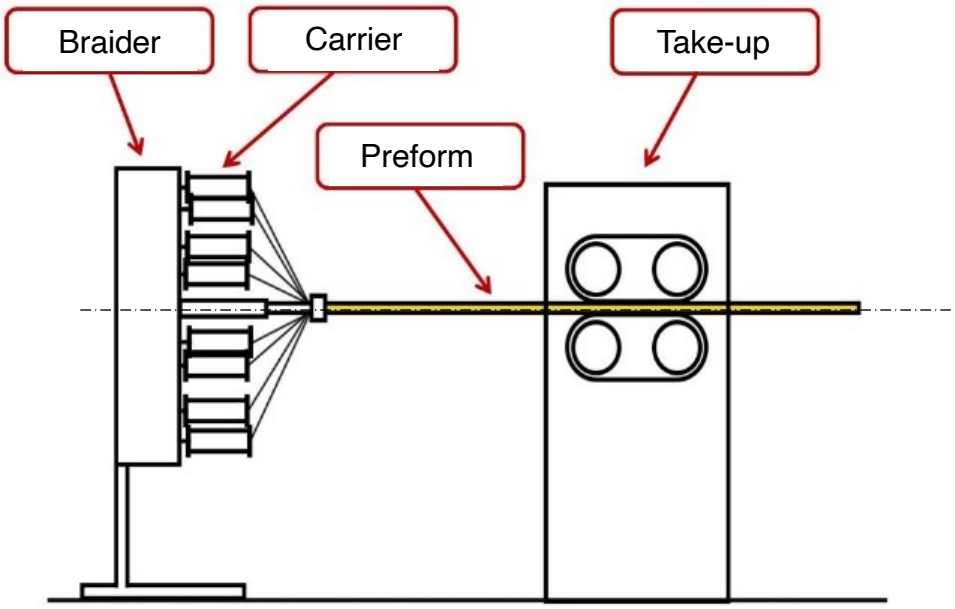

Figure 2.6 Schematic of the braiding line showing different elements of TBC manufacturing. Carriers are loaded with yarns which rotate about the translating mandrel. Rotational motion is controlled by the braider and translational motion is controlled by the puller.

By altering the parameters of the braiding process, the resulting geometry of the preform can also be changed. This allows for further classification of 2D braids. Braids are typically classified in two ways. The first is the pattern of overlap of the braid. By controlling the motion of the carriers and the order in which yarns interlace, different patterns can be manufactured. A diamond braid is formed when a yarn moves over one yarn and under one yarn. A regular braid is formed when a yarn moves over two yarns and under two. A Hercules braid is formed when a yarn moves over three yarns and under three yarns. Other classifications for overlap exist, however, these are the most relevant to this work. Figure 2.7 shows schematics of the three different braided preform patterns.

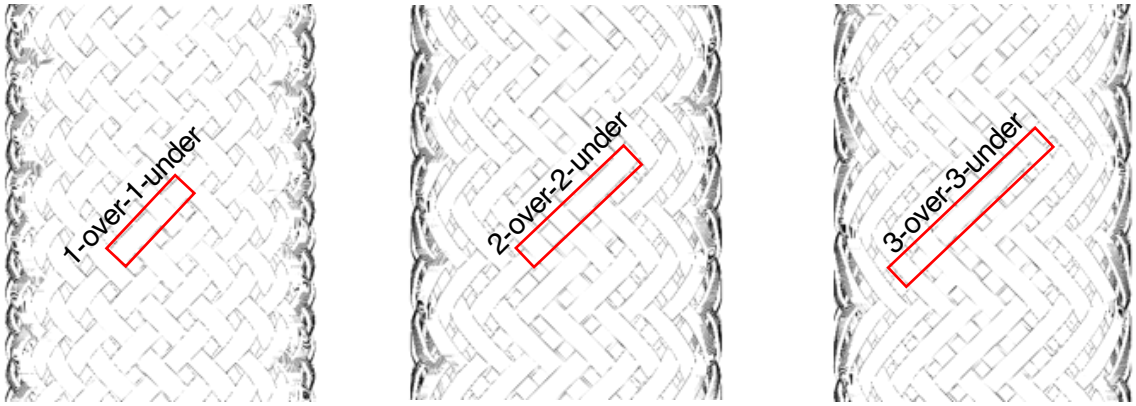

(a) (b) (c)

Figure 2.7. Schematic representations of the three common braiding patterns, (a) Diamond (1/1) (b) Regular (2/2) and (c) Hercules (3/3) braids. Red boxes highlight the differences in overlay and underlay per repeating unit.

The other method for defining the geometry of the preform is the braid angle. This is the most important parameter that defines the overall behaviour of the braided preform (and the resulting composite). Braid angle is defined as the angle formed between the interlacing yarns and the longitudinal axis of the preform. Due to the nature of the braiding process, yarns interlace at two (identical but opposite) angles about the axis of the preform. The braid angle has a significant effect on the overall mechanical properties of the resulting composite. Smaller braid angles result in composites with fibres oriented along the longitudinal direction of the structure, promoting longitudinal properties. Conversely, larger braid angles result in composites with fibres oriented closer to the perpendicular direction, resulting in improved transverse properties. Figure 2.8 shows the braid angle defined on a braided preform.

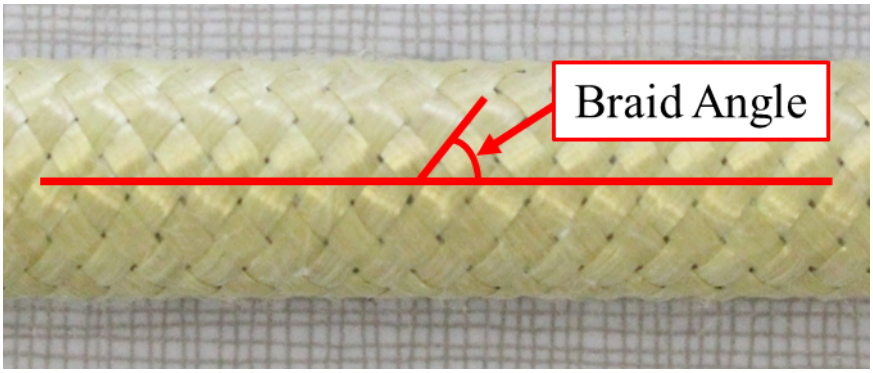

Figure 2.8. Image of a TBC preform depicting the braid angle as the angle formed between the longitudinal axis of the preform and a vector following the path of the yarn.

Once preforms are manufactured, the next step is to add the matrix to form the braided composite. For braided composites, matrix impregnation is either a manual process or a vacuum-assisted process. Manually impregnation is often a more rapid process, particularly for research purposes. Vacuum-assisted matrix impregnation can be used in industrial settings and reduces the number of inherent flaws produced during this step. For this work, manual impregnation was used. To do this, samples are first placed on PTFE rods of the same inner diameter. These rods ensure the preform structure minimally changes during impregnation. Once secured, resin and hardener are mixed and manually massaged onto the samples. Once impregnated, samples are loaded onto a jig and cured. Curing is a process that allows the chemical bonds within the matrix to completely form. The resulting composite from the aforementioned described braiding and impregnation processes is known as a 2D tubular braided composite.

2.2.2 Applications of Braided Composites

Textile composites are used in many different fields including in maritime applications[23], aircraft and aerospace design[24,25], high performance automobile components[26] and civil applications including bridges and buildings[27]. Due to their tailorable mechanical and physical properties, textile composites can be designed to meet the specifications of these different applications. For braided composites, readers are directed to Carey for numerous current applications of these advanced materials[28]. Croon also summarizes some of the potential applications of braided fabrics in his earlier work[29]. Braided fabrics were the first fibre preform architecture to reinforce composites due to the high through-thickness properties achievable in 3D braided fabrics. A wealth of research has attempted to characterize and understand the elastic properties and impact resistance for applications in bone support and fixation[30,31], tubing[32], structural design[33], automobile engines[34], aerospace[35] and satellite components[36], underwater vessels[37], gas-turbines[38] and orthodontics[39]. Some of these are briefly described below.

In structural applications, 2D braided composites are used in concrete reinforcement and concrete confinement. Additionally, concrete members are often reinforced with steel rebars which

provide the required tensile strength. The high density of steel along with its susceptibility to corrosion and structural degradation has resulted in a shift towards braided composite material-based rebar as a viable alternative[1].

In aerospace, braided composites have been used for several components including ducts, fuselage frames and helicopter blade spars. Due to the excellent thermal and wear properties of carbon, carbon braided composites have been used in rocket nozzles. The improved impact and fatigue strength with increased manufacturing efficiency have encouraged the use of braided composites as the fan case of jet engines[1].

In the automotive industry, braided composites have many uses. Braided composites are used as a reinforcement for different structures such as the fuel lines and bellows. In addition to supporting tubular structures in the car, the high specific stiffness of braided composites has resulted in the use in components of vehicle body (window frame and roof pillars) and the chassis (drive shafts and shock absorber tubes). Further, braided composites are considered a suitable material for crash energy dissipation[1].

In biomedicine, braided composites have been studied as suitable materials for reinforced tubing in cardiovascular catheters and microcatheters for cerebral catheterization. Braided composites can be configured to achieve the required rigidities of catheters that helps clinicians avoid invasive surgical procedures. The self-expansive properties of braided composites have presented opportunities for the implementation of braided composites in bone stents and orthodontic wires[1].

2.3 2D Tubular Braided Composite Characterization

In all the presented applications, braided composites represent viable alternatives to typical materials used in these industries. Braiding is a versatile manufacturing process. The high repeatability and precision of the braiding process allows for manufacturing near net shape components of superior quality. For these materials to be used in their intended applications, several studies have attempted to characterize TBCs from their manufacture to their final mechanical and physical properties.

2.3.1 Yarn Properties and Braiding Kinematics

TBC manufacture has been investigated thoroughly in the literature. Joff looked into the geometrical modelling the manufacture of tubular braided preforms in his dissertation. In this study, relationships were established between the fibre parameters (number of filaments, strand diameter and strand shape) and the resulting preform geometries. Experimental tests were conducted on diamond and regular braids to confirm the applicability of the developed model[4]. Following this initial work, research focused on the development and testing of different geometry based kinematic models for the braiding process. Du and Popper developed a detailed model of the braiding process that relates the resulting braid geometry to the speeds of the braider and the take-up mechanism. In addition to general braid geometry, the model also is able to predict micro-geometry including braid angle, cover factor and jamming limits[5]. Zhang et al. conducted a two-part theoretical study into the kinematics of the braiding process. Previous work typically neglected the friction between the yarns and between the yarns and mandrel, but Zhang et al. accounted for it. Experimental results were conducted and showed that accounting for friction improved the ability of the model to predict the final braid geometry[6,7]. By simulating the yarn paths with three-dimensional vectors, these models relate the final preform geometry to the spatial translation and rotation of the yarn path vectors. Several assumptions are used to simplify these models, each with their limitations in predicting the final preform geometry. The results of these studies have been developing an equation that relates the final braid angle of the preform to the radius of the mandrel, the rotational speed of the braider and the translational speed of the take-up mechanism.

To improve yarn handling, yarn twist is often implemented prior to braiding. Yarn twist is a geometrical effect that has been commonly introduced in textile applications used to improve the handling and mechanical properties of short-fibre staple materials. Yarn twist is defined as the rotation of a yarn about its longitudinal axis, achieved by fixing one end of the yarn and twisting the free end relative to the fixed end [40]. Yarn twist is measured by several different methods. A common method is a count of turns per unit of length measurement such as turns per meter (TPM) or turns per inch (TPI). Although these are simple measures of twist, they do not account for change in diameter caused by twist. Other measures such as twist factor and twist multiplier take these into account. For high-performance fibres, twist influences the modulus, strength and elongation of the yarns. Several studies have investigated the impact of twist on the properties of

these high-performance fibres and composite yarns [41–43]. Weinberg and Schwartz investigated the influence of twist on Kevlar 29/epoxy strands. The results showed that increasing twist (in the range of 1-3 tcpm) resulted in an overall decrease in strength and modulus of the yarns [44]. Naik and Madhavan developed a geometrical model that confirmed the results of Weinberg and Schwartz, predicting a substantial decrease in the longitudinal modulus with increasing twist [45]. Analytical models such as DeGauff $\cos^2\theta$ model and the Rao and Farris models have attempted to capture the influence of yarn twist on the mechanical properties of the yarns [46,47]. Shah et al. modified the DeGauff model with consideration of the rule of mixtures and orientation factors to produce a new geometrical model. This model was compared against experimental data and showed to be highly agreeable [48]. Recently, Carey and Cheung modelled the influence of low-angle twist on the mechanics of yarns using the DeGauff model and the Rao and Farris models. Experimental results showed a bilinear curve for Aramid samples. The DeGauff model was poor at predicting the elastic performance of the yarns, while the Rao and Farris models were better [41]. Although researchers have attempted to study multifilament yarns and their properties, few studies have investigated the influence of twist on the geometry of multifilament yarns. Mertová et al. modelled the influence of twist on several geometrical and structural parameters of multifilament yarns. The results showed that an increase in twist did not influence cross-sectional area significantly at low levels of twist. At higher levels, cross-sectional area increased [49]. Studies on the geometry of the twisted yarns are limited, however, predominately focus on yarn compactness.

The integrity of yarn structures is maintained through some form of compactness between the filaments of the yarn. Inter-filament contact, due to lateral forces, maintain this structure throughout the length of multifilament yarns. In the case of spun yarns, twisting and wrapping are used to maintain the structure. Yarn compactness is a measure of the space between the filaments of the yarn and have a direct effect on porosity and compressibility. This can ultimately influence the properties of yarns when used in particular applications where stress is applied over the length of the yarn. Geometrically, compactness is directly related to yarn circularity. The cross-sectional geometry of a yarn can take on many shapes and has been modelled in textile fabrics as circular, elliptical and lenticular [50–52]. Circular cross-sections for yarns have been used extensively in textile modelling due to simplicity, however, no studies have investigated directly the influence of twist on the yarn cross-section. Some studies have attempted to include this “distortion” in cross-section

in modelling the overall behavior of the textiles, however, they have not investigated the influence on the entire textile geometry.

2.3.2 Mechanical and Physical Properties of 2D TBCs

In addition to the studies focusing on the manufacturing aspect of TBCs, much research has been conducted in the characterization of the mechanical properties of TBCs. Some of these studies are highlighted below.

Carey developed an analytical model based on a flat braid unit cell to predict the elastic and flexural moduli of TBCs. The model showed good agreement with experimental data and and a parametric study was performed to identify the sensitivity of the model to the composite properties[8]. Ayranci and Carey further developed the model to predict the elastic and flexural moduli of TBCs based on a curved braid unit cell[9]. Ayranci and Carey provide a review of the studies that have investigated the elastic tensile stiffness properties of braided composites. Their review presents a summary of the manufacturing challenges with using braided composites, applications that require high stiffness properties and the experimental, numerical and analytical studies that have explored the characterization of the linear elastic properties of braided composites[10]. Melenka et al. conducted a thorough experimental investigation into the tensile and torsional properties of TBCs manufactured at different configurations. Higher braid angles resulted in lower tensile and improved torsional properties[11]. These results have been also been mirrored in many other studies. Ead et al. looked into the creep behaviour or TBCs. Virtual extensometery was used to measure the strain of TBCs tested to 60% of their failure strength over a duration of 2 hours. Results showed that as the braid angle decreased, the extrapolated time to failure increased for tested samples[12]. Bruni-Bossio conducted an experimental investigation into the tensile properties of green composites comprised of natural fibres and resin. Their results showed similar results in terms of the relationship between braid angle and the stiffness of TBCs, though the values were less than TBCs manufactured of synthetic fibres and epoxy[13]. Cheung and Carey looked into the implementation of yarn twist in the manufacturing of TBCs and the result twist has on the resulting TBC stiffness and strength. Their results showed that result can improve the elastic modulus and strength[53]. One important observation from the results of these studies has been the range of values obtained for tested samples. Although samples are prepared in the same manner,

variations in the modulus and strength are often in the range of 5-10%. Some work has attempted to explain these variations, but addressing them remains largely unanswered.

In addition to a full understanding of the tensile stiffness and strength properties, the thermal behaviour of TBCs is important. As mentioned earlier, TBCs have potential applications in aerospace and construction. One important parameter that must be understood for TBCs to be used in these applications is the thermal behaviour, particularly the coefficient of thermal expansion. In aerospace, structural members on orbital satellites are exposed to temperature changes over the range of -160 °C to 120 °C[54]. Typical materials experience thermal expansion and contraction that create residual stresses in the components designed from these materials. Some research has been conducted on the use of composites to minimize the thermal expansion experienced by these structures. This research has focused mainly on the use of carbon in these composites due to its low expansion coefficient[55]. Woven textiles and laminates have been the focus of this research, with few experimental, analytical and numerical studies exploring the behaviour of TBCs. Experimental studies have been poorly documented in literature and to the knowledge of the author, no standard exists on measuring the thermal expansion of polymer-based composites[56,57]. All existing experimental methods are contact based, often relying on push-rod dilatometry that requires specific sample shapes. For analytical modelling, the only existing work in the literature is the dissertation work of Yan[14]. In this work, force balance equations were created to calculate the thermomechanical properties of TBCs, however, results were never experimentally verified[14]. Numerical modelling has been the forefront of research into the thermal behaviour of 3D TBCs, but these methods require extensive computational power and provide approximations rather than exact solutions.

Lastly, increasing environmental awareness and concerns with climate change have resulted in shifts in all industries to more sustainable practices with less of an environmental impact. In composite research, many studies have also attempted to characterize and investigate the properties of these composites when manufactured. The unpredictability in the properties of natural fibres and their susceptibility to damage under moisture, UV radiation and acidic and alkali environments results in even larger variations in the properties of composites reinforced with natural fibres. In TBC research, very limited work has been conducted. Some studies have shown that natural fibres can be used in the braiding process without damage to the fibres and that the properties of triaxial braided green composites can be analytically modelled. With an exception to the work of Bruni-

Bossio et al., no studies have investigated the properties of green TBCs. An important obstacle in the introduction of these materials is an actual investigation into the environmental impact of synthetic fibres and whether natural fibres can have a positive impact.

2.4 Gaps in TBC Research

Due to their excellent mechanical properties and low weight, TBCs are suitable materials for various applications including construction, aerospace and automotive. Much research has been conducted on the mechanical properties of TBCs. These studies have looked into characterizing the tensile, compressive, creep and fatigue properties of TBCs. One area that remains largely unexplored is the thermal expansion behaviour of TBCs. Due to the diversity of potential applications of these materials, the viability of TBCs extends beyond mechanical properties. Thermal properties must be understood fully to confidently use TBCs in applications where temperatures can range over 100 °C.

Furthermore, current research on the mechanical properties has helped understand the relationship between manufacturing parameters and resulting properties of TBCs. Modelling tools exist that allow the prediction of these properties and the design of TBCs for their stiffness-critical applications. One observation in the experimental studies on the mechanical properties is the variation between the measured properties. This variation is typically in the range of 5-10%. Although some explanation has been offered throughout the literature, many areas of sample variation remain unexplored. Two of these potential areas that are hypothesized to have an influence are the stress-free aging and displacement rate of tensile tests. Stress-free aging refers to the time elapsed between sample manufacture and sample testing. Some research suggests that resin fully sets after a period from curing, altering the properties of these TBCs. Displacement rate refers to the speed at which tensile testing is conducted. Although ASTM standards do exist for this, they only specify testing at a rate that results in sample failure within a certain time. The viscoelasticity of polymers (fibres and matrices) are hypothesized to be influenced by these testing rates.

Lastly, green TBCs face many obstacles in their introduction in industry due to the lack of research on their mechanical and thermal properties. One extremely important aspect that has not

been investigated is the full extent of the impact that using natural fibres and resin may have on the environment. Comparisons between the use of synthetic fibres and natural fibres are unavailable in literature, adding an additional hurdle when attempting to use green TBCs.

2.5 Thesis Direction

With the aforementioned gaps in the literature of 2D TBCs, the lack of understanding their behaviour is an obstacle in the introduction of these materials in their intended applications. Accordingly, this work sought to investigate these gaps and address the following aspects of TBC characterization:

I. Review the available literature on the thermal properties of textile composites with a particular focus on research conducted on 2D TBCs.

II. Develop a repeatable and precise non-contact experimental method for measuring the longitudinal coefficient of thermal expansion of 2D Kevlar®/epoxy TBCs due to the lack of standards in this area. Kevlar® has a large negative coefficient of thermal expansion. This makes it a viable material to achieve a zero coefficient of thermal expansion when combined with epoxy. Three different braid angles will be tested (35-, 45- and 55-degrees) to represent a range of TBCs that have already been tested and documented in the literature and to compare trends to existing trends in the mechanical properties.

III. Develop an analytical model based on classical laminate plate theory that can predict the longitudinal coefficient of thermal expansion of 2D Kevlar®/epoxy TBCs. Unlike the existing model in literature, results from this model will be verified against existing experimental research on laminates and against the experimental results collected in II. This model will also be expanded to predict the behaviour of Kevlar®/epoxy 2D TBCs at different braid angles.

IV. Conduct an experimental study on 2D Kevlar®/epoxy TBCs manufactured at three angles (35-, 45- and 55-degrees) to investigate the relationship between stress-free aging time and the tensile modulus and tensile strength of braids. Three aging times are tested (0, 2 and 6 weeks) that are within typical experimental research times.

V. Investigate the relationship between tensile testing displacement rate and the tensile modulus of 2D Kevlar®/epoxy TBCs. Three different braid angles (35-, 45- and 55-

degrees) and displacement rates (1, 2 and 6 mm/min) were selected. Braid angles were selected due to the existing experimental data and displacement were rates to meet requirements of existing ASTM standards.

VI. Conduct a Life Cycle Analysis based literature review to investigate the environmental impact of using green composites as a potential replacement to typical synthetic composites. This literature review will go through procurement, use and end-of-life phases to identify the viability of green composites as better environmental choices compared to synthetic composites.

2.6 Intended Impact of Thesis

Through addressing the aforementioned gaps, the work presented in this thesis is meant to aid in the introduction of 2D TBCs in their intended applications. For aerospace and construction, thermal properties of these materials must be understood. Achieving a zero coefficient of thermal expansion has been sought in both these industries and through this work, 2D TBCs are presented as a viable alternative to the typical metal alloys that have been used in these applications. Further, a model is developed and presented to aid in the design of 2D TBCs for temperature-sensitive applications by predicting the coefficient of thermal expansions using the properties of the fibre and matrix. Two potential hypotheses are presented as reasons for the variability seen in the mechanical properties. By addressing these two aspects of 2D TBC manufacture and testing, consistent properties are more achievable, aiding in TBC research and use in all stiffness and strength sensitive applications. Lastly, a literature review on the environmental impact is presented to encourage the further development, testing and characterization of TBCs manufactured with natural fibres and natural resins. By addressing the gaps highlighted in 2.5, the intended outcomes are:

I. Provide an elaborate summary of the studies that have investigated the experimental, analytical and numerical characterization of the thermal coefficient of expansion of laminate and textile composites. This summary is meant to serve as an accessible means to identify gaps in the thermal expansion literature and offers readers with potential avenues for research not addressed in this work.

II. Introduce an alternative method for measuring the CTE of tubular polymer-based composites that is repeatable and does not interfere with the sample. This would provide

a more consistent method for measuring CTE, promoting further investigation into the thermal expansion properties of TBCs.

III. Present a model that can be used for the design of TBCs in temperature-sensitive applications. Ideally this would reduce the need for experimental testing by relying on the properties of the fibres and the matrix to predict the thermal behaviour in TBCs. The model can be implemented to shortlist viable materials which can then be experimentally investigated using the methods developed in II.

IV. Improve repeatability for tensile characterization studies of TBCs by acknowledging the significance of stress-free aging time and displacement rate on the resulting properties. Accounting for these variables in sample manufacture and testing are intended to reduce the variability in measured stiffness and strength, promoting the use of TBCs in stiffness-sensitive applications.

V. Expand on the current list of materials used in TBC research by including green fibres and green matrices as viable alternatives with a significantly reduced environmental impact. The presented review of literature is meant to serve as a motivation for investigating the properties of green TBCs in future work, despite the obstacles explained earlier in this chapter.

CHAPTER 3 - Textile Braided Composites: A Review of Thermal Expansion Literature

Although the mechanical properties of braided composites have been well documented in the literature, the thermal properties remain largely unexplored. For applications where thermal expansion is important such as aerospace components and structural members, this lack of research is an obstacle to introducing braided composites. Through this chapter, we present a review of the literature conducted on textile composites to identify gaps in research for further investigation. A version of this chapter was submitted for publication in the Journal of Engineered Fibres and Fabrics under the title "Textile Braided Composites: A Review of Thermal Expansion Literature". This article was written by me and edited by Dr. Jason Carey and Dr. Cagri Ayranci.

3.1 Introduction

Textile composites are a subset of fibre reinforced polymer composites (FRPCs) in which the smallest unit (traditionally referred to as the unit cell) consists of fibre bundles in several orientations[58]. The reinforcement phase for these composites is typically in the form of unidirectional (UD) preforms composed of various fibre or yarn architectures. These preforms are impregnated with a polymer matrix to form the textile composite[59]. Textile composites are preferentially selected over basic laminate structures due to the simpler handling and storage requirements[58]. The method in which the fabric structure is produced from the individual fibres allows for the classification of textile composites into three main categories: knit composites, woven composites and braided composites[60].

Within these categories, textile composites may be further classified as two- or three-dimensional. Although all fabric geometries are three-dimensional in nature, when the thickness of the fabric is sufficiently small, less than three yarns in the thickness direction, it can be considered two-dimensional. Three-dimensional textile composites are those with textile reinforcement in the through-thickness directions[58]. Figure 3.1 shows these general textile composite classifications as adapted from Carey et al[60]. Figure 3.2 shows simplified schematic comparisons of the textile fabrics pertinent to this work.

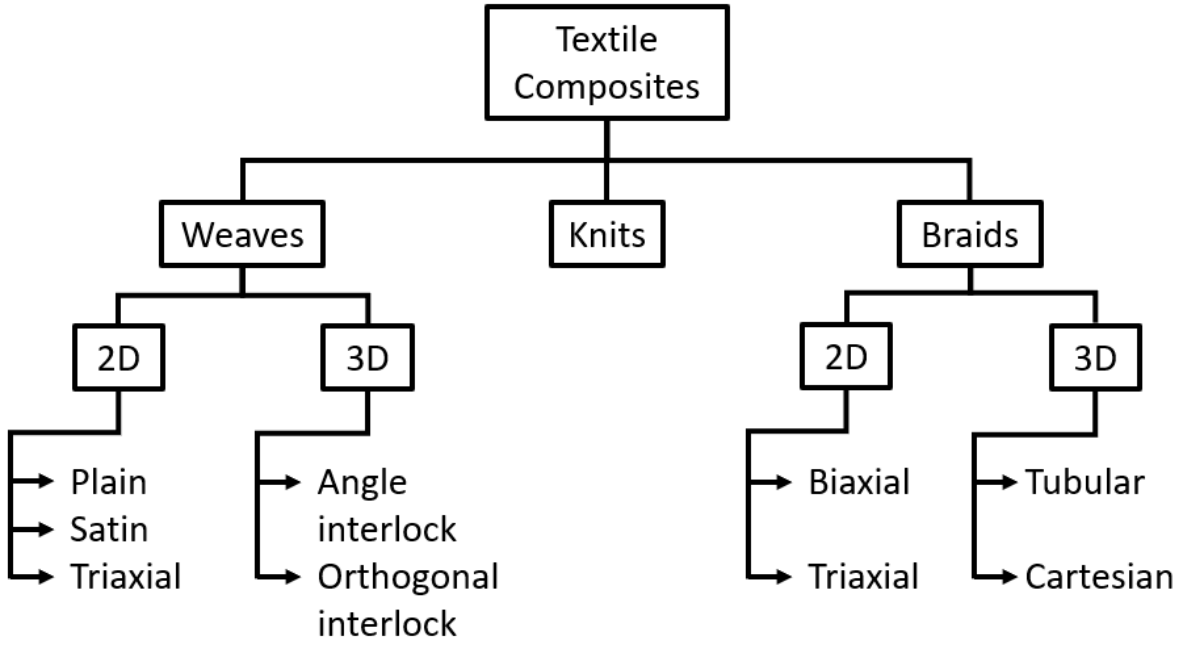

Figure 3.1. Schematic showing typical classification of textile composites pertaining to this investigation.

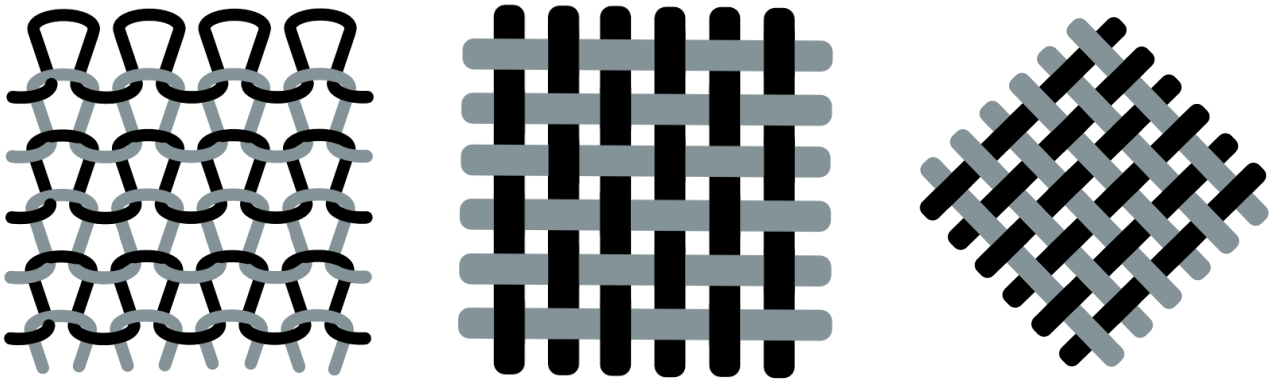

(a) (b) (c)

Figure 3.2. Schematics of the 2D textile structures considered in this work, specifically (a) Knits, (b) Weaves and (c) Braids.

Knitting is a manufacturing process in which yarns are fed by a guide over needles to create loops. Needles are fixed on a needle bar which moves with the guide to allow the continuous formation of loops. These loops are repeated in either the weft or warp directions to form weft-knitted or warp-knitted fabrics respectively[61].

Weaving is a manufacturing technique in which two sets of yarns are interlaced orthogonally through a loom. These yarn sets are referred to as warp and weft yarns. Fibres are fed through harnesses and are displaced on the bed in the cast of warp yarns. Fill yarns are combed and displaced in the perpendicular direction, repeating over the size of the woven fabric. Readers are guided to the work of Lord and Mohamed for further details on the weaving process[58,62].

Lastly, braiding is a textile composite manufacturing technique in which three or more parallel yarns are intertwined over the length of a mandrel to create a preform. Braided preforms are typically manufactured using a maypole braider. In these machines, carriers spooled with a fibrous material move along predefined paths. The motion of the carriers is provided by horn gears. As the carriers move along the tracks in a serpentine motion, the yarns are deposited and interlaced on a translating mandrel to create the preform. Figure 3.3 shows a typical braiding manufacture line. As shown in Figure 3.1, braiding may further be classified into two-dimensional (2D) or three-dimensional (3D). Both of these processes involve interlacing of yarns, however, are distinguished by the axes over which the yarns are interlaced. When yarns are also interlaced in the through thickness direction, 3D braids are formed. 2D braids are typically manufactured on a maypole braider, whereas 3D braids are manufactured on a cartesian or a rotary braider. Several manufacturing parameters influence the properties of the final braided composite. Of these parameters, braid angle is the most significant in determining the effective thermoelastic properties of the composite. Braid angle is defined as the angle formed between the yarns and the longitudinal axis of the braid. Figure 3.4 shows the braid angle labelled on a braided preform. For further details on the braiding process, users are guided to the work of Ko, Head and Pastore[63] and the work of Carey[28].

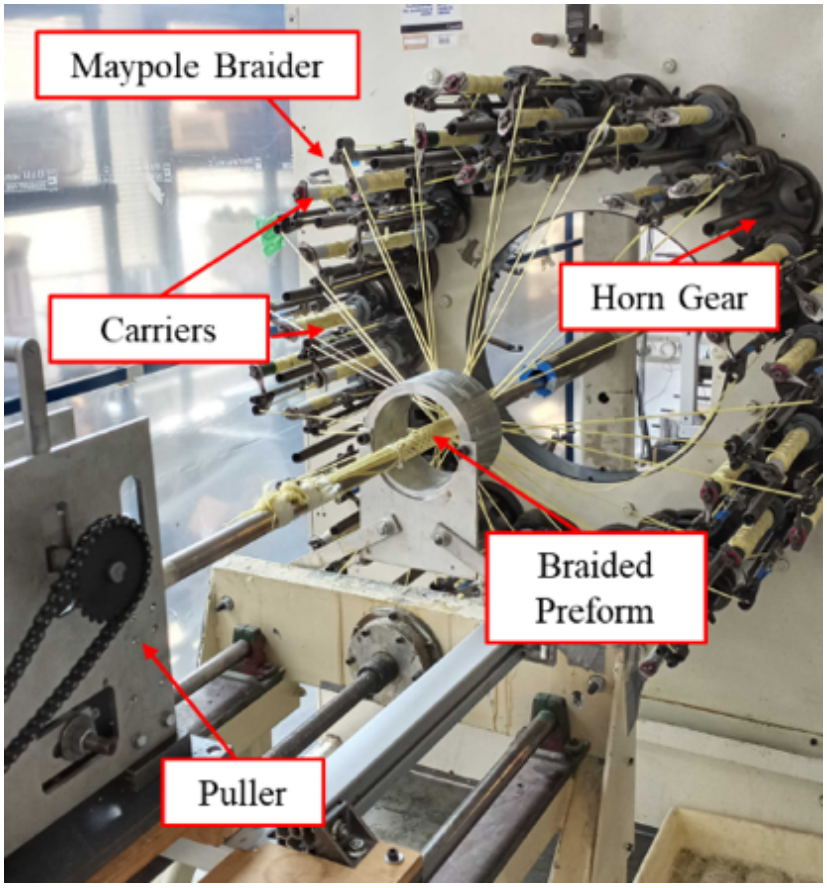

Figure 3.3. Typical manufacturing line used to manufacture TBCs, highlighting the different components of the braider and take-up mechanism

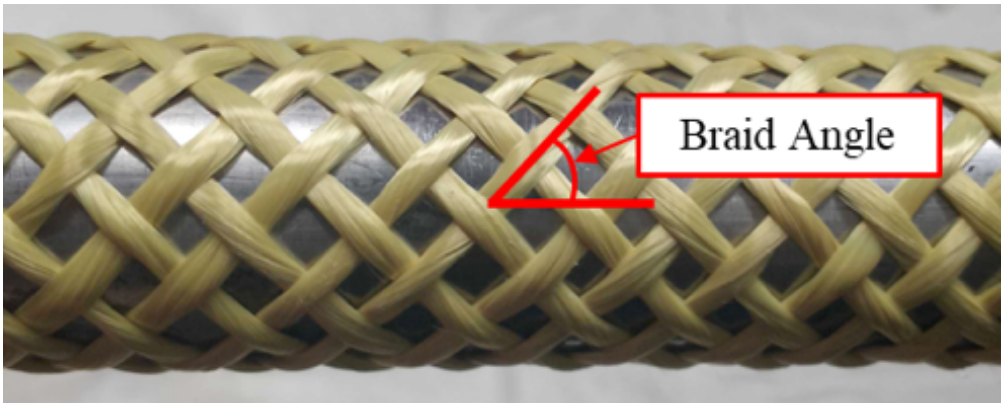

Figure 3.4. Image of a preform showing the braid angle as the angle between the interlacing yarns and the longitudinal axis of the braid

Once the textile preform is formed, it is impregnated with a matrix, typically a polymer, to form the final textile composite. The matrix binds the yarns together and helps in load transfer between the reinforcing fibres. Many different processes can be used to impregnate the preform with a matrix, however, this work focuses mainly on manual or vacuum-assisted impregnation. Composite braiding is a highly repeatable and flexible process that can rapidly produce near net shape components and structures.

3.2 Modelling Background

Many of the studies presented in later sections rely on a fundamental understanding of some aspects of composite modelling. Although many different methods exist to model composite materials, this section is meant to concisely present the broad aspects of classical laminate plate theory (CLPT). Although developed primarily to model the behaviour of laminate composites, the theory has been extended to model the behaviour of textile composites. For more in-depth information on CLPT including the different micromechanical models and derivations of the presented equations, readers are directed to Kaw[15].

3.2.1 Lamina Micromechanics

To accurately model the stress and strain relationships for a composite material, the properties of the constituents are important. In CLPT, the impregnated continuous yarns of textile composites are modelled as thin unidirectional composite lamina. A lamina (also called a ply) is defined as a single layer of fibres arranged in a single direction in a matrix. Figure 3.5 shows a schematic of a unidirectional lamina. A local coordinate system is defined for a lamina such that the 1-direction is in the same direction as the reinforcing fibres [15].

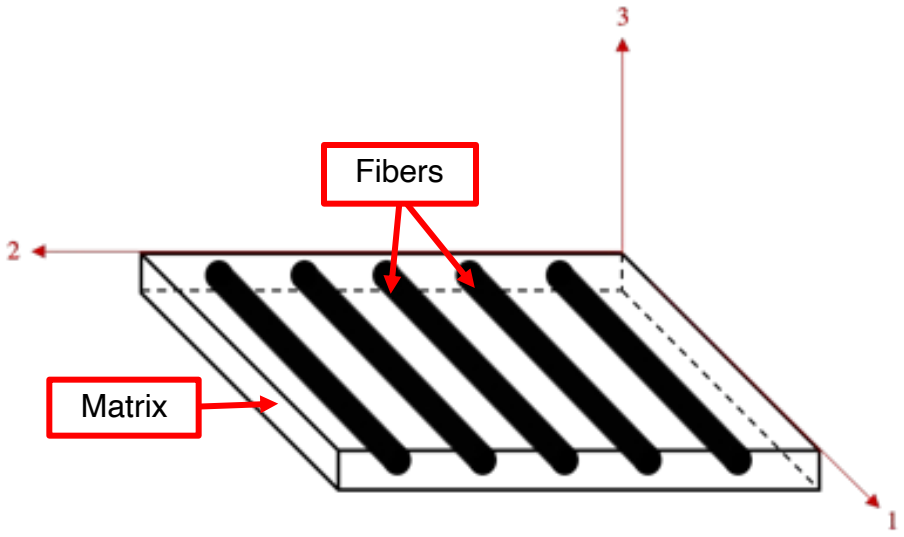

Figure 3.5. Schematic representation of a unidirectional lamina with the local coordinate system defined according to the fibre orientation.

Several models can be used to derive the properties of the lamina from the constituent fibre and matrix. These models differ in the representative volume element (RVE) selected and the distribution of fibres within the RVE. The rectangular block model (RBM) is presented here due to its simplicity [15].

In RBM, the fibres and matrix are idealized as joined blocks. The underlying assumptions for RBM include identical fibre dimensions, perfect bonding between the fibres and matrix, no voids in the lamina and that the fibres and matrix are linear elastic isotropic materials with a uniform distribution of stress and strain in the fibre and matrix blocks. Figure 3.6 shows a schematic representing how a unidirectional lamina RVE is simplified to the RBM. Using force equilibrium and assuming states of iso-stress and iso-strain, the properties of the lamina in the principle directions can be related to the properties of the constituents. Equations 3.1-3.6 show these relationships.

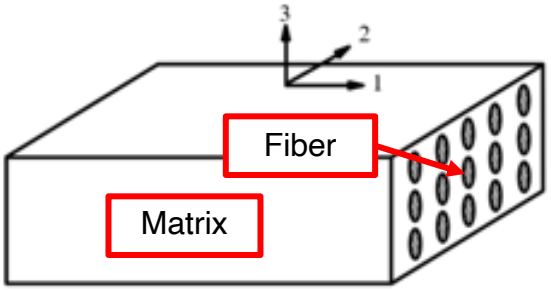

(a)

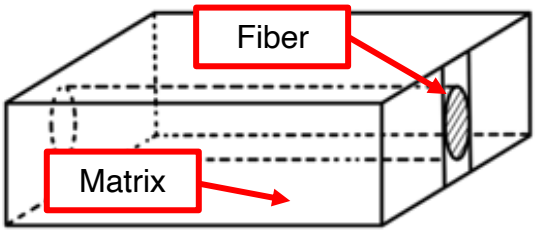

(b)

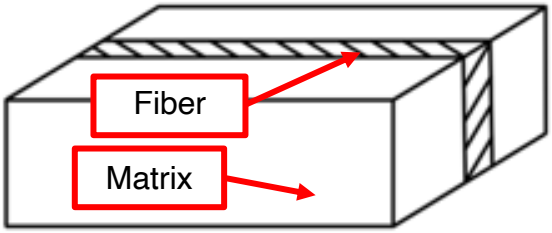

(c)

Figure 3.6. Schematic representation of simplifying a (a) unidirectional lamina to a (b) RVE element with a single fibre and finally to its equivalent (c) RBM representation.

$$E_1 = E_f V_f + E_m V_m \tag{3.1}$$

$$\frac{1}{E_2} = \frac{V_f}{E_f} + \frac{V_m}{E_m} \tag{3.2}$$

$$v_{12} = v_f V_f + v_m V_m \tag{3.3}$$

$$\frac{1}{G_{12}} = \frac{V_f}{G_f} + \frac{V_m}{G_m} \tag{3.4}$$

$$\alpha_1 = \frac{\alpha_f E_f V_f + \alpha_m E_m V_m}{E_f V_f + E_m V_m} \tag{3.5}$$

$$\alpha_2 = \left[\alpha_f - V_f(\alpha_1 - \alpha_f)\right]V_f + [\alpha_m - V_m(\alpha_1 - \alpha_m)]V_m \tag{3.6}$$

where E is the elastic modulus, V is the volume fraction, v is the Poisson's ratio, G is the shear modulus and α is the coefficient of thermal expansion. Subscripts f, m refer to fibre and matrix respectively and subscripts 1 and 2 refer to the local principal lamina directions.

3.2.2 Lamina Macromechanics

Macromechanics translate the properties of the lamina from its local coordinate system to a generalized global coordinate system. To facilitate this, laminae are generally modelled as orthotropic materials. The small thickness of the lamina allows for a plane-stress assumption, reducing the matrices from three dimensions to two dimensions [15]. Equations 3.7-3.12 show this stress strain relationship and how the constants are related to the elastic constants of the lamina found from equations 3.1-3.6 [15].

$$\{\sigma\}_i = Q_{ij}\{\varepsilon\}_j \tag{3.7}$$

$$[Q] = \begin{bmatrix} Q_{11} & Q_{12} & 0 \\ Q_{12} & Q_{22} & 0 \\ 0 & 0 & Q_{66} \end{bmatrix} \tag{3.8}$$

$$Q_{11} = \frac{E_1}{1 - v_{12}v_{21}} \tag{3.9}$$

$$Q_{22} = \frac{v_{12}E_2}{1 - v_{12}v_{21}} \tag{3.10}$$

$$Q_{12} = -\frac{E_2}{1 - v_{12}v_{21}} \tag{3.11}$$

$$Q_{66} = G_{12} \tag{3.12}$$

where $\{\varepsilon\}$ is the local strain tensor, $[Q]$ is the local stiffness matrix and $\{\sigma\}$ is the local stress tensor. Subscripts $11, 22, 12$ and 66 refer to the elements of the stiffness matrix. Subscript $i = (1,2,12)$ and subscript $j = (1,2,12)$

A transformation matrix is then used to convert this local stiffness matrix $[Q]$ into a global stiffness matrix $[\bar{Q}]$. This transformation matrix uses the angle between the local and global coordinate systems [15]. Equations 3.13-3.19 highlight the relationships between the terms in the global stiffness matrix and the local terms presented earlier in equations 3.7- 3.12).

$$\bar{Q} = \begin{bmatrix} \bar{Q}_{11} & \bar{Q}_{12} & \bar{Q}_{16} \\ \bar{Q}_{12} & \bar{Q}_{22} & \bar{Q}_{26} \\ \bar{Q}_{16} & \bar{Q}_{26} & \bar{Q}_{66} \end{bmatrix} \tag{3.13}$$

$$\bar{Q}_{11} = Q_{11}\cos^4\theta + 2(Q_{12} + 2Q_{66})\sin^2\theta\cos^2\theta + Q_{22}\sin^4\theta \tag{3.14}$$

$$\bar{Q}_{12} = Q_{12}(\sin^4\theta + \cos^4\theta) + (Q_{11} + Q_{22} - 4Q_{66})\sin^2\theta\cos^2\theta \tag{3.15}$$

$$\bar{Q}_{22} = Q_{11}\sin^4\theta + 2(Q_{12} + 2Q_{66})\sin^2\theta\cos^2\theta + Q_{22}\cos^4\theta \tag{3.16}$$

$$\bar{Q}_{16} = (Q_{11} - Q_{12} - 2Q_{66})\sin\theta\cos^3\theta + (Q_{12} - Q_{22} + 2Q_{66})\sin^3\theta\cos\theta \tag{3.17}$$

$$\bar{Q}_{26} = (Q_{11} - Q_{12} - 2Q_{66})\sin^3\theta\cos\theta + (Q_{12} - Q_{22} + 2Q_{66})\sin\theta\cos^3\theta \tag{3.18}$$

$$\bar{Q}_{66} = (Q_{11} + Q_{22} - 2Q_{12} - 2Q_{66})\sin^2\theta\cos^2\theta + Q_{66}(\sin^4\theta + cos^4\theta) \tag{3.19}$$

where $\bar{Q}$ is the global stiffness matrix and θ is the angle between the local and global coordinate systems. Subscript numbers refer to terms in a 3x3 compliance matrix reduced to the form shown in equation due to plane-stress and transverse isotropic material assumptions.

Although equations 3.1-3.19 allow for calculating the stress-strain relationships for lamina, laminates are constructed from multiple laminae of many different materials with fibres in different orientations. When laminae are combined, the global stiffness matrices $[\bar{Q}]$ of the stacked lamina are also combined together through classical laminate plate theory (CLPT) [15]. This involves integrating over the entire thickness of the composite to relate the forces and moments experienced by the laminate to the midplane strains and curvatures of the laminate structure. Equations 3.20-3.23 present these relationships [15].

$$\boldsymbol{A_{ij}} = \sum_{k=1}^{N} [\bar{Q}]_k (h_k - h_{k-1}) \tag{3.20}$$

$$\boldsymbol{B_{ij}} = \sum_{k=1}^{N} [\bar{Q}]_k \frac{1}{2} (h_k^2 - h_{k-1}^2) \tag{3.21}$$

$$\boldsymbol{D_{ij}} = \sum_{k=1}^{N} [\bar{Q}]_k \frac{1}{3} (h_k^3 - h_{k-1}^3) \tag{3.22}$$

$$\begin{bmatrix} N_x \\ N_y \\ N_{xy} \\ M_x \\ M_y \\ M_{xy} \end{bmatrix} = \begin{bmatrix} \boldsymbol{A} & \boldsymbol{B} \\ \boldsymbol{B} & \boldsymbol{D} \end{bmatrix} \begin{bmatrix} \varepsilon_x^0 \\ \varepsilon_y^0 \\ \gamma_{xy}^0 \\ K_x \\ K_y \\ K_{xy} \end{bmatrix} \tag{3.23}$$

where h is the thickness of the lamina, N is the total number of lamina in the structure, N_x, N_y and N_{xy} are resultant forces on the composite, M_x, M_y and M_{xy} are resultant moments on the composite, $\varepsilon_x^0, \varepsilon_y^0$ and γ_{xy}^0 are midplane strains and K_x, K_y and K_{xy} are midplane curvatures. Subscript k refers to a particular lamina in the stacking sequence and subscripts x and y refer to the directions in the global coordinate system. The $\boldsymbol{A_{ij}}, \boldsymbol{B_{ij}}$ and $\boldsymbol{D_{ij}}$ are commonly referred to as the extensional, coupling and bending matrices respectively.

3.3 Motivation

Due to their favourable mechanical, hygrothermal and physical properties, textile composites have numerous applications. Polymer composites reinforced with 2D fabrics have been used in maritime craft[23], aircraft and aerospace[24,25], high performance automobile applications[26] and civil applications including bridges and buildings[27]. In a review by Mouritz et al., many of the applications of woven composites are discussed. Woven composites are used in I-beam construction and H-joint connectors in aircrafts. Other potential uses include floor beams of trains and ferries and load trays in trucks[64]. For braided composites, readers are directed to Carey for numerous current applications of these advanced materials[28]. Croon also summarizes some of the potential applications of braided fabrics in his earlier work[29]. A wealth of research has attempted to characterize and understand the elastic properties and impact resistance for applications in bone support and fixation[30,31], tubing[32], structural design[33], automobile engines[34], aerospace[35] and satellite components[36], underwater vessels[37], gas-turbines[38] and orthodontics[39]. To function as intended in all these applications, the properties of textile composites need to be fully understood.

Ayranci and Carey provide a thorough review of the literature on the elastic stiffness properties of woven and braided composites[10]. An aspect of textile composites that has not received much attention are the thermal properties. One of the most sensitive applications for textile composites is aerospace structures such as antennas, solar panels and structural components on spacecrafts[54]. These structures are exposed to temperature ranges of -160 °C to 120 °C[54]. Understanding the thermal properties of these advanced materials becomes paramount to confidently design for these applications. Arguably the most significant property is the coefficient of thermal expansion (CTE). The CTE of a material is defined as the strain experienced by the material per unit change in temperature.

CTE mismatch between the reinforcement and the matrix can have significant effects on the composite. These effects become pronounced during the curing and heating/cooling cycles of these materials and result in residual thermal stresses[65–68]. Ultimately, this can cause fibre-matrix debonding[54] that would lead to premature failure[69,70]. Despite its importance, no studies have reviewed the literature conducted to characterize the CTE of textile composites.

Accordingly, this chapter provides a review of the literature on textile composite CTE. Due to the sheer volume of literature on thermal properties, studies on thermal conductivity and specific latent heat were not included. “Braided composites, textile composites, coefficient of thermal

expansion, woven composites" were used as keywords to find the studies in this work. Articles addressing hygrothermal, hydrothermal, thermal aging and residual stresses were not included for brevity. Analytical, experimental and numerical studies on CTE are presented for each of the major categories of textile composites including FRP composites in general (including laminates), woven composites and braided composites. For each section and sub-section, studies are presented chronologically.

3.4 Analytical Modelling Literature

3.4.1 Analytical CTE of General Composites

The investigation of the CTE for composite materials is not simple. The compounding effects of the different CTE for the constituents, their geometry, their adhesion and the method of interaction and failure often create a need for assumptions and simplifications to predict the overall composite behaviour. Chamis and Sendeckyi provide a summary of the extent of the analytical work done to model the thermal properties of composites in their critique in 1968[71]. The summary covers the netting analysis methods (disjointed constituent response), the mechanics of material approaches (expressing the properties of the composite in terms of its constituents using equilibrium and force balance), self-constituent modelling (representing the material in terms of its atomic structure) and the variational methods (energy principles and elasticity theory to produce bounds)[71]. Limited experimental verification was conducted throughout the analytical research predicting the CTE of composites. One potential explanation for this observation was difficulty in material procurement and the lack of standards.

Although most fundamental work in predicting the thermal behaviour of composites used a mechanics of material approach[72], available literature points at the work of Turner as the first to explore the thermomechanical behaviour of reinforced polymer composites in-depth[73]. In their work, the influence of material geometry, constituent moduli, moisture content, temperature and constituent CTE are discussed as important factors influencing the behaviour of the composite. Following a constrained aggregate expansion of the composite and neglecting shear deformation, the work presents a modified volume averaging method for calculating the longitudinal CTE for reinforced composites. Results showed that for metal composites, the produced model was able to accurately predict the CTE of the composites within an error of less than 1μm/m°C. The formulation was then used to predict the CTE of glass-fibre reinforced phenol-formaldehyde resin

composites. Limited experimental data was compared to the model, with deviations of more than 5 μm/m°C at a fibre volume fraction of 25%[73]. The investigation of the CTE of generic heterogenous structures was developed extensively in Russia up until the late 1960's, however, access to these studies is quite limited[74–77].

Schapery was one of the earliest to investigate the CTE for isotropic and anisotropic fibrous composite materials using thermoelasticity and energy principles[78]. The energy principles were used on two- and three-phase isotropic composites and a fibre reinforced composite. Boundary stresses were applied and minimized to reduce the difference between the upper and lower bounds of the analytical solutions. Schapery's results presented formulae for the transverse and longitudinal CTE bounds for unidirectional FRP composites. No experimental validation was conducted[78]. Following Schapery's energy approach, classical laminate theory was introduced as a method for predicting the thermoelastic properties of composite laminates. Halpin is often credited for this work[79]. In CLT, laminae stress-strain relations are transformed from lamina axes to the laminate axes using transformation matrices. These equations are often simplified by the assumption that the laminate is symmetric and balanced. This reduces the complexity of the calculation significantly[79]. Rosen and Hashin expanded on the work of Schapery by applying the analytical energy principles to investigate the relationship between the geometry of the composite's constituents and the effective composite properties. Their work focused on the CTE as well as the specific heat of the composites. The energy principles were combined with elements of the extensional and coupling matrices to derive bounds for CTE and specific heat. Although their results confirmed Schapery's results, no experimental validation was conducted[80]. Holliday and Robinson presented a literature review on the thermal expansion of polymer-based composites. Although predominately focused on particulate-reinforced composites, their work briefly touches on fibre-reinforced composites. The results of the review show that the CTE of short fibre-reinforced composites is closely predicted by Turner's volume averaging equation[73,81]. Their work also sheds light on other analytical methods and semi-analytical expressions to calculation the CTE in unidirectional composites[81].

Although continuous fibres are typically used for applications involved FRPCs, analytical study of the CTE is not limited to composites with continuous fibres. Wakashima et al. looked into predicting the thermal expansion of heterogenous solids with ellipsoidal fillers[82]. The study used

theory of transformation of stress and strain states of the inclusions to calculate the thermal coefficients of expansion of the entire aggregate composite. The model was used to predict the CTE of tungsten fibre, copper matrix composites and experimental validation was conducted to compare to the model. The results of the work showed that the ellipsoidal filler model was able to predict the overall shape of the relationship between longitudinal CTE and fibre volume fraction, however, deviation between the model and the experimental data was around 15% at lower fibre volume fractions[82]. Craft and Christensen derived the effective coefficient of thermal expansion for composites with randomly oriented fibres[83]. Linear thermoelasticity theory under the assumption of isotropic fibre and matrix is used to derive the expressions for the CTE. The results of the work suggest a strong relationship between the elastic moduli ratio of the constituents and the longitudinal CTE. Further, increasing the volume fraction at a given elastic moduli ratio is expected to reduce the error between the analytical and experimental data[83].

Yalvac and Tastistcheff attempted to extend the previously developed theories to predict the thermoelastic properties of short random fibre reinforced thermoplastic composites[84]. The fundamental theories of Schapery[78] and Halpin's models[79] were adapted and applied to predict the CTE of glass-fibre reinforced polypropylene (PP) matrix and glass-fibre reinforced polyethylene (PE) matrix composites. The results of the work showed that the Halpin modelling techniques predicted the CTE of short fibre reinforced composites at the midpoint of the tested temperature range for both low temperatures and high temperatures. CTEs measured for the PP and PE composites were found to be in the range 2 μm/m°C to 10 μm/m°C with CTE values decreasing with increasing fibre volume fraction (up to 25%). Maximum deviation between measured and predicted values was around 1.5 μm/m °C, suggesting good agreement between modelling and experimental data. The results of the study extended the applicability of these theories from continuous fibre composites to short fibre reinforced composites as well[84].

3.4.2 Analytical CTE of Unidirectional/Bidirectional Composites

In addition to the analytical derivation of the CTE of general anisotropic fibre-reinforced composites, several studies have specifically investigated the CTE of unidirectional and bidirectional composites. Micromechanics are typically the starting point for analysing the thermoelastic properties of laminae. Chamis provides a summary of the elastic, hygral and thermal micromechanics equations[85]. Ishikawa conducted an analytical and experimental investigation of

the CTE of carbon/epoxy and glass/epoxy unidirectional composites[86]. Unlike previous work, fibre anisotropy and temperature dependency of the composite constituents were considered during derivation. The developed equations related the CTE in the three principal directions to the elastic moduli and the constituents' CTE. Experimental validation was conducted for the carbon/epoxy unidirectional composites. For the measured range of temperatures (25 °C to 150 °C), the experimental longitudinal CTE of the carbon/epoxy laminae varied from -0.4 μm/m°C to -0.1 μm/m °C. Maximum deviation between the model and the experimental data was around -0.3 μm/m°C at 100 °C, though again the general shape of the modelled unidirectional lamina CTE agreed with experimental data. Results of the work conducted by Ishikawa showed better agreement than the CTE values predicted by Schapery[86].

Although scattered, some earlier references sought to consolidate the available information on the CTE of textile composites. Johnson et al. summarized the studies conducted to identify the thermal properties of laminates and woven composites analytically and experimentally[87]. Their report summarizes the factors shown to influence the CTE including the fibre volume, void content, reinforcement angle, stacking sequence and moisture effects. Furthermore, the CLPT derivation for CTE of composites is thoroughly explained while highlighting previous micromechanical models. A summary of the experimental methods used to measure CTE is also listed. Lastly, thermal expansion data of a wealth of composites is presented to the reader[87]. Bowles and Tompkins also provided a summary of the major analytical models conducted on composites as well as their developed FE model[55]. The models were applied to unidirectional graphite/epoxy laminae and laminates and the produced CTEs were compared to each other and to experimental data. For the range of fibre volume fraction investigated (10% to 80%), the modelling data showed an exponential decrease of longitudinal CTE with increasing fibre volume fraction. Values of CTE decreased from 3.2 μm/m°F at 10% fibre volume fraction to -0.2 μm/m°C at 80% fibre volume fraction. All models showed excellent agreement with the limited experimental data of the study. The maximum deviation from experimental data was less than $0.1 \times 10^{-6}/°C$ in the range of 30-40% fibre volume fraction [55].

All of the fundamental theories used to develop the thermomechanical models for unidirectional composites mentioned to this point assumed surfaces of interaction to be perfect surfaces. Consequently, composites are treated as consisting of multiple constituents with perfect interfaces.

This simplifying assumption is commonly used in CLPT as well. Titomanlio and Piccarolo related the experimentally observed thermoelastic anisotropy of laminate composites to these simplifying assumptions[88]. To better account for this, interlaminar shear stress across the surface of the laminae was estimated following elasticity approaches highlighted in earlier work by Pagano and Pipes[89]. The additional strains resulting from the interlaminar shear stress were related to the stress-free temperature. Experimental results showed favourable agreement through the inclusion of these additional components of stress[88]. Some studies investigated the fibre-matrix interactions further. Sideridis argued that the region between the matrix and the reinforcement is far from perfect and has significant implications on the overall mechanical and thermal properties of the composite. This region, called the interphase, was used to develop a model to account for the behaviour of the interphase in the overall thermal expansion behaviour of the material. A linear, hyperbolic and parabolic mathematical variation model is used to account for interphase irregularities. An experimental study on the CTE of glass/epoxy unidirectional was conducted to supplement the work and compare the developed model to its predecessors. The models were used to predict the longitudinal CTE for fibre volume fractions between 0 and 90%. Longitudinal CTE values non-linearly decreased from 53 μm/m°C at 0% to 5-10 μm/m°C at 90%. The results of the study showed that the developed model and the Schapery model were almost identical in predicting the behaviour of the composites. Both models were better at predicting the longitudinal and transverse CTE than the law of mixtures. Deviations between the developed model and the experimental data did not exceed 1 μm/m°C whereas the law of mixtures showed a difference of 11 μm/m °C[90].

Following the work of Sideridis[90], work on the CTE of laminates seems to have been absent in literature for almost two decades due to the sufficiently accurate predictions made by the models highlighted in Section 3.4.1. Ran et al., however, mention the discrepancy in predicted transverse CTE of unidirectional composites seen in the predictions of the models, encouraging further investigation[91]. In their work, a novel model is proposed in which the RVE of the laminate is treated a cylinder rather than a block, with a transversely isotropic fiber embedded in an isotropic matrix. The main assumptions include that the interface can be neglected and that the RVE does not deform (no thermomechanical coupling occurs). An FEM model is used to calculate the longitudinal and transverse CTE of carbon reinforced composites with epoxy, metal and ceramic matrices. The results of the tests conducted on the composites showed improvements for the

longitudinal CTE (18.58% deviation rather than 35%). However, the Schapery model[78] was still the best in predicting the transverse CTE of the majority of carbon/epoxy laminae tested[91].

One of the fundamental works in the analytical prediction of the CTE of fabric composites was conducted by Ishikawa and Chou in 1983[92]. In their work, they examine two important thermal properties of fabric composites: the CTE and the thermal bending coefficients. Three models were adopted for their work – the "mosaic" model (MM), the "fibre undulation" model (FUM) and the "2D bridging" model (BR). These are fundamental models in textile composite modelling. The MM neglects yarn undulation and treats the periodic repetitions within the composite as laminate stacks. The FUM accounted for the undulations, however, only accounted for undulations in the weft yarn direction but not in the warp. The BR expands on the FUM, applying it to the analysis of satin weave composites. The authors show in their work the applicability of these models in determination of the thermoelastic properties of graphite/epoxy weave composites. Experiments were conducted to validate the models, showing good agreement between BR and the experimental data. Maximum deviation was 2.7 μm/m°C predicted by the model against 2.5 μm/m°C determined from the experimental data for a tested sample [92]. Naik and Ganesh expanded on this work to calculate the elastic properties of woven composites to predict the thermomechanical properties of three different types of woven composites (carbon/epoxy and e-glass/epoxy)[93,94]. The developed model uses CLT as the fundamental starting point, however, this model takes into consideration the actual strand geometries and cross-sections. A geometrical description of the yarns and the undulation patterns is provided in the work and used to select a unit cell which contains both warp and weft yarns. Two modelling approaches are then introduced to apply CLPT to the selected unit cell, the slice array model (SAM) and the element array model (EAM). In SAM, the unit cell is divided into three slices which are idealized as laminates. In EAM, the slices are further divided into elements which improves on the geometrical averaging limitations of SAM. Figure 3.7 represents these two different modelling techniques. Table 3.1 compares the experimental and model data along with percentage difference, showing reasonable agreement between the two[93,94]. No explanation was provided for the differences in the models ability to predict longitudinal CTE for the different composites.

TABLE 3.1. RESULTS OF THE SAM MODELLING TECHNIQUES AS ADAPTED FROM NAIK AND GANESH [93,94]

Composite Type	$\boldsymbol{\alpha_{L-MODEL}}$ $(\boldsymbol{ppm/°C})$	$\boldsymbol{\alpha_{L-EXP}}$ $(\boldsymbol{ppm/°C})$	% difference
carbon/epoxy, $V_f = 0.44$	4.61	4.40	4.77
e-glass/epoxy, $V_f = 0.42$	15.92	14.20	12.11%

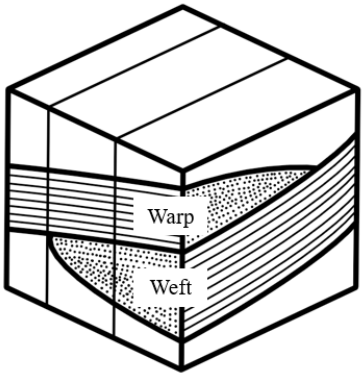

(a)

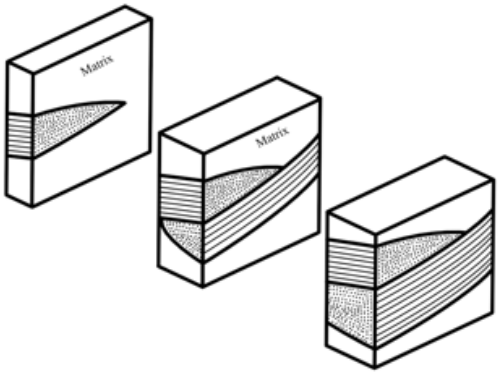

(b)

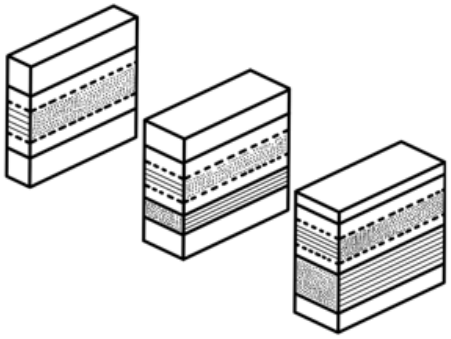

(c)

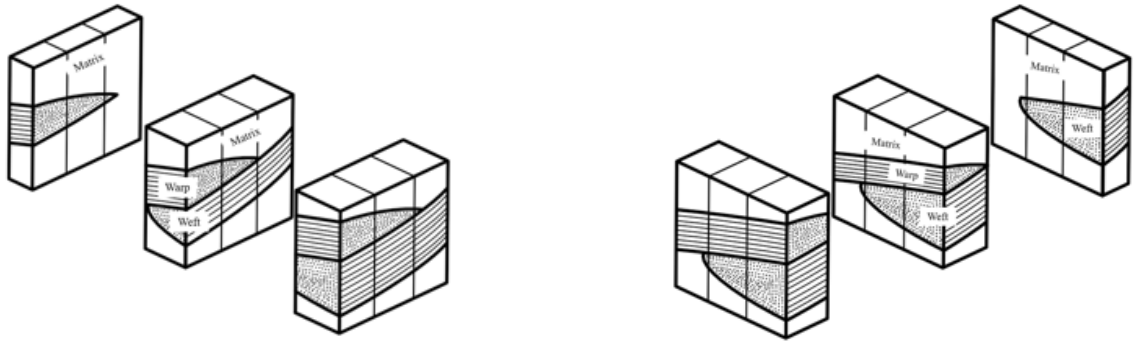

(d) (e)

Figure 3.7. Schematic representations of the two modelling approaches used by Naik and Ganesh to predict the thermal expansion properties of a (a) woven composite unit cell, the (b,c) SAM and (d,e) EAM approaches.

Sankar and Marrey addressed some of the limitations of previously developed analytical models and introduced the selective averaging method to predict the thermoelastic constants of textile composites (unidirectional and woven)[95]. Typically, analytical approaches reduce the complexity of the problem using one of two methods. Stiffness averaging assumes a state of iso-strain. Compliance averaging assumes a state of iso-stress. In the newly developed method, both approaches are averaged on the microscale. The properties are then homogenized for the unit cell to compute the extensional, coupling, and bending matrices for different types of graphite/epoxy weaves. The authors compare the calculated CTEs to available FEM data, showing good agreement with maximum deviation around 35%[95].

3.4.3 Analytical CTE of Braided Composites

One of the earliest works attempting to predict the coefficient of thermal expansion of braided composites was the work of Powell[96]. In this study, an analytical model was created that combined aspects of mechanics of materials and CLPT. These results were compared with experimental data in which a knockdown factor was used to account for braiding. The results of the work showed that the developed model for the longitudinal CTE was sensitive to the axial spacing of the yarns on the braided sample[96].

Following the initial work of Powell, Naik expanded on the analytical work done to model the behaviour of fabric composites to predict the thermoelastic properties of both woven (plain and

satin) and braided (2D and 2D triaxial) graphite/epoxy composite structures while accounting for the internal yarn architecture[97]. A representative unit cell was selected for each of the textile types considered and the yarn centreline path was described. Yarn cross section was modelled as lenticular. A method of discretizing the yarns was implemented and for each "slice", the effective properties were calculated. The properties were then averaged under the assumption of an iso-strain state within the representative unit cell. A parametric study was also done on the influence of yarn geometry on the resulting properties. The results showed that for a 2D braided graphite/epoxy composite, the negative longitudinal CTE initially decreased non-linearly with increasing braid angle up to 30° and a CTE value of -2.5 μm/m °C. After 30° braid angle, the CTE increased again, beginning to plateau around 75° braid angle and a CTE value of 16 μm/m °C. For 2D triaxial braided composites, the longitudinal CTE decreased linearly with increasing fibre volume fraction. The method, however, was unsuccessful in composites with preferential yarn reinforcement[97].

Yan applied a CLPT based approach to calculate the thermomechanical properties of braided composites[14]. This section of the work closely resembles the methodologies highlighted earlier for laminae and woven composites. Similar to these materials, a unit cell is selected on the sample and a force balance is used to calculate the effective elastic constants of the composite. Hygrothermal constants are calculated by using an identical unit cell, but following the virtual work method. The result of the derivation is an expression for the effective CTEs of the braid as functions of terms of the extensional matrix, the volume fraction, the filament packing factor and the axial yarn content of braided preform. The results of the modelling showed that increasing the braid angle and yarn spacing increased the effective transverse CTE while the longitudinal CTE seemed to attain a maximum at a braid angle of 45°[14].

3.5 Experimental Literature

Experimental determination of the CTE of textile composites is difficult due to the diverse shapes and structures in which these composites are manufactured. Unlike the determination of mechanical properties, no standard exists specifically for the determination of the CTE of polymer-matrix composites[98]. For the experimental measurement of CTE, many studies have used some form of dilatometry. In this test method, samples are constrained in an insulated chamber. When temperature is changed, the sample dimension changes which is then registered by the

displacement of a push rod. This displacement is then relayed and used to calculate CTE. Figure 3.8 shows a schematic of a dilatometer highlighting the basic components. Although no standard exists specifically for polymer-matrix composites, the reader is directed to ASTM standards E831: "Standard Test Method for Linear Thermal Expansion of Solid Materials by Thermomechanical Analysis" and E228: "Standard Test Method for Linear Thermal Expansion of Solid Materials with Push-Rod Dilatometer" for further information on the experimental measurements of the CTE of textile composites[56,57].

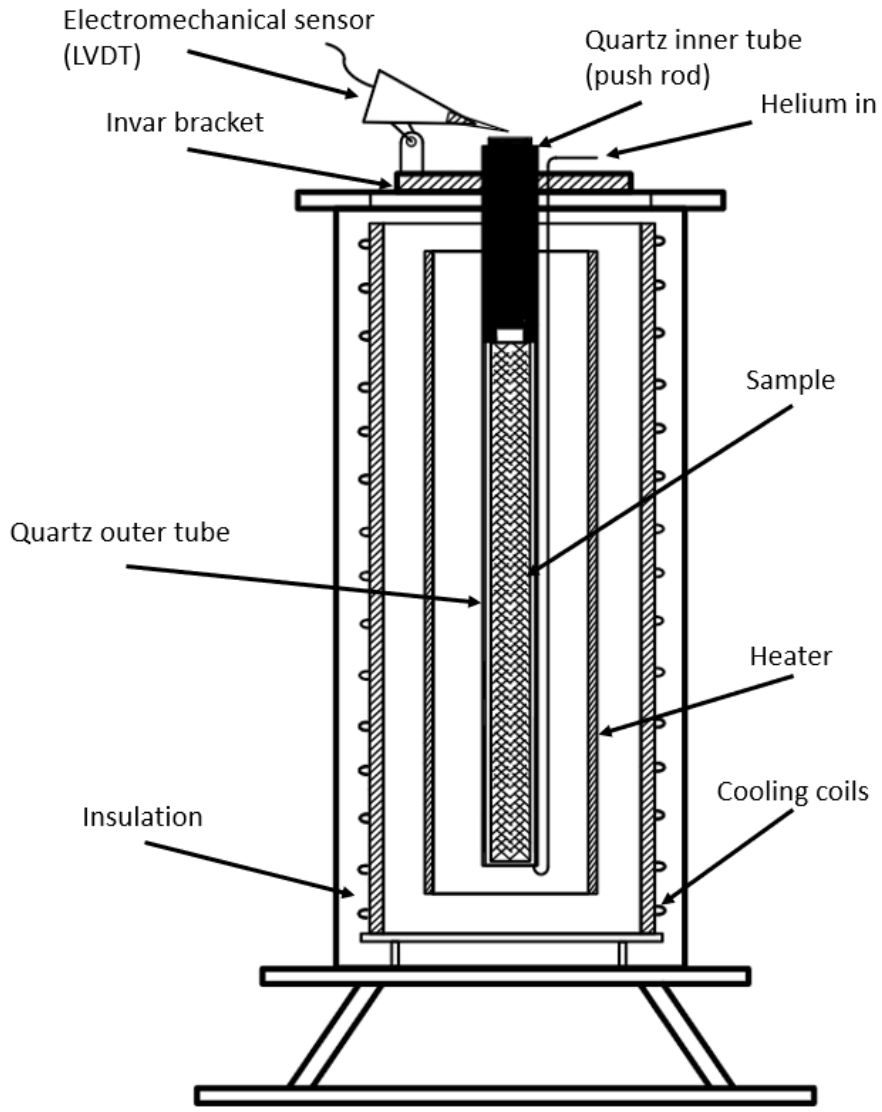

Figure 3.8. Schematic of the main components typically found in an electromechanical dilatometer as adapted from Johnson et al[87]. Sample dimensions typically are in the scale of 100 mm.

3.5.1 Experimental Studies on Composites

For laminae and laminates, Fahmy and Ragai conducted an experimental study on the thermal expansion behaviour of unidirectional, balanced angle-ply and complex graphite/epoxy laminates[99]. Experimental data was compared to a previously derived theoretical model based on the rule of mixtures. Unidirectional samples were heated at a rate of 1°C/min from 20°C to 160°C and the coefficient calculated at 100°C. Balanced angle-ply samples were heated at a rate of 1°C/min from 20°C to 180°C and the coefficient calculated at 100°C. Change in length was measured in both the longitudinal and transverse direction. The results showed excellent agreement between the theoretical model and the experimental data for unidirectional samples, with less agreement for the angle-ply laminates. For angle-ply laminates, the model deviates by more than 50% at approximately 23 °C. These deviations were attributed to inaccuracies in the calculations of the transverse modulus and in-plane shear modulus [99]. Freeman and Campbell conducted an extensive experimental investigation into the thermal expansion characteristics of graphite reinforced composite materials as well[100]. The longitudinal and transverse CTE of different types of laminates (unidirectional lamina, 0/±60 and 0/±45/90) were measured over the temperature range of – 186 °C to 288 °C. The results showed that moisture content had a significant effect on the measured strains. The results also indicated that for all samples except the unidirectional laminate, the CTE increases nonlinearly with temperature. The authors suggest that achieving near zero CTE is possible by careful selection of the laminae[100].

Yates et al. investigated the thermal expansion behaviour of carbon-fibre reinforced polymer-matrix composites[101]. More specifically, they sought to understand the influence of fibre volume fraction on the CTE. This work was also unique in testing the matrix independently from the combined composite systems. The results confirmed the applicability of theoretical modelling techniques including the work of Schapery[78] and Rosen[80] in the range of fibre volume fractions of 0.5 to 0.8[101].

Strife and Prewo expanded on the materials used for studying the CTE of composites[102]. Typical materials used in the majority of work up to their study were carbon fibre or glass fibre reinforced polymer composites. Their work, however, involved the experimental investigation of the thermal expansion behaviour of Kevlar/Epoxy unidirectional and bidirectional (±22, ±30, ±45, ±60 and ±68 degrees orientation) composites. Samples were heated at a rate of 2°C/min. Results of the

work showed that Kevlar®/Epoxy composites are considerably more anisotropic than Carbon/Epoxy composites. The relationship between the angle and the CTE was also presented. In both unidirectional and bidirectional composites, CTE initially becomes more negative but at larger angles increases and becomes more positive. Their results also showed that Kevlar®/epoxy bidirectional laminates achieve a zero CTE at an angle of ±43 degrees[102]. Adams conducted an experimental study which sought to find the CTE of automotive sheet molding compound reinforced with glass fibre. A numerical model known as the *"Scheffe special cubic model"* was used to predict the CTE for the composites and compare them to the experimental data[103].

Raghava conducted an experimental study to confirm the validity of CLT on glass/epoxy unidirectional laminae and laminate composites[104]. Glass/epoxy laminates were heated from room temperature to 100 °C with the temperature and the deformation of the samples measured and recorded. Excellent agreement was found between the experimental data and the Schapery[78] and Halpin CLT models[79]. The largest percentage difference was for the longitudinal CTE of 60° unidirectional laminae, where the predicted CTE was 14.8 μm/m°F and the measured was 17.03 μm/m°F (15.07%). The Chamberlain model[105] theoretical values were found to be lower than the experimental values. A crucial conclusion from the work, however, is that heating and cooling cycles do not influence the values of CTE[104]. Following this work, Raghava et al. compared the thermal properties of thick (2.125") glass/epoxy laminates to thin (0.212") laminates. The results of their work suggest that in thick laminates, localized strains are produced, violating the iso-strain assumption necessary for CLPT. Further, the CTE values measured for the thick laminates were dependent on the mounting positions of the strain gages. Lastly, thick laminates experienced large hysteresis loops in heating and cooling cycles. This suggests that residual stresses are developed during the curing of thick laminates[106]. Akay et al. indicated in their study the significance of moisture on the mechanical and thermal properties of laminates[107]. An experimental study was conducted in which Kevlar/epoxy laminates were prepared in two methods and exposed to moisture in an environmental chamber. The results of the work showed that oven-cured laminates had higher void content resulting in greater moisture absorption. Higher moisture content was correlated with a decrease in the glass-transition temperature and overall thermomechanical properties of the laminate[107].

Tezvergil et al. conducted an experimental study that looked into the influence of fiber orientation on the CTE of FRPs[108]. FRP samples were made into the shape of a bar in a mould and cut to cubical test specimens. To eliminate the influence of moisture, samples were stored in a desiccator for 7 days prior to conducting the thermomechanical analysis. CTE was measured as the temperature of the sample was increased up to 160 °C. Results of the study showed that all samples exhibited an increase in CTE between 37 °C and 67 °C. As expected, samples with lower filler content had higher CTE values. Although only two orientations of filler were tested, results suggest a relationship between filler orientation and exhibited CTE. Samples with longitudinal fillers showed lower CTE values[108]. Rupnowski et al. conducted an interesting combined experimental-analytical study which sought the thermal properties of different types of graphite fibres from measuring the CTE of the unidirectional and woven composites[109]. Length dilatometry was used in the work to experimentally measure the longitudinal and transverse CTE of the materials. From the measured values, the Mori-Tanaka model was used to back calculate the fibre properties from the unidirectional composites[110]. For the woven composites, an FEM optimization technique was used. The results on the CTE of the T650-35 graphite fibres from the unidirectional and woven composites showed excellent agreement between each other and the experimental data[109].

For woven composite work, Rogers et al. studied the thermal expansion characteristics of laminates reinforced with carbon fibre weaves over the temperature range of 90 K to 400 K[111]. The results showed that the thermal behaviour of the composites were influenced by tow densities in the principal fibre directions, the crimp in the reinforcing fibres and the laminate stacking sequence. Reported CTE values were reported as $-2.6 \times 10^{-7}\ °C^{-1}$ in the longitudinal direction and $2.6 \times 10^{-5}\ °C^{-1}$ in the transverse direction[111]. Liao et al. conducted an experimental investigation on the thermal expansion properties of 2D and 3D woven carbon/carbon composites[112]. Chemical vapor infiltration (CVI) was used to prepare samples and the CTE was measured using dilatometry by heating the samples at 3 °C/min to a temperature of 1300 °C. The results of the experimental study showed an inverse relationship between porosity and the longitudinal CTE in the temperature range of 25 °C to 100 °C. The comparison between the CTE of 2D and 3D woven composites also showed lower CTE for 2D (which ranged from $-0.4 \times 10^{-6}\ °C^{-1}$ to $7.0 \times 10^{-6}\ °C^{-1}$) compared to 3D woven composites (which ranged from $-0.8 \times 10^{-6}\ °C^{-1}$ to $3.0 \times 10^{-7}\ °C^{-1}$)[112].

The earliest documented experimental investigation into the general thermal behaviour of braided composite materials was conducted by Antonio in their dissertation[37]. Braided composite samples (glass/epoxy, carbon/epoxy and Kevlar®/epoxy) were examined with respect to their resistance to heat. Out of the tested materials, Kevlar/epoxy braided panels demonstrated the least resistance. The author commented on how thermal expansion mismatch between fibres and matrix result in the formation of voids and microgaps, ultimately accelerating stress damage[37].

Braided composites are seldom found in literature following this initial work. Zhang et al. looked into the thermal behaviour of 2D woven and 3D braided C/SiC composites from room temperature to 1400 °C. Samples were manufactured using CVI[113]. To measure CTE, a dilatometer was attached to samples to record displacements as temperature was increased. Similar to the results reported from Liao et al. on woven composites[112], the longitudinal CTE of 3D braids was lower than the 2D woven composites. Although the braided composites had a small braid angle of 22 °C, the contribution of the through-thickness fibres was significant. Residual stresses and the development of microcracks in the braided composites, however, were attributed to the large difference between the CTE of the carbon fibres and the SiC matrix[113]. Zhang et al. used precursor infiltration and pyrolysis (PIP) to test the influence of different 3D braided structures on the thermal expansion of hybrid C/SiC composite[114]. The three braided structures used were 3D3d, 3D4d and 3D5d. Dilatometry was used to measure the longitudinal and transverse CTE between -150 °C to 25 °C. For longitudinal CTE, near-zero CTEs were achieved by 3D3d braided C/SiC samples between -120 °C to -40 °C and by 3D5d samples between -40 °C and 0 °C. For transverse CTE, near-zero CTEs were achieved exclusively by the 3D3d braided C/SiC samples over the tested temperature range[114].

3.5.2 Related Experimental Studies

Furusho et al. investigated the thermal degradation of several halogen containing polymers by torsional braid analysis (TBA)[115]. TBA involves a composite system composed of a polymer matrix with a mechanically inactive supporting braid. The results primarily focus on the influence of halogens on the thermal stability and overall chemical reactions involved in the experimental study[115].

Mackowski et al. measured the CTE of several epoxies in the range of 4 K to 300 K to supplement the experimental work looking into the CTE of composite materials[116]. To conduct the study, samples were manufactured to standardized lengths and the temperature was measured using a copper-constantan thermocouple imbedded in the sample. The reverse junction was immersed in liquid nitrogen. Change in the length of the sample was measured relative to a standard copper reference of the same initial length. Results of the study showed an inversely non-linear relationship between temperature and the CTE of the tested epoxies[116]. Adamson conducted an experimental investigation into the thermal expansion and swelling behaviour of an epoxy resin system and two graphite/epoxy systems exposed to moisture[117]. Important findings of the work include the sensitivity of thermal expansion to moisture content in epoxy resin. Epoxy resin saturated with water demonstrated more than double the thermal expansion of dry epoxy resin[117]. Joshi conducted an experimental study of the influence of moisture on the shear properties of carbon fibre composites[118]. Unidirectional samples were immersed in boiling water or aged in a hot-humid atmosphere and the tensile strength and interlaminar shear strength measured. Results showed that at testing temperatures above 70 degrees, tensile strength decreased due to the increased tendency of the composite to absorb moisture. Interlaminar shear strength varied significantly depending on the amount of water absorbed[118]. Fabric composites are typically used in applications where shear strength is significant, implying that further investigation of the influence of moisture on thermoelastic properties should be investigated[29].

3.6 Numerical Studies

A review of the numerical studies conducted to predict the properties of textile composites is presented in this section. Typically, numerical analysis is a multi-step process which involves modelling the yarn (microscale), modelling the unit cell (mesoscale) and finally the composite structure (macroscale). The micro- and mesoscale involve some application of the analytical models presented in section 3.4. Homogenization is often used to treat the different elements of the model as a continuous structure with single properties. A generalized representation of the different classifications and the inputs and expected outputs for each when numerically modelling the thermoelastic behaviour of textile composites, adapted from Dixit and Mali, is shown in Figure 3.9[59].

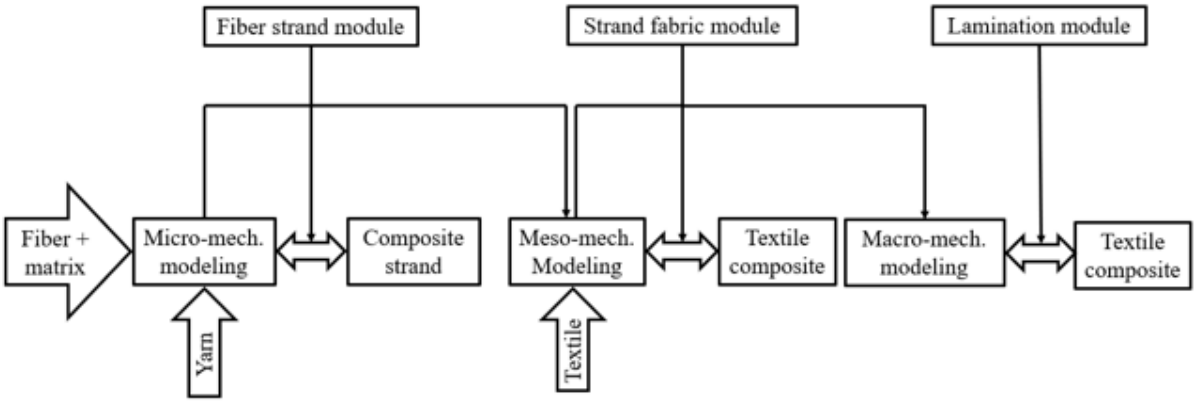

Figure 3.9. Schematic showing the different scales of modelling textile composites along with the inputs and expected outputs of each level.

3.6.1 Numerical Studies on Laminates and Woven Composites

Numerical simulations of the thermal behaviour of composites were practically non-existent before the late 1970s due to the computational complexity required. Research in composites started with looking at laminates. Bowles is often cited as the first to develop a finite element (FE) code for composite analysis[119]. In this analysis, a generalized plane strain assumption in a composite consisting of two or more orthotropic constituents is used. The code was designed for both mechanical and thermal loads, allowing the user to calculate the elastic and thermal properties of the composite[119]. Bowles and Tompkins later used the developed code to predict the CTE of unidirectional composites using two different unit cell geometries, a double period square and a hexagonal pattern[55]. Liu and Cheng used a homogenization method to predict the properties of unidirectional lamina[120]. Islam et al. looked into the CTE of unidirectional composites using a FEM approach based on the double period square unit cell geometry developed by Bowles and Tompkins. In addition to predicting CTE, however, the authors were interested in understanding the influence of debonding on the CTE. The results on the intact carbon/epoxy composites showed very similar results to that of Bowles and Tompkins. As expected, increasing the fibre volume fraction from 0.60 to 0.70 resulted in a decrease of the longitudinal CTE from $6.77 * 10^{-6}\ °C^{-1}$ to $6.26 * 10^{-6}\ °C^{-1}$. The results did show, however, that the presence of cracks in the region between the fibres and matrix can change the transverse CTE significantly[90,121]. Karadeniz and

Kumlutas conducted a numerical study investigating the influence of fibre volume fraction on the predicted longitudinal and transverse CTE of unidirectional composites[122]. For the FEM simulation, the representative volume element was selected to be a cylinder imbedded in a unit cube. The fibres were assumed to have a square packing arrangement in the unit cell. The FEM approach neglected coupling between the different directions and models the CTE of each direction as a function of the local displacement and global temperature increment. The values predicted from the modelling approach were then compared to those obtained from the analytical models previously discussed in section 3.4. The results of the study showed excellent agreement in the longitudinal CTE, with maximum deviation below 0.2 μm/m °C. For the transverse CTE, discrepancies were attributed to the sensitivity of the transverse CTE to the modulus ratio of the fibres and matrices used, a conflicting result with the previous work of Craft and Christensen[83,122].

For woven composites, Raju et al. were one of the earliest to explore the implementation of FEM to predict the thermal coefficients of expansion[123]. An analytical mosaic model was combined with a superposition method to facilitate the FEM. The model was then used to predict the coefficients of expansion for a plan weave, a 5-harness satin and an 8-harness satin. Different meshing was used to account for the increasing complexity of the structures (ranging from 50 nodes for a coarse mesh for plain weaves to 3077 nodes for the fine mesh for an 8-harness satin). The results showed good agreement (less than 0.5 μm/m°C with the experimental data) with the BR model and the limited experimental data available at the time[123]. Hahn and Pandy expanded on previous numerical simulations conducted on laminates to develop a FEM-based micromechanics model for predicting the thermoelastic properties of plain weave fabric composites[124]. An RVE in the plain weave fabric is selected and sinusoidal functions are used to described the undulations. An iso-strain assumption and volume averaging is used to calculated the effective stiffness of the RVE. A similar process is conducted assuming iso-strain and zero total induced stress to calculate the effective CTE. The results of the FEM-based model showed that the CTE slightly increased with reduction in the fibre volume fraction[124]. Dasgupta et al. used a two-scale asymptotic homogenization scheme to calculate the effective thermomechanical properties of woven fabric composites[125]. Similar to the work of Hahn, a representative unit cell is selected and orthotropic tensors for the effective mechanical stiffness, coefficient of thermal expansion and thermal conductivity are calculated numerically. An FEM approach is used to solve the BVPs of the elements of the selected unit cell. The results of the numerical work highlight the effectiveness of

the developed methodology in predicting the properties of woven composites when the microscale of the irregularities (voids, crimping, etc.) are small compared to the scale of the composite[125].

Although Whitcomb is often credited for introducing three-dimensional finite element modelling to predict the thermoelastic constants, his work was limited to predicting the effective elastic constants of plain weaves. The study did, however, perform a parametric study on the influence of tow waviness on the predicted properties[126]. Marrey and Sankar performed a finite element analysis on the unit cell of textile composites assuming that they can be modelled as beams. The results of their work showed that the beam/plate thermal properties could not be predicted from the properties of the constituents and assumed beam geometry[127].

Ishikawa et al. developed a simple mechanical model to predict the thermoelastic constants of three-dimensional graphite/epoxy, carbon/epoxy and glass/epoxy woven composites[128]. CLT is once again used as the basis for this modelling technique, closed form formulae are developed for the unidirectional laminae representing the yarns. Parallel and series linkages are then used to combine the unidirectional composites to form the overall composite and predict its properties through homogenization. The thermomechanical values obtained from the model were compared to very limited experimental data, showing good agreement (within 5%)[128]. Tan et al. developed a three-dimensional modelling technique for predicting the properties of woven fabric unit cells[129]. In their method, the different unit cells of woven fabrics were considered assemblages of three different types of micro-blocks. The micro-block properties are derived from laminate modelling. These micro-blocks are assembled along each of the X, Y and Z axes to represent the "*X Model", "Y Model"* and "*Z Model*" respectively. Elasticity theory can then be used to predict the effective properties of each of the *X, Y* and *Z* models which can be combined in different ways to predict the effective elastic properties of the unit cells[129]. Tan et al. expanded on their initial work to predict the CTEs for 3D orthogonal carbon/epoxy woven fabric composites[130]. Furthermore, the developed models were used to perform a parametric study on the relationship between the yarn-cross sectional shape, micro-block thickness, through thickness yarn volume fraction and the CTE. Results showed some agreement between the developed model and experimental data. Minimum deviation in the longitudinal CTE was 22% [130].

Zuorong et al. expanded on this work by attempting to create an FEM-based model that evaluated the thermoelastic properties of three-dimensional (rather than plain two-dimension)

woven composites[131]. Previously developed work assumed thermoelastic exclusivity in each of the orthogonal directions in 3D textile composites. An essential assumption in CLT is a balanced symmetric laminate structure to remove coupling effects. This assumption might provide satisfactory analytical results, however, Zuorong et al. took into account these coupling effects in their developed FEM model by following a homogenisation scheme used earlier by Chen et al. to evaluate the elastic properties of three-dimensional braided composites[131]. The results of the numerical study showed better agreement than the previous work by Tan et al.[130].

Dixit and Mali provide a summary of some of the modelling techniques used to predict the mechanical properties of woven composites[59]. Although predominately focusing on mechanical properties, some studies looking into the CTE are also cited in the review. The review highlights some of the analytical, numerical and experimental studies conducted. It is important, however, to highlight that some of the studies mentioned in the review that supposedly predict CTE only focus on the mechanical properties of woven composites, such as the studies of Sun and Vaidya[132], Naik and Shembekar[133] and Shembekar and Naik[59,134]. The reference still provides a summary of the work conducted including general assumptions and limitations[59].

3.6.2 Numerical Studies on Braided Composites

Wang and Wang were the first to attempt to bridge the manufacture parameters of three-dimensional braided composites to the effective properties through numerical analysis[135]. In this study, the braid was divided based on the topology of the yarn in different regions of the unit cell (interior RVE, surface RVE and corner RVE). Yarn interactions in each of the regions differ, creating a need to define and model each region separately. From these yarn topologies a micromechanics approach is followed then to estimate the local and global properties of the unit cells. Using the developed model, the relationship between the braid angle and CTE was calculated. Their results showed that as braid angle increased, the CTE initially decreased for the braided interior RVE but then increased at approximately 42 degrees[135]. Mohajerjasbi also conducted a study in the numerical analysis for the thermomechanical properties of braided composites[136,137]. In this study, an FE method for the prediction of the CTE for 3D braided composites was introduced. The model considered the different fibre architectures in the three regions of the composite braid: the interior, edges and corners. The results showed that the

relationship between the braid angle and the longitudinal CTE was similar to the relationship between the ply angle and the CTE of laminate composites[136,137].

Xu and Zhang conducted an FEM-based investigation to predict the CTE of 3D braided C/SiC composites[138]. A sequential homogenization scale is carried out from the fibres to the yarns to the selected representative volume cell. In each of these homogenization steps, micromechanics based on a strain energy model are used to calculate the effective CTE of the structure. The results from the modelling technique were compared to the authors' previous work[113]. Results of the work show good agreement between theoretical and experimental values of the longitudinal CTE, but large discrepancies for the transverse CTE. [138].

Some references point to earlier studies which investigated the CTEs of 3D braided composites, however, these studies are either in Mandarin or could not be found by the authors. These studies are referenced here for completion[139–142]**.** Lu et al. conducted a numerical investigation into the influence of the interfacial region between the braiding yarns and matrix on the thermophysical properties of 3D braided composites[143]. Yarns were modelled as unidirectional lamina and used to construct a homogenized representative volume element with a collision algorithm. To model the interfacial region, a thin layer of interface is introduced between the yarns and the matrix. Additionally, a periodic nonadiabatic temperature boundary condition was used in the simulation. Results of the study showed that as the braid angle increased, the longitudinal CTE became more negative. Furthermore, the inclusion of the interfacial region for the mesoscale modelling reduced errors by up to approximately 18.5%[143].

Jiang et al. also conducted an FEM based study on the thermo-mechanical properties of 3D braided composites[144]. Typical representative unit cells treat the yarns as straight rods. In this work, a helix geometry model was implemented for the yarn centreline directions in the unit cells. The unit cell is then discretized into rectangular blocks and the CTE is solved for in each block using a 27-point Gauss quadrature function. The influence of braiding angle and fibre volume fraction is also investigated in the study. The results showed that longitudinal CTE initially decreases with braid angle before hitting a minimum at around 40 degrees, after which it increases with braid angle. Fibre volume fraction seemed to have a much less significant influence on longitudinal and transverse CTE[144]. Hu et al. also looked into numerically modelling the longitudinal CTE of 3D braided carbon/carbon composites[145]. An FEM based program was developed using VC++

programming language. The Rosen and Hashin model[80] was implemented to calculate the properties of the fibres for the finite element analysis. A parametric study was also performed to understand the influence of porosity, fibre volume fraction and braiding angle on the CTE. Results showed that CTE increased when porosity decreased, fibre volume fraction decreased and/or lower braid angles were used. The relationship with porosity was almost linear whereas non-linear relationships were seen with fibre volume fraction and braid angle[145]. The results were also extended to investigate the thermal conductivity and temperature distribution. This study also attempted to lay the foundation for thermo-mechanical coupling to be investigated numerically[146]. Pan et al. looked into the thermomechanical properties of basalt/epoxy 3D rectangular braided composites under different temperatures[147]. Yarn geometry modelling follows an earlier redacted article. Thermomechanical modelling was conducted using the Chamis model[85]. Results of the model mostly focus on the thermal stresses induced in the braided composite. As expected, maximum stress is carried by the straight segments of fibres. Interestingly, the results seem to indicate that the surface and corner structures reduce the thermal stress[147].

Wang et al. also conducted a numerical analysis of the CTE in carbon/epoxy 3D braided composite materials in the temperature range of -100 °C to 140 °C [148]. The authors sought to further understand the relationship between braid angle and the CTE and thermal stresses. Results showed that the axial CTE initially decreases to a minimum at around 30 degrees before increasing and becoming zero at approximately 40 degrees. Transverse CTE was found to decrease non-linearly with increasing braid angle[148]. Zhai et al. also conducted a finite element analysis on carbon/epoxy 3D braided composite that relies on a technique called multiscale asymptotic expansion homogenization (MAEH)[149]. This was presented as the authors' developed method to successfully predict the stiffness properties of 3D braided composites[149] and was extended to predict thermal properties. The results of the numerical analysis showed almost identical results to the study by Wang et al.[148], namely a local minimum in the longitudinal CTE at approximately 40 degrees braid angle and an inverse non-linear relationship between the braid angle and the transverse CTE[150].

Viscoelastic response pertains primarily to the temperature and time sensitivity of polymer composites. Experimental research has shown the significance of viscoelasticity in determining the long-term behaviour of braided composites[151]. Cai and Sun conducted a numerical study looking into the thermo-viscoelastic properties of 3D braided composites[152]. A unique aspect of this numerical study was the assumption of an equivalent thermal expansion coefficient which is

a function of time, following the same relationship as relaxation modulus and time. The thermal expansion strain calculated agreed well with the developed numerical model[152].

3.7 Discussion

This chapter presents the literature available on the investigations of the CTE of textile composites. Studies on the thermal expansion behaviour of unidirectional laminae, angle-ply laminates, 2D and 3D woven composites and 2D and 3D braided composites were presented as concisely as possible. “Braided composites, textile composites, coefficient of thermal expansion, woven composites” were used as keywords to find the studies presented in this review. Articles addressing hygrothermal, hydrothermal, thermal aging and residual stresses were not included for brevity. The referenced studies cover the analytical, experimental and modelling work conducted from 1948 to 2022 on this subject. Resources for this literature review were collected from Scopus, Google Scholar and Elsevier.

Several points arise when examining the literature presented here. These can be briefly summarized as the following:

1. Exceptional progress on the predicition of the CTE has been made in analytical, experimental and numerical modelling of unidirectional laminae, angle-ply laminates and woven composites. Recent numerical studies have shown the ability of the Schapery model[78], one of the earliest models to the knowledge of the authors, to effectively predict the CTE of unidirectional laminae. Many of the analytical modelling techniques implemented to predict the properties of lamina extend to predicting the properties of textile composites through CLT, encouraging the use of these analytical modelling techniques.
2. Transverse CTE modelling is an aspect of weakness in analytical modelling that has been often attributed to the assumptions that are used to develop the models. Different models result in various levels of accuracy and care should be taken when selecting a model and justifying its use for modelling the transverse CTE.
3. For braided composites, the current review suggests a significant gap in the investigation into the thermal expansion behaviour of 2D braided composites. Although the through-thickness properties of 3D braided composites are superior, the relative manufacturing ease and analysis of 2D braided composites present these materials as viable alternatives. Since

the work of Yan in 1998[14], no study has investigated the thermal expansion behaviour of 2D braided composites, analytically, experimentally or numerically. Despite the analytical derivation in Yan's model, no experimental validation was conducted.

4. Investigations into the thermal properties stem from potential applications of textile composites in aerospace applications. The predominant material that has been used in almost all the studies cited in this review has been carbon fibre. Although the negative CTE of the fibre allows for zero or near-zero composite CTE, the current review suggests a huge limitation on available data on the expansion behaviour of other FRPCs, particularly Kevlar® based composites. Data on the CTE of composites designed from fibres other than carbon, both synthetic and natural, is necessary for better implementation of FRPCs in their intended applications. Evaluation of the developed analytical models with different materials other than carbon is paramount.
5. Experimental investigations into the CTE of textile composites have not undergone change. The methods introduced in the earliest work are improved on, but fundamentally the same. ASTM standards do not exist specifically on polymer-matrix composites, and current standards suggest the use of a dilatometer to measure CTE. Non-contact methods of measuring the CTE need to be documented and presented as viable and precise alternatives to measuring the CTE in samples that cannot be designed for a dilatometer.
6. Some of the factors presented in the earlier work of Johnson on the CTE of laminae must be considered when investigating the thermal behaviour of textile composites[87]. Moisture content, fibre volume fraction, fibre orientation, heating cycles, void content and porosity have been investigated and have shown to have correlations with the measured CTE. These results have been shown for laminates, weaves and braids. Careful consideration of the testing environment and testing conditions is important for repeatability when measuring the CTE of textile composites.
7. Conflicting results are seen with regards to the inclusion of the fibre-matrix interface in modelling. Logically, the inclusion of the interface would improve the accuracy of the predicted CTE. Assuming perfect mathematical surfaces of interactions seems to yield acceptable results in most 2D analytical models. Inclusion of the interface (through homogenization or interface modelling or other methods) has shown varying degrees of success in reducing the errors seen in numerical modelling.

3.8 Conclusion

Textile composites offer numerous advantages over traditional composites. Knits, weaves and braids offer tailorability and precision in manufacturing and designing for applications that require high strength, high stiffness and low weight. One aspect of the behaviour of these materials that has not been consolidated is the CTE. Accordingly, a literature review was conducted on the studies that have investigated the CTE of textile composites. A quick summary of the CLPT method is presented to the reader in the scope of calculating the CTE of a laminate from the properties of the fibre and the matrix. The literature is divided into analytical methods, experimental investigations and numerical modelling studies. Within these sections, the literature is further divided into the three categories of laminates, knits and weaves and braids. The literature review on the CTE of textile composites suggests that although extensive research has been conducted on laminates and woven composites, braided composites remain largely unexplored with a single analytical study conducted without experimental verification.

These gaps in characterizing and predicting the thermal expansion of braided composites must be addressed for them to be used in their potential applications. Many areas remain unexplored including the influence of geometrical parameters of braided composites on the final thermal expansion behaviour as well as a general lack of materials tested. No analytical model exists to predict the thermal expansion behaviour, resulting in cumbersome experimental testing for designing components for aerospace and construction, among other applications.

CHAPTER 4 - Thermal Expansion Coefficient of 2D Braided Composites: Analytical Model development and Experimental validation

The literature review presented in Chapter 3 suggests that research into the thermal expansion behaviour of braided composites remains unexplored. With an exception to one study, no research has looked into experimentally testing and modelling the thermal expansion behaviour of two-dimensional tubular braided composites. Accordingly, this chapter presents a novel non-contact method to experimentally measure the thermal expansion of tubular braided composites for which no standard currently exists. Additionally, an analytical model based on classical laminate plate theory is used to predict the thermal expansion behaviour which can also be used to design tubular composites for specific application requirements. This chapter was submitted for publication in the journal of engineered fibres and fabrics as two articles titled "Thermal Expansion Coefficient of 2D Braided Composites, Part 1: Development of non-contact experimental measurement technique based on optical methods" and "Thermal Expansion Coefficient of 2D Braided Composites, Part 2: Classical Laminate Plate Theory analytical model development and verification". Both articles were written by me and edited by Dr. Jason Carey and Dr. Cagri Ayranci.

4.1 Introduction

Composites have gained popularity over the last 70 years due to the tailorable properties that are not possible by using traditional materials. Composite materials consist of two or more constituents joined together to produce a non-homogenous material. There are different types of composites; this work will focus on fibre reinforced polymer matrix composites (FRP composites or FRPCs) which consist of continuous or discontinuous small diameter fibres reinforcing a polymer matrix. The small diameter of fibres minimizes material flaws and improves the overall bond between the matrix and reinforcement, resulting in improved overall properties of FRPCs[153].

Textile composites are a subset of fibre-reinforced polymer composites in which the smallest repeating unit, traditionally referred to as the unit cell, consists of fibre bundles in several orientations[58]. Braiding is a textile manufacturing method in which three or more parallel strands of fibre are intertwined together at nonorthogonal angles. To create this braided structure, two

motions happen simultaneously, one rotational and the other translational. The rotation of the yarns about a common axis allows for the braided pattern to be formed circumferentially around a mandrel. The translational component of motion ensures that this pattern is repeated along a length. By combining these two motions, yarns are interlaced and a braided preform is created.

The rotational motion of the yarns is provided by the braiding machine (or braider). Figure 4.1 shows a 2D braider. In these machines, yarns of the fibre that is desired for the final product are first spooled on carriers. The carriers are then loaded onto the braider. The carriers move along predetermined serpentine paths to create the interlacing pattern on a mandrel of the desired shape of the final component. To ensure that the final braided pattern is produced, each set of carriers move in opposite clockwise and counter-clockwise directions. This motion is controlled by horngears[154]. Figure 4.2 shows a schematic of the motion of the carriers on a maypole braider.

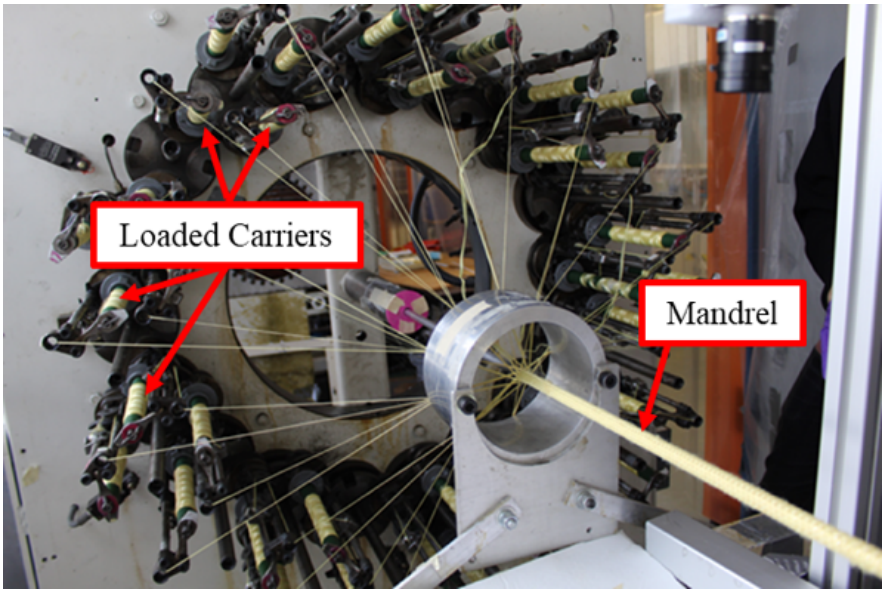

Figure 4.1. Image of a maypole braider highlighting the carriers spooled with Kevlar ® 49 fibres interlacing on the mandrel.

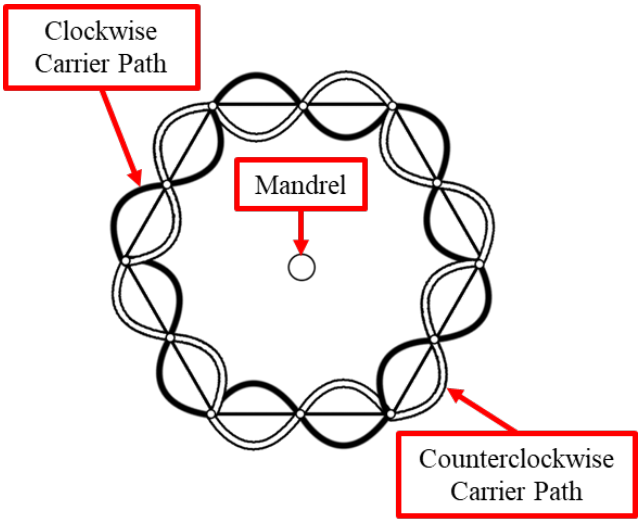

Figure 4.2. Schematic showing the front cross-sectional view of a maypole braider centred at the mandrel. Clockwise and counterclockwise paths represented the direction of motion of carriers along those paths.

To ensure that the yarns are not constantly intertwining at a single point, a take-up mechanism provides the translational motion of the mandrel. This moves the formed braided preform further down the production line, allowing new parts of the yarns to interlace. This is repeated until the desired length of the braided pattern is produced[154]. Figure 4.3 shows a schematic of the entire braiding and take-up process combined.

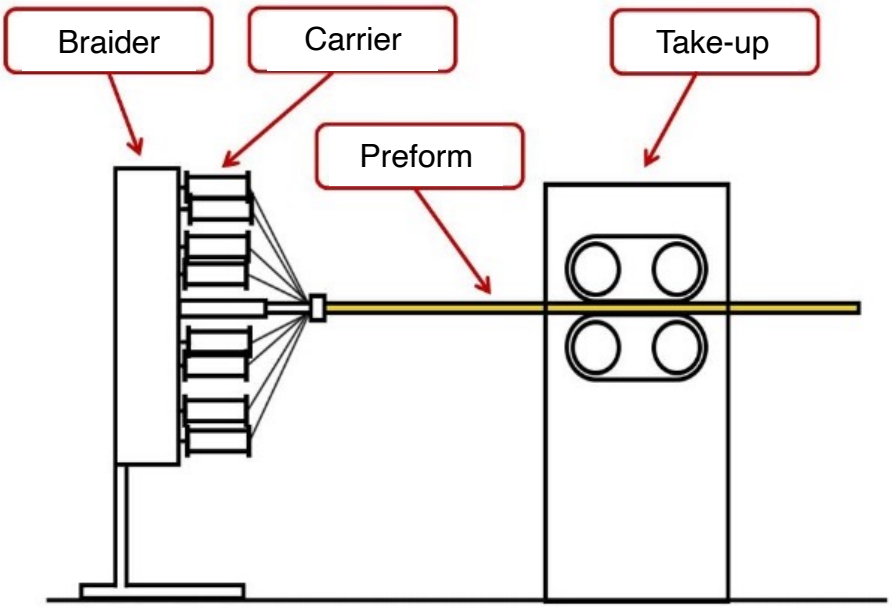

Figure 4.3. Schematic of the braiding line showing different elements of TBC manufacturing. Carriers are loaded with yarns which rotate about the translating mandrel. Rotational motion is controlled by the braider and translational motion is controlled by the take-up mechanism or puller.

Once preforms are manufactured, the matrix is added to the preform to form the braided composite. When the braid is formed on a cylindrical mandrel, the resulting braided composite is commonly referred to as a tubular braided composite (TBC).

By altering the parameters of the braiding process, the resulting geometry of the TBC can also be changed. This allows for further classification of braids by the pattern of yarn overlap and by the braid angle. Braided preforms may be classified as diamond (1/1 or one-over one-under), regular (2/2 or two-over two-under) or Hercules (3/3 or three-over three-under). Figure 4.4 shows schematics of the three different braided preform patterns.

(a) (b) (c)

Figure 4.4. Schematic representations of the three common braiding patterns, (a) Diamond (1/1) (b) Regular (2/2) and (c) Hercules (3/3) braids.

The other parameter of TBCs is the braid angle that defines the overall behaviour of the composite. Braid angle is defined as the angle formed between the interlacing yarns and the longitudinal axis of the preform. The braid angle has a significant effect on the overall mechanical properties of the resulting composite. Figure 4.5 shows the braid angle defined on a TBC.

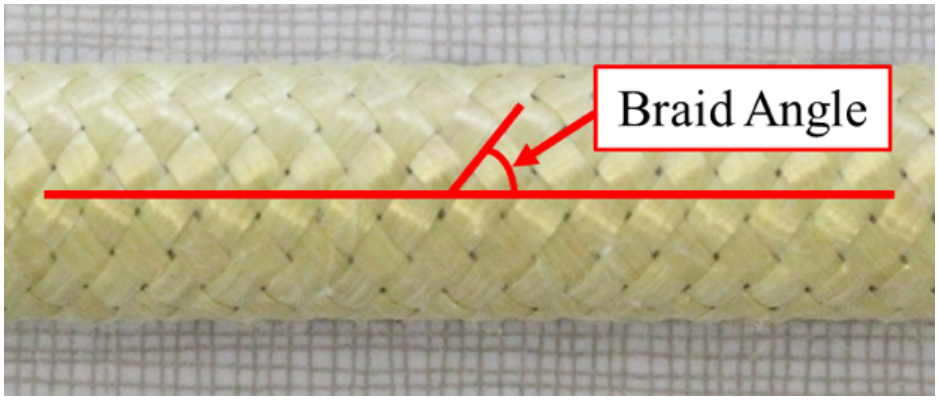

Figure 4.5. Image of a TBC preform depicting the braid angle as the angle formed between the longitudinal axis of the preform and a vector following the path of the yarn.

4.2 Literature Review

Braided composites offer advantages in terms of the properties, rapid production, design flexibility and precision and near-net shape manufacturing compared to other structures and

materials. These advantages have resulted in the investigation and use of braided composite materials in numerous applications.

Croon et al. provides an early summary of the potential applications of braided fabrics in earlier conference proceedings[29]. More recently, Carey highlights some of the current uses of braided composites in jet engine stator vanes, hockey sticks and bone casts[1]. A wealth of studies have identified the suitability of braided composite materials for applications in bone fixation[30,31], tubing support[32], truss design[155], car engine elements[63], aerospace[35] and satellite components[36], underwater vehicles[37] and orthodontics[39].

Numerous works have investigated the mechanical properties of braided composites. These studies have explored the strength and stiffness properties of 2D braided composites in relation to the braid parameters[156–163]. Ayranci and Carey provide a review of the developments in the stiffness testing and modelling of 2D braided composites within the elastic-region of the material behaviour[10]. In addition to tensile properties, relatively few studies have examined the compressive[164–166], fatigue[167,168] and creep[12] behaviour of 2D braided composites.

One aspect of 2D braided composites that has not been explored extensively is the thermal expansion behaviour. For aerospace structures, structural elements and automobile composites defining the thermal properties of the used materials is extremely important. The coefficient of thermal expansion (CTE) is defined as the strain experienced by a material per unit change in temperature. One of the difficulties in composite manufacturing is the thermal stresses induced during curing. Due to the CTE mismatch between the fibres and the matrix, residual stresses are developed in the composite[65–68]. These residual stresses accelerate failure of the composite by fibre-matrix debonding and crack formation[54]. This failure typically manifests as fibre pull-out at the fracture surface[69,70].

Despite the importance of characterizing the thermal expansion behaviour of 2D braided composites, few studies have investigated this. Powell conducted a preliminary analytical and experimental study on the thermal expansion behaviour of 2D carbon/epoxy triaxial braided composites[96]. A model based on mechanics of material and classical laminate theory was developed to predict the CTE and tested against the measured experimental data. The results of the work showed that the experimental values for longitudinal and transverse CTE were greater than the estimates of the model. Within lower temperature ranges (-129 °C to 21 °C), the model

and experiment results for longitudinal CTE agreed within 17.2%. For the transverse CTE, experimental data was significantly higher than model predictions[96]. Naik employed a yarn-discretization method to predict the CTE of 2D and 2D triaxial graphite/epoxy braided composites[96]. Results showed that for 2D braided composites, the negative longitudinal CTE initially decreased non-linearly with increasing braid angle up to 30° and a CTE value of -2.5 μm/m °C. After 30° braid angle, the CTE increased again, beginning to plateau around 75° braid angle and a CTE value of 16 μm/m °C. Results also showed an inverse relationship between fibre volume fraction and longitudinal CTE[97]. Yan applied a laminate plate theory approach to calculate the thermomechanical properties of 2D braided composites using a virtual work method [14]. The effective CTEs of the braids were derived as functions of the terms of the extensional matrix, the volume fraction, the filament packing factor and the axial yarn content of braided preform. Modelling results suggested that longitudinal CTE attained a maximum at a braid angle of 45 degrees[14]. Outside of these three studies, no literature has investigated the thermal expansion behaviour of 2D braided composites.

Experimental determination of the CTE of braided composites is poorly documented in literature. To the knowledge of the author, the two ASTM standards currently available for measuring the CTE of composites are ASTM E831: “Standard Test Method for Linear Thermal Expansion of Solid Materials by Thermomechanical Analysis” and E228: “Standard Test Method for Linear Thermal Expansion of Solid Materials with Push-Rod Dilatometer”. Although these are not explicitly for composites, most studies that have explored measuring the longitudinal and/or transverse CTE of textile composites have used the latter standard of a push-rod dilatometer. Figure 4.6 shows a schematic of the typical components of a push-rod dilatometer. In these devices, an enclosed sample is exposed to a temperature increase. As the temperature increases, the sample dimensions shift, causing a displacement in rods that are in contact with opposite faces of the sample. This relative displacement is then recorded by a linear variable differential transformer (LVDT) sensor at the specific temperature. These are then used to calculate CTE.

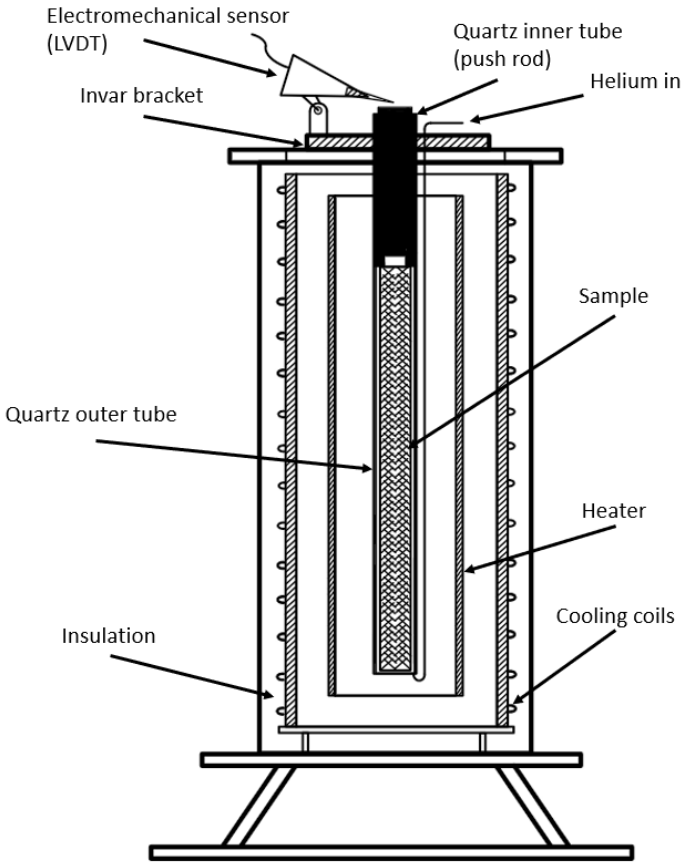

Figure 4.6 Schematic of the typical components of a dilatometer used to measure the CTE of a sample.

Typically, dilatometers have been used to measure the CTE of metals and alloys with excellent results due to the large difference between the CTE of the sample and the push rod material. Vitreous silica, a commonly used push rod material, has a CTE of the order of $0.5 \times 10^{-6}\ \mathrm{C}^{-1}$, making it suitable for metals and alloys where the range of values of CTE typically is of the order of $5 \times 10^{-6}\ \mathrm{C}^{-1}$ to $25 \times 10^{-6}\ \mathrm{C}^{-1}$. As the difference between the CTE of the tested sample and the push rod material decreases, errors increase. Additionally, to accurately measure the CTE of the sample, push-rod dilatometers require samples to have flat or round smooth ends to minimize the errors from edge effects and stress concentrations. Lastly, errors become more prominent when the melting point of the material is close to the temperature at which the sample is being tested. Due to softening effects, the contact between the sample and the push rod is affected, resulting in erroneous displacement measurements and, consequently, incorrect CTE values[169].

In addition to limited data on experimental measurement techniques for CTE, many studies have shown the sensitivity of the measured values to conditions of testing and sample preparation. Freeman and Campbell conducted an experimental investigation into the influence of moisture on the CTE of graphite fibre reinforced composites. They concluded that moisture and temperature both have significant influence on the CTE[100]. These conclusions were supported by other studies. Akay et al. confirmed the significance of moisture on the thermal properties of laminates. Higher moisture was associated with a decrease in the glass-transition temperature and overall thermomechanical properties[42].

4.3 Objectives

The limited data on the thermal expansion behaviour of 2D braided composites is an obstacle in introducing these materials in their intended applications. Further, the presented concerns with the experimental measurement of the CTE of polymer-based composites motivated an investigation into an alternative contact-free method to measure CTE. This method would be suitable for specimens of any shape and size and would overcome all the obstacles with measure the CTE of TBCs using dilatometry. This study attempts to address the gaps in the presented experimental and analytical literature on the CTE of 2D braided composites. Accordingly, the objectives of this work are:

I. Devise a non-contact imaging based experimental method to measure the longitudinal CTE of 2D TBCs.
II. Develop an analytical model to predict the longitudinal CTE of 2D Kevlar®/epoxy TBCs.

4.4 Methodology

4.4.1 Experimental Investigation of 2D TBC CTE

4.4.1.1 Materials

To manufacture TBC samples for this work, 1420 denier Kevlar® 49 (DuPont, Wilmington, Delaware, USA) was selected as the fibre material. Previous research has used this Kevlar® when investigating the thermal properties of composites[102]. Kevlar® is a high-strength and stiffness synthetic fibre with good thermal stability. Additionally, the slight negative coefficient in the

longitudinal direction is comparable to carbon. This allows for designing composites with zero or near-zero CTEs.

The resin-hardener combination selected for this work was Epon 826 epoxy resin (Hexion Inc., Ohio, USA) with Lindau LS-81K hardener (Lindau Chemicals Inc., South Carolina, USA). Epon 826 / LS-81K is a thermoset bisphenol A based matrix system with good thermal stability up to 300 °C. The relevant properties of the selected materials are presented in Table 4.1.

TABLE 4.1. ELASTIC AND THERMAL PROPERTIES OF THE MATERIALS SELECTED FOR THIS WORK

Material	Elastic Modulus (GPa)		Shear Modulus (GPa)	Poisson's Ratio	Thermal Conductivity (W/mK)	Tg (°C)	CTE (μm/m °C)	
Kevlar® 49	E_{1f}	E_{2f}	2.3	0.33	0.04	-	α_{1f}	α_{2f}
	79.7	5.9					-4.9	53
Epon 826	2.73		1.3	0.35	-	136	30	

4.4.1.2 TBC Sample Manufacturing

TBC samples were manufactured following the procedure highlighted in the previous work of Ead et al.[12]. Kevlar® fibre was manually spooled onto 36 bobbins and loaded onto the carriers of a horizontal maypole braiding machine (Steeger HS140/36-91; Steeger GmbH and Co., Wuppertal, West Germany) connected to a pressure-controlled take-up mechanism. A 11.11 mm aluminium mandrel was secured in the take-up mechanism pressurized at approximately 90 psi as specified by the manufacturer. Varying the speeds of the braider and the take-up mechanism can be directly related to the produced preform braid angle by equation 4.1[170].

$$\theta_{\infty} = \tan^{-1}\frac{\omega}{v}R_m \tag{4.1}$$

where θ_{∞} is the steady-state angle of the produced preform, ω is the rotational speed of the braider, v is the take-up speed and R_m is the mandrel radius.

This was used to produce Kevlar® preforms at three braid angles for this work, 35°, 45° and 55°. Braid angles were selected to sufficiently represent the range of angles possible with the available manufacturing setup. Further, these angles allow for a more quantitative examination of the behaviour of manufactured samples. All samples for this work were manufactured in a diamond, one-over-one-under pattern. Figure 4.7 shows the combined braider and take-up mechanism that were used to manufacture preforms for this study.

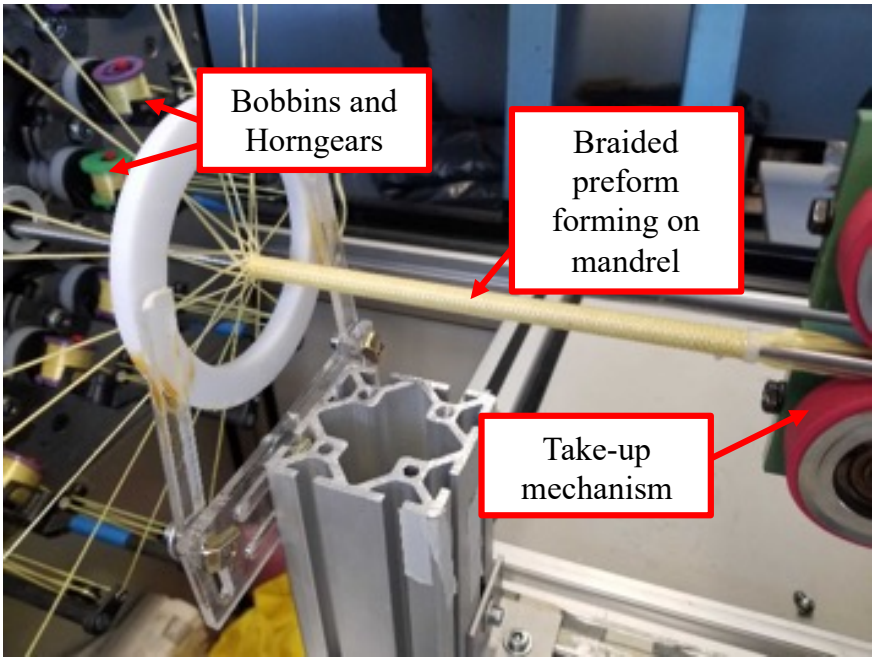

Figure 4.7. Image of a TBC preform depicting the braid angle as the angle formed between the longitudinal axis of the preform and a vector following the path of the yarn.

Once manufactured, preforms were carefully loaded onto 11.11 mm diameter polytetrafluoro-ethylene mandrels for matrix impregnation. Epon 826 and LS-81K were measured and mixed in a 1:1 ratio. Preforms were then manually coated using a manual impregnation technique to ensure sufficient penetration of the mixture through the fibres. Once coated, samples were then transferred to an electronically controlled square oven (Thelco 31480, GCA/Precision Scientific, Chicago, IL). Following the resin manufacturer data sheet, wet TBC samples were cured at 66 °C for 1.5 hours, 85 °C for 1 hour and 150 °C for 3 hours. After curing, samples were removed from the polytetrafluoro-ethylene mandrels and cut into six-inch-long samples. Figure 4.8 shows a sample of each Kevlar®/epoxy TBC configuration used in this work.

Figure 4.8. Kevlar/epoxy TBC samples manufactured at the three braid angles used in this work, 35°, 45° and 55°.

4.4.1.3 Sample Dimension Measurement and Quality Assurance

To assess the quality of the manufactured TBCs, various measurements were taken post curing. Length was measured using a meter rule. To measure the braid angle, high-resolution images were taken using a CMOS camera (Apple, CA). Images taken were then loaded onto ImageJ (Image Processing and Analysis in Java, National Institute of Health, Maryland) and used to measure the angle formed between the yarns and the longitudinal axis of the braid. Inner diameter measurements were using a microscopic gauge set (Mitutoyo Series 155, Mitutoyo, Kanagawa, Japan). Outer diameter measurements were taken using a Vernier micrometer (Mitutoyo 115-225, Mitutoyo, Kanagawa, Japan). For each measurement, five data points were taken per sample and averaged. The cross-sectional area of the TBC samples were assumed to be ring-shaped and were calculated using equation 4.2.

$$A = \frac{\pi}{4}(d_o^2 - d_i^2) \qquad (4.2)$$

where A is the cross-sectional area of the TBC, d_o is the outer diameter and d_i is inner diameter.

Table 4.2 shows the averaged measurements from all manufactured samples. As can be seen from Table 4.2 and Figure 4.9, variation of braid angle for manufactured samples was ± 2 degrees. This was deemed satisfactory for the current study.

TABLE 4.2 MEASURED SAMPLE DIMENSIONS

Sample #	**Length** (mm)	$\boldsymbol{\theta}$ (°)	$\boldsymbol{d_i}$ (mm)	$\boldsymbol{d_o}$ (mm)	$\boldsymbol{A}$ (mm^2)
35_01	152.2	35.199	11.92	12.202	5.358
35_02	151.2	34.980	11.77	12.188	7.857
35_03	156.6	35.543	11.53	12.260	13.630
35_04	152.2	35.293	11.86	12.250	7.408
35_05	157.8	35.280	11.86	12.280	8.117
35_06	151.4	35.230	11.69	12.262	10.784
35_07	157.6	35.446	11.70	12.200	9.431
35_08	152.0	35.488	11.88	12.232	6.619
35_09	158.0	35.235	11.81	12.322	9.693
35_10	155.4	35.202	11.61	12.260	12.171
45_01	153.2	45.736	11.49	12.274	14.692
45_02	150.4	46.141	11.60	12.668	20.419
45_03	152.6	44.302	11.71	12.370	12.478
45_04	150.6	43.848	11.83	12.302	9.016
45_05	154.2	45.353	11.42	12.438	19.107
45_06	155.0	45.405	11.67	12.586	17.609
45_07	152.0	45.467	11.52	12.467	17.770
45_08	152.6	45.392	11.55	12.412	16.171
45_09	153.2	45.475	11.56	12.158	11.176
45_10	150.4	45.146	11.56	12.314	14.105
55_01	153.8	55.492	11.86	12.522	12.656
55_02	153.8	55.492	11.63	12.216	10.868

55_03	150.0	55.135	11.58	12.150	10.660
55_04	152.4	55.284	11.23	12.224	18.235
55_05	155.6	55.266	11.55	12.824	24.456
55_06	156.5	55.906	11.73	12.188	8.663
55_07	151.6	55.752	11.63	12.518	16.917
55_08	156.0	55.068	11.76	12.912	22.221
55_09	155.2	55.703	11.66	12.212	10.299
55_10	155.2	55.260	11.65	12.618	18.560

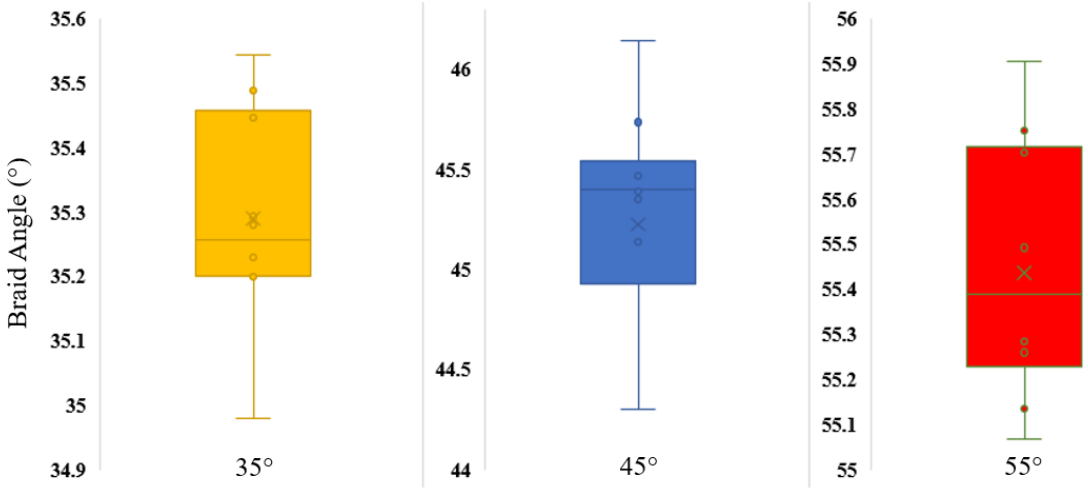

Figure 4.9. Box-and-Whisker plots of the measured sample dimensions highlighting braid angle variation for manufactured TBCs.

4.4.1.4 CTE Pilot Study

Pilot tests were conducted for the following reasons:

1. Identify the suitability of non-contact methods in measuring the strain (and in extension, the CTE) of TBCs.
2. Identify necessary sample treatment required to minimize influence of factors such as moisture content, manufacturing errors and stress concentrations on measured CTE.

To conduct pilot tests, a methodology used by Ead et al.[12] in previous work was followed. Samples were manufactured following previously mentioned steps. Samples were then placed in a vacuumed thermocouple-controlled oven (V0914A1 Series Vacuum Oven, Lindberg/Blue M, Riverside, Michigan, USA). To measure the strain experienced by the sample over the duration of the test, a virtual extensometer was employed. Manufactured samples are painted in a matter black paint (Painter's Touch Flat Black, Rust-Oleum Corp, Concord, ON, Canada) and two white marks are painted (4230 Transparent White, Auto Air-Colors, East Granby, CT) around the gage length of the sample. Samples are then placed in the oven at the intended temperature and images taken using a scientific camera (Basler acA3800-10gm, Basler AG, Ahrensburg, Germany). As the sample deforms, strain is measured using an error fitting code developed by Aldrich et al.[171]. The error function tracks the displacement of the mark in each successive image relative to the first image taken. Displacement is then used to calculate strain. Figure 4.10 shows a sample image taken of the TBC samples tested with the virtual extensometer strain measurement method.

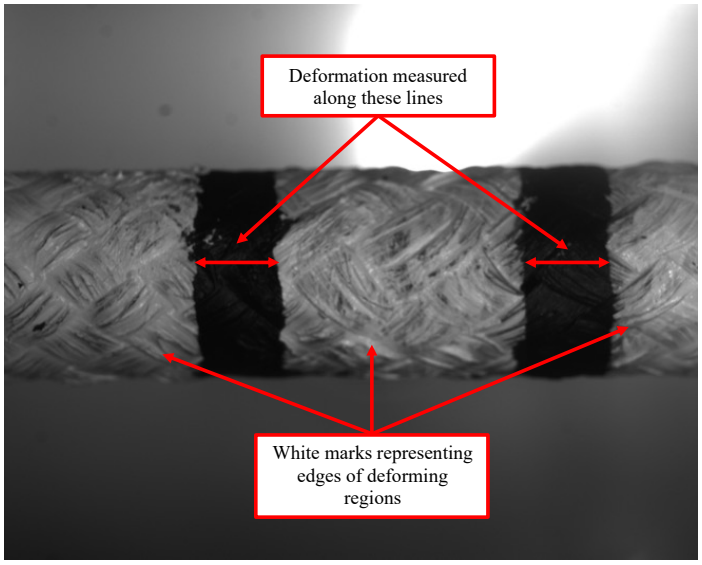

Figure 4.10. Sample image used to measure strain by following the deformation along contrasting regions over the duration of the test.

Primary pilot tests confirmed that measuring strain using optical methods was possible, however, sample preparation was crucial. Figure 4.11 shows the warpage experienced by some samples that were tested after manufacturing without treatment. The resulting warpage shifting the contrasting marks too significantly for proper displacement correlation.

(a)

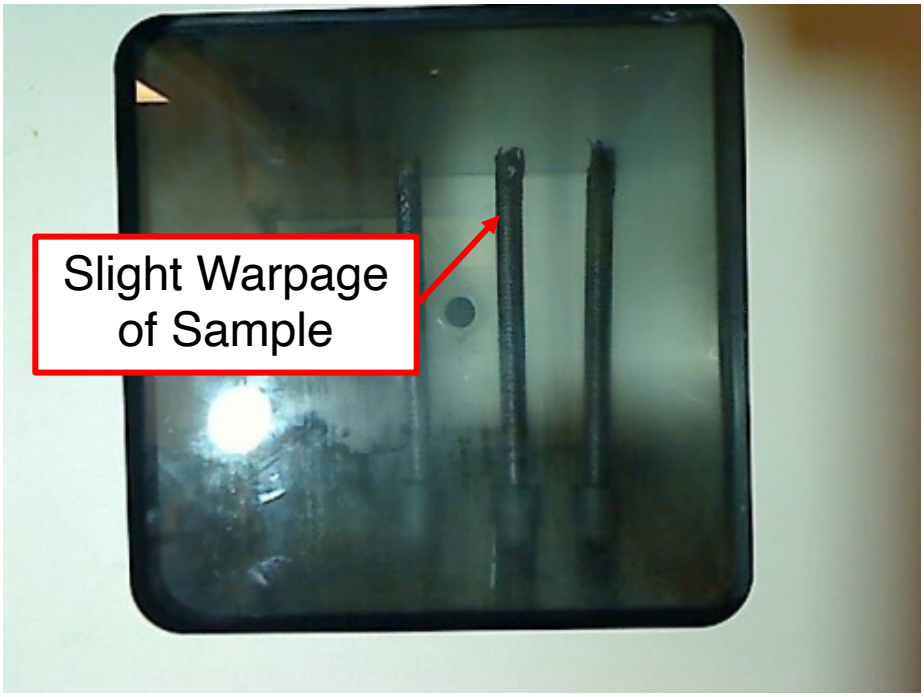

(b)

Figure 4.11 Images showing the warpage of samples (a) before and (b) after applying heat.

An experimental design matrix was used to determine the factors most significant in minimizing the warpage. The results of the pilot test showed that samples were most influenced by moisture content during manufacture and testing. This finding is supported by previous work in literature[100]. Accordingly, an additional step was added to sample preparation in which samples were placed in a desiccator (Space-Saving Desiccator F420310000, Bel-Art & SP Scienceware, Warminster, Pennsylvania, USA) from the end of manufacturing until the start of testing.

4.4.1.5 Thermal Testing and Strain Measurement

To measure the strain experienced by the samples, 2D Digital Image Correlation (DIC) was employed. DIC is an optically based contact-free method for measuring the 2D or 3D changes on a surface over time[172]. To prepare samples for DIC, each manufactured TBC was attached to a stainless-steel end tab using two-part epoxy (Henkel AG & Company, KHaA, Düsseldort, Germany). This ensured that samples were attached to a flat surface for measurement of strain along the longitudinal axis. Once cured, manufactured samples were spray-painted in a black matte paint (Painter's Touch Flat Black, Rust-Oleum Corp, Concord, ON, Canada). A white speckle pattern (4230 Transparent White, Auto Air-Colors, East Granby, CT) was applied to the sample using an airbrush (Paasche H Series, Paasche Air Brush Co., Chicago, IL) at a pressure of 16 psi and approximately 5 inches from the surface of the TBCs. This ensured that a random contrasting speckle pattern was marked on the surface for strain measurement as per DIC recommendations[172]. Figure 4.12 shows an example of the speckling pattern produced on a TBC sample.

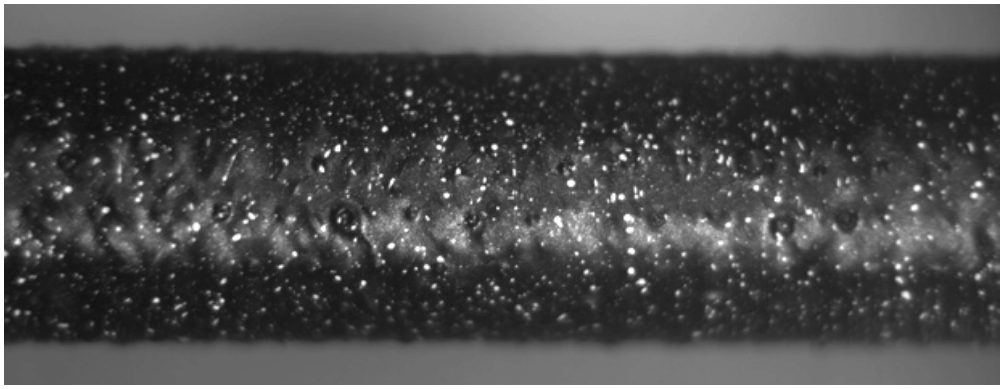

Figure 4.12. Image of TBC sample showing contrasting white speckle pattern on painted black sample.

Once painted and speckled, samples were transferred from the desiccator to the vacuumed oven for thermal expansion testing. To take images of the sample over the duration of the test, an experimental setup was devised as shown in Figure 4.13. A CMOS (complementary metal oxides semiconductor) scientific camera (Basler acA3800-10gm, Basler AG, Ahrensburg, Germany) was positioned along the radial plane of the TBC sample at a distance of 20 cm. Camera zoom and focal length were adjusted to capture a region of interest with at least ten unit cells in the frame. To ensure sufficient light for camera acquisition, two LED lights were placed at oblique angles to the sample plane to prevent glare. An additional camera was used to take images of the temperature and time reading of the oven. Pairs of images were captured every five minutes over the duration of the test.

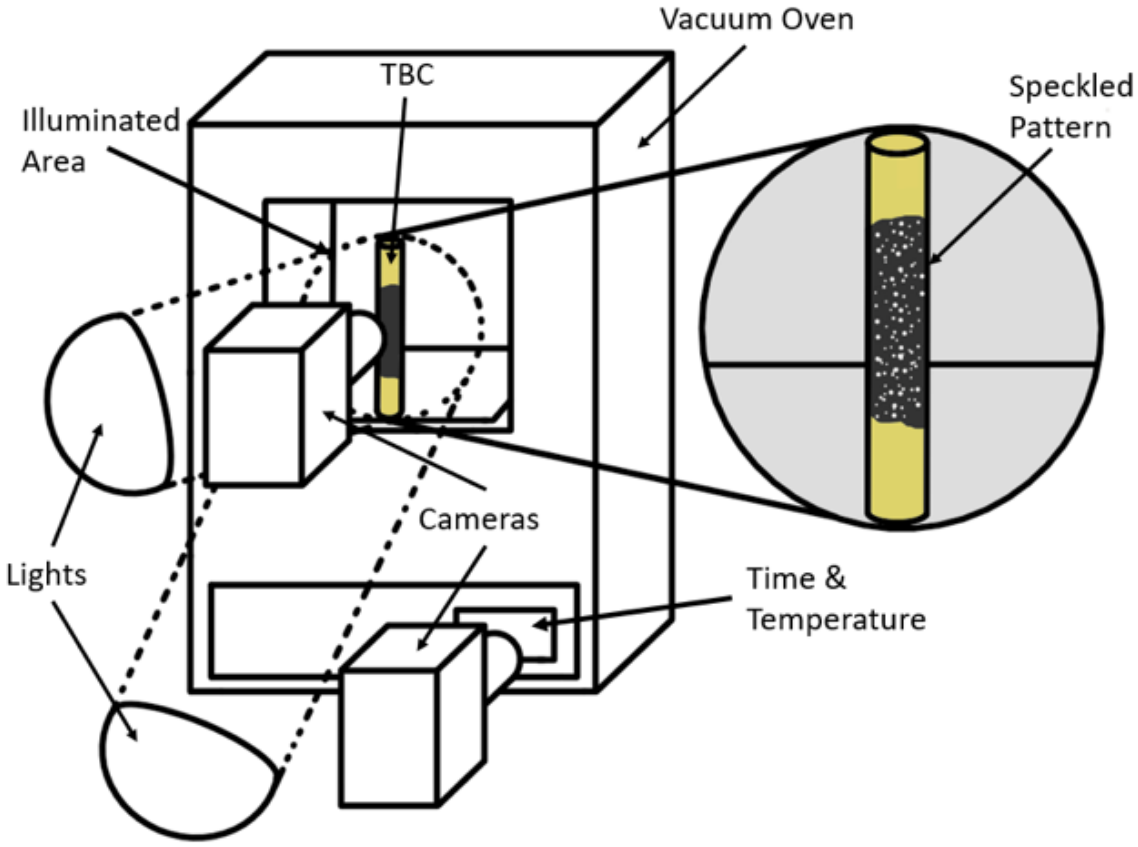

Figure 4.13. Images showing the warpage of samples (a) before and (b) after applying heat.

4.4.1.6 DIC Image Analysis

The CMOS images of the sample taken by the scientific camera were uploaded into a digital image correlation processing software (DaVis version 8.2.0 StrainMaster 3D, LaVision GmbH, Gottingen, Germany) for processing. The steps for processing the images were as follows:

- **Calibration**: Calibration images taken before the sample testing were used to convert the local camera 2D pixel coordinate system into an equivalent physical coordinate system. This converted images from the pixel domain into the physical domain.
- **Pre-processing**: Two filters were applied to the sample to improve the accuracy of the correlation algorithm in measuring the displacements of the speckles. A normalization filter and a sliding average gaussian filter were applied. These ensured smoother images with lower peaks for better correlation results.
- **Correlation:** A least-squares matching algorithm is then applied to the pre-processed image pairs to calculate the displacement of the speckle patterns with respect to the first image in the set over the entire sample surface. Strain elements were then calculated as the derivatives of these displacements with respect to the spacing between the vectors.
- **Virtual Extensometer:** The calculated strains were finally used to calculate the overall longitudinal strain experienced by the sample by using the virtual extensometer feature in the software. These values were exported into a data processing software.
- **CTE Calculation:** Using the reported strain values and the temperature readings recorded by the second camera, the CTE was calculated using equation 4.3.

$$\alpha_{yy-exp} = \frac{1}{\Delta T} \times \frac{\Delta L}{L} \tag{4.3}$$

where α_{yy-exp} is the experimental longitudinal coefficient of thermal expansion, ΔT is the change in temperature and $\frac{\Delta L}{L}$ is the strain collected from the image processing software.

4.4.2 Predictive model for CTE of 2D TBCs

This section highlights the theoretical derivation and prediction of CTE of 2D TBCs based on classical laminate plate theory (CLPT). This theory expands on the previous work of Carey et al., which is a generalization of the theory developed by Raju and Wang for woven composites[8]. In CLPT, yarns of the textile composite are modelled as unidirectional lamina with fibres oriented in the yarn directions. The interactions of the differently oriented yarns within the unit cell are then aggregated into a laminate approximation, for which a theoretical understanding has been thoroughly developed. This approximation allows the calculation of the effective elastic, thermal and hygral properties of the textile unit cell.

The general assumptions that underline the theoretical derivation for laminate equations can be found in Agarwal et al. These assumptions are summarized here for clarity:

- Each lamina is considered to be homogenous, with uniform properties throughout.
- A plane-stress state is assumed for the constitutive stress-strain equations of the lamina.
- Lamina are assumed to be transversely isotropic.
- Bonds between the laminae in the laminate are perfect with no slip.
- Laminate deformations follow the Kirchhoff-Love assumption for thin plate deformations, namely that the normal plane to the midplane of the laminate remains normal throughout deformation.

Further assumptions are needed for modelling the behaviour of 2D TBCs using CLPT, and these can be summarized as follows:

- Yarn cross section is assumed to be rectangular throughout the path of the yarn. The cross-sectional area is defined by the yarn width, W_y and yarn thickness, h_c.
- Volume fractions of the yarns (and in extension the unidirectional lamina) are assumed to be 0.6 for this work.

4.4.2.1 Geometrical Description of TBC Unit Cell

Figure 4.14 shows a schematic representation of the unit the unit cell of a TBC. This unit cell consists of three different types of regions, a yarns-only region (in yellow), a matrix-only region

(in orange) and a fibre-overlap or undulation region (in red). Each of the regions have the same total thickness (which is the thickness of the unit cell).

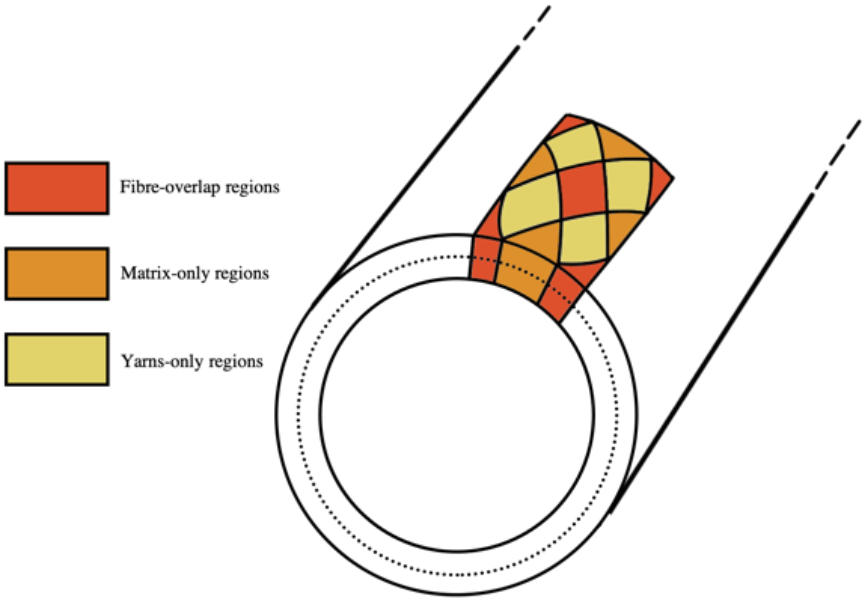

Figure 4.14. Schematic highlighting a single unit cell on the outer surface of a TBC. Yarns-only regions are shown in yellow, matrix-only regions are shown in orange and undulation regions are shown in red.

For the theoretical derivation of the CTE of 2D TBCs, this unit cell is modelled as flat, following the work of Carey et al.47,[9]. Figure 4.15 shows a representative schematic of the flat braid unit cell with all included regions.

To describe the unit cell, several geometrical parameters need to be defined. These are summarized as follows:

- Two-dimensional axes originate from the bottom left corner of the unit cell.
- The unit cell is defined by the total length (X) and total width of the unit cell (Y). These also allow for the definition of the braid angle (θ) as the angle between the yarns and the longitudinal axis of the braid and the complimentary braid angle (γ). The thickness of the unit cell (t) is constant throughout the unit cell.

- Each unit cell can be divided into 13 regions (labelled R1-R13 in Figure 4.15). These can be further sub-divided into fibre-overlap regions (R1-R5), matrix-only regions (R6-R9) and fibre-only regions (R10-R13).
- The 13 regions of the unit cell are defined by the lines L1-L10 in Figure 4.15. For the flat braid model, unit cell symmetry is assumed along the line $x = 0.5X$. This implies that L1, L2, L3, L8 and L10 are parallel to each other. Further, L5, L6, L7, L4 and L9 are also parallel to each other.
- The lengths of L4, L8, L9 and L10 are the same and equal to the effective length, L_e, which is a geometrical function of the yarn width, W_y. The two parameters can be related by equation 4.4.

$$L_e = \frac{W_y}{\cos\left(\frac{\pi}{2} - 2\theta\right)} \tag{4.4}$$

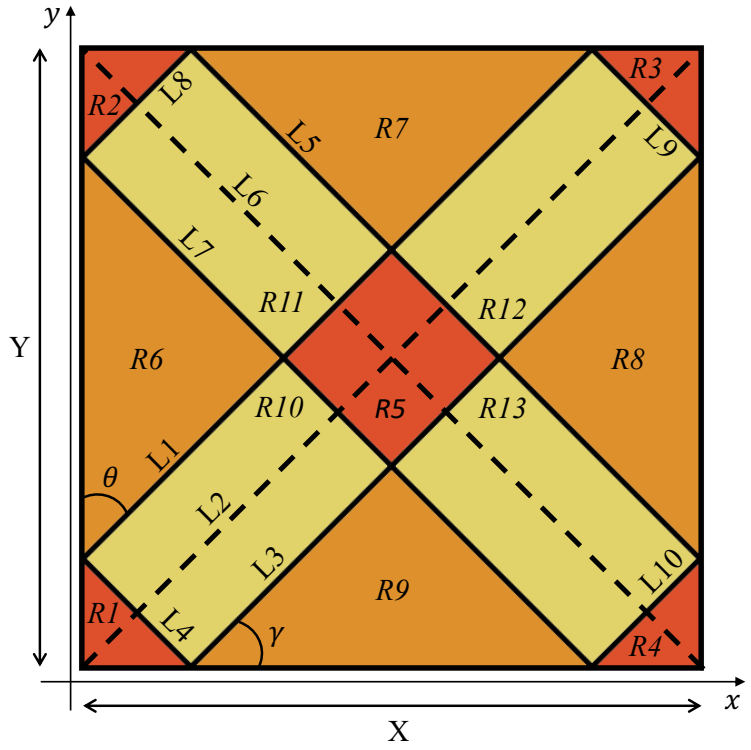

Figure 4.15. Schematic of the flat braid unit cell used in this study. Lines of the unit cell are labelled as L1-L10. Regions of the unit cells are labelled as R1-R13. Red regions (R1-R5) indicate the fibre-

overlap regions, orange regions (R6-R9) indicate matrix-only regions and yellow regions (R10-R13) indicate yarn-only regions.

Lines L1-L13 are described as functions of the overall dimensions of the unit cell as well as the braid angle, complimentary braid angle and the effective length. Table 4.3 summaries the equations of the lines.

TABLE 4.3: EQUATIONS OF LINES DEFINING THE FLAT BRAID UNIT CELL MODEL USED IN THIS WORK

Line #	Equation
L1	$y_1 = x\tan(\gamma) + L_e\sin(\gamma)$
L2	$y_2 = x\tan(\gamma)$
L3	$y_3 = x\tan(\gamma) - L_e\sin(\gamma)$
L4	$y_4 = -x\tan(\gamma) + L_e\sin(\gamma)$
L5	$y_5 = -x\tan(\gamma) + Y + L_e\sin(\gamma)$
L6	$y_6 = -x\tan(\gamma) + Y$
L7	$y_7 = -x\tan(\gamma) + Y - L_e\sin(\gamma)$
L8	$y_8 = x\tan(\gamma) + Y - L_e\sin(\gamma)$
L9	$y_9 = -x\tan(\gamma) + 2Y - L_e\sin(\gamma)$
L10	$y_{10} = x\tan(\gamma) - Y + L_e\sin(\gamma)$

Figure 4.16 shows a sectional view of the undulating regions (R10-R13) of the unit cell. These regions are defined as follows for this work:

- The fibre orientation is assumed to be inclined to the yarn centreline by an angle β. The front rectangular surface is assumed to be perpendicular to the braid centreline path. This is demonstrated in Figure 4.17.
- The projected undulation length of the yarns (a_u) is measured with respect to the y-axis.
- The thickness of the matrix layer (t_m) in the yarn-only regions (R10-R13) is given by the difference between the total unit cell thickness (t) and the thickness of the yarn (h_c).
- The thickness of the matrix layer (t_m) in the overlap regions (R1-R5) is given by the difference between the total unit cell thickness (t) and two yarns ($2h_c$).

- The undulation path ($h(d)$) is a function of the variable d which is the length along the undulating yarn. This path is assumed to follow a cosine function given by equation (4.5).

$$h(d) = \frac{h_c}{2}\left(1 \pm \cos\left(\frac{\pi d}{a_u}\right)\right) \qquad 0 < d \leq a_u \qquad (4.5)$$

- The undulation path can then be used to mathematically define the fibre orientation angle β using equation (4.6).

$$\tan\beta = \frac{dh(d)}{dd} = \mp\frac{h_c\pi}{2a_u}\sin\left(\frac{\pi d}{a_u}\right) \qquad (4.6)$$

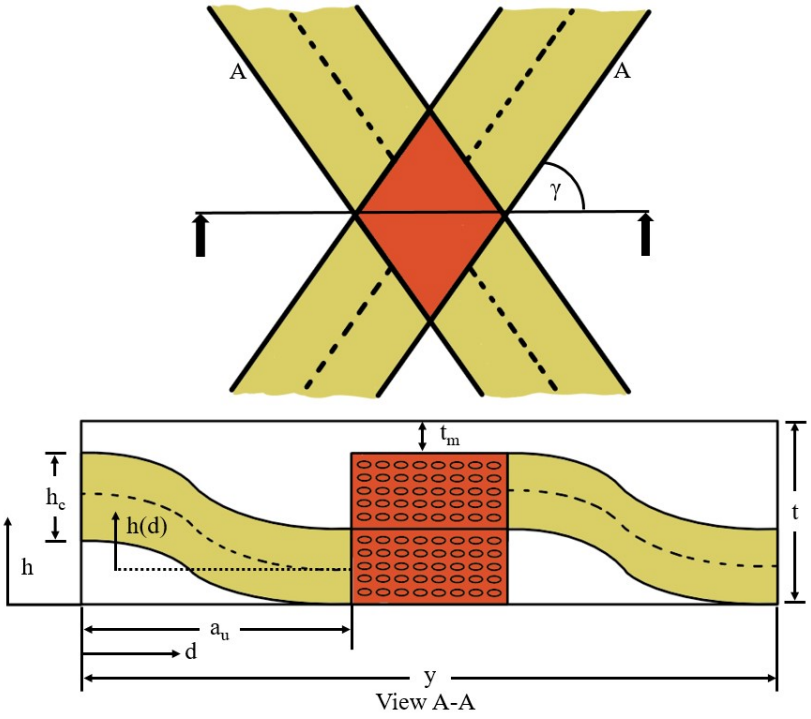

Figure 4.16. Sectional schematic view of the undulating regions, showing the overall dimensions of the unit cell as well as the trajectory path $h(d)$ of the yarns as adapted from Carey et al[47].

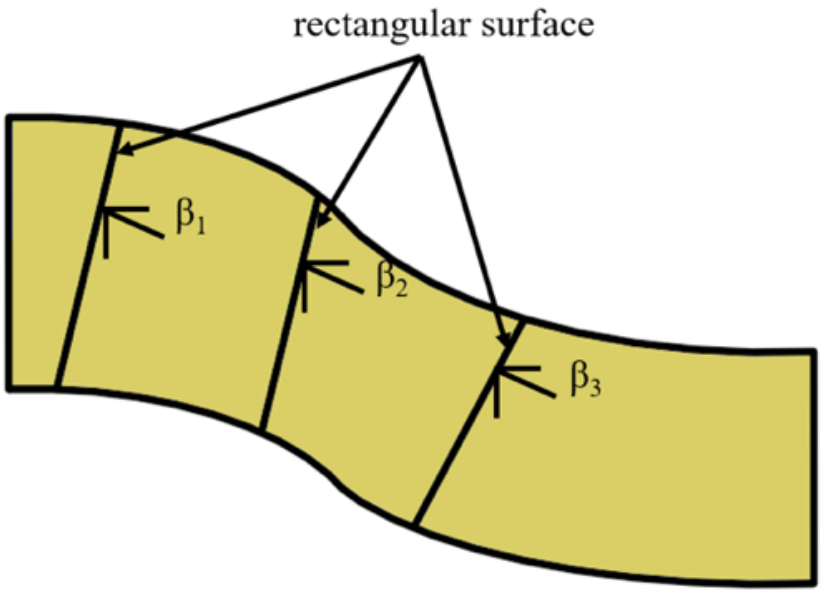

Figure 4.17. Close up schematic of the undulation path of the yarns in the TBC unit cell defined by the angle β between the rectangular surface and the y-axis as replicated from Carey et al.[47]

4.4.2.2 Mechanical Modelling of TBC Properties

In this model, each region is considered to be a laminate consisting of different types of lamina. This is also highlighted in Figure 4.16. Fibre-overlap regions (R1-R5) consist of two angle-ply lamina and one matrix-only lamina. Matrix-only regions (R6-R9) consist of a single matrix-only layer. Finally, the undulation regions (R10-R13) consist of one undulating angle-ply lamina and one matrix-only lamina.

To calculate the properties of these different lamina from the properties of the selected fibres and matrix, different micromechanical models are used. For the calculation of the longitudinal modulus E_1 and the major Poisson's ratio v_{12}, the rectangular block model in Figure 4.18 was used with the assumption of iso-strain.

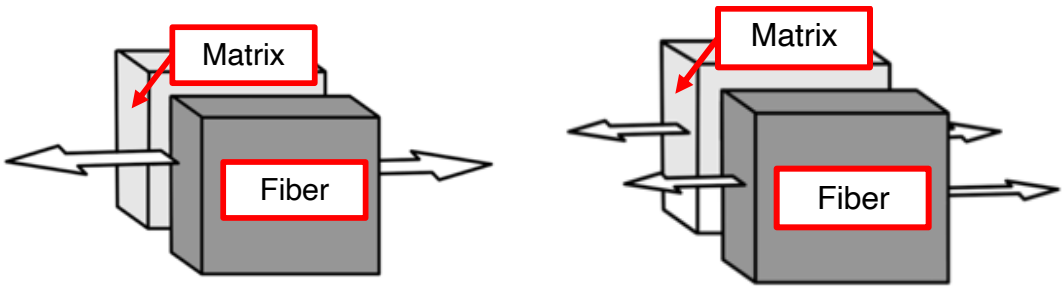

(a) (b)

Figure 4.18. Schematic showing the method for deriving the longitudinal properties in the RBM. Here, (a) a load is applied to the composite along the fibre direction and (b) the load is "split" between the fibre and the matrix.

To calculate the transverse modulus E_2 and the in-plane shear modulus G_{12}, the semi-empirical formulae of Halpin-Tsai were used. These formulae are shown in equations 4.9-4.12. The Halpin-Tsai equations are simplified approximations of Hill's generalized self-consistent composite cylinder model. In this model the composite is assumed to be equivalent to a square arrangement of perfectly aligned cylindrical fibres[173].

To calculate the out-of-plane shear modulus G_{23} and the out-of-plane Poisson's ratio v_{23} the empirical formulae of Ko et al. were used. These are presented in equations 4.13 and 4.14.

Lastly, the Schapery energy-based model was used to calculate the longitudinal CTE of the composite due to its excellent agreement with literature[78]. The transverse modulus was calculated using the Tsai-Hahn formula[153]. These are shown in equations 4.15 and 4.16.

$$E_1 = E_{1f}V_f + E_mV_m \tag{4.7}$$

$$v_{12} = v_fV_f + v_mV_m \tag{4.8}$$

$$E_2 = \frac{1 + \eta_E V_f}{1 - \eta_E V_f} E_m \tag{4.9}$$

$$\eta_E = \frac{\left(\frac{E_{2f}}{E_m}\right) - 1}{\left(\frac{E_{2f}}{E_m}\right) + 1} \tag{4.10}$$

$$G_{12} = \frac{1 + \eta_G V_f}{1 - \eta_G V_f} G_m \tag{4.11}$$

$$\eta_G = \frac{\left(\frac{G_f}{G_m}\right) - 1}{\left(\frac{G_f}{G_m}\right) + 1} \tag{4.12}$$

$$G_{23} = \frac{G_m}{(1 - V_f^{0.5}\left(\frac{G_m}{G_{f23}}\right))} \tag{4.13}$$

$$v_{23} = V_f v_{f23} + V_m(2v_m - v_{21}) \tag{4.14}$$

$$\alpha_1 = \frac{1}{E_1}(\alpha_{1f} E_f V_f + \alpha_m E_m V_m) \tag{4.15}$$

$$\alpha_2 = \left(1 + v_f\right)\alpha_{2f} V_f + (1 + v_m)\alpha_m V_m - \alpha_1 v_{12} \tag{4.16}$$

where E is the elastic modulus, V is the volume fraction, v is the Poisson's ratio, G is the shear modulus, η is an empirical constant, α is the CTE. Subscripts f, m refer to fibre and matrix respectively, subscripts E and G refer to young and shear modulus respectively and subscripts 1 and 2 refer to the local principal directions of the lamina.

The elastic and thermal properties in equations 4.7-4.16 are used to calculate the local stiffness matrices of the laminae. Once calculated, these properties are then transformed from the local 1-2 coordinate system of the lamina to the global $x - y$ coordinate system of the braided composite. Due to the assumed isotropic nature of the matrix, the local and global stiffness and thermal coefficient matrices for the matrix-only regions are identical. Equations 4.17-4.23 show these steps for regions R1-R9.

$$[\bar{Q}_\theta] = [T_\theta]^{-1}[Q_\theta][R][T_\theta][R]^{-1} \tag{4.17}$$

$$[\bar{\alpha}_\theta] = [R][T_\theta]^{-1}\begin{bmatrix}\alpha_1\\ \alpha_2\\ 0\end{bmatrix} \tag{4.18}$$

$$[Q_\theta] = \begin{bmatrix}\dfrac{E_1}{1-v_{12}v_{21}} & \dfrac{v_{12}E_2}{1-v_{12}v_{21}} & 0\\ \dfrac{v_{12}E_2}{1-v_{12}v_{21}} & \dfrac{E_2}{1-v_{12}v_{21}} & 0\\ 0 & 0 & G_{12}\end{bmatrix} \tag{4.19}$$

$$[T_\theta] = \begin{bmatrix}c^2 & s^2 & 2sc\\ s^2 & c^2 & -2sc\\ -sc & sc & c^2-s^2\end{bmatrix} \tag{4.20}$$

$$[R] = \begin{bmatrix}1 & 0 & 0\\ 0 & 1 & 0\\ 0 & 0 & 2\end{bmatrix} \tag{4.21}$$

$$[\bar{Q}_m] = [Q_m] = \begin{bmatrix}\dfrac{E_m}{1-v_m^2} & \dfrac{v_m E_m}{1-v_m^2} & 0\\ \dfrac{v_m E_m}{1-v_m^2} & \dfrac{E_m}{1-v_m^2} & 0\\ 0 & 0 & G_m\end{bmatrix} \tag{4.22}$$

$$[\bar{\alpha}_m] = \begin{bmatrix}\alpha_m\\ \alpha_m\\ 0\end{bmatrix} \tag{4.23}$$

where $[\bar{Q}_\theta]$is the 3×3 global stiffness matrix of the angle-ply lamina, $[T_\theta]$ is the transformation matrix for the angle-ply lamina, $[Q_\theta]$ is the 3×3 local stiffness matrix of the angle-ply lamina, $[R]$ is the Reuter's matrix, $[\bar{\alpha}_\theta]$ is the 3×1 global thermal coefficient matrix for the angle-ply lamina, c and s are the cosine and sine of the braid angle θ, $[\bar{\alpha}_m]$ is 3×1 global thermal coefficient matrix for the matrix-only lamina and $[\bar{Q}_m]$ and $[Q_m]$ refer to the 3×3 global and 3×3 local stiffness matrices of the matrix only lamina.

For the fibre-undulation regions (R10-R13), the global stiffness and thermal matrices must also account for the undulation of the fibre. Equations 4.24-4.31 show the formulae for these regions as adapted from Ishikawa and Chou[174,175].

$$[\bar{Q}_u(\beta)] = [T_\theta]^{-1}[Q_u(\beta)][R][T_\theta][R]^{-1} \quad (4.24)$$

$$[Q_u(\beta)] = \begin{bmatrix} \frac{E_x(\beta)}{D_v} & \frac{E_y(\beta)v_{21}(\beta)}{D_v} & 0 \\ \frac{E_y(\beta)v_{21}(\beta)}{D_v} & \frac{E_y(\beta)}{D_v} & 0 \\ 0 & 0 & G_{xy}(\beta) \end{bmatrix} \quad (4.25)$$

$$E_x(\beta) = \frac{1}{\frac{\cos^4\beta}{E_1} + \left(\frac{1}{G_{13}} - \frac{2v_{31}}{E_1}\right)\cos^2\beta\sin^2\beta + \frac{\sin^4\beta}{E_3}} \quad (4.26)$$

$$v_{21}(\beta) = E_x(\beta)[\frac{v_{31}\cos^2\beta}{E_1} + \frac{v_{23}\sin^2\beta}{E_3}] \quad (4.27)$$

$$G_{12}(\beta) = \left[\frac{\cos^2\beta}{G_{12}} + \frac{\sin^2\beta}{G_{23}}\right]^{-1} \quad (4.28)$$

$$E_y(\beta) = E_2 = E_3 \quad (4.29)$$

$$D_v = 1 - \frac{\left(v_{21}(\beta)\right)^2 E_{22}}{E_x(\beta)} \quad (4.30)$$

$$[\bar{\alpha}_u(\beta)] = [R][T_\theta]^{-1}\begin{bmatrix} \cos^2\beta\,\alpha_1 + \sin^2\beta\,\alpha_2 \\ \alpha_2 \\ 0 \end{bmatrix} \quad (4.31)$$

4.4.2.3 Modelling of TBC Properties

The basis of this model is CLPT, highlighted in equation (4.32). This relates the forces N and moments N experienced by the entire laminate to the midplane strains $\tilde{\varepsilon}^o$ and curvatures $\tilde{\kappa}^o$.

$$\begin{Bmatrix} N \\ M \end{Bmatrix} = \begin{bmatrix} A & B \\ B & D \end{bmatrix}\begin{Bmatrix} \tilde{\varepsilon}^o \\ \tilde{\kappa}^o \end{Bmatrix} - \begin{Bmatrix} N \\ M \end{Bmatrix}^{\Delta T} \quad (4.32)$$

where A is the extensional matrix of the laminate, B is the coupling matrix of the laminate, D is the bending matrix of the laminate. Superscript ΔT refers to temperature induced forces and moments.

To derive the expressions for the longitudinal CTE of the composite, the total strains $\tilde{\varepsilon}_k^{total}$ in each lamina k may be expressed as a combination of the mechanical $\tilde{\varepsilon}_k^{M}$ and thermal strains $\tilde{\varepsilon}_k^{\Delta T}$ as:

$$\tilde{\varepsilon}_k^{total} = \tilde{\varepsilon}_k^{M} + \tilde{\varepsilon}_k^{\Delta T} \qquad (4.33)$$

Rearranging for the mechanical strain in the layer and calculating stress by multiplying by the global stiffness matrix for each layer results in:

$$\tilde{\sigma}_k = [\bar{Q}]_k \tilde{\varepsilon}_k^{M} = [\bar{Q}]_k \tilde{\varepsilon}_k^{total} - [\bar{Q}]_k \tilde{\varepsilon}_k^{\Delta T} \qquad (4.34)$$

Integrating by dz over the entire laminate consisting of n layers of laminae results in the following integral form of equation (4.34):

$$\sum_{k=1}^{n} \int_{h_{k-1}}^{h_k} \tilde{\sigma}_k \, dz = \sum_{k=1}^{n} \int_{h_{k-1}}^{h_k} [\bar{Q}]_k \tilde{\varepsilon}_k^{total} dz - \sum_{k=1}^{n} \int_{h_{k-1}}^{h_k} [\bar{Q}]_k \tilde{\varepsilon}_k^{\Delta T} dz \qquad (4.35)$$

where h_k and h_{k-1} are the thickness coordinates of the lamina.

The LHS of equation (4.35) represents the total external forces by the laminate, namely N from equation (4.32). When measuring the CTE of a laminate, no external forces are applied, resulting in a zero value for the 3x1 N matrix. This allows equation (4.35) to be written as:

$$\sum_{k=1}^{n} \int_{h_{k-1}}^{h_k} [\bar{Q}]_k \tilde{\varepsilon}_k^{total} dz = \sum_{k=1}^{n} \int_{h_{k-1}}^{h_k} [\bar{Q}]_k \tilde{\varepsilon}_k^{\Delta T} dz \qquad (4.36)$$

The total strain in each layer can be written as the sum of the midplane strains ε^o and the curvatures κ^o. The thermal strains may be written as the multiplication of the change in temperature and the global CTE $[\bar{\alpha}]$ for each lamina expanding equation (4.36) into:

$$\sum_{k=1}^{n}\int_{h_{k-1}}^{h_k}[\bar{Q}]_k(\tilde{\varepsilon}^o + z_k\tilde{\kappa}^o)dz = \sum_{k=1}^{n}\int_{h_{k-1}}^{h_k}[\bar{Q}]_k\Delta T[\bar{\alpha}]_k dz \qquad (4.37)$$

From fundamental definitions of CLPT, each of the terms in equation (4.37) represents a variable from the previous equation (4.32). Accordingly, equation (4.37) may be partly written as:

$$[A \quad B]\begin{Bmatrix}\tilde{\varepsilon}^o \\ \tilde{\kappa}^o\end{Bmatrix} = \{N\}^{\Delta T} \qquad (4.38)$$

Alternatively integrating equation (4.35) by $z\,dz$ over the entire laminate consisting of n layers of laminae results in the following:

$$\sum_{k=1}^{n}\int_{h_{k-1}}^{h_k}[\bar{Q}]_k(\tilde{\varepsilon}^o + z_k\tilde{\kappa}^o)\,zdz = \sum_{k=1}^{n}\int_{h_{k-1}}^{h_k}\Delta T[\bar{Q}]_k[\bar{\alpha}]_k z\,dz \qquad (4.39)$$

$$[B \quad D]\begin{Bmatrix}\tilde{\varepsilon}^o \\ \tilde{\kappa}^o\end{Bmatrix} = \{M\}^{\Delta T} \qquad (4.40)$$

Combining equations (4.38) and (4.40) results in the following form of the CLPT equation:

$$\begin{bmatrix}A & B \\ B & D\end{bmatrix}\begin{Bmatrix}\tilde{\varepsilon}^o \\ \tilde{\kappa}^o\end{Bmatrix} = \begin{Bmatrix}N \\ M\end{Bmatrix}^{\Delta T} \qquad (4.41)$$

Although the previous developed equation is suitable for calculations pertaining to a laminate comprised of lamina of the same area, Raju and Wang expanded this equation to account for a composite assembly of different laminate regions with different areas. A similar approach was followed in this work in which the CLPT equation was modified to:

$$\begin{bmatrix}[A]^* & [B]^* \\ [B]^* & [D]^*\end{bmatrix}\begin{Bmatrix}\tilde{\varepsilon}^o \\ \tilde{\kappa}^o\end{Bmatrix} = \begin{Bmatrix}[N]^* \\ [M]^*\end{Bmatrix}^{\Delta T} \qquad (4.42)$$

Here, the 3x3 matrices $[A]^*$, $[B]^*$ and $[D]^*$ on the LHS of equation (4.42) are defined as the area-weighted sums of the stiffness, coupling and bending matrices of the regions of the unit cell as:

$$[A]^* = \frac{1}{P_A}\sum_{k=1}^{13}A_k \qquad (4.43)$$

$$[B]^* = \frac{1}{P_A}\sum_{k=1}^{13} B_k \qquad (4.44)$$

$$[D]^* = \frac{1}{P_A}\sum_{k=1}^{13} D_k \qquad (4.45)$$

where P_A is the projected area of the unit cell at the midplane.

Equations 4.43-4.45 sum the influence for each of the 13 regions of the unit cell to calculate the stiffness, coupling and bending matrices for the entire unit cell which is then divided by the projected area P_A of the midplane of the unit cell. For each region k, the different matrices A_k, B_k and D_k are calculated as:

$$A_k = \left[\int_x \int_y \left(\int_z [\bar{Q}_k]\, dz\right) dy\, dx\right]_k \qquad (4.46)$$

$$B_k = \left[\int_x \int_y \left(\int_z [\bar{Q}_k]\, z\, dz\right) dy\, dx\right]_k \qquad (4.47)$$

$$D_k = \left[\int_x \int_y \left(\int_z [\bar{Q}_k]\, z^2\, dz\right) dy\, dx\right]_k \qquad (4.48)$$

Further details on the calculation of these terms for the different regions can be found in the work of Carey et al.[8]. For the RHS of equation (4.42), the terms $[N]^{*\Delta T}$ and $[M]^*$ may be written as:

$$[N]^{*\Delta T} = \frac{1}{P_A}\sum_{k=1}^{13} [N]_k^{\Delta T} \qquad (4.49)$$

$$[M]^{*\Delta T} = \frac{1}{P_A}\sum_{k=1}^{13} [M]_k^{\Delta T} \qquad (4.50)$$

Again, equations 4.49 and 4.50 sum the thermal influence for each of the 13 regions of the unit cell to calculate the fictitious forces and moments created by thermal stresses for the entire unit

cell. An area-weighted approach over the projected area P_A is once again used. For each region k, the fictitious thermal forces $[N]_k^{\Delta T}$ and thermal moments $[M]_k^{\Delta T}$ are calculated as:

$$[N]_k^{\Delta T} = \Delta T \times \left[\int_x \int_y \left(\int_z [\bar{Q}_k]\,[\bar{\alpha}_k]\,dz \right) dy\,dx \right]_k \tag{4.51}$$

$$[M]_k^{\Delta T} = \Delta T \times \left[\int_x \int_y \left(\int_z [\bar{Q}_k]\,[\bar{\alpha}_k]\,z\,dz \right) dy\,dx \right]_k \tag{4.52}$$

4.4.2.4 Sample calculations for different regions

Fibre-Overlap Regions (R1-R5)

Each of the five fibre-overlap regions can be idealized as a laminate consisting of a negative angle-ply lamina, a positive angle-ply lamina and a matrix layer. The thickness of the angle-plies is equal to the impregnated yarn thickness h_c. For each of these regions, equations 4.43-4.52 can be applied to calculate the A_k, B_k, D_k, $[N]_k^{\Delta T=1}$ and $[M]_k^{\Delta T=1}$ matrices for k=1 to 5. As an example, the calculations for R1 are presented in this sub-section. Figure 4.19 shows a schematic of the magnified region within the unit cell presented earlier in figure 4.15.

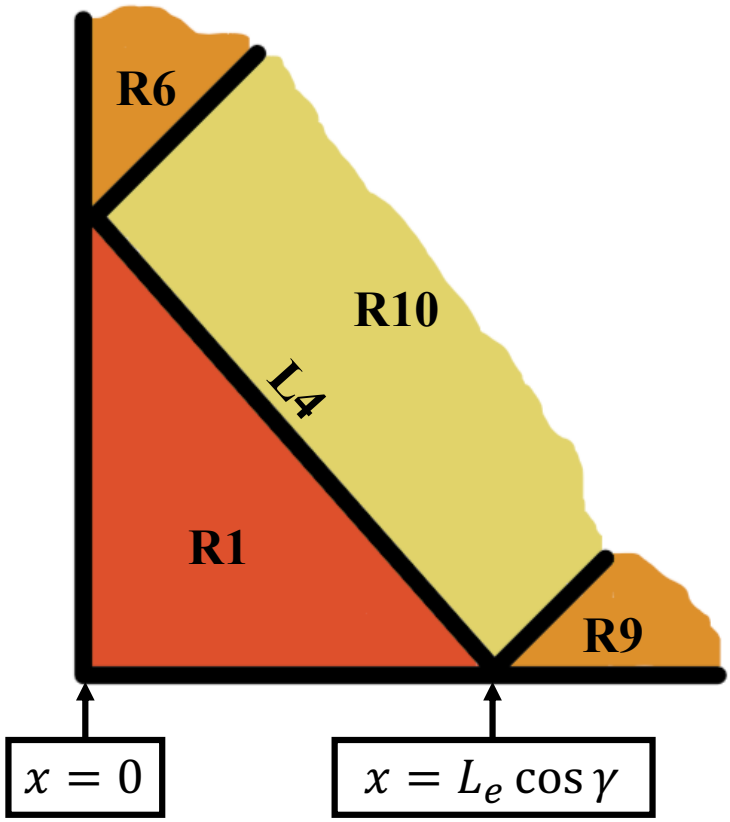

Figure 4.19. Schematic of R1 highlighting the defining lines and adjacent regions.

For R1, the region is defined in the x-direction by $x = 0$ as a lower bound and $x = L_e \cos\gamma$ as an upper bound. In the y-direction, R1 is defined by $y = 0$ and L4, where $y = -x\tan(\gamma) + L_e \sin(\gamma)$. Accordingly, A_1, B_1 and D_1 may be written as:

$$A_1 = \left[\int_0^{L_e\cos\gamma} \int_0^{-x\tan(\gamma)+L_e\sin(\gamma)} \left(\int_z [\bar{Q}_1]\, dz\right) dy\, dx\right]_{k=1} \tag{4.53}$$

$$B_1 = \left[\int_0^{L_e\cos\gamma} \int_0^{-x\tan(\gamma)+L_e\sin(\gamma)} \left(\int_z [\bar{Q}_1]\, z\, dz\right) dy\, dx\right]_{k=1} \tag{4.54}$$

$$D_1 = \left[\int_0^{L_e\cos\gamma} \int_0^{-x\tan(\gamma)+L_e\sin(\gamma)} \left(\int_z [\bar{Q}_1]\, z^2 dz\right) dy\, dx\right]_{k=1} \tag{4.55}$$

The integral of the stiffness matrix $[\bar{Q}_1]$ over the z is independent of the x and y directions, allowing the integral for A_1 for example to be changed into:

$$A_1 = \int_z [\bar{Q}_1]\, dz \int_0^{L_e \cos\gamma} \int_0^{-x\tan(\gamma)+L_e\sin(\gamma)} dy\, dx \qquad (4.56)$$

The integrals of R1 over the x and y direction simple result in the area of the region, a_{xy-1}, allowing equation 4.56 to be rewritten as:

$$A_1 = a_{xy-1} \int_z [\bar{Q}_1]\, dz \qquad (4.57)$$

$$\text{where } a_{xy-1} = -\frac{L_e \cos^2\gamma \tan\gamma}{2} + L_e^2 \cos\theta \cos\gamma \qquad (4.58)$$

For the integral term in equation 4.57, this is divided into three integrals over each of the lamina in R1. The laminate z-axis originates from the centre of the laminate with positive upwards. This results in the following:

$$\int_z [\bar{Q}_1]\, dz = \int_{-\frac{t_m}{2}}^{-\frac{t_m}{2}+h_c} [\bar{Q}_\theta]\, dz + \int_{-\frac{t_m}{2}-h_c}^{-\frac{t_m}{2}} [\bar{Q}_{-\theta}]\, dz + \int_{-\frac{t_m}{2}+h_c}^{\frac{t_m}{2}+h_c} [\bar{Q}_m]\, dz \qquad (4.59)$$

Similar steps are followed for each of B_1 and D_1, but are not included here for brevity. The final answers for the integrals are:

$$A_1 = a_{xy-1} \times (([\bar{Q}_\theta] + [\bar{Q}_{-\theta}]) * h_c + [\bar{Q}_m] * t_m) \qquad (4.60)$$

$$\begin{aligned} B_1 = \frac{1}{2} a_{xy-1} \times ([\bar{Q}_\theta] \times & \left(-\left(-\frac{t_m}{2}\right)^2 + \left(h_c - \frac{t_m}{2}\right)^2 \right) \\ & + [\bar{Q}_{-\theta}] \times \left(\left(-\frac{t_m}{2}\right)^2 - \left(-h_c - \frac{t_m}{2}\right)^2 \right) * h_c \\ & + [\bar{Q}_m] \times \left(\left(h_c - \frac{t_m}{2}\right)^2 - \left(h_c - \frac{t_m}{2}\right)^2 \right)) \end{aligned} \qquad (4.61)$$

$$D_1 = \frac{1}{3} a_{xy-1} \times ([\bar{Q}_\theta] \times \left(-\left(-\frac{t_m}{2} \right)^3 + \left(h_c - \frac{t_m}{2} \right)^3 \right) + [\bar{Q}_{-\theta}] \times \left(\left(-\frac{t_m}{2} \right)^3 - \left(-h_c - \frac{t_m}{2} \right)^3 \right) * h_c + [\bar{Q}_m] \times \left(\left(h_c - \frac{t_m}{2} \right)^3 - \left(h_c - \frac{t_m}{2} \right)^3 \right)) \quad (4.62)$$

For the fictitious thermal loads $[N]_1^{\Delta T=1}$ and thermal moments $[M]_1^{\Delta T=1}$ for R1, equations 4.51 and 4.52 are applied with the previously stated x-axis and y-axis bounds. This results in an integral of the following form:

$$[N]_1^{\Delta T=1} = \left[\int_0^{L_e \cos\gamma} \int_0^{-x \tan(\gamma) + L_e \sin(\gamma)} \left(\int_z [\bar{Q}_1] \, [\bar{\alpha}_1] dz \right) dy \, dx \right]_{k=1} \quad (4.63)$$

$$[M]_1^{\Delta T=1} = \left[\int_0^{L_e \cos\gamma} \int_0^{-x \tan(\gamma) + L_e \sin(\gamma)} \left(\int_z [\bar{Q}_1] \, [\bar{\alpha}_1] \, z \, dz \right) dy \, dx \right]_{k=1} \quad (4.64)$$

Applying the same steps used for the calculations of A_1, B_1 and D_1 allows us to rewrite the previous equations as:

$$[N]_1^{\Delta T=1} = a_{xy-1} \int_z [\bar{Q}_1] \, [\bar{\alpha}_1] \, dz \quad (4.65)$$

$$[M]_1^{\Delta T=1} = a_{xy-1} \int_z [\bar{Q}_1] \, [\bar{\alpha}_1] \, z \, dz \quad (4.66)$$

The integrals on the RHS of equations 4.65 and 4.66 can be split into an integral over the positive angle-ply, the negative angle-ply and the matrix-only ply to give:

$$\int_z [\bar{Q}_1][\bar{\alpha}_1] \, dz = \int_{-\frac{t_m}{2}}^{-\frac{t_m}{2}+h_c} [\bar{Q}_\theta] \, [\bar{\alpha}_\theta] \, dz + \int_{-\frac{t_m}{2}-h_c}^{-\frac{t_m}{2}} [\bar{Q}_{-\theta}][\bar{\alpha}_{-\theta}] \, dz + \int_{-\frac{t_m}{2}+h_c}^{\frac{t_m}{2}+h_c} [\bar{Q}_m] \, [\bar{\alpha}_m] \, dz \quad (4.67)$$

$$\int_z [\bar{Q}_1][\bar{\alpha}_1]\, z\, dz$$

$$= \frac{1}{2} \times \left(\int_{-\frac{t_m}{2}}^{-\frac{t_m}{2}+h_c} [\bar{Q}_\theta]\, [\bar{\alpha}_\theta]\, z\, dz + \int_{-\frac{t_m}{2}-h_c}^{-\frac{t_m}{2}} [\bar{Q}_{-\theta}][\bar{\alpha}_{-\theta}]\, z\, dz \right. \tag{4.68}$$

$$\left. + \int_{-\frac{t_m}{2}+h_c}^{\frac{t_m}{2}+h_c} [\bar{Q}_m]\, [\bar{\alpha}_m]\, z\, dz \right)$$

Matrix-Only Regions (R6-R9)

Each of the four matrix-only regions can be idealized as a laminate consisting of a single matrix layer of thickness t. This simplifies the equations considerably. For each of the matrix-only regions, equations 4.43-4.52 can be applied with k=6 to k=9 to calculate the A_k, B_k, D_k, $[N]_k^{\Delta T=1}$ and $[M]_k^{\Delta T=1}$ matrices. As an example, the calculations for R6 are presented in this sub-section. Figure 4.20 shows a schematic of the magnified region within the unit cell presented earlier in Figure 4.15.

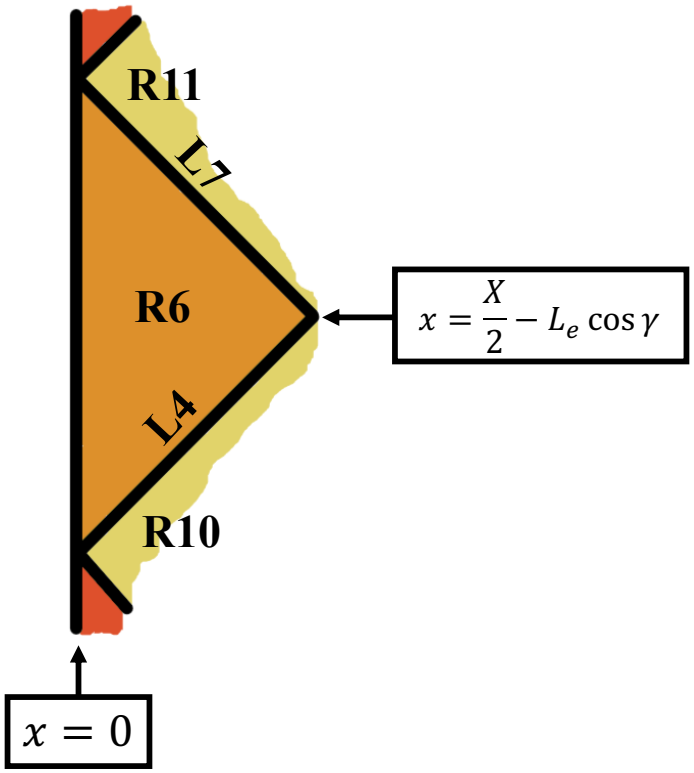

Figure 4.20. Schematic of R6 highlighting the defining lines and adjacent regions.

For R6, the region is defined in the x-direction by $x = 0$ as a lower bound and $x = \frac{X}{2} - L_e \cos\gamma$ as an upper bound. In the y-direction, R6 is defined by the difference between two lines, namely L7 and L4. Hence the bounds become $y = x\tan(\gamma) + L_e \sin(\gamma)$ and $y = -x\,tan(\gamma) + L_e\,sin(\gamma)$. Accordingly, A_6, B_6 and D_6 may be written as:

$$A_6 = \left[\int_0^{\frac{X}{2}-L_e\cos\gamma} \int_{x\tan(\gamma)+L_e\sin(\gamma)}^{-x\tan(\gamma)+Y-L_e\sin(\gamma)} \left(\int_z [\bar{Q}_6]\,dz\right) dy\,dx\right]_{k=6} \tag{4.69}$$

$$B_6 = \left[\int_0^{\frac{X}{2}-L_e\cos\gamma} \int_{x\tan(\gamma)+L_e\sin(\gamma)}^{-x\tan(\gamma)+Y-L_e\sin(\gamma)} \left(\int_z [\bar{Q}_6]\,z\,dz\right) dy\,dx\right]_{k=6} \tag{4.70}$$

$$D_6 = \left[\int_0^{\frac{X}{2} - L_e \cos\gamma} \int_{x\tan(\gamma) + L_e \sin(\gamma)}^{-x\tan(\gamma) + Y - L_e \sin(\gamma)} \left(\int_z [\bar{Q}_6]\, z^2 dz \right) dy\, dx \right]_{k=6} \tag{4.71}$$

Similar to the previous simplifications conducted on the fibre-overlap regions, the integrals over the x-direction and y-directions give the area of the region. The A_6 matrix can therefore be written as:

$$A_6 = a_{xy-6} \int_z [\bar{Q}_6]\, dz \tag{4.72}$$

$$\text{where } a_{xy-6} = -\frac{X^2 L_e \cos^2\gamma \tan\gamma}{4} + (Y - 2L_e \sin\gamma)\left(\frac{X}{2} L_e \cos\gamma\right) \tag{4.73}$$

The integral on the RHS of equation (4.72) can be simply replaced with an integral over the stiffness of the matrix layer:

$$\int_z [\bar{Q}_6]\, dz = \int_{-\frac{t_m}{2} - h_c}^{\frac{t_m}{2} + h_c} [\bar{Q}_m]\, dz \tag{4.74}$$

Similar steps are followed for the B_6 and D_6, but are not included here. The final results for the three matrices of R6 are:

$$A_6 = a_{xy-6} \times ([\bar{Q}_m] * (2h_c + t_m)) \tag{4.75}$$

$$B_6 = \frac{1}{2} a_{xy-6} \times ([\bar{Q}_m] \times \left(\left(h_c + \frac{t_m}{2} \right)^2 - \left(-h_c - \frac{t_m}{2} \right)^2 \right)) \tag{4.76}$$

$$D_6 = \frac{1}{3} a_{xy-6} \times ([\bar{Q}_m] \times \left(\left(h_c + \frac{t_m}{2} \right)^3 - \left(-h_c - \frac{t_m}{2} \right)^3 \right) \tag{4.77}$$

For the fictitious thermal loads $[N]_6^{\Delta T=1}$ for R6, equations 4.51 and 4.52 are applied with the previously specified x and y bounds:

$$[N]_6^{\Delta T=1} = a_{xy-6}\int_z [\bar{Q}_6]\,[\bar{\alpha}_6]\,dz = a_{xy-6}\int_{-\frac{t_m}{2}-h_c}^{-\frac{t_m}{2}-h_c} [\bar{Q}_m]\,[\bar{\alpha}_m]\,dz \tag{4.78}$$

$$[M]_6^{\Delta T=1} = a_{xy-6}\int_z [\bar{Q}_6]\,[\bar{\alpha}_6]\,z\,dz = a_{xy-6}\int_{-\frac{t_m}{2}-h_c}^{-\frac{t_m}{2}-h_c} [\bar{Q}_m]\,[\bar{\alpha}_m]\,z\,dz \tag{4.79}$$

Undulation Regions (R10-R13)

Each of the four fibre-only undulation regions can be idealized as a laminate consisting of a single angle-ply layer of thickness h_c undulating through the laminate and two matrix-only lamina. For each of the undulation regions, equations 4.43-4.52 can be applied with k=10 to k=13 to calculate the A_k, B_k, D_k, $[N]_k^{\Delta T=1}$ and $[M]_k^{\Delta T=1}$ matrices. As an example, the calculations for R10 are presented in this sub-section. Figure 4.21 shows a schematic of the magnified region within the unit cell presented earlier in Figure 4.15.

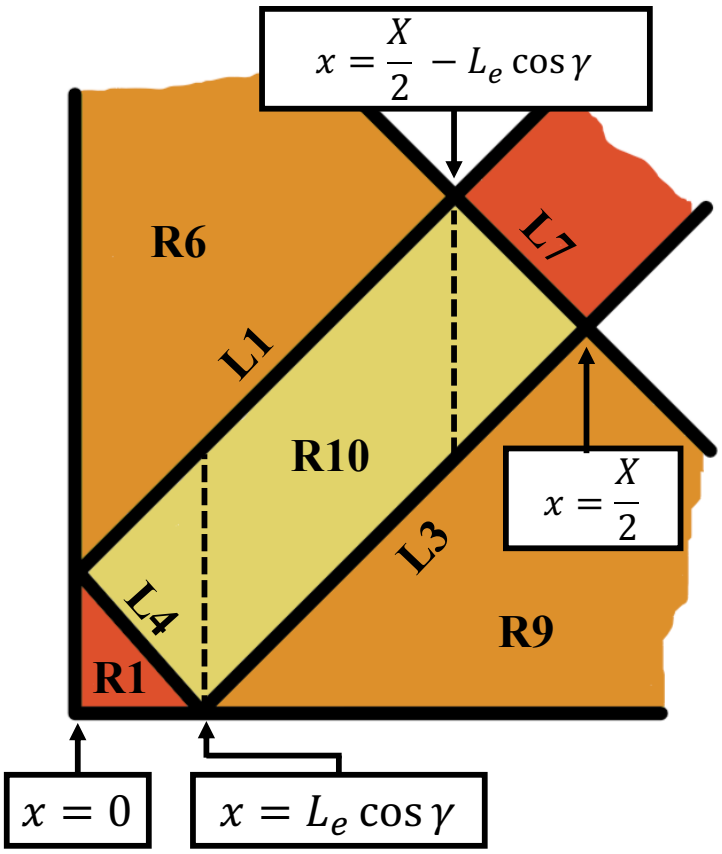

Figure 4.21. Schematic of R10 highlighting the defining lines and adjacent regions.

The undulating nature of yarns in R10 results in a slightly different approach to calculating the stiffness, coupling, bending and fictitious thermal load matrices. The area of the region is defined by three sub-areas as shown in Figure 4.21. The equations for A_{10}, B_{10} and D_{10} may be then written in terms of the area of the region a_{xy-10} as:

$$\begin{aligned} a_{xy-10} = &\int_0^{L_e\cos\gamma} \int_{-x\tan(\gamma)+L_e\cos(\theta)}^{x\tan(\gamma)+L_e\cos(\theta)} dy\,dx \\ &+ \int_{L_e\cos\gamma}^{\frac{X}{2}-L_e\cos\gamma} \int_{x\tan(\gamma)-L_e\cos(\theta)}^{x\tan(\gamma)+L_e\cos(\theta)} dy\,dx \\ &+ \int_{\frac{X}{2}-L_e\cos\gamma}^{\frac{X}{2}} \int_{x\tan(\gamma)-L_e\cos(\theta)}^{-x\tan(\gamma)+Y-L_e\sin(\gamma)} dy\,dx \end{aligned} \tag{4.80}$$

$$A_{10} = \left[a_{xy-10} \int_z [\bar{Q}_{10}]\, dz\right]_{k=10} = \left[a_{xy-10} \int_z [\bar{Q}_u(\beta)]\, dz\right]_{k=10} \quad (4.81)$$

$$B_{10} = \left[a_{xy-10} \int_z [\bar{Q}_{10}]\, z\, dz\right]_{k=10} = \left[a_{xy-10} \int_z [\bar{Q}_u(\beta)]\, z\, dz\right]_{k=10} \quad (4.82)$$

$$D_{10} = \left[a_{xy-10} \int_z [\bar{Q}_{10}]\, z^2\, dz\right]_{k=10} == \left[a_{xy-10} \int_z [\bar{Q}_u(\beta)]\, z^2\, dz\right]_{k=10} \quad (4.83)$$

Due to the undulating nature of the yarns in R10-R13, the integrals in equations on the RHS of equations 4.81 – 4.83 cannot be solved exactly. A Gauss-Legendre (GL) numerical integration approach was used to calculate the integrals over 10 points along the direction of the yarn. For each of these points, the stiffness matrix $\bar{Q}_u(\beta)$ is first calculated and then multiplied by the integral form of the height of the yarn at that point. The final value is multiplied by the weight of the point according to the GL formulation. The contribution of all the points is then summed and multiplied by the range of the function. Finally, the GL sum is multiplied by L_e to calculate the integral over the effective length of the region.

To calculate the fictitious thermal loads and moments for the region, an identical approach is followed, however, the stiffness matrices for each point of the numerical integration is also multiplied by the global CTE matrix of the composite at that point, $\bar{\alpha}_u(\beta)$. Equations 4.84 and 4.85 show the integral form of these calculations.

$$[N]_{10}^{\Delta T=1} = \left[a_{xy-10} \int_z [\bar{Q}_u(\beta)] * [\bar{\alpha}_u(\beta)]\, dz\right]_{k=10} \quad (4.84)$$

$$[M]_{10}^{\Delta T=1} = \left[a_{xy-10} \int_z [\bar{Q}_u(\beta)] * [\bar{\alpha}_u(\beta)] z dz\right]_{k=10} \quad (4.85)$$

4.4.2.4 Longitudinal CTE Calculation for Flat Braid TBC Unit Cell

After the calculation of each of the terms in equation 4.42, the CTE can then be derived by rearranging the equation to:

$$\begin{Bmatrix} \tilde{\varepsilon}^o \\ \tilde{\kappa}^o \end{Bmatrix} = \begin{bmatrix} a & b \\ b & d \end{bmatrix} \begin{Bmatrix} [N]^* \\ [M]^* \end{Bmatrix}^{\Delta T} \tag{4.86}$$

CTE is defined as the change in length per unit length per degree Celsius increase in temperature. Accordingly, setting the ΔT term to 1 °C allows for the CTE of the entire unit cell to be written as:

$$\begin{Bmatrix} \alpha_{yy} \\ \alpha_{xx} \\ \alpha_{yx} \end{Bmatrix}_{UC} = [a][N]^{*\Delta T=1} + [b][M]^{*\Delta T=1} \tag{4.87}$$

The longitudinal CTE of the unit cell, α_{yy-UC} is then simply equal to:

$$\begin{aligned} \alpha_{yy-UC} = a_{1,1}[N_1]^{*\Delta T=1} + a_{1,2}[N_2]^{*\Delta T=1} + a_{1,3}[N_3]^{*\Delta T=1} \\ + b_{1,1}[M_1]^{*\Delta T=1} + b_{1,2}[M_2]^{*\Delta T=1} + b_{1,3}[M_3]^{*\Delta T=1} \end{aligned} \tag{4.88}$$

Similarly, transverse CTE of the unit cell, α_{xx-UC} is equal to:

$$\begin{aligned} \alpha_{xx-UC} = a_{2,1}[N_1]^{*\Delta T=1} + a_{2,2}[N_2]^{*\Delta T=1} + a_{2,3}[N_3]^{*\Delta T=1} \\ + b_{2,1}[M_1]^{*\Delta T=1} + b_{2,2}[M_2]^{*\Delta T=1} + b_{2,3}[M_3]^{*\Delta T=1} \end{aligned} \tag{4.89}$$

Finally, the in-plane CTE of the unit cell, α_{yx-UC} is equal to:

$$\begin{aligned} \alpha_{yx-UC} = a_{3,1}[N_1]^{*\Delta T=1} + a_{3,2}[N_2]^{*\Delta T=1} + a_{3,3}[N_3]^{*\Delta T=1} \\ + b_{3,1}[M_1]^{*\Delta T=1} + b_{3,2}[M_2]^{*\Delta T=1} + b_{3,3}[M_3]^{*\Delta T=1} \end{aligned} \tag{4.90}$$

A Matlab™ script was written to perform the calculations for all the different regions and calculate the CTE of the unit cell.

4.5 Results and Discussion

4.5.1 DIC Local Strain Data

Images collected from the acquisition system presented earlier in Figure 4.13 were processed as described in section 4.4.1.6. Local strain vectors were calculated for each of the TBC samples for

each image over the duration of the heating cycle. Table 4.8 shows the strain maps as exported from DaVis® for a sample 35º, 45º and 55º TBC.

As can be seen from Table 4.8, for each TBC sample exposed to a heating cycle, the deformation vectors and longitudinal strain increase with increasing temperatures. This thermal dilation behaviour has been well documented for a plethora of materials, including Kevlar®/epoxy composites. Over the duration of a single heating cycle, each sample exhibits higher values of strain as the temperature reaches the target temperature. This is clearly demonstrated by the changes in the local strain vectors shown in Table 4.8. In the 35º samples shown in Figure 4.22, increasing the temperature results in higher strains in regions exhibiting the largest deformation. Along the edges of the tubular sample, however, strains become increasingly negative. This suggests that 3D DIC would capture more accurately the behaviour of the TBC along the rims of the samples. Similar patterns can be seen for the 45º and 55º TBC samples tested.

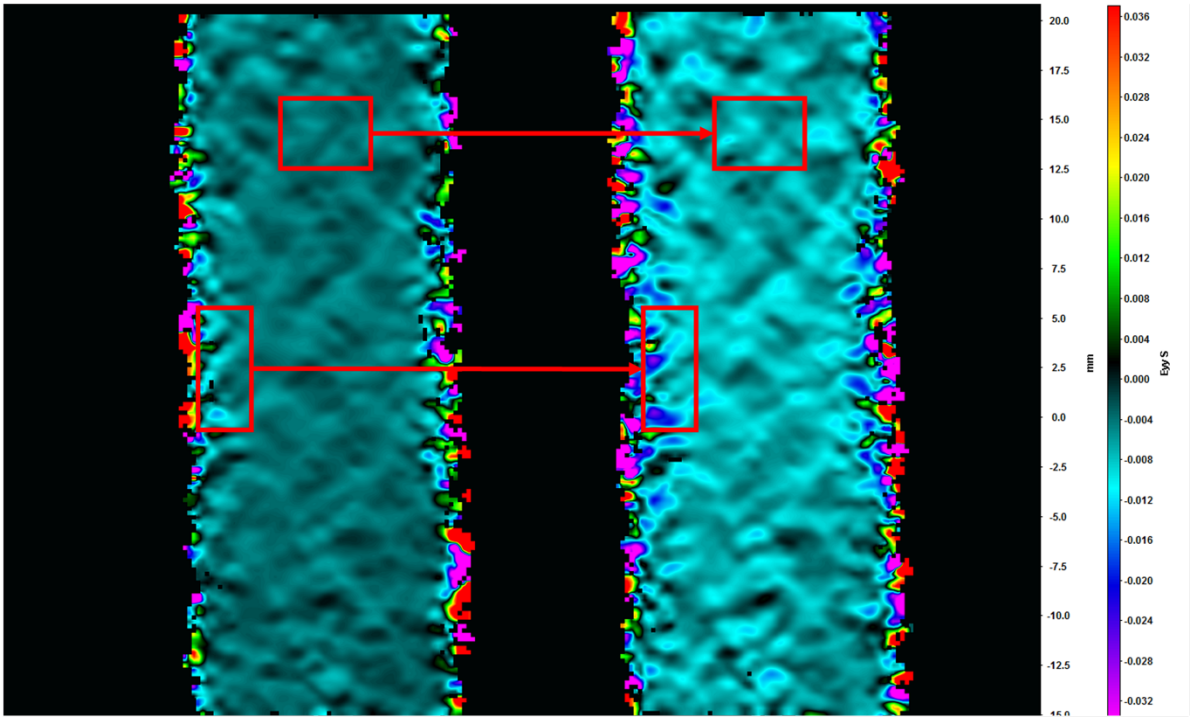

Figure 4.22. Local strain map images of 35º samples over the heating cycle of the study. Top box highlights the increase in deformation and strain in the centre regions of the TBC. Bottom box suggests that 2D DIC might not be able to fully capture the behaviour of the samples at the edges of the sample.

In addition to the expected thermal dilation behaviour, the different samples exhibited different strain behaviours over the duration of the heating cycles. Using equations 4.15 and 4.16, the longitudinal and transverse CTE of the yarns can be calculated. These are presented in Table 4.4. As can be seen in Figure 4.22, the 35° samples exhibited predominately negative strains over the duration of the test (the blue regions in Figure 4.22), with few regions within the sample exhibiting positive strain (black and green in Figure 4.22). These positive strain regions are likely matrix-rich regions. Due to the isotropic large positive CTE of the epoxy selected for this work (30 μm/m°C), these regions have relatively positive strains. The impregnated yarns, however, have a negative CTE along the fibre direction due to the negative CTE of Kevlar. For 35° TBC samples, the yarns are more closely aligned to the longitudinal direction. Accordingly, the negative CTE of the yarns contributes more to the negative strain exhibited by the entire sample in the longitudinal direction. As the braid angle increases, however, the transverse CTE of the impregnated yarns dominates the overall thermal behaviour of the samples. This results in more positive local strains for the 55° TBC samples. The 45° samples show a combination of the behaviour exhibited by 35° and 55°. Along the direction of the yarns, the samples exhibit large negative CTEs. Transversely, the yarns contribute more along with more matrix-rich regions. Figure 4.23 shows a comparison of the local strains experienced by the 35°, 45° and 55° samples at the target temperature for the experimental testing of these samples. As can be seen, increasing the braid angle results in a shift in the longitudinal strain from negative to positive.

TABLE 4.4. CALCULATED CTE VALUES FOR IMPREGNATED YARNS USING SCHAPERY MODELS, μm/m°C

Longitudinal CTE, α_1	-5.44
Transverse CTE, α_2	29.125

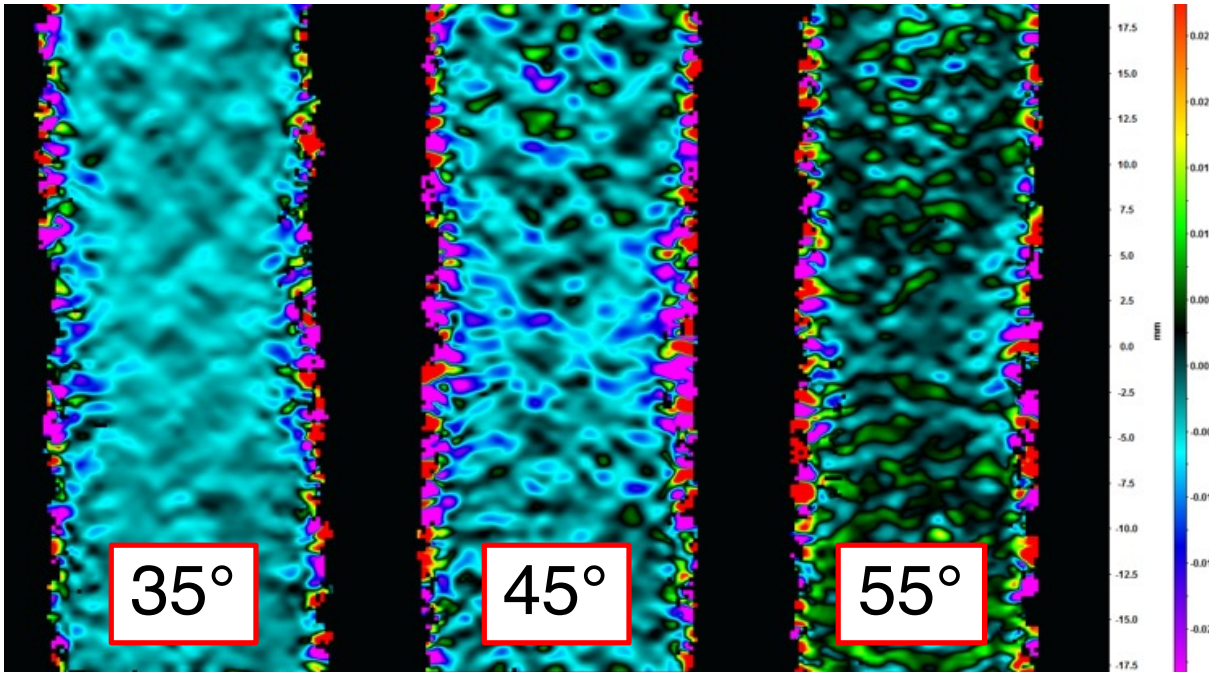

Figure 4.23. Local strain maps on three braid samples at three different braid angles (35°, 45° and 55°). As braid angle increases, the longitudinal local strain shifts from negative to positive.

4.5.2 Experimental CTE Values

Longitudinal strain data from the image processing software was exported and plotted against the temperature data from the second camera for each of the TBC samples tested. Figure 4.24 shows the results for all samples of each of the 35º, 45º and 55º TBC samples. As mentioned earlier, for each braid angle, ten samples were tested. Each sample was heated to 150ºC and data points collected every five minutes. Figure 4.24 shows the strain against temperature data for each of the 30 samples tested in his study.

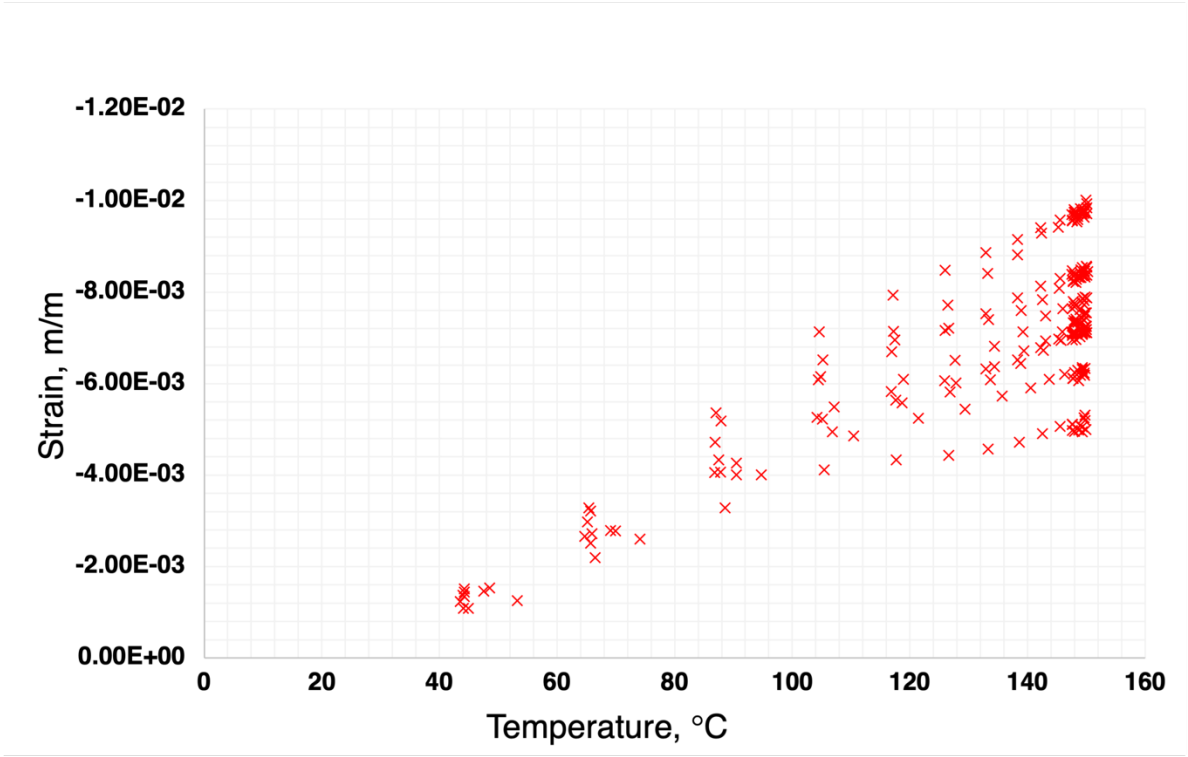
-1.20E-02
-1.00E-02
-8.00E-03
-6.00E-03
-4.00E-03
-2.00E-03
0.00E+00
Strain, m/m
0
20
40
60
80
100
120
140
160
Temperature, °C

(a)

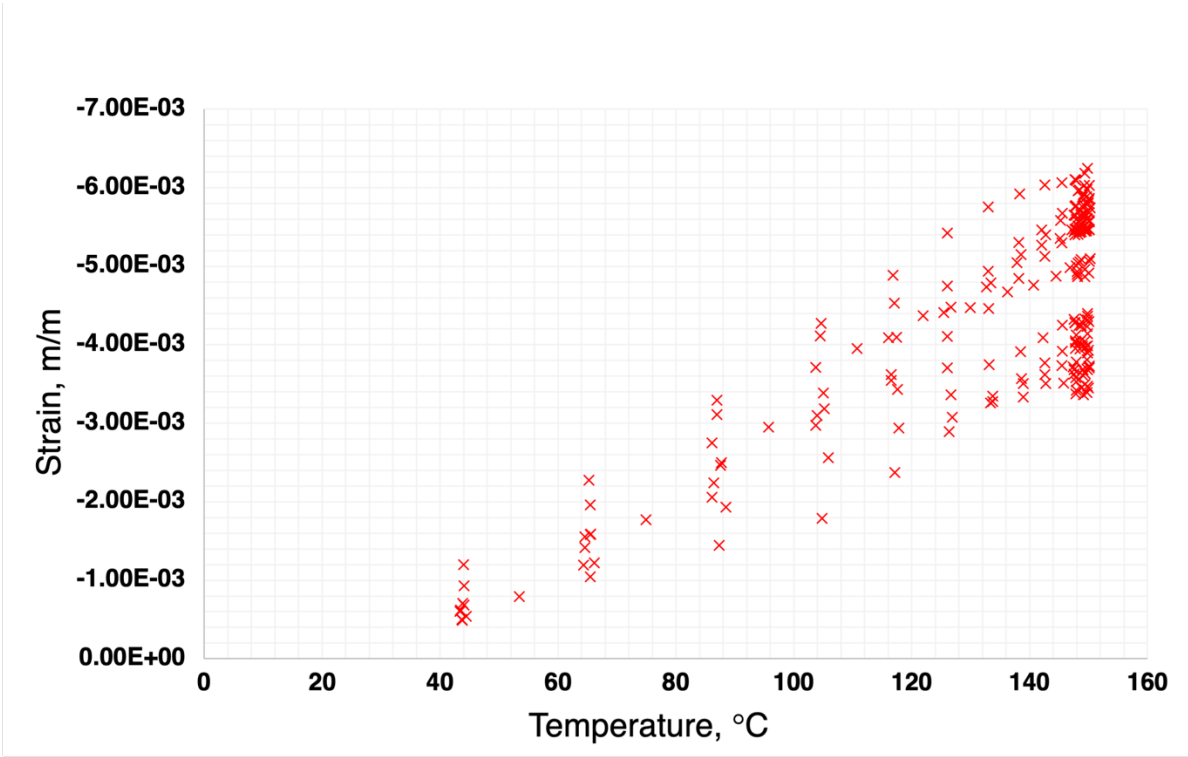
-7.00E-03
-6.00E-03
-5.00E-03
-4.00E-03
-3.00E-03
-2.00E-03
-1.00E-03
0.00E+00
Strain, m/m
0
20
40
60
80
100
120
140
160
Temperature, °C

(b)

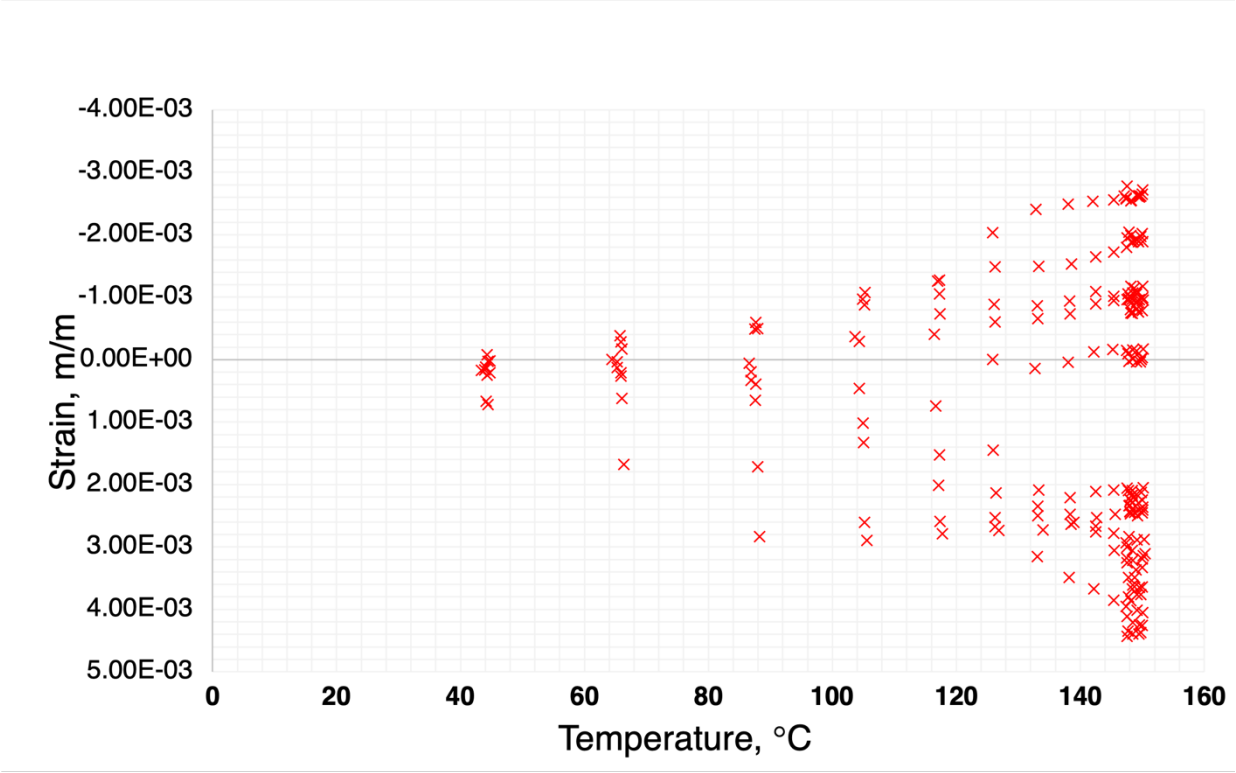

(c)

Figure 4.24. Plots of the strain measured by the DIC processing software against the temperature for (a) 35, (b) 45 and (c) 55-degree braids.

As can be seen from Figure 4.24, the relationship between the thermal strains and the braid angles follows an expected trend. For the 35-degree TBCs, the strains at the target temperature ranged from -0.00495 to -0.00958. For the 45-degree TBCs, the strains at the target temperature ranged from -0.00337 to -0.00584. Finally, for the 55-degree TBCs, the strains at the target temperature ranged from -0.00260 to 0.00443. The 35-degree TBCs experience the largest negative strains. At lower braid angles, yarns are aligned closer to the longitudinal axis of the braid. Given that the longitudinal CTE of the yarns is negative, the large negative strains produced in the 35^{o} samples are to be expected. Conversely, increasing the braid angle, results in a larger contribution from the transverse CTE of the yarns. Given the large anisotropy of the fibres in the longitudinal and transverse directions, the transverse CTE of the yarns is largely positive and results in a reduced negative strain of the TBC samples at higher braid angles. Consequently, the

45-degree TBCs show less negative longitudinal strains. The 55-degree TBCs show even lower negative longitudinal strains and some samples show positive strains. Due to the variation of the braid angle of the 55-degree samples, samples at the lower end of the range exhibit small negative expansion behavior. Samples at the higher end exhibit slightly positive behavior. This would imply that the 55-degree braids are close to the zero-CTE of the Kevlar®/epoxy TBCs. For each of the braid angles shown in Figure 4.24, the average of all the samples were calculated. These averaged plots are shown in Figure 4.25.

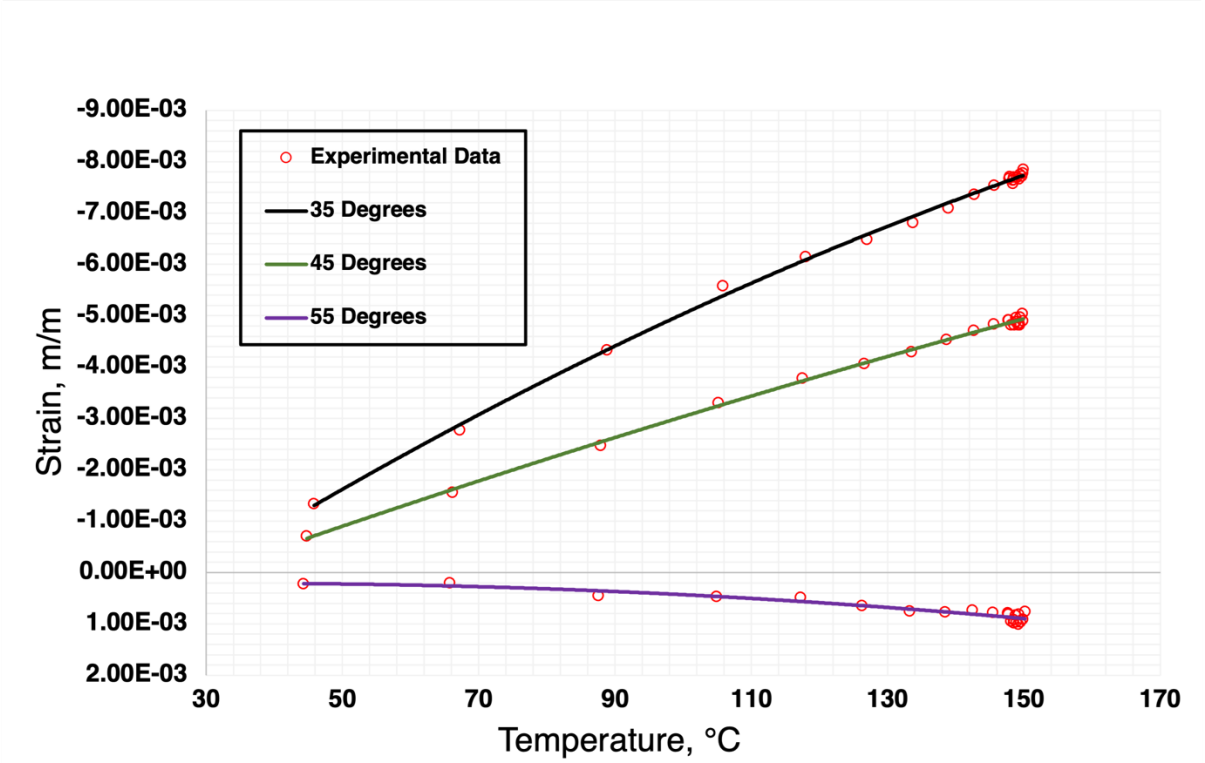

Figure 4.25. Averaged plots of the thermal strain against the temperature for the three TBC samples tested in this study.

As can be seen in Figure 4.25, the strains experienced by the TBC samples is dependent on the braid angle. Lower braid angles result in more negative strains, and larger braid angles result in relatively positive strains. Interestingly, another important conclusion from the averaged plots is the relationship between strains and temperature. Between 100 °C-110 °C, the relationship between strain and temperature shifts slightly. Figure 4.24 also highlights this and suggests a relationship between the properties of the materials in the work and the temperature at which the

thermal expansion tests are conducted. Strife and Prewo recognized the dependence of the CTE of Kevlar® to the testing temperatures. For temperatures between 0-100 °C, the CTE of Kevlar® fibres is -2 µm/m°C and between 100-200 °C, the CTE of Kevlar® fibres is -4 µm/m°C[102]. Furthermore, the glass transition temperature of the matrix used in this work is 121 °C according to the manufacturer data sheet[176]. Previous literature has highlighted the relationship between the glass transition temperature and thermal properties of Kevlar®/epoxy composites[177]. Although the effects are reduced in the averaged plots in Figure 4.25, the current results of the work suggest that the change in CTE of the fibres at 100 °C and the glass-transition temperature of the epoxy must be considered during thermal expansion studies. The spread of the data is also likely to be a consequence of the varying fibre volume fraction of the TBC samples, promoting the glass transition temperature and change in the CTE of Kevlar® fibres to be more pronounced.

Collected strain data was used to calculate the longitudinal CTE of each sample at each data point by using equation 4.3. Figure 4.26 shows the plots of CTE against temperature for each of the 10 samples tested per braid angle.

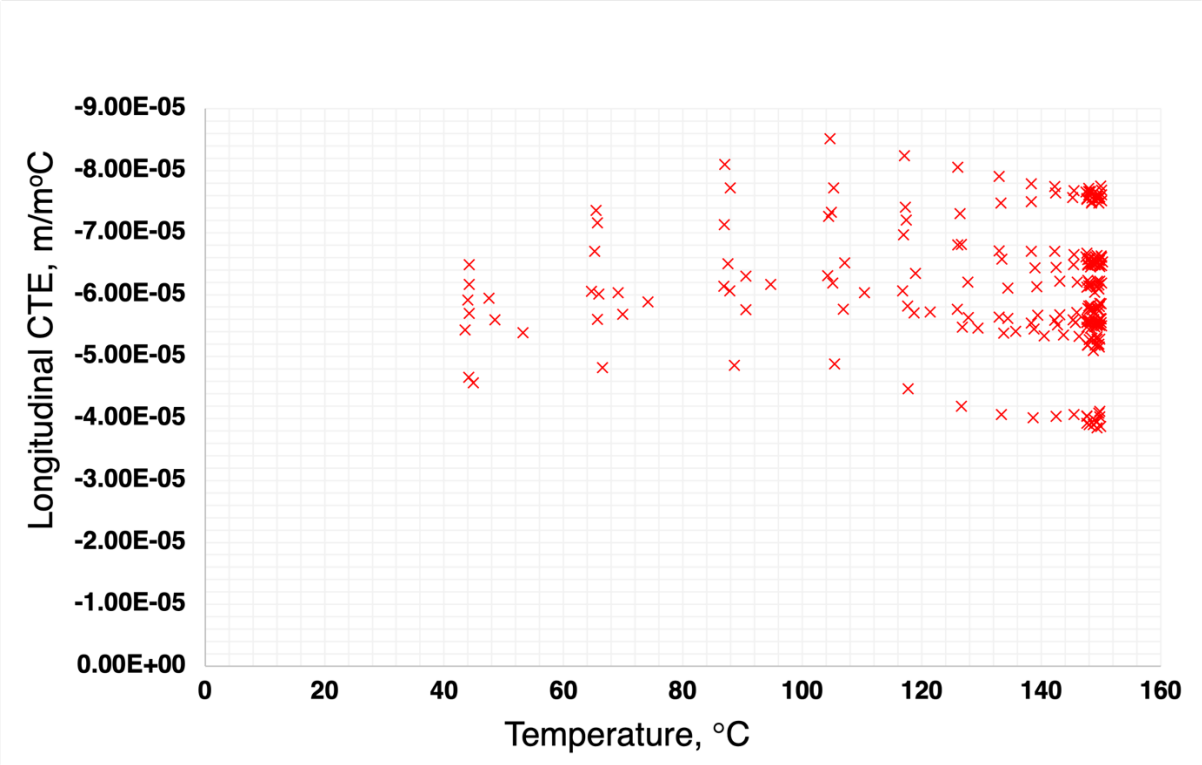

(a)

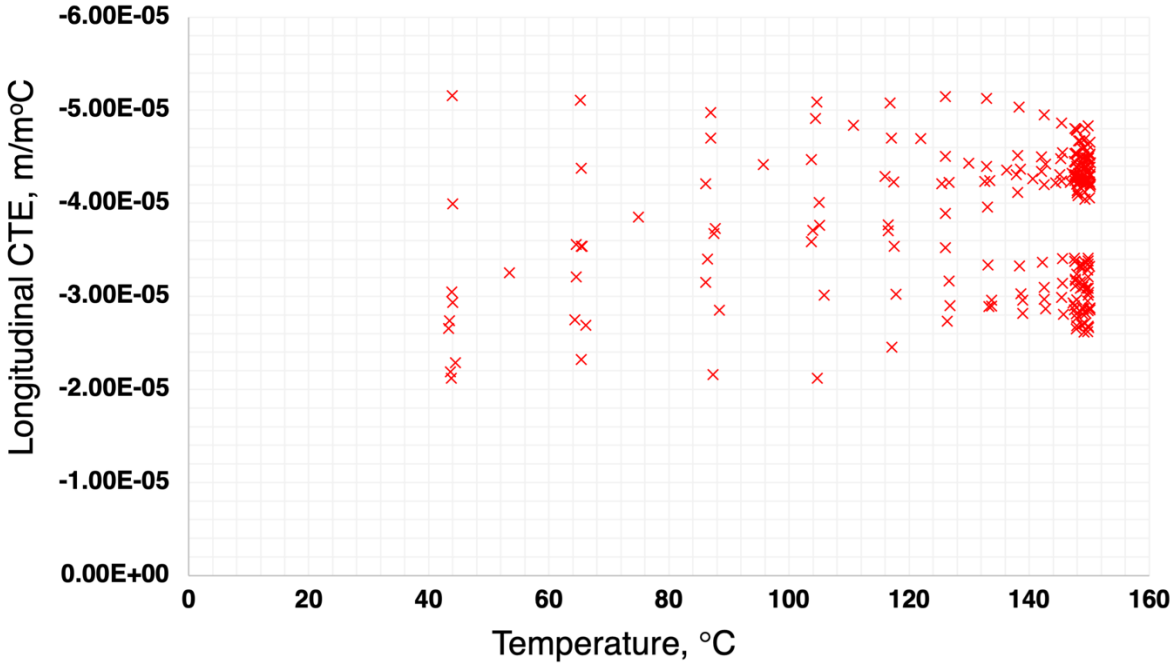
-6.00E-05
-5.00E-05
-4.00E-05
-3.00E-05
-2.00E-05
-1.00E-05
0.00E+00
Longitudinal CTE, m/m°C
0
20
40
60
80
100
120
140
160
Temperature, °C

(b)

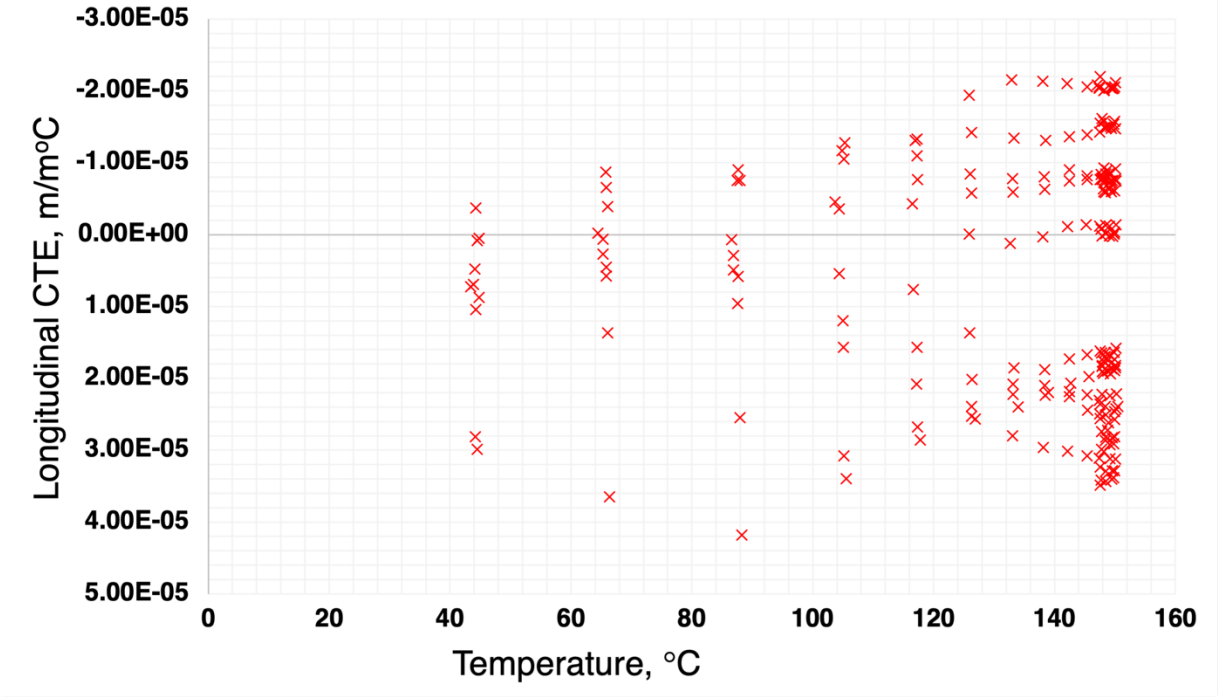

(c)

Figure 4.26. Plots of the CTE calculated from strain and temperature data for (a) 35, (b) 45 and (c) 55-degree braids.

As can be seen in Figure 4.26, experimental CTE values were most negative for the 35-degree TBC samples and became more positive with increasing braid angles. 55-degree braids showed mix of positive and negative CTE values. For the 35-degree braids, longitudinal CTE initially increases with temperature but begins to drop at 100 °C. These observations confirm the relationship between the CTE of the fibres and the temperature. As the CTE of the fibres change from -2 µm/m°C to -4 µm/m°C, the CTE of the braid reflects this with the sudden drop in CTE values. Similar drops in the CTE-temperature plots can be seen for the 45-degree and 55-degree braids. Figure 4.27 shows the average CTE data for each braid angle combined in a single graph.

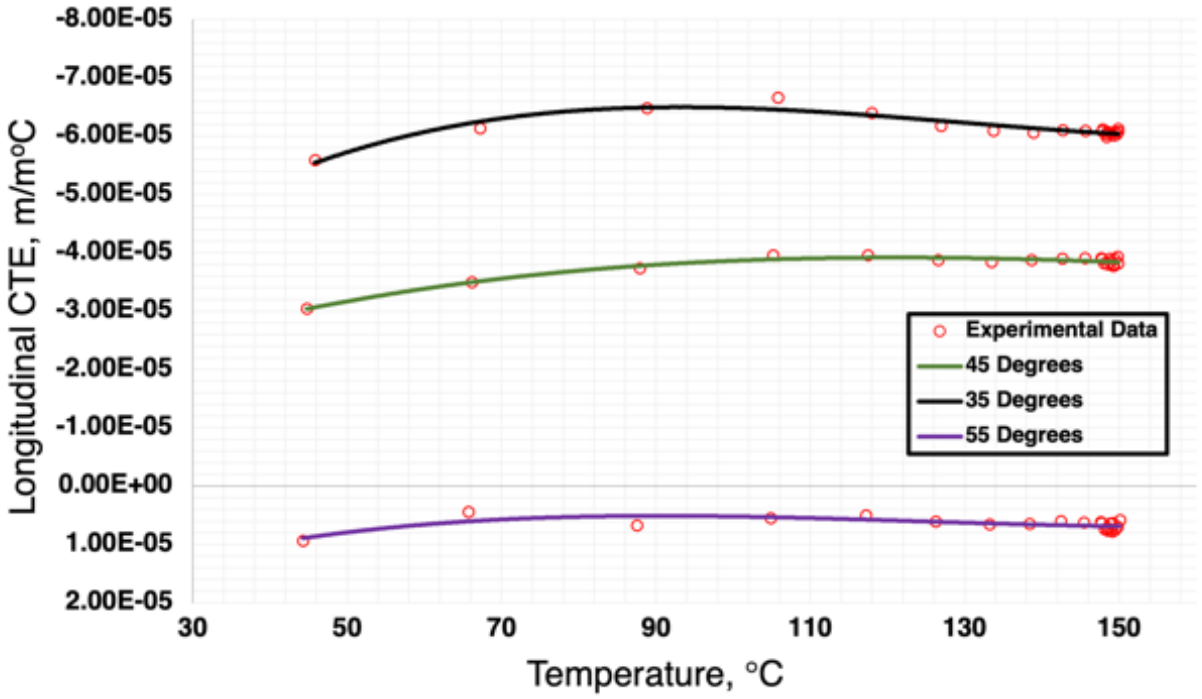

Figure 4.27. Averaged plots of the CTE against temperature for the three TBC samples tested in this study.

As shown in Figure 4.27, the average CTE of 35-degree TBC samples is the largest negative CTE, with values increasing with increasing braid angle. Although all samples show some level of variation in longitudinal CTE up to 100 °C, longitudinal CTE values seem to not change after. The experimental CTEs of all the samples at the targe temperature of 150 °C were calculated and averaged. Table 4.5 shows the values of longitudinal CTE for each tested sample. Table 4.6 shows the average longitudinal CTE and standard deviation for each braid angle.

TABLE 4.5: EXPERIMENTAL CTE VALUES FOR KEVLAR®/EPOXY TBCS AT 150 °C

Sample #	**Longitudinal CTE, α_{yy-exp}** (μm/m°C)
35_01	-55.2
35_02	-61.5
35_03	-52.1

35_04	-58.1
35_05	-55.8
35_06	-65.7
35_07	-65.1
35_08	-75.7
35_09	-39.6
35_10	-76.3
45_01	-41.5
45_02	-42.6
45_03	-28.9
45_04	-43.3
45_05	-45.3
45_06	-43.4
45_07	-33.5
45_08	-31.3
45_09	-27.0
45_10	-46.7
55_01	24.4
55_02	-6.66
55_03	17.0
55_04	18.7
55_05	28.5
55_06	-2.06
55_07	-15.3
55_08	-0.33
55_09	33.4
55_10	-8.25

TABLE 4.6. AVERAGE EXPERIMENTAL LONGITUDINAL CTE AND STANDARD VARIATION FOR EACH BRAID ANGLE CONFIGURATION TESTED

Braid Angle	**Longitudinal CTE, α_{yy-exp}** (μm/m°C)
35	-60.5 ± 11.02
45	-38.3 ± 7.37
55	7.08 ± 19.51

As seen in Table 4.6, the average CTE values are mostly negative for the 35-degree TBCs and become more positive as braid angle increases. An important conclusion from Table 4.6 and the previous figures of strain against temperature and CTE against temperature is the sensitivity of the CTE to braid angle. The variation in the braid angle of the samples can be directly related to the variation in the final strain and CTE results. Figure 4.9 presented a box and whisker plot of the measured braid angle of the tested samples in this work. The box and whisker plots showed that the 45-degree samples showed the smallest measured range, followed by the 35 degree braids and finally the 55 degree braids. These ranges are mirrored in the collected averaged CTE data presented in Table 4.6. 45-degree TBCs demonstrated the lowest longitudinal CTE deviation is due to the relatively low deviation in the recorded braid angles for the 45-degree TBC samples. Conversely, 55-degree braids had the relatively largest angle deviation, resulting in the largest deviation in the measured longitudinal CTE. Reducing errors in the manufacturing process can help reduce the variation of the braid angle, likely reducing the spread of the strain and ultimately the CTE data. Although measured braid angles were deemed satisfactory for this work, it is important to acknowledge that the averaged data presented can more closely represent the behaviour of these materials by improving the manufacturing process. Furthermore, an important underlying assumption in averaging the braid angle data and the strain data is that all samples are perfect, symmetric tubes.

4.5.3 CLPT Model Validation

Limited data is present in the literature on the behaviour of Kevlar®/epoxy composites. Strife and Prewo conducted an experimental and analytical study into the longitudinal CTE of

unidirectional laminae and bidirectional Kevlar®/epoxy laminates. In their work, the CTE of the tested composites were plotted against the angle of the laminae used. To validate the current model, the CTE of unidirectional and bidirectional composites were calculated. The obtained CTEs were then compared to the results of Strife and Prewo. Table 4.7 lists the material properties adapted from Strife and Prewo. Figures 4.28 and 4.29 shows the plots obtained from this work against the orientation angle for each of the unidirectional Kevlar® /epoxy laminae and the Kevlar®/epoxy bidirectional composites using the same properties.

TABLE 4.7: PROPERTIES ADAPTED FROM STRIFE AND PREWO FOR MODEL VALIDATION OF CTE OF UNIDIRECTIONAL LAMINAE AND BIDIRECTIONAL COMPOSITES

Property	**Value**
Volume Fraction	0.5
Fibre Longitudinal Modulus	117.75 GPa
Fibre Longitudinal CTE	-2 μm/m °C
Fibre Transverse CTE	59 μm/m °C
Epoxy Longitudinal Modulus	4.07 GPa
Epoxy CTE	66.1 μm/m °C

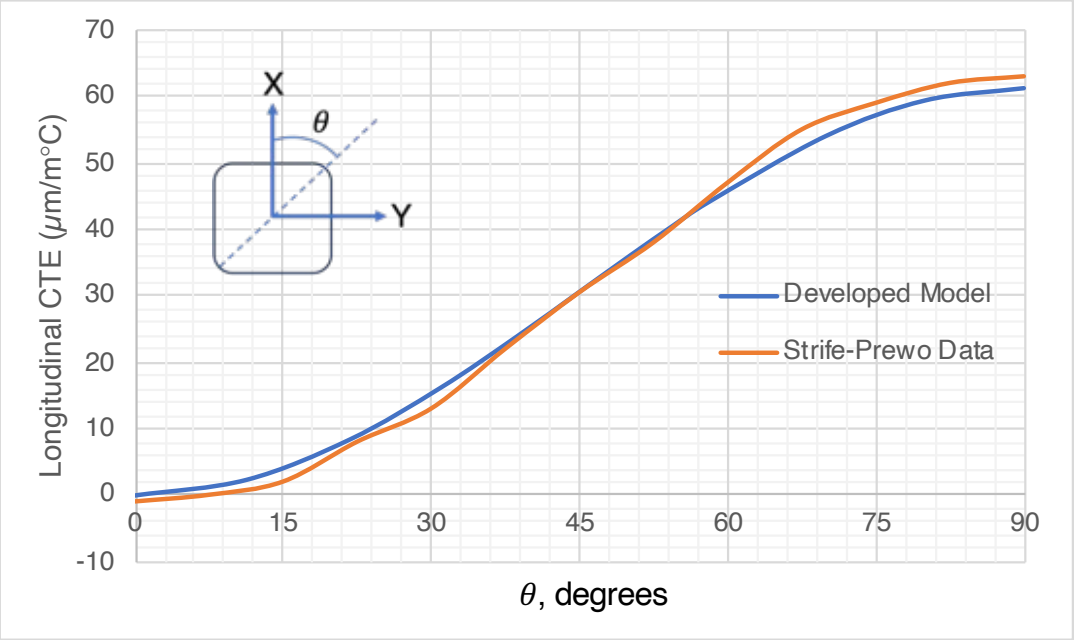

Figure 4.28. Plot of longitudinal CTE vs angle for unidirectional Kevlar®/epoxy laminae.

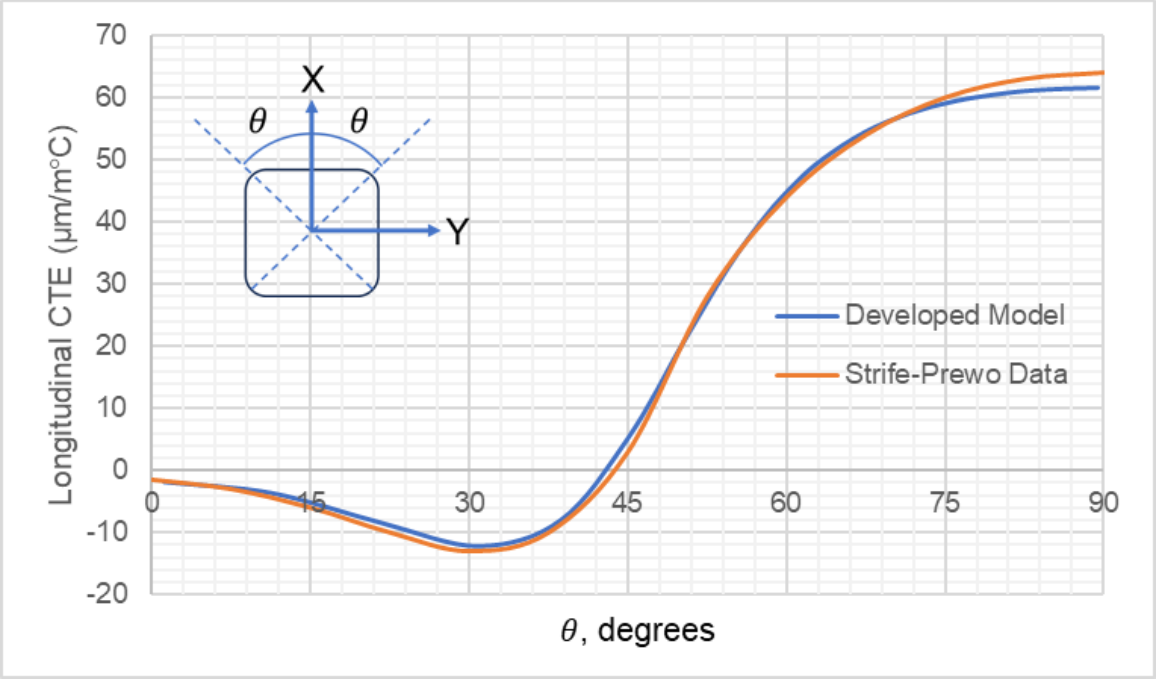

Figure 4.29. Plot of longitudinal CTE vs angle for bidirectional Kevlar®/epoxy laminates.

The work of Strife and Prewo only specified that symmetric balanced laminates were used to plot the data in Figure . To compare to the data in Figure, the material properties in Table were used to calculate the longitudinal CTE for a symmetric balanced laminate consisting of six plies. As can be seen from Figure 4.28 and Figure 4.29, the currently developed CLPT-based model is able to accurately replicate the data from Strife and Prewo. For unidirectional Kevlar®/epoxy laminae, the maximum deviation was -3.38 μm/m^{o}C at an angle of approximately 30^{o}. For the bidirectional Kevlar®/epoxy laminates, the maximum deviation was 2.51 μm/m^{o}C at an angle of ±90^{o}. Strife and Prewo comment on the influence of the anisotropy between the Kevlar® fibre and the matrix on the expected shapes of the graph. At large braid angles that approach 90^{o}, the transverse properties of the fibre dominate the behaviour, resulting in higher sensitivity and accordingly, more deviation. Additionally, both the Strife and Prewo data as well as the currently developed model suggest that Kevlar®/epoxy composites can be designed with a zero or near-zero CTE. Strife and Prewo predicted achieving a zero longitudinal CTE at a bidirectional laminate angle of ±43^{o}. Through linear interpolation, the current model suggests that a zero longitudinal CTE can be achieved at an angle of ±42.48^{o}.

Although the current model accurately predicts the behaviour of unidirectional laminae and six-ply bidirectional composites, the sensitivity of the CTE to the bidirectional stacking sequence was further investigated. The developed model was used to calculate the CTE of two-ply, four-ply and eight-ply bidirectional laminate composites. The results are presented in Figure 4.30.

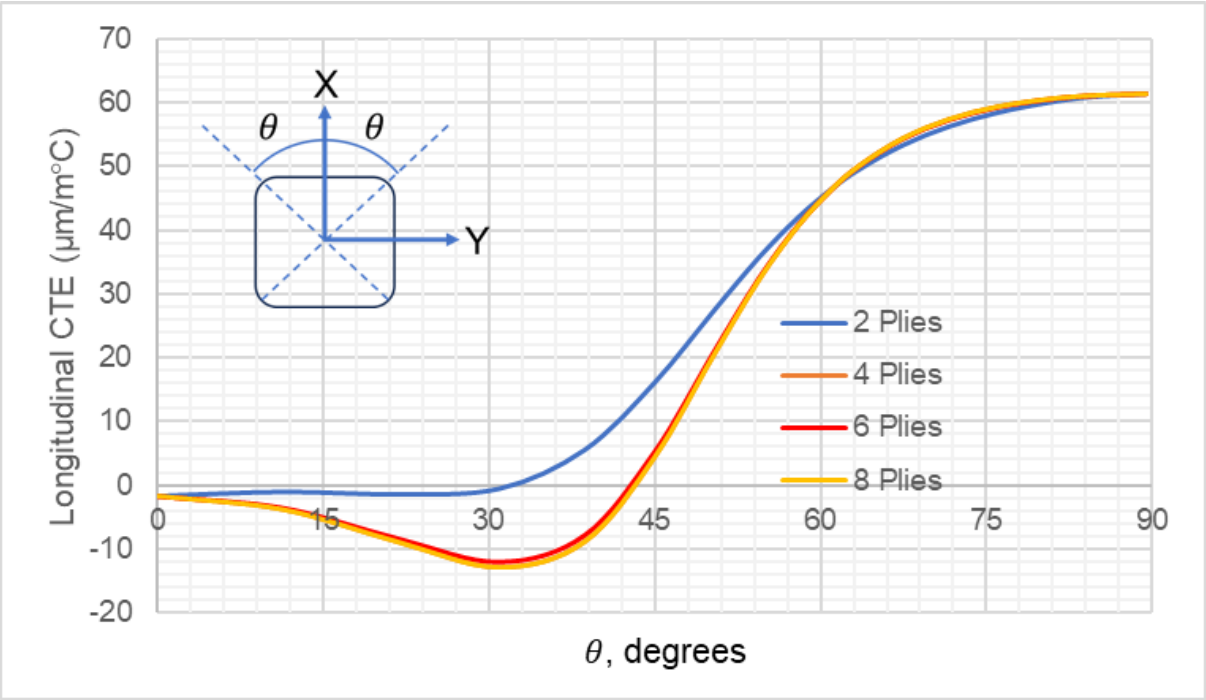

Figure 4.30. Plot of longitudinal CTE vs angle for bidirectional Kevlar®/epoxy laminates of varying plies as calculated from the developed model.

Figure 4.30 shows the influence of increasing the number of plies on the longitudinal CTE of bidirectional laminates. At two plies, the CTE of the laminate is negative for angles under approximately ±32°, increasing afterwards. The behaviour of the four-ply and eight-ply laminates are identical. This suggests that any laminate consisting of an even number of plies around the midplane will have identical behaviour. The six-ply laminate shows that an odd number of plies around the midplane results in similar trends over the range of angles, however, values deviate slightly, particularly in the range of angles between ±15° and ±43°. The behaviour of the two-ply composite may suggest that at these angles, the negative CTEs of the plies compound, resulting in a larger negative CTE for the entire laminate. This conclusion has also been supported by the previous work of Strife and Prewo[102].

The developed model was used to calculate the longitudinal CTE of a flat braid unit cell for the three tested braid angles in this work, 35-, 45- and 55-degrees. Figure 4.31 shows a plot of the longitudinal CTE against the braid angle combined with the experimental data.

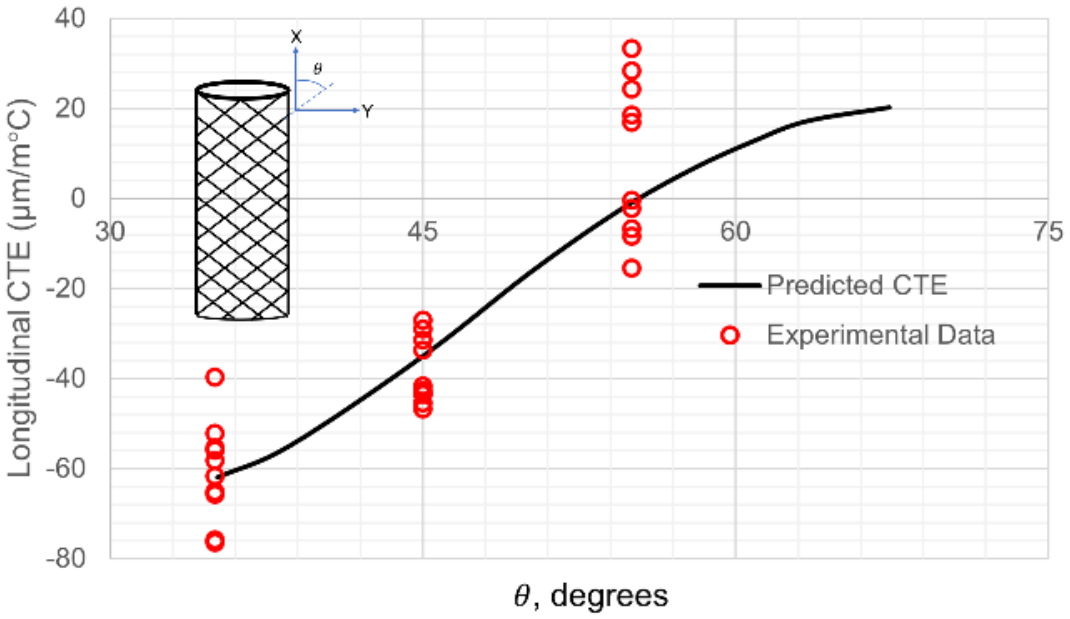

Figure 4.31. Plot of longitudinal CTE from developed CLPT model against the braid angle of TBCs

As can be seen from Figure 4.31, the model is able to predict the average longitudinal CTE of TBCs over the range of angles tested. The current experimental data suggests, however, the sensitivity of the model to the thermal expansion properties of the constituents. Although the reported CTE of Kevlar® fibres is typically in the range of -1 µm/m°C to -7 µm/m°C at room temperature, the results of this work suggest that the values are in fact more negative at elevated temperatures. A potential explanation for this observation is the degradation of the fibres and matrix. This would result in a change in the thermomechanical properties, reflected in the overall thermal expansion behaviour of the TBC. An important conclusion is that the manufactured Kevlar®/epoxy TBC samples achieve a zero-CTE at a predicted values of approximately 53-degree braid angle.

4.6 Conclusion

TBCs have a wide variety of applications due to their high mechanical properties and low density. Although the tensile, compressive, fatigue and creep behaviour has been investigated in the literature, a large gap remains in the thermal expansion behaviour of these materials. This gap is both in the experimental measurement of CTE and analytical modelling of the behaviour. Accordingly, this work sought to develop a new non-contact method based in DIC to measure the

CTE of these materials and develop a CLPT based model to predict the CTE of TBCs. Results of the work showed that DIC was able to repeatably measure the CTE of TBCs. Behaviour of the strain followed the expected trend with higher absolute thermal strains and lower braid angles. Averaged values of the experimental longitudinal CTE for each of the 35-degree, 45-degree and 55-degree TBCs were -60.5 μm/m °C, -38.3 μm/m°C and 7.08 μm/m °C. The experimental data, however, suggests the sensitivity of the CTE to braid angles. The largest deviation in the measured CTE correlated to the largest deviation in the measured braid angles. The CLPT based model developed was tested against limited CTE data from laminates from previous work and showed excellent agreement. The CLPT model was then used to predict the CTE of TBCs at the three theoretical braid angles tested in this work and showed good agreement with the experimental data. The current model for the flat braid unit cell is highly sensitive to the thermal properties of the constituents. Testing a larger range of braid angles at different temperatures would allow for further refinement of the model.

The results of this chapter show that experimental measurement of the CTE of tubular polymer composites is possible using digital image correlation. This can be expanded to measure the thermal dilation behaviour of non-standard shaped composites. Furthermore, current data suggests that braid angle has a significant effect on the CTE of Kevlar®/epoxy 2D TBCs. At lower braid angles, the overall longitudinal CTE of Kevlar®/epoxy TBCs is negative, increasing with braid angle, turning positive at a braid angle of approximately 53 degrees. For composite applications where minimal thermal expansion behaviour is required, Kevlar®/epoxy TBCs is a viable material.

TABLE 4.8. EXPORTED THERMAL STRAIN DATA FROM DAVIS FOR A 35-DEGREE, 45-DEGREE AND 55-DEGREE SAMPLE, SHOWING THE CHANGE OF STRAIN OVER TIME.

Braid Angle				
35º	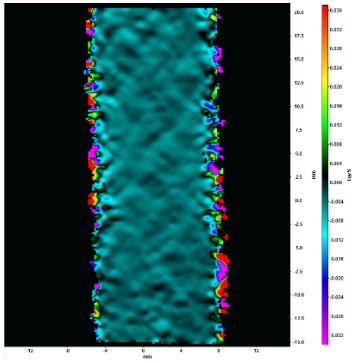	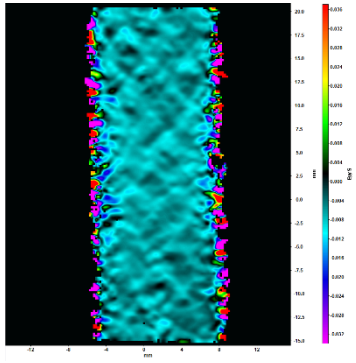	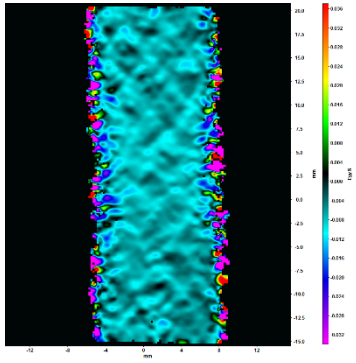	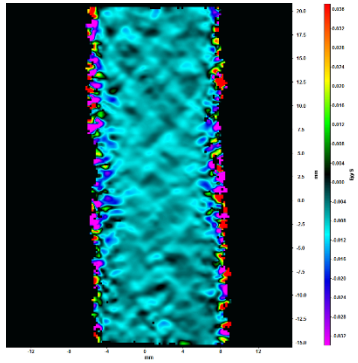
45º	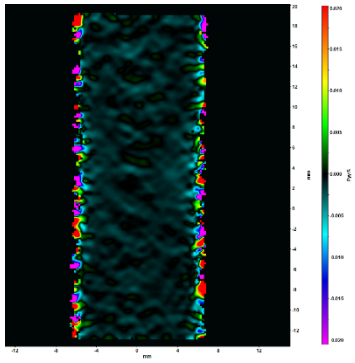	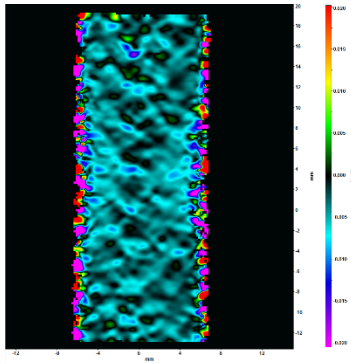	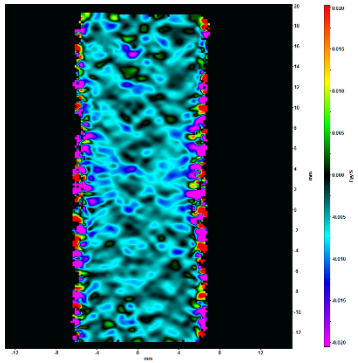	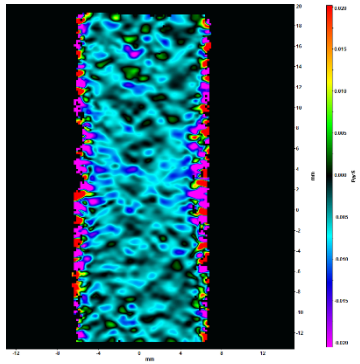

55º	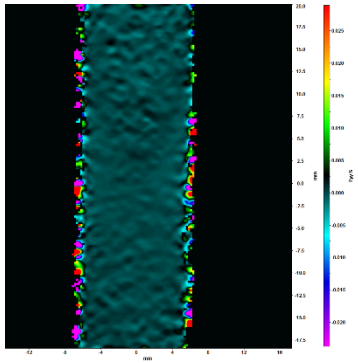	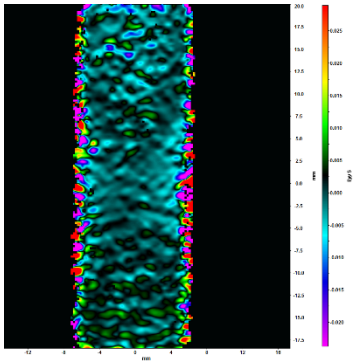	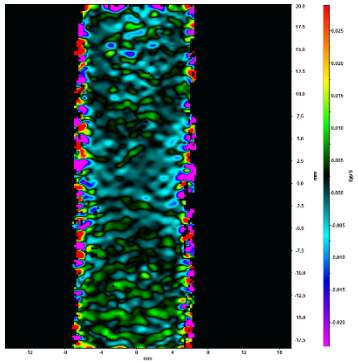	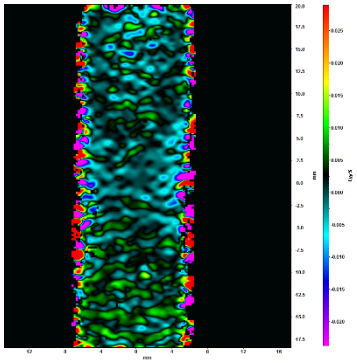

CHAPTER 5 - Influence of Displacement Rate on Elastic Modulus of 2d Kevlar®/epoxy Tubular Braided Composites

In chapter 3, thermal expansion of braided composites is shown to be an area where further research is needed to understand the type of behaviour demonstrated by these materials. In chapter 4, an experimental method is developed along with an analytical model to measure and predict the thermal expansion behaviour. The results, however, show the large variability between the samples tested. This variation is not specific to thermal properties. As mentioned in chapter 2, tensile testing of the properties of tubular braided composites shows a variability between the modulus and strength of tested samples in the range of 5-10%. For advanced applications where high specific strength and specific stiffness are crucial, these variations can present an obstacle in fully implementing composites. In this chapter, we present displacement rate – the rate at which tensile properties are tested – as a variable that influences the variability between samples. A version of this chapter was submitted as a conference paper to CANCOM 2024 under the title "Influence of Displacement Rate on Elastic Modulus and Strength of 2d Kevlar®/epoxy Tubular Braided Composites".

5.1 Introduction

Composite materials consist of two or more constituents joined together to produce a non-homogenous material. A plethora of manufacturing processes can be employed to combine these constituents. These different processes result in complex composite materials with tailorable mechanical and physical properties. Braiding is a textile composite manufacturing technique in which three or more parallel yarns are intertwined over the length of a mandrel to create a preform. Braided preforms are typically manufactured using a maypole braider. In these machines, carriers spooled with a fibrous material move along predefined paths. The motion of the carriers is provided by horn gears. As the carriers move along the tracks, the yarns are deposited and interlaced on a translating mandrel to create the preform. Figure 5.1 shows a typical braiding manufacture line.

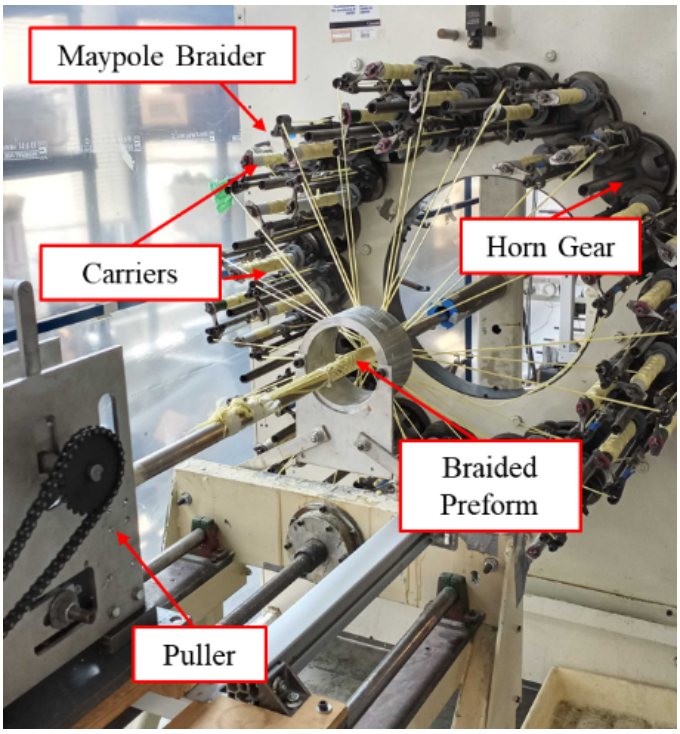

Figure 5.1. Image of a typical braided preform manufacturing line showing the maypole braider, horn gears, carriers, puller and the braided preform.

Once braided, the preform is impregnated with a matrix, typically a polymer, to form the final braided composite. The matrix binds the yarns together and helps in load transfer between the reinforcing fibres. Matrix impregnation is either a manual or vacuum-assisted process. Composite braiding is a highly repeatable and flexible process that can rapidly produce near net shape components and structures. Several manufacturing parameters influence the properties of the final braided composite. Of these parameters, braid angle is the most significant in determining the final tensile and compressive strength, stiffness and rigidity of the composite. Braid angle is defined as the angle formed between the yarns and the longitudinal axis of the braid. Figure 5.2 shows the braid angle labelled on a braided preform.

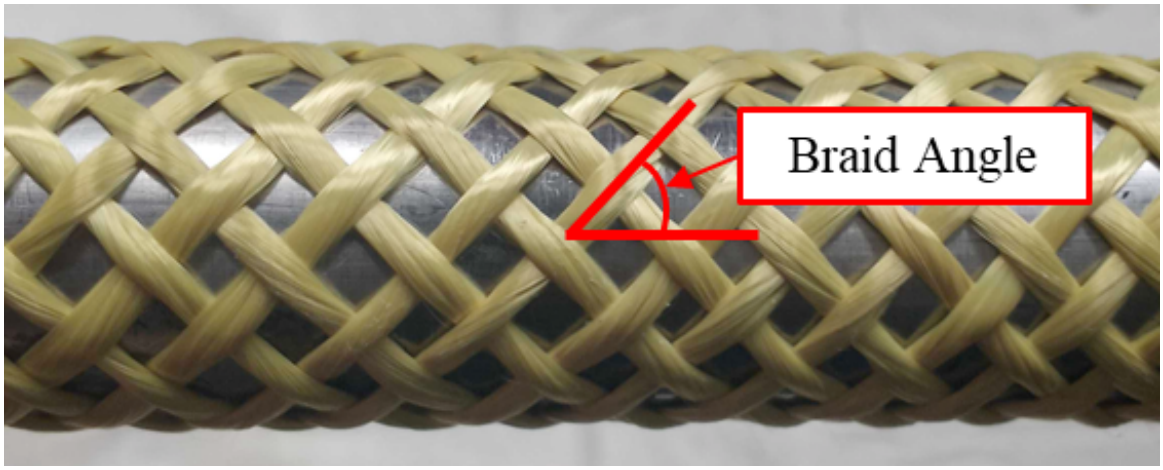

Figure 5.2. Image of a preform showing the braid angle as the angle between the interlacing yarns and the longitudinal axis of the braid

Tubular braided composites (TBCs) are the most common type of braided composites and are manufactured using a cylindrical mandrel. Due to their high specific strength and specific stiffness, TBCs have numerous applications including construction, sports, medicine and aerospace. Figure 5.3 shows a typical TBC manufactured using the equipment shown in Figure 5.1.

Figure 5.3. Image of Kevlar®/Epoxy TBC.

5.2 Literature Review

Several studies have investigated the manufacture of TBCs, focusing on the kinematics of the braiding process[178–181]. Models have been produced that predict the influence of the braider rotational speed and puller translation speed on the geometry of resulting preforms. Some studies have also attempted to understand the relationship between yarn twist and inter-yarn friction and their impact on the final braid angle[182–184]. The relationship between these manufacturing parameters and TBC preform structure is well documented.

In addition to the manufacturing of braided preforms, the characterization and mechanical properties of TBCs have also been thoroughly explored in literature. These studies have investigated the tensile, compressive, torsional, creep and fatigue behaviour of TBCs[11,12,167,185–189]. The relationships between the final geometry of TBCs and the resulting properties are documented

in these articles. Many studies have even examined the failure modes of braided composites under different loading scenarios.

From the studies that have characterized TBCs, the documented tensile mechanical properties have shown large variation between samples. TBC samples manufactured following identical processes will often show variations exceeding 10%. An explanation for the variations in TBC properties is the testing procedure followed by studies. ASTM standard D3039 is typically followed to test and measure the tensile properties of polymer matrix composite materials. Section 11 of this standard describes the recommended procedure for conducting the test. For one parameter, "Speed of Testing", the standard document suggests selecting a strain rate "so as to produce failure within 1 to 10 min[utes]"[190]. This is a wide range of sample loading rates. The differences in loading rates between studies might explain the disparity in the mechanical properties of TBCs manufactured under the same conditions.

In regard to investigating the influence of loading rate on the behaviour of composite materials, the majority of studies have looked into very high rates that mimic impact. May and Kilchert studied the effect of loading rate on the in-plane shear stress of carbon fibre triaxial braided composites. Samples were manufacture at three different braid angles (30^o, 45^o and 60^o) and tested at two strain rates (0.001 s^{-1} and 3 s^{-1}). The results showed that samples tested under higher strain rates had higher shear strength and more scattering in the data collected[191]. Böhr et al. experimentally investigated the strain rate dependent behaviour of 2D biaxial and triaxial carbon fibre braided composites. Biaxial samples were manufactured at three braid angles (30^o, 45^o and 70^o) and triaxial samples were manufactured at two braid angles (30^o and 45^o). Samples were tested at four different strain rates rates (2 mm/min, 10 mm/s, 100 mm/s and 1 m/s). The results of the study concluded that tensile strength and damage onset were significantly dependent on strain rate[192]. Jiang et al. looked into the influence of strain rate on the dynamic tensile properties of braided carbon fibre composites. Samples were tested at six strain rates (1 s^{-1}, 10 s^{-1}, 100 s^{-1}, 250 s^{-1}, 500 s^{-1}, and 800 s^{-1}). The study found that increasing strain rate resulted in an increase in tensile elastic modulus by 10-30% and tensile strength by 30-40%[193].

Other studies have looked into the influence of strain rate on the properties of woven and laminate composites. Hou and Ruiz explored the influence of a large range of strain rates on the tensile properties CFRP woven composites. The results of the work indicated that fibre dominated

properties are strain rate independent[194]. Naresh et al. examined the effect of high strain rate on laminated glass/epoxy, carbon/epoxy and hybrid glass/carbon/epoxy composites. Strain rates ranging from 0.0016 s^{-1} to 542 s^{-1} were tested on the manufactured samples. The results indicated that higher strain rates resulted in increased tensile strength and elastic modulus and decreased failure strain[195]. Gilat et al. conducted an experimental study on the strain-rate-dependent behaviour of carbon/epoxy composite laminates. Manufactured samples were tested in tension at three strain rates (0.00005 s^{-1}, 1 s^{-1} and 500 s^{-1}). The results of the study showed that elastic modulus and tensile strength both increased with strain rate, though not linearly. The authors suggest that rate dependent properties are primarily influenced by the resin more than the fibres[196]. Al-Zubaidy et al. investigated the relationship between the tensile properties and strain rates of CFRP laminates used in structural reinforcement applications Their results showed a positive linear relationship between elastic modulus and strain rate[197].

As mentioned, although some studies have looked into the relationship between strain rate and the tensile properties of composites, these studies are limited to very high strain rates. These strain rates are not reflective of the rates used during tensile testing of composites. Additionally, the results of the studies that have been conducted seem to indicate a relationship between testing rate and the elastic modulus and tensile strength, though the results are inconclusive. This relationship provides a plausible explanation for the variation seen in the experimental data collected from TBCs. Accordingly, the objective of this study is to experimentally investigate the influence of displacement rate on the elastic modulus of TBCs.

5.3 Methodology

5.3.1 Materials

TBCs in this study were manufactured using 1420 den Kevlar® 49 fibres (DuPont, Wilmington, Delaware, USA), Epon 826 epoxy resin (Hexion, Ohio, USA) and Lindau LS-81K hardener (Lindau Chemicals Incorporated, South Carolina, USA). Material selection was based on the previous work done by Ead et al.[12]. Table 5.1 shows the elastic modulus and failure strain of the fibres and matrix used in this study.

TABLE 5.1. MATERIAL USED IN STUDY AND MECHANICAL PROPERTIES AS FOUND IN [1] AND [198]

Material	Tensile Modulus (GPa)	Failure Strain (%)
Kevlar® 49	112-138	2.4
Epon 826 (with LS-81K)	2.7	5

5.3.2 TBC Manufacturing

Samples were manufactured following the procedure highlighted in previous work by Ead et al.[12]. Braided preforms were manufactured using a maypole braider (Steeger HS140/36-91, Steeger GmbH and Co. Wuppertal, West Germany) and an in-house caterpillar puller. The speed of the braider and puller were controlled through a voltage DAQ calibrated to the kinematics of the system. Yarns of Kevlar® were spooled on 36 carriers using an automatic spooling machine (Steeger SK2257-84, Steeger GmbH and Co. Wuppertal, West Germany). Following spooling, the carriers were secured on the braiding machine. Yarns were interlaced onto a 7/16-inch diameter aluminium mandrel. A LabVIEW™ software was used to control the braider rotational speed and puller translational speed and consequently, the braid angles of manufacture samples. Preforms in this work were manufactured at three different braid angles (35°, 45° and 55°) in a diamond (one-over one-under) pattern. Figure 5.4 shows an image of a manufactured 45° degree preform with the unit cell highlighted.

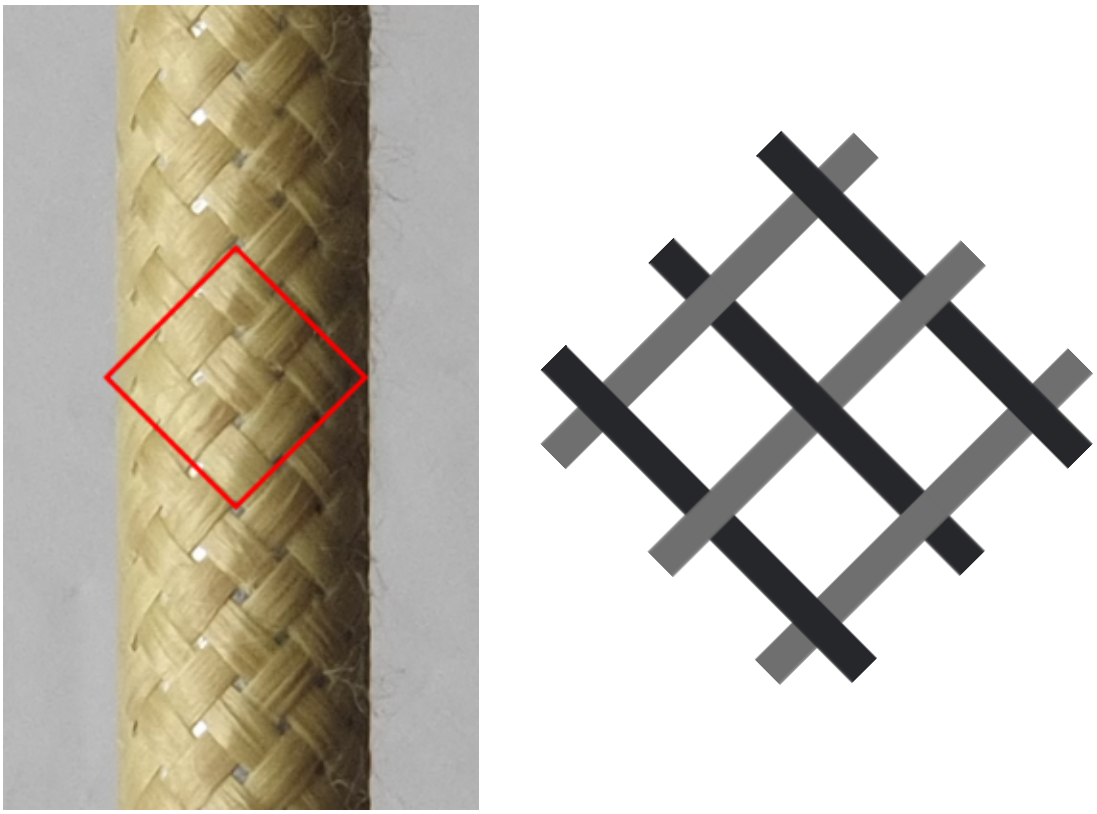

(a) (b)

Figure 5.4. Image of a (a) 45º preform highlighting the one-over-one under pattern and a (b) unit cell schematic for a regular braid preform.

Once braided, preforms were carefully placed over Teflon mandrels for resin and hardener impregnation. Epon 826 and LS-81K were mixed in a 1:1 ratio and manually massaged onto preforms. Following the manufacturer data sheet, samples were then carefully added to a rack and cured vertically in a square oven at 66ºC for 90 mins, 85º for 60 minutes and 150ºC for 180 minutes. After curing, samples were removed and cut down to a length of 7 inches. Figure 5 shows three fully cured TBCs manufactured at the three braid angles used in this study. Edges of the sample were filed to ensure uniform ends and reduce edge effects. Inner and outer diameters of the samples were measured and recorded using a microscopic gauge and a digital Vernier caliper. Sample cross-section was assumed to be a ring, and area was calculated using the inner and outer diameters at three different points along the length of the sample and averaged.

5.3.3 Sample Pre-Testing Preparation

Prior to testing, TBC samples were attached to steel end tabs using two-part epoxy (Henkel AG & Company, KHaA, Düsseldort, Germany) and left to fully set in for 24 hours. Samples were secured on an aluminium rail with hose clamps to ensure sample alignment during testing. Figure 5.5 shows a sample TBC sample prepared for testing.

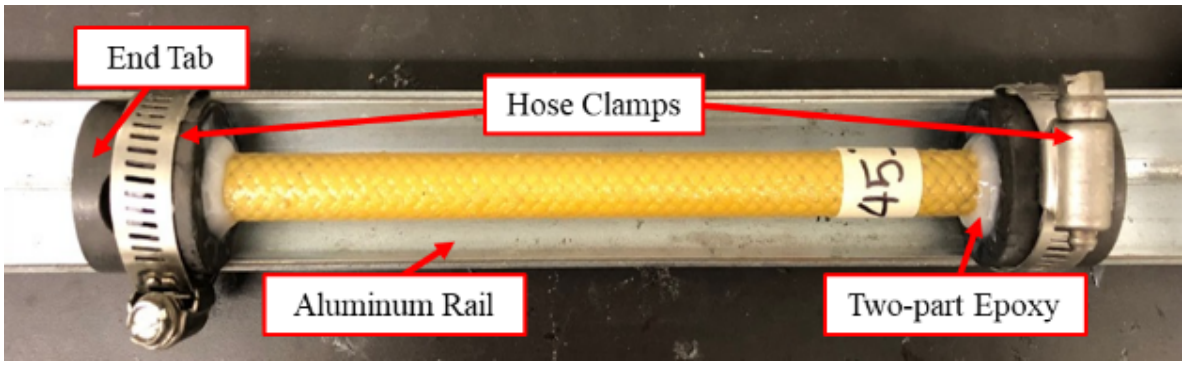

Figure 5.5. Image showing the setup used to prepare samples for testing.

To prepare samples for strain measurement during testing, settled samples were spray-painted in a black matte paint (Painter's Touch Flat Black, Rust-Oleum Corp, Concord, ON, Canada) and speckled with white paint (4230 Transparent White, Auto Air-Colors, East Granby, CT) using an airbrush (Paasche H Series, Paasche Air Brush Co., Chicago, IL). Air pressure and nozzle outlet size for speckling were selected to ensure sufficient speckle density and contrast for accurate strain measurement during the tensile test. Figure 5.6 shows a zoomed in image of the samples after painting and speckling.

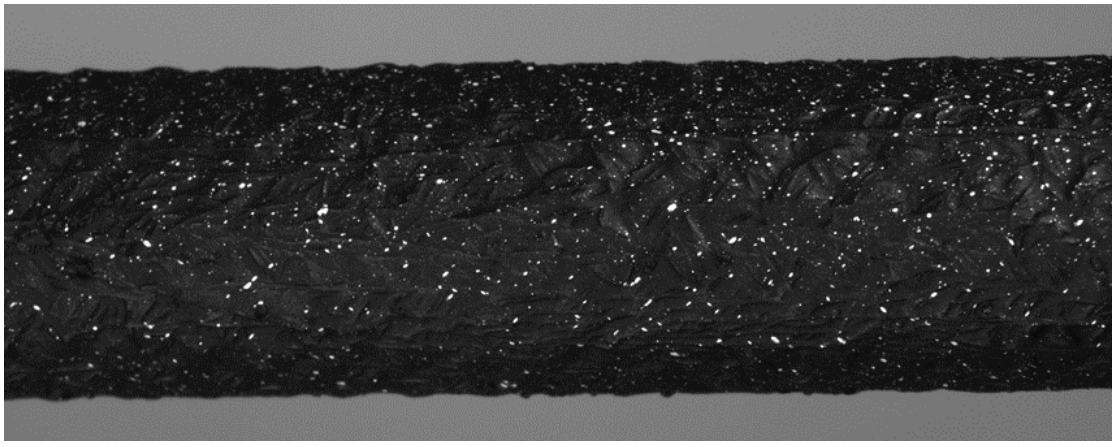

Figure 5.6. Zoomed in image of a 55º speckled TBC sample.

5.3.4 Displacement-Rate Pilot Study

Prior to testing, a pilot study was run to ensure the tensile testing machine was calibrated and correctly output the loading rate specified by the user. Furthermore, the pilot study was necessary to determine an acceptable range of loading rate values that ensured samples failed within the specifications of ASTM standard D3039. Based on these pilot tests, three displacement rates were determined for this work (1 mm/min, 2 mm/min and 6 mm/min). These speeds have been used in characterization studies and also ensured that samples failed within 1-10 min of loading. For each testing configuration, three samples were to be tested. Table 5.2 shows the experimental matrix of this study.

TABLE 5.2. TBC SAMPLE EXPERIMENTAL MATRIX

Angle	**Displacement Rate (mm/min)**	**Number of Samples**
35°	1	3
	2	3
	6	3
45°	1	3
	2	3
	6	3
55°	1	3
	2	3
	6	3

5.3.5 Tensile Testing and Strain Measurement

Quasi-static testing of the samples was performed using an Instron tensile testing machine (Instron 1000, Instruments and Systems for Advanced Materials Testing, Canton, Massachusetts). Samples were loaded into the testing frame and secured using steel dowel pins. Once secured, displacement rate was set to the specific value for each sample and load was initiated. A MATLAB® code was written to collect and record the load experienced by the sample over the duration of the test.

To measure strain during tests, a stereo digital image correlation (DIC) setup was used. DIC is a contact-free strain measurement method in which correlation fields are used to measure displacement of the sample. In DIC, images are taken of the sample at set intervals over the duration of the test being conducted. These images capture the contrasting speckles on the sample and their movement. The time-dependent change in the correlation fields are used to calculate displacement vectors over the surface of the sample. These displacement vectors are then averaged to calculate the strain experienced by the samples in the principal directions. The validity and accuracy of using DIC to measure the strain experienced by TBC samples has been shown by Melenka et al. . For collecting strain data with DIC, the procedure highlighted by Lepp and Carey was followed. Two scientific cameras (Basler acA3800-10gm, Basler AG, Ahrensburg, Germany) were positioned approximately 20 cm from the sample at an angle offset of approximately 22^{o} from the horizontal. Images of the sample were taken at two-second intervals and controlled by a MATLAB® code. Testing was conducted until sample experienced yielding or failure. Figure 5.7 shows a schematic of the setup used for applying loads at the specified displacement rates and collecting images for DIC.

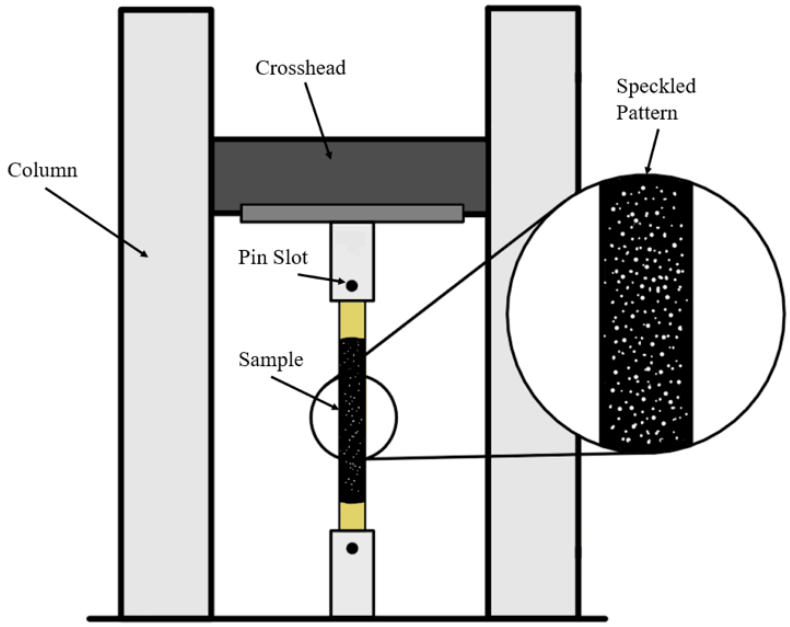

Figure 5.7. Schematic of experimental setup used for quasi-static tensile testing of TBC samples

5.3.6 DIC Image Analysis

Images collected from the testing highlighted in 3E were processed using DaVis® (LaVision, Göttingen, Germany). To further improve the results, an intensity normalization filter and a sliding average Gaussian filter were applied to each pair of images per time interval. A correlation algorithm is then used by DaVis® to produce a deformation vector map on the sample. A macro virtual extensometer function within DaVis® is finally used to average the deformation vectors and report the total average global longitudinal strain experienced by the sample over the duration of the test.

5.4 Results

Load data was assumed to be uniformly distributed over the cross-sectional area. The stress experienced by the sample was calculated by dividing load data by the previously recorded cross-sectional area. Strain data collected from DaVis® was matched to the stress data by using the time stamps from the MATLAB® code. Stress and strain data were then plotted against each other for

each sample tested in this work. For each configuration, the stress and strain data were averaged to produce a single plot. The averaged plot for each of the configurations is shown in Figure 5.8.

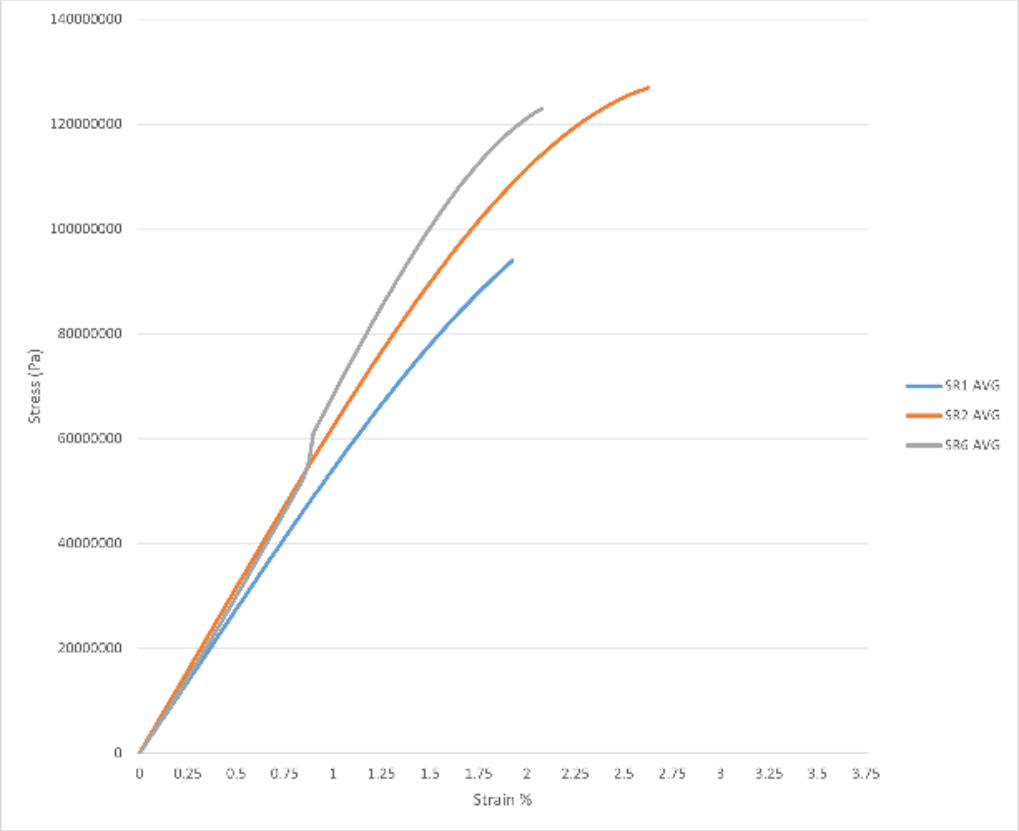

(a)

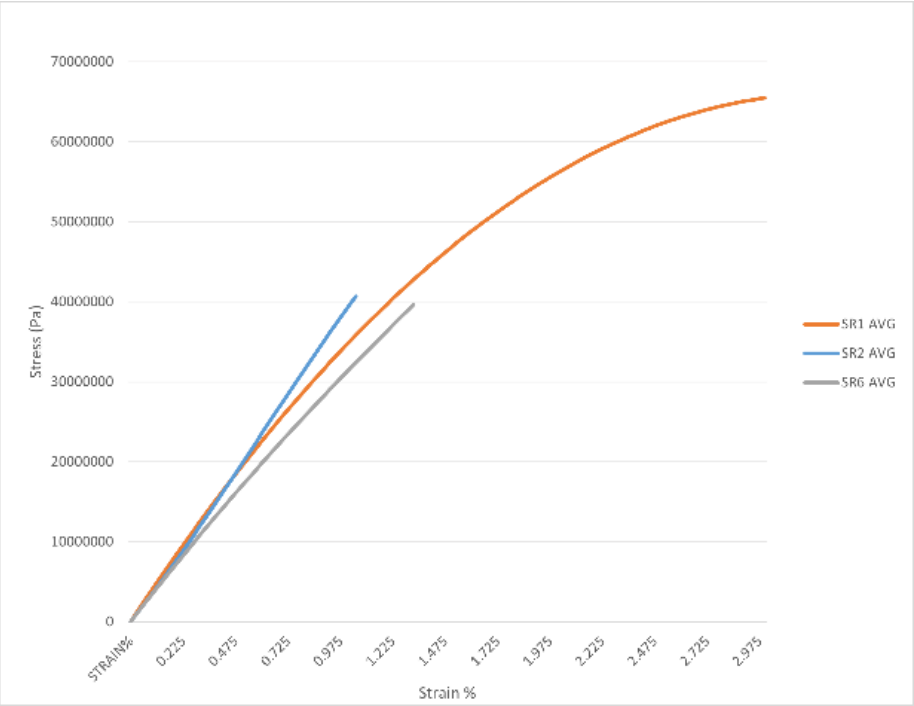
70000000
60000000
50000000
40000000
30000000
20000000
10000000
0
Stress (Pa)
STRAIN%
0.225
0.475
0.725
0.975
1.225
1.475
1.725
1.975
2.225
2.475
2.725
2.975
Strain %
SR1 AVG
SR2 AVG
SR6 AVG

(b)

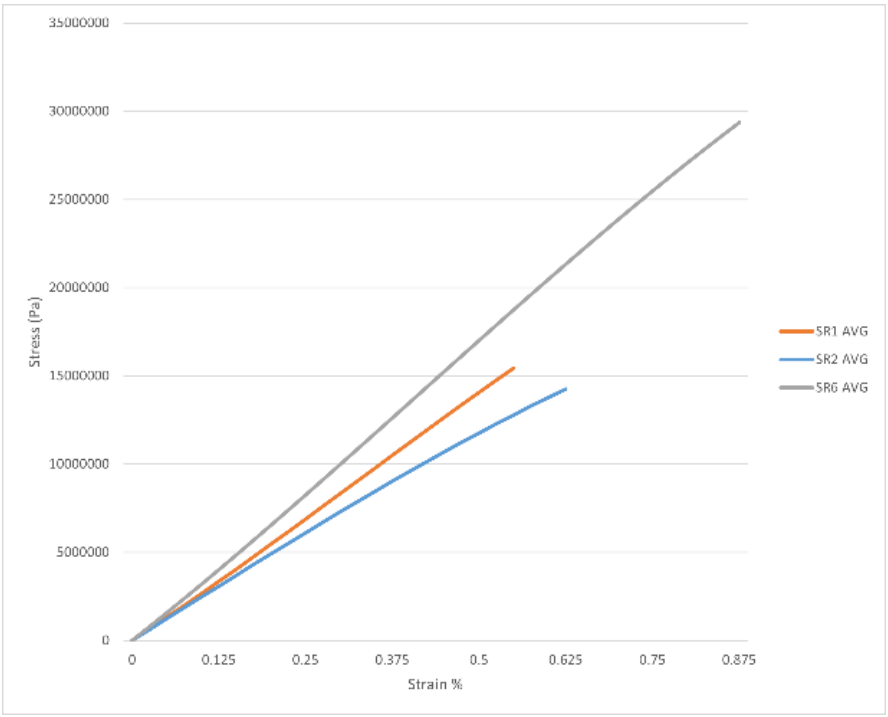
35000000
30000000
25000000
20000000
15000000
10000000
5000000
0
Stress (Pa)
0
0.125
0.25
0.375
0.5
0.625
0.75
0.875
Strain %
SR1 AVG
SR2 AVG
SR6 AVG

(c)

Figure 5.8. Averaged plots of the stress-strain behavior of each strain-rate for (a) 35°, (b) 45°and (c) 55°.

To calculate the elastic modulus for each sample, a regression-based formula was used following ASTM standard D3039. This formula is shown in equation 5.1. For each configuration, the longitudinal elastic moduli values calculated were averaged between the three samples. The standard deviation of the elastic moduli was calculated using the formula shown in equation 5.2. The calculated results are shown in Table 5.3.

$$E_x = \frac{\sum_i^K (\sigma_i \varepsilon_i) - K\bar{\sigma}\bar{\varepsilon}}{\sum_i^K \sigma_i^2 - K\bar{\sigma}^2} \tag{5.1}$$

where E_x is longitudinal elastic modulus, σ_i and ε_i are the stress and strain values of a data point, K is the total number of data points and $\bar{\sigma}$ and $\bar{\varepsilon}$ are the average stress and strain for all data points.

$$s_x = \sqrt{\frac{\sum_i^K (E_x - \bar{E}_x)^2}{K - 1}} \tag{5.2}$$

where s_x is the standard deviation of the longitudinal elastic modulus and $\bar{E}_x$ is the average longitudinal elastic modulus per strain rate configuration.

TABLE 5.3. AVERAGE MODULUS VALUES CALCULATED FROM THE TESTED TBC SAMPLES

Braid Angle (°)	**Displacement Rate (mm/min)**	E_x **(GPa)**	s_x **(GPa)**
35	1	5.49	0.560
	2	6.32	0.438
	6	5.91	0.453
45	1	3.74	0.364

	2	3.67	0.243
	6	3.24	1.20
	1	2.83	0.135
55	2	2.41	0.581
	6	3.40	2.11

5.5 Discussion

The stress-strain plots shown in Figure 5.8 coupled with the values in Table 5.3 describe the typical behavior of TBC under tensile testing. As can be seen, the longitudinal elastic modulus trends shown are to be expected from these materials. At lower braid angles (35^{o}) the architecture of the composites promotes the reinforcement phase to contribute more significantly to the overall longitudinal elastic modulus. Conversely, for larger braid angles (55^{o}), the reinforcement phase is less able to promote the stiffness of the composites, resulting in lower overall longitudinal elastic moduli values. The elastic modulus values of the 45^{o} braids are in between the 35^{o} and 55^{o} samples. These known properties of TBCs are further confirmed by the results of this work.

The influence of strain rate on the elastic modulus of TBCs can also be observed from Table 5.3. The average elastic modulus values seem to be independent of the strain rate. Within a particular braid angle, strain rate does not result in a clear increase or decrease in the averaged elastic modulus values.

The data presented in Table 5.3, however, suggests that strain rate can influence the variation between the samples. For the 35^{o} TBC samples tested, the data from this study suggests that strain rate does not influence the scatter of the data. For the 45^{o} and 55^{o}, however, the influence of strain rate is more pronounced. Between the 1 mm/min and 2 mm/min strain rates, the average deviation does not change. At the 6 mm/min strain rate, however, the variation between the 45^{o} and 55^{o} samples increases by a noticeable amount. The standard deviation for the 45^{o} tested at 6 mm/min is 1.20 GPa (compared to 0.364 GPa and 0.243 GPa at 1 mm/min and 2 mm/min respectively) and for the 55^{o} tested at 6 mm/min is 2/11 GPa (compared to 0.135 GPa and 0.581 GPa at 1 mm/min

and 2 mm/min respectively). These preliminary results indicate that at higher braid angles the influence of strain rate on the variation is more pronounced. At higher braid angles, the matrix has a more significant impact on the overall behavior of the composite. The results from the study might provide an explanation for the variation documented in the tensile properties of braided composites. Samples tested with higher strain rates may exhibit higher variation due to the more pronounced contribution of the viscoelastic matrix phase. These results seem to support the findings presented Gilat et al., however, further experimental work and analysis is required to verify these initial findings[196].

5.6 Conclusion

Although the tensile behavior of TBCs has been thoroughly investigated in literature, documented properties of these materials exhibit large variations. These variations often exceed 10% for identical samples. One potential explanation for this variation is the different testing strain rates used in studies. Although few studies have looked into the influence of loading rate on composites, most of these studies have focused on extremely high strain rates that mimic impact loading scenarios.

The purpose of this study was to investigate the hypothesis that testing strain rate influences the tensile properties of TBCs. TBC samples were manufactured at three braid angles (35^{o}, 45^{o} and 55^{o}) and tested in tension at three displacement rates (1 mm/min, 2 mm/min and 6 mm/min). Load and extension data were collected and used to plot stress-strain curves and calculate the elastic moduli of the tested samples. Initial results from this work suggest that displacement rate does not have a significant effect on TBCs at lower braid angles. For the 35-degree braids, deviation was less than 10% for all displacement rates used. At higher braid angles tested in this work (45-degrees and 55-degrees), no significant difference in deviation was noted for the 1mm/min and 2mm/min displacement rates. At the higher displacement rates of 6 mm/min, deviation increased significantly to 37% for the 45-degree braids and 62% for the 55-degree braids. These large deviations at the higher displacement rate are theorized to be a result of the pronounced effect on the matrix phase of the composites. The results of this work suggest that this manifests as increased scatter of the data. When measuring the elastic properties of 2D TBCs, the results of this work indicate that higher strain rates of 6 mm/min should be avoided to reduce data scatter.

In this chapter, we present displacement rate as a potential explanation for the variation observed in the measured tensile properties of tubular braided composites. For these materials to be used in their potential applications, this variability in reported properties can discourage selecting composites. The results of this work suggest that a potential reason for the observed variability in properties is the range of displacement rates that can be used during tensile testing. ASTM standards only suggest a rate which guarantees sample failure within a specific time frame. The results of this work suggest that for 2D TBCs, lower displacement rates (between 1 mm/min and 2 mm/min) are recommended for lower variation between the samples. Higher displacement rates (6 mm/min) should be avoided, particularly for higher braid angle TBCs. These results lend themselves to further characterization of TBCs and potentially reducing reported variation in properties by controlling displacement rate during testing.

CHAPTER 6 - Influence of Stress-free Aging on Modulus and Strength of 2D Kevlar® Tubular Braided Composites

Although the potential to achieve zero thermal expansion in braided composites was shown in chapters 3 and 4, and while chapter 5 addressed the second major component of the thesis in the variation in tensile properties of tubular braided composites. In chapter 5, we showed that at higher displacement rates, higher variation was reported in the stiffness modulus of higher angle TBCs. In this chapter, we present stress-free aging time – the time between sample manufacture and tensile testing – as a variable that influences the variability in the tensile properties of TBC samples. A version of this chapter was submitted and accepted and published in the proceedings of the CSME 2023 conference under the title "Influence of Stress-free Aging on Modulus and Strength of 2D Kevlar® Tubular Braided Composites".

6.1. Introduction

Composites consist of two or more constituents joined together to produce a non-homogenous material with tailorable properties. Braiding is a composite manufacturing technique in which yarns of one or more materials are interlaced over the length of a mandrel to create a preform. This preform is impregnated with a matrix, typically a polymer, to create the braided composite. When a cylindrical mandrel is used, the resulting hollow braided composite is called a tubular braided composite (TBC). Figure 6.1 shows a typical TBC. Due to their high strength-to-weight and stiffness-to-weight ratios, TBCs have a wide range of potential applications including construction, sports and medicine [1].

Braided preforms are typically manufactured using a rotary braider in which carriers with bobbins of the fibrous material move in predefined serpentine paths. During this motion, yarns are deposited on a translating mandrel to create the braided preform. Figure 6.2 shows a schematic of the preform braiding process. Matrix impregnation is either a manual or vacuum assisted process [154]. Several manufacturing parameters influence the final properties of TBCs, however, braid angle is the most significant in determining the final stiffness, strength and rigidity of the composites. Braid angle is defined as the angle between the yarns and the longitudinal axis of the braid. Figure 6.3 shows the braid angle labelled on a preform.

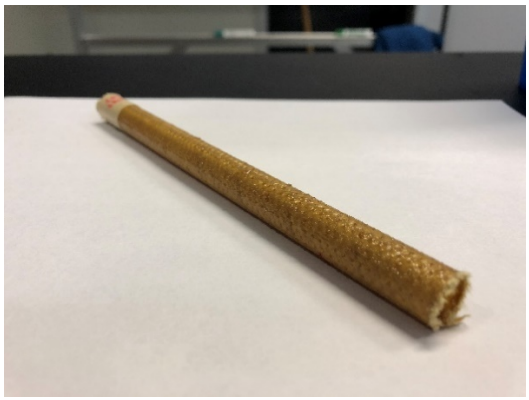

Figure 6.1. A tubular braided composite

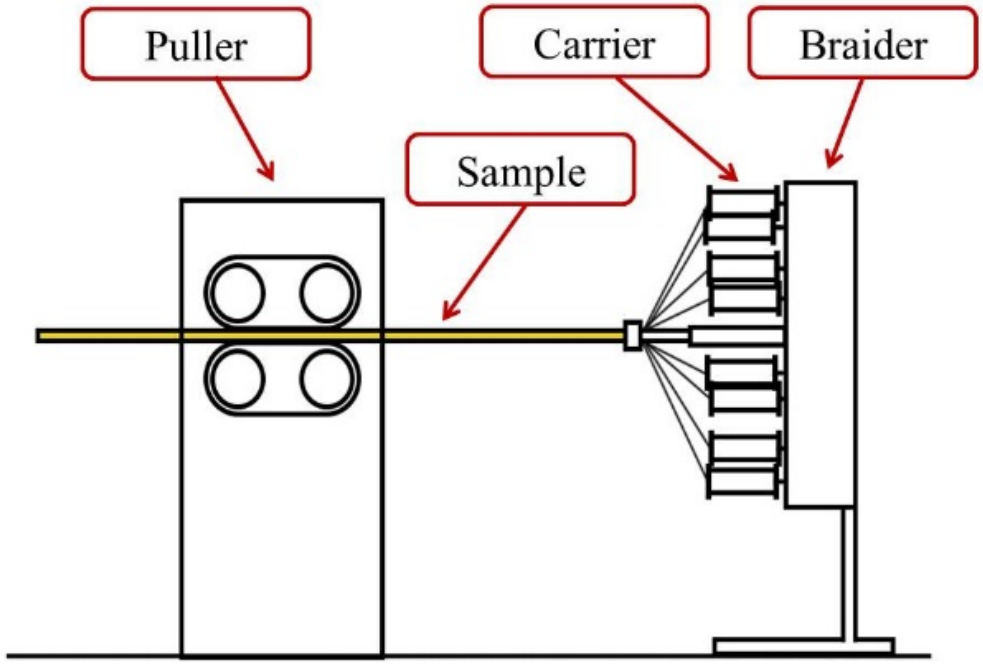

Figure 6.2. Schematic of braid manufacture line. Yarns from carriers are deposited on the mandrel pulled forward at a predetermined speed.

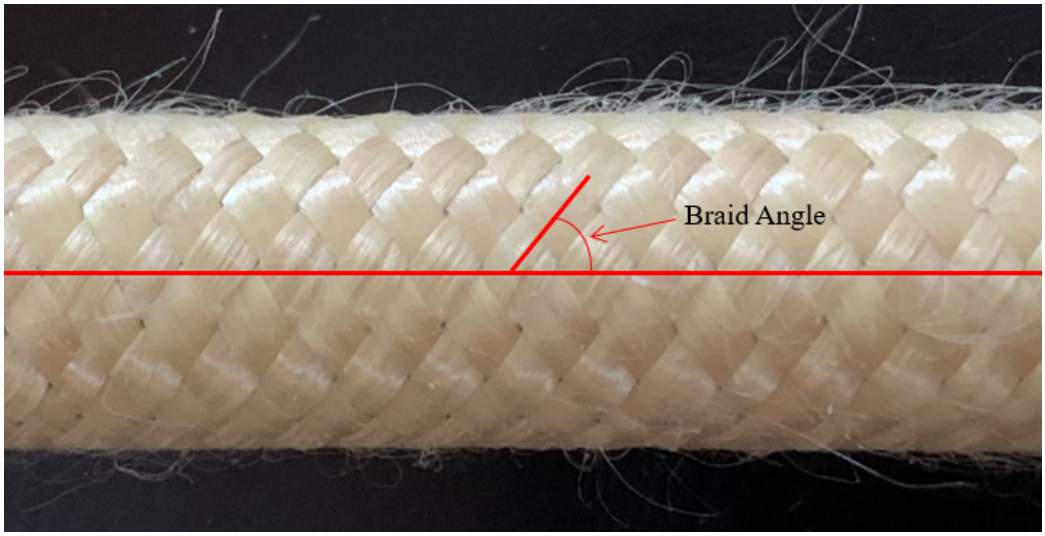

Figure 6.3. Preform showing the braid angle as the angle between the interlacing yarns and the longitudinal axis of the braid.

6.2 Literature Review

The mechanical properties of TBC are well documented in the literature. Several studies have looked into the kinematics of the braiding process. These studies have focused on developing equations that relate braider rotational speed and puller translational speed to the final braid angle [5–7,179,199]. A wealth of literature exists on the characterization of TBCs and studying their mechanical properties [9,10,13,151,160,200].

Studies with TBCs have shown high variation between the documented properties of composites manufactured with the same parameters. These variations can often exceed 10% between samples. Sample manufacturing is a primarily manual process and sample repeatability is difficult to attain. One potential aspect of sample repeatability is the stress-free aging of the manufactured composite samples post cure. This is defined as the elapsed time from cure to testing for the composites. The effect of aging on the mechanical properties of thermoset polymers and some polymer composites has been documented in a few studies. Si et al. investigated the influence of thermal-oxidative aging on the mechanical properties of epoxy asphalt. Results showed that the tensile strength of the epoxy asphalt increased due to post-cure aging [201]. Kong et al. showed that the elastic modulus of network epoxy resin increased with post-curing time over the course of seven days. Results

were explained to be a consequence of an excess of trapped free volume in the thermoset polymer after curing. As the thermoset resin approaches thermodynamic equilibrium post cure, free volume is lost. This limits the molecular mobility within the resin, increasing elastic modulus [202]. Although a wealth of literature is available on the effect of hygrothermal aging on composite behaviour, very few have looked into stress-free aging. Chiao et al. found that Kevlar® and epoxy composites displayed no change in strength after stress-free aging for five and ten years [203]. Odegard and Bandyopadhyay concluded that the studies investigating the influence of aging on the mechanical properties contradicted each other. Their review indicates that several studies disagreed as to the positive or negative impact of stress-free aging on the elastic modulus and strength of epoxy resins and epoxy composites [204].

While some studies have investigated the influence of aging on epoxy and epoxy composites, results have been inconclusive. Further, no studies have investigated the influence of the stress-free aging on braided composites. With the repeatability issue that arises during manufacturing, the post-cure aging phenomenon found in previous studies provides a plausible explanation to the high variation seen in the experimental data collected from TBCs. Accordingly, the objective of this study is to experimentally investigate the influence of stress-free aging on the mechanical properties of TBCs.

6.3 Methodology

6.3.1 Materials

To manufacture TBCs for this work, 1420 Den Kevlar® 49 (DuPont, Wilmington, Delaware, USA), Epon 826 (Hexion Inc., Ohio, USA) epoxy resin with Lindau LS-81K (Lindau Chemicals Inc., South Carolina, USA) hardener were used. Table 6.1 shows the mechanical properties of the materials used.

TABLE 6.1. MATERIAL USED IN STUDY AND MECHANICAL PROPERTIES AS FOUND IN [1] AND [198]

Material	Tensile Strength (GPa)	Tensile Modulus (GPa)	Failure Strain (%)
Kevlar 49	3.6	112-138	2.4

Epon 826 (with LS-81K)	0.074	2.7	5

6.3.2 Sample Manufacturing

Samples were manufactured following the methodology highlighted in previous work by Ead et al. [151]. Braided preforms were manufactured using a rotary maypole braider (Steeger HS140/36-91, Steeger GmbH and Co., Wuppertal, West Germany) and a puller mechanism. Yarns of Kevlar® were spooled onto 36 carriers. Carriers were loaded onto the rotary braider. Yarns were interlaced onto a 7/16'' aluminium mandrel at three different braid angles (35°, 45° and 55°). A LabVIEW™ software was used to control braider rotational speed and puller translational speeds. Preforms for this study were manufactured in a diamond one-over-one-under pattern. Figure 6.4 shows an image of a sample preform manufactured at 35° and a schematic of the unit cell of the manufactured TBC preforms.

Braided preforms were carefully transferred onto Teflon mandrels and manually impregnated with a 1:1 weight mixture of Epon 826 epoxy resin and Lindau LS-81K hardener. Following the resin manufacturer data sheet, samples were cured in a square oven at 66°C for 90 mins, 85°C for 60 minutes and 150°C for 180 minutes [198]. Once the cure cycles were completed, composite TBC samples were removed from the Teflon mandrels and cut to a sample length of 7 inches. The cross-sectional area of the TBCs was measured using a digital Vernier caliper (Mastercraft Digital Caliper 6-inch, Mastercraft tools, Kirkwood, MO) and recorded. For each sample, cross-sectional area was measured and calculated at three points along the length of the TBC sample. Cross sectional area measurements were then averaged. Figure 6.5 shows three manufactured TBC samples, one at each of the tested braid angles used in this study.

For post-cure aging, TBC samples were stored in airtight containers at standard ambient temperature and pressure. Three aging periods were chosen for this work: 0 weeks, 2 weeks and 6 weeks based on previous research [202]. Three samples were tested per braid angle and aging interval for a total of 27 samples. Table 6.2 shows the experimental matrix of this study.

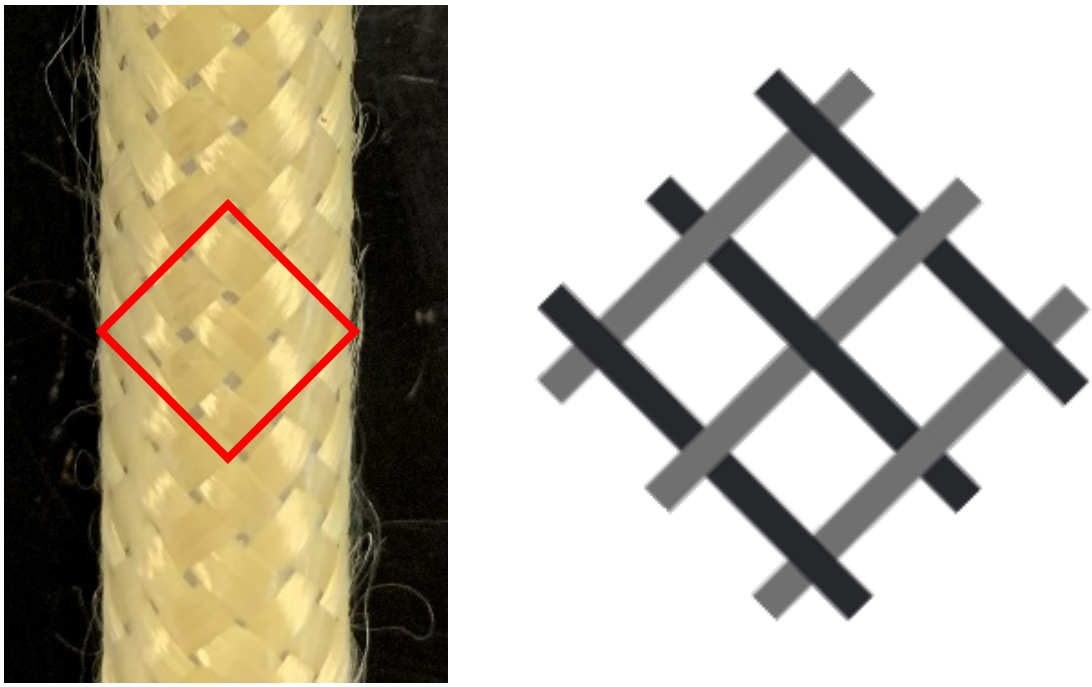

(a) (b)

Figure 6.4. Image of a (a) 45º preform highlighting the one-over-one under pattern and a (b) unit cell schematic for a regular braid preform.

Figure 6.5. Cured TBC samples manufactured at three braid angles, 35, 45 and 55 degrees.

TABLE 6.2. TBC SAMPLE EXPERIMENTAL MATRIX

Angle	Aging Time (weeks)	Number of Samples
35°	0	3
	2	3
	6	3
45°	0	3
	2	3
	6	3
55°	0	3
	2	3
	6	3

6.3.3 Sample Testing

Prior to testing, each sample was attached to steel end tabs using two-part epoxy (Henkel AG & Company, KHaA, Düsseldort, Germany). With end tabs attached, TBC samples were tied to aluminium rails with hose clamps for 24 hours to allow the two-part epoxy time to cure while maintaining braid alignment. To prepare samples for strain measurement, tabbed TBC samples were painted in black matte paint (Painter's Touch Flat Black, Rust-Oleum Corp, Concord, ON, Canada). Once painted and dried, a white speckle pattern (4230 Transparent White, Auto Air-Colors, East Granby, CT) was applied to the sample using an airbrush (Paasche H Series, Paasche Air Brush Co., Chicago, IL). The white speckles against the black TBC samples provided enough contrast for strain data collection. A sample TBC prepared for testing is shown in Figure 6.6.

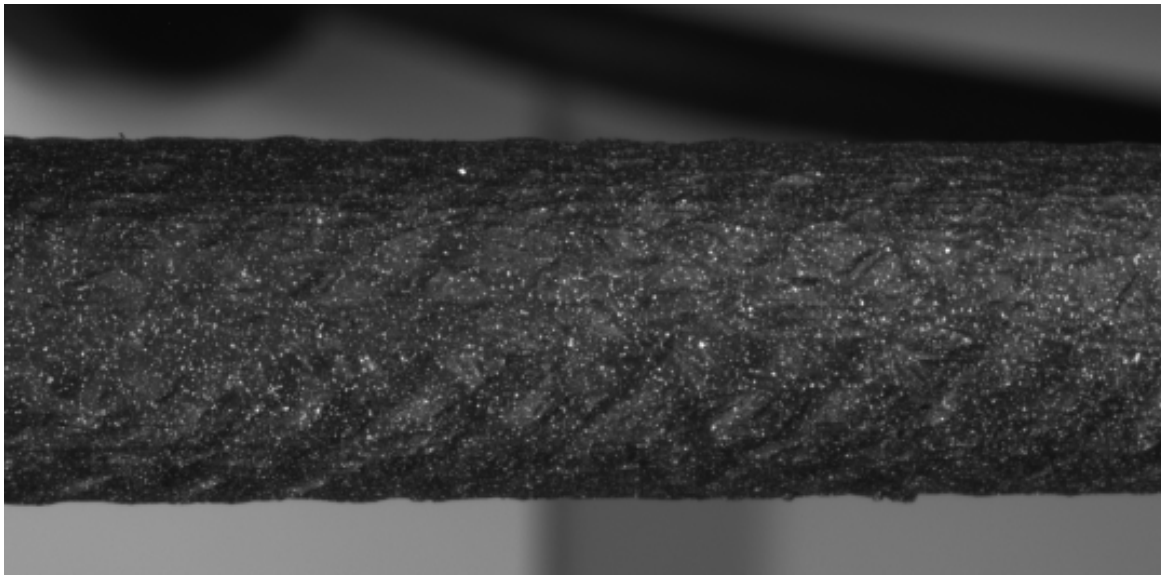

Figure 6.6. Zoomed in image of a 45° speckled TBC sample.

Quasi-static tensile testing of TBC samples was performed using a hydraulic MTS machine (MTS Systems, Eden Prairie, MN) following ASTM standard D3039 [98]. Samples were pinned to the MTS grips using metal dowels. To apply the tensile loads to the samples, a 1000 lb load cell was used. For this study, samples were loaded at a strain rate of 1 mm/min as this resulted in sample failure within 1 to 10 minutes of test initiation as specified by ASTM standards. A data acquisition program collected the load data from the MTS machine every 0.01 seconds. To collect the strain data, an imaging technique similar to that highlighted in Lepp and Carey was followed [205]. Two scientific cameras (Basler acA3800-10gm, Basler AG, Ahrensburg, Germany) were positioned at an approximately 22° offset from the horizontal. The cameras acquired images of the samples every two seconds throughout the duration of the tensile test. A MATLAB® code was written to control image acquisition and file storage for each sample tested. Tensile load was increased until yielding was observed in the load response of the sample or pseudo-necking occurred. Figure 6.7 shows the experimental setup for the quasi-static tensile tests conducted in this study.

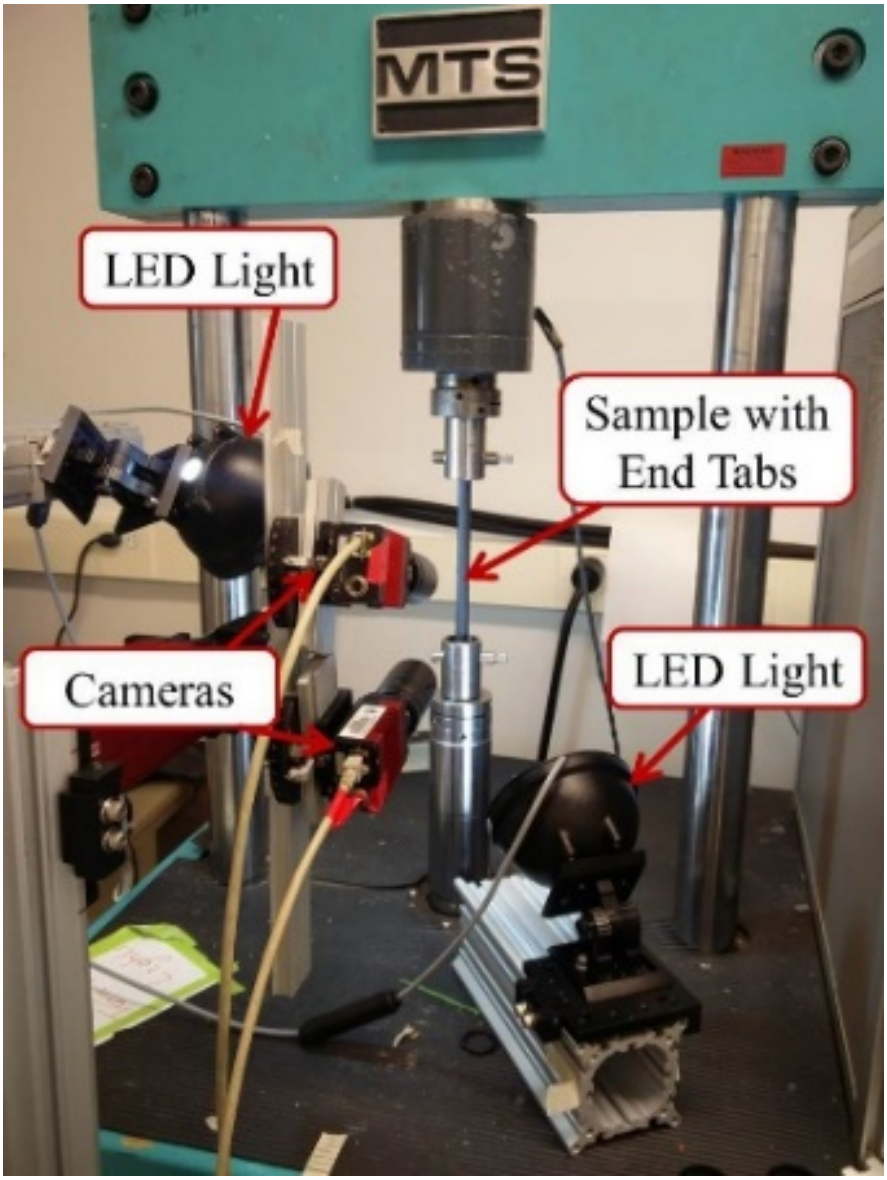

Figure 6.7. Experimental setup used for quasi-static tensile testing of aged TBC samples

6.3.4 DIC Image Analysis

Images collected during the tensile tests were processed using 3D digital image correlation in image processing software DaVis® (LaVision, Göttingen, Germany). DIC is a contact-free strain measurement technique that traces the motion of speckles between images throughout the tensile test and uses a correlation algorithm to calculate deformation vectors between successive images. These deformation vectors can then used to produce a strain map along the braid in the three

principal directions. The validity and precision of using 3D DIC to analyse strain across a tubular braided composite has been justified by Melenka et al. [11]. Once a strain map is produced, DaVis® allows users to calculate the average global strain over a length of the sample with a virtual extensometer function. Prior to producing deformation and strain results, an intensity normalization filter and sliding average Gaussian filter were applied to each pair of images. These improve the ability of the software to accurately calculate the displacements of the speckles on the braid surface. Once displacements were calculated for each pair of images, a virtual extensometer was used to calculate the average global longitudinal strain from each pair of images. Figure 6.8 shows the strain map on a sample with the virtual extensometer highlighted.

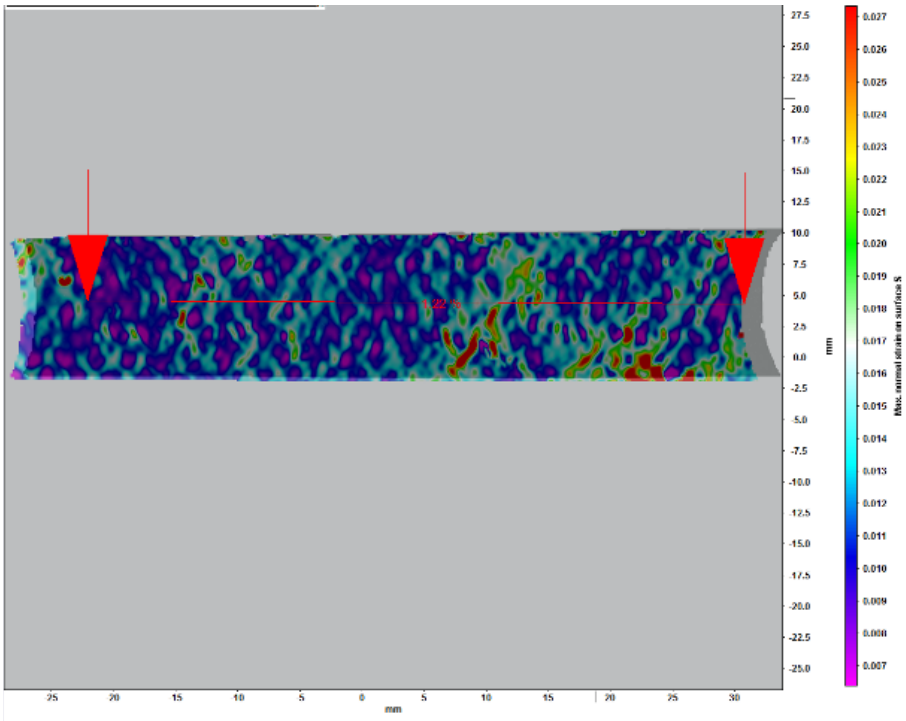

Figure 6.8. Maximum surface strain on 55° braid immediately before failure. Virtual extensometer length is indicated by the red line between the two arrows.

6.4 Results

Load data collected and converted from the load cell was converted to stress data by dividing by the cross-sectional areas measured post-sample manufacture. Stress data was plotted against the corresponding strain data produced from DaVis for each of the 27 tested samples. For each

three samples tested at a particular braid angle and aging time, the stress-strain plots were averaged. Figure 6.9 shows the average stress-strain results for each of the testing conditions.

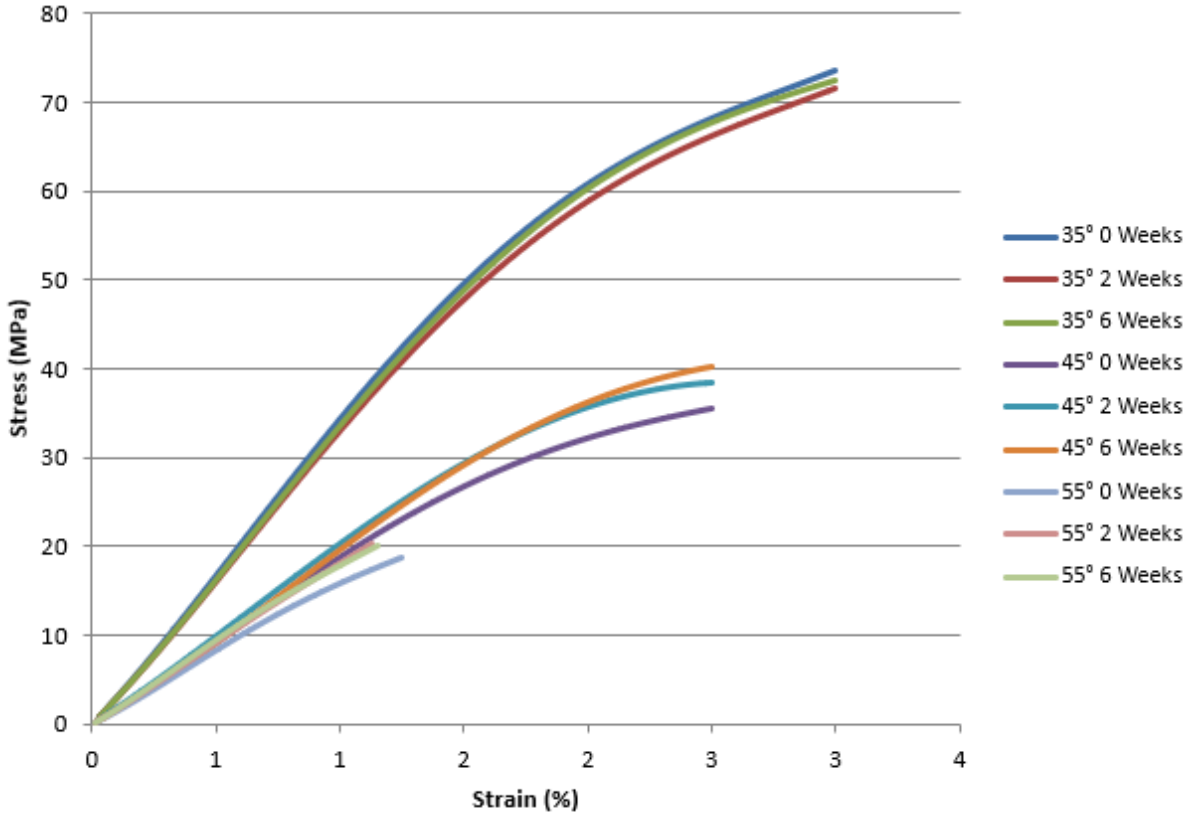

Figure 6.9. Plots of the average stress-strain behavior of each experimental condition tested.

To calculate the longitudinal elastic modulus of the tested samples, ASTM standard E111-17 for measuring young modulus was followed. Equation (6.1) shows the statistical formula used to calculate the longitudinal elastic modulus from the collected stress and strain data [206]. Yield strength was measured using the 0.2% strain offset method. Table 6.3 shows the results of elastic modulus and yield strength from the data collected.

$$E_x = \frac{\sum_i^K (\sigma_i \varepsilon_i) - K\bar{\sigma}\bar{\varepsilon}}{\sum_i^K \sigma_i^2 - K\bar{\sigma}^2} \tag{6.1}$$

where E_x is longitudinal elastic modulus, σ_i and ε_i are the stress and strain values of a data point, K is the total number of data points and $\bar{\sigma}$ and $\bar{\varepsilon}$ are the average stress and strain for all data points.

TABLE 6.3. AVERAGE MODULUS AND STRENGTH VALUES CALCULATED FROM THE DIFFERENT TESTED TBC SAMPLES

Braid Angle (°)	**Aging Time (weeks)**	**Average Elastic Modulus (GPa)**	**Average Yield Strength (MPa)**
35	0	3.45±0.15	59.9±0.32
	2	3.34±0.13	57.7±2.08
	6	3.39±0.02	59.8±1.02
45	0	2.03±0.05	32.5±2.49
	2	2.05±0.05	34.7±2.39
	6	2.13±0.02	35.7±1.87
55	0	1.78±0.05	18.65*
	2	1.92±0.09	22.08*
	6	1.94±0.07	20.83*

* values for yield data could not be collected due to sample failure, fracture strength is reported for these samples.

6.5 Discussion

Stress-strain plots in Figure 6.9 as well as the average experimental results in Table III show typical properties of TBCs. TBCs manufactured at lower braid angles have higher longitudinal modulus and strength. At these lower angles, orientation of the yarns is closer to the longitudinal direction of the braid results in higher stiffness imparted by the reinforcement phase. The opposite

is seen at higher braid angles. These results agree with the available literature on the tensile properties of TBCs.

For the influence of aging time on the mechanical properties of tubular braided composites, initial results from this study seem to indicate that stress-free aging does not have a significant impact on the stiffness and strength of TBCs. Percentage changes in the average elastic modulus ranged from -3.30% for the 35° TBC samples between 0 and 2 weeks to 7.65% for the 55° TBC samples between 0 and 2 weeks. Data collected for this study shows that percentage changes become larger and more positive as braid angle increases. One possible explanation for this phenomenon is related to braid architecture. At higher braid angles, the resin contributes more significantly to the overall longitudinal behavior of the TBC. The influence of stress-free aging on the resin found by Kong et al. would explain the increased stiffness and strength of resin and the increase in TBC stiffness and strength at higher braid angles. Similar results were found for the yield strength data [202].

6.6 Conclusion

The purpose of this study was to investigate the influence of post-cure stress-free aging on the properties of TBCs. Although some literature has investigated the influence of aging on epoxy and epoxy composites, results from these studies have showed mixed results with regards to the changes in the properties of composites as related to post-cure aging time. Stress-free aging was hypothesized to be a potential reason behind the large variation seen in the tensile data collected from TBC. No literature is available on the impact of stress-free aging on the behaviour of TBCs.

TBC samples were manufactured at three different braid angles (35°, 45° and 55°) and tested in tension after 0, 2 and 6 weeks of curing. Three TBC samples were tested for each configuration. DIC was used to collect strain data for this study. Initial results from this work seem to indicate that post-cure aging time does not have a significant on lower braid angles, however, might have a higher impact on the behaviour of higher angle TBCs. More experimental studies involving more braid angles and large post-cure aging times are critical to confirm the preliminary results of this work.

In this chapter, we presented stress-free aging time as a potential explanation for the variation observed in the measured tensile properties of tubular braided composites. The results of this work

suggest that a potential reason for the observed variability in properties is the time elapsed between sample manufacture and tensile testing. The results of this work suggest that for 2D TBCs, longer stress-aging times (between 2 weeks and 6 weeks) increase the measured tensile strength and modulus for 45-degree and 55-degree braids, but had no significant effect on 35-degree braids. Future characterization studies on TBCs should consider the time between sample manufacturing and testing that can influence the measured properties, increasing the variability between the tested samples.

CHAPTER 7 - Life cycle analysis for green composites – a review of literature including considerations for local and global agricultural use

The previous chapters present experimental and analytical research to address some of the gaps in introducing tubular braided composites in their intended applications. In chapters 3 and 4 we investigate the thermal expansion behaviour of Kevlar®/epoxy TBCs and in chapters 5 and 6 we show the importance of considering displacement rate and stress-free aging time in characterizing the tensile properties of Kevlar®/epoxy TBCs. Although this thesis has focused on Kevlar®/epoxy, synthetic fibres and matrices have a significant environmental impact. The use of natural fibres and matrices in tubular braided composites has been sparsely investigated in the literature. In addition to a lack of studies characterizing these materials, the difference in environmental impact between synthetic and green TBCs has not been documented in literature. In this chapter, a life cycle analysis comparison is conducted to evaluate the influence of selecting green fibres and matrices. A version of this chapter has been submitted and accepted as an article in the Journal of Engineering Fibres and Fabrics under the title "Life cycle analysis for green composites – a review of literature including considerations for local and global agricultural use".

7.1 Introduction

With increasing awareness of human-driven climate change, there is a push to take steps to reduce environmental impact and carbon footprint. One approach to decrease the amount of carbon dioxide and other greenhouse gases (GHG) released to the atmosphere is to incorporate sustainable practices into commercial production and consider the environmental effects of the product for production, use, and end of life-cycle/recycling phases. Although industrialization has enabled inexpensive mass production, the vast amount of resources used and waste produced contributes to the depletion of natural resources and pollution.

Life cycle assessment (LCA) is a tool that can be utilized to determine the total environmental impact of a product throughout its lifetime [207]. An important aspect within LCA is tracking and estimating the inputs and outputs of resources for a specific product and/or process. By completing an LCA, the environmental impact of a product can be compared to another product and improved upon. The different stages of a product's life can be assessed to determine where the most resources

are used or the most GHG are released so that the process can be improved upon towards a more sustainable approach.

Fibre-reinforced composites are materials composed of fibre bundles embedded in a matrix material. In this review we will focus on polymeric fiber reinforced composites where, typically, a polymeric resin, that is homogeneous and isotropic, is used as the matrix material. Composite materials are designed and built to combine the properties of their constituents to produce a superior end-product. Fibre-reinforced composites can be manufactured in several ways depending on the size and orientation of the reinforcement, as well as the type of matrix material used. Synthetic fibres are conventionally used in these composites because their properties are more consistent and controllable than naturally sourced fibres. However, entirely synthetic composites can have a large, negative environmental impact. This is a result of the resources required and waste disposed to produce and process these materials. Composites made of synthetic fibres are not biodegradable and cannot be recycled at the end of their life due to the dissimilarity between the fibres and the matrix.[208] Furthermore, most composites are manufactured using petroleum-based synthetic polymer matrices. These non-biodegradable artificial polymer matrices contribute to global warming, accelerate land fill deposits and promote toxic environmental effects.[209]

In contrast, natural fibres are biodegradable at their end-of-life, or they can be incinerated for energy return. Further, if the matrix is also biodegradable, the entire composite can be decomposed at the end of its usable life.[210] Usage of biopolymer matrices made from renewable materials also minimizes human dependence on non-renewable fossil fuels. A bio-composite is made from either a natural fibre reinforcement or natural matrix. A “green” composite is made from bother natural fibres and natural matrix. Thus, developing “green” composites with significantly lower environmental impact than synthetic-based composites is promising. Life Cycle Analysis (LCA) can be applied to present environmental comparisons between natural fibre composites and synthetic fibre composites in all stages of their life cycle. These comparisons are important to determine the sustainability of further developing green composites.

The purpose of this review is to present and examine the requirements of LCA when applied to green composites while incorporating aspects of economic impacts (life cycle costing) and durability. Additionally, this review will cover an introduction to choosing a type of natural fibre with a consideration of location. This will include consideration for a case study of natural fibre

cultivation in Alberta, Canada. This paper aims to demonstrate the value of this analysis in all future work that wish to undertake valuable R&D and technological development using green composites.

7.2 Life Cycle Assessment

LCA is "*an analytical tool specifically designed to assess the environmental impacts relating to the whole production chain of a good*".[211] To ensure a complete analysis, LCA also examines the product's impacts during use and at the end-of-life disposal. As a tool, LCA is very broad and can be applied to various industries, areas and types of products. Thus, a guideline cannot specify how to carry out each individual step because the exact procedure can vary drastically between products. Rather, the International Organization for Standardization (ISO) has organized a general protocol to follow and necessary steps to complete an LCA. However, as ISO defines LCA, it does not involve an analysis of other factors apart from environmental, such as social or economic factors which are important considerations.[207]

LCA is useful to analyze a single product, but can be used to compare two products. In this case, LCA assists in determining if a new product, when compared to a previous one, would be more or less environmentally friendly.[212] In the process of performing an LCA, the steps of a product's life are broken down so that data of each significant input and output of resources and energy can be accounted for. This rigorous procedure is vital to the design process so that changes can be made in phases of the product's life cycle where there is potential to improve environmental effects.[213] Accordingly, LCA is an important step in the development of green composites as it enables the production of material with much lower environmental impacts than its synthetic equivalents.

7.2.1 Basic Requirements

ISO has established guidelines for LCA to harmonize the basic procedure of studies. ISO 14040 outlines the principles and framework of LCA, and ISO 14044 outlines the requirements and guidelines of LCA.[214,215] From the standards, the steps are (1) identify the goal and scope of the analysis, (2) compile a life cycle inventory (LCI), (3) complete a life cycle impact assessment (LCIA) and (4) interpret the results.[207] These steps are described below.

7.2.1.1 Goal and Scope

From ISO 14040, the first step of LCA is to define and clearly state the goal of the study. This involves explaining the purpose of the analysis and the applications of the results.[207] The scope of the study must also be defined, which includes setting system boundaries. The system boundary defines where the system is separated from the environment so that all inputs and outputs can be tracked. With the system boundary, it should also be stated and reasoned what stages of the product's life cycle will be analyzed. Most studies use a cradle-to-grave approach, which is defined from production to disposal.[216] It is important to distinguish the boundary for the production and the end-of-life stages, where systems like forests, fields and landfills are involved. Consistency is critical when determining where the system is divided from the environment.

A functional unit must be established in this step. The functional unit is a set amount of product which is to be analyzed, or some other quantity that describes what is being studied. By establishing a functional unit, all the input and output flows of all processes in a system can be compared and compiled. Further, a functional unit is useful for a comparative study of two different materials.[217] In this case, the overall input and output value units are equivalent between the two types of materials so that individual environmental impacts are simpler to compare. While the functional unit is often an amount of product, it can also be a value of time for the product to be in use. This definition depends on the function of the product. An example of a time-based functional unit is illustrated in an LCA study by Pegoretti et al.[218], which compared three acoustic panels in the Brazilian automotive sector. One was made of mainly synthetic plastics and the other two were made of recycled cotton. By following ISO 14040, the goal was defined to "*evaluate and compare the potential environmental impacts of the three acoustic panels… considering the environmental concerns of the automotive industry in Brazil.*". For the scope of the study, it was stated that the LCA would consider three phases: production, use and end-of-life. The functional unit of the study was "*maintaining an acceptable acoustic level inside a vehicle during 10 years.*" Although this is not a unit to describe the amount of product made, it is applicable for this study. The panels are made such that they would all maintain the acceptable acoustic level throughout their use over a 10-year period. They all achieve the same function, although the amount of product used for each panel may be different. It is important to note that there are no calculations for data collection completed in this step.

7.2.1.2 Life Cycle Inventory

The second step of LCA is life cycle inventory (LCI) analysis. As the most time-consuming and extensive phase, LCI requires identifying and quantifying the resource flows for the system.[216] The purpose of LCI is to create an inventory of all inputs and outputs of materials, wastes and natural resources for all processes, in relation to the functional unit.[219] Before a quantitative analysis, all unit processes must be defined inside the system boundaries. Unit processes are elementary steps in a product's life that can consist of a single or grouped operation. All the unit processes can be connected to form the product system.[207] Next, all flows of water, energy and raw materials into the system, the waste released to the atmosphere, land and water and use of land are traced and recorded for each unit process.[213] Here, it is important to be detailed and consistent with system boundaries. A flow chart can then be made to visualize and connect the flows for unit processes.[207] The flows must be quantified so that they are relatable in terms of the functional unit. To help with data accuracy and consistency for LCA, databases have been created for common areas of study such as energy, waste treatment and chemical production.[213] However, it would not be practical to have a complete database for LCA due to the vast number of different materials and specific processes that are possible. Hence, the databases could be too general for a thorough analysis or for LCA in a different sector. For these reasons, or for lack of available data, some processes would require the collection of primary data for a complete analysis of a more specific case study. Once data collection is completed, it is organized into a list or "inventory table" to be further analyzed in the next step.

In a study by Leejarkpai et al.[220], three boxes of polystyrene (PS), polyethylene terephthalate (PET) and polylactic acid (PLA) were compared for their impact on global warming using cradle-to-grave LCA. PS and PET are both petroleum-based plastics, whereas PLA is a bio-based plastic. In the LCI step, the system was broken down into unit processes. However, unit processes were compiled into two generalized stages of the product's life cycle: production and waste management. For production, data for all three boxes were gathered from a previous LCA study. Waste management was separated into transportation of used boxes, sanitary landfill and controlled composting. The transportation data was estimated based on the distance travelled and the amount of product transported. Sanitary landfill disposal and controlled composting data were obtained from a primary biodegradation study.

The LCI method described here is used in what is called "process-LCA", which is the most extensive and most popular method. There are ways to simplify this method, such as vertical cut-

offs to reduce the detail in the information required for each unit process. An alternative method exists based on industry input/output called "I/O-LCA". Modelled with supply chains using economic databases, I/O-LCA focuses more on combining economic analysis with environmental assessment. Applications suitable for I/O-LCA utilization include assessing the overall environmental impact of a system or for comparing highly dissimilar options on a regional, national or international level.[213]

7.2.1.3 Life Cycle Impact Assessment

The third step of an LCA process is a life cycle impact assessment (LCIA). The purpose of LCIA is to determine and evaluate the overall environmental impacts within the system. This step builds on the analysis completed in LCI because the outcome of LCI, the inventory table, is usually very long and complicated, and requires further assessment.[207] To do this, LCIA converts the results of the inventory analysis to common units within several impact categories. In the ISO standard for LCA, LCIA is broken down into steps, some of which are not mandatory. In order, these steps are: (1) selection of impact categories, (2) selection of impact category indicators, (3) classification of inventory results into categories, (4) characterization, (5) normalization, (6) grouping and (7) weighting. The first four steps are mandatory, whereas the remaining three are optional.[207,221]

First, impact categories must be selected. Impact categories are groupings of resource flows and environmental factors that cause a common and general type of damage. The impact categories must also follow the goal and scope of the study. In general, ISO defines three broad impact categories to be included: damage to human health, ecosystem health and resources.[207] If the LCA uses these general categories, the study can be classified as an "end-point damage" model. However, a "mid-point damage" model can instead be used when impact categories are made more specific.[216] For example, some of these categories used could be climate change, ozone depletion, human toxicity and acidification. Further, land use is an impact category that has been used more frequently. Although it may seem unnecessary, land use is an important impact to consider since an occupied area is a limited resource.[212] Once the impact categories are established, they must be further defined in terms of characterization model, category indicators and characterization factors. This definition is usually based on global models unless the category is a local issue. Characterizing the impact categories will assist in the third step, which is the process of assigning inventory results. Each inventory result is classified into an impact category in a qualitative manner

for further analysis. In step four, characterization is when all the results in each impact category are given a common unit so that the numbers can be aggregated to get a final value for the category, called the category indicator result. The complete list of category indicator results is then called the environmental profile.[207]

The first four steps in LCIA are required but three further steps can be taken to recognise the information and prepare it to relate to current trends and previous studies. Normalization is the first optional step, which involves expressing the category indicator results in relation to reference information.[207] When compared, the magnitude of the results cannot be interpreted as the degree of impact on the environment. For instance, a category with a large value could cause less critical damage than a category with a smaller value. This is due to impact categories often having different units, so the values after characterization may not reflect the actual impact. In the grouping step, the results of all impact categories are organized by ranking based on the importance of their impact.[221] Weighing occurs in the final step for the normalized, grouped indicator results. For each result, a numerical weighting factor is generated based on the determined importance. This factor is then multiplied by the indicator result value to yield a weighted value.[207]

7.2.1.4 Interpretation of Results

The final step of LCA is an overall analysis and interpretation of the results in LCI and LCIA with the purpose of answering the initial study goal.[217] This step evaluates and analyzes the results so that conclusions and recommendations can be made.[207] Part of this analysis is to determine the consistency and reliability of the data and procedure. Limitations presented by the study should also be discussed. To fulfill the purpose of the LCA, the results must meet the goal and be within the initial scope. If not, the LCA may have to be redefined and repeated as it is not complete.[217]

Although the above information is comprehensive, more information about the LCA process can be found in literature.

7.2.2 LCA of Green Composites

LCA is a valuable tool for the production and development of green composites. Considering time and resource investments, LCAs aid in determining if advancing these composites is worthwhile. To accomplish this, LCA is typically used as a comparison tool for petroleum-based

composites and biodegradable composites. Between fully synthetic composites and fully degradable composites, a natural fibre reinforced petroleum-based matrix is also possible. LCAs can have a "cradle-to-gate" analysis, where only the production phase is analyzed to compare to other studies. However, "cradle-to-grave" assessments could be more important for green composites since the end-of-life disposal can vary significantly from those of synthetic composites.[222]

A central aspect of an LCA study is the choice of impact categories such that they reflect the goal and scope of the study. Green composites are typically sourced from crops produced by agricultural processes. Therefore, it is likely the LCA will have impact categories that are influenced by agriculture. For example, some common impact categories for these studies are: global warming potential, acidification, eutrophication, abiotic depletion, and land use.[212,218,223–225]

7.2.2.1 Production Phase

The production phase is typically where the most materials and resources are used, and the most wastes are produced. Both the fibres and the matrix must be considered separately in this phase as they both will contribute significantly to resource flow.[226] For the fibres, production typically includes crop growth, harvesting, transportation and manufacturing. The matrix likely requires an extraction or processing of raw material, then transportation and manufacturing. Like natural fibres, many biodegradable matrices are made from agricultural crops.[222] During the production phase in an LCA for green composites, it is important to consider location. First, the crops must be grown in a climate that supports their growth. Then, if that optimal growth location is far from the manufacturing location, the raw material must be transported. Additionally, location can be significant for determining how the area responds to certain practices. For these reasons, it may be less accurate to use secondary data rather than collect primary data for the study.

Since the production of raw materials for green composites requires land and influences the surrounding area, LCA should incorporate land use impacts as well. In recent studies, natural land is considered a resource as the use of land for agriculture reduces the amount of available land.[224] As the characteristics of land varies with geographical region, the impact on the land will also change, meaning the location of the production should be considered.

The production of natural fibres involves plowing and sowing of land, irrigation, fertilization, pest control, then harvesting and processing. Environmental impacts of each production step can vary significantly between fibre types based on what the crop requires for optimal growth. For instance, hemp cultivation typically does not require the use of pesticides or herbicides since it naturally deters insects and suppresses harmful fungi growth.[212] Plowing and sowing requires use of machinery and fossil fuels for power, with equipment also releasing pollutants into the air. Depending on the system boundaries, the impact of the machinery can be considered as well.[227] Agricultural land often lacks the necessary nutrients for crops to thrive. Consequently, usage of fertilizers is common, but contributes to eutrophication in the surrounding ecosystems. Eutrophication occurs when high levels of nutrients are present and encourage excess biomass production in aquatic and terrestrial ecosystems, resulting in a harmful imbalance in the environment. During growth, herbicides and pesticides are usually required to protect crops from invasive weeds and insects. Although this practice will provide protection for the agricultural land, the chemicals used will negatively impact the surrounding area.[224] Once fully grown, the crops will again require machinery to be harvested.

After harvesting, transportation is likely to occur to move the raw, harvested waste to a manufacturing location, and then again to transport the final product to the consumer. The transportation aspect is typically characterized by distance travelled and estimating the type and weight of the vehicle, which then leads to the amount of gas used.[227,228]

Processing of raw material prior to production of the final product could vary significantly between types of plants and the intended use. Further, different machines could be used depending on the manufacturing technique. Therefore, the focus is to determine significant resource inputs and outputs for the process. Waste produced by harvesting and processing could be used as fuel to burn and produce heat for a different process. In a study by la Rosa et al.[228] on cork polymer composites, the scraps from the production were burned for heat for the boiling process. Accordingly, utilizing industrial by-products as fuel sources can minimize the environmental impacts of harmful, non-renewable fuels.

7.2.2.2 Use Phase

Typically, the use phase can be omitted in an LCA because the products compared in the study have the same, or similar, uses. Therefore, they should produce and consume a similar amount of resources over their use phase.[222] In a study by la Rosa et al.[212], a comparison LCA of glass fibre and a natural fibre composite was performed. The composites were manufactured to be elbow-fittings for a pipeline. The use stage of this study was excluded because it was assumed that this stage would be equal for both composites. Although such assumptions are common amongst LCA studies, they are not always valid. Often, material durability has considerable influence on environmental impact, since longer service lives lead to less material maintenance and replacement. However, inadequate knowledge of use phase behavior and deterioration processes limit proper consideration of the use phase within LCA studies, especially for unconventional materials like green composites.[229] Applications of green composites are limited due to many durability-related parameters, including ambient moisture content, biodegradation, UV exposure and weathering effects.[229–233] A weathering study conducted on green composites by Miller et al.[229] has signified the importance of geographic location and weather conditions on use phase material degradation, with warm, moist climates inducing faster degradation rates and more severe ecological effects.

Differences between natural and synthetic fibre use should be noted when the product's purpose is influenced by the weight of the component.[222] Natural fibres in green composites can have a higher volume fraction, but lower density than synthetic fibre composites. A benefit of this property is the reduced weight of green composites. In the automotive sector, green composites are attractive since components can be made to be lightweight by substitution of synthetic fibres for natural fibres, thereby improving fuel efficiency.[234] Several advantages arise from enhancing fuel efficiency within automobiles. A lower rate of fuel consumption is economically beneficial as money can be saved on fuel cost overtime. Additionally, better fuel efficiency decreases environmental impacts as less non-renewable resources are used and less pollution is released to the atmosphere. However, it is important to note again life expectancy of the component in this analysis and consequently the need for replacement parts.

7.2.2.3 End-of-Life Phase

For natural fibre composites, consideration should be shown for how the composite will be disposed of at the end of its usable life. Green composites could potentially have favorable end-of-life-phase environmental effects compared to typical synthetic fibre composites. Composites with synthetic fibres and a non-biodegradable matrix typically cannot be reused or recycled inexpensively, often ending up in landfills instead. However, using landfills is expensive and may not fully prevent the leaching of waste into the environment.[235] It is important to find a way for all composites to be waste-free at the end of their usable life.

Incineration is an alternate option for natural fibre composites. Plant fibres have stored carbon when harvested, which is retained throughout its use. At the end of the composite's service life, these fibres can be incinerated to release the stored carbon as energy. Burning natural composite will still produce carbon dioxide. However, this carbon was sequestered by the plant from the atmosphere and stored throughout its life, so there is theoretically no increase in emissions.[234]

Another option is to only use materials that are biodegradable, so that at the end of their life, they can be broken down naturally without any waste left. Further, if both the matrix and the fibres are biodegradable, they do not need to be separated at disposal. Biodegradable materials need controlled conditions and bacteria or enzymes to break them down. If the material is fully compostable, it can break down naturally in a compost pile with other biodegradable scraps under suitable temperature and oxygen conditions.[235]

7.3 Life Cycle Costing

While LCA is focused on the environmental concerns caused by a product or system, the process does not consider the economic implications of the product's life cycle. Often, further studies must be done to form a more complete analysis of the impact of the product. One way to accomplish this is by performing a life cycle costing (LCC) study. LCC serves as a tool to analyze, from the short to long term, the full costs and benefits of a product.[236] Like LCA, there is no single, broad methodology to follow for all LCC.[237] Instead, there are many standards and guides to assist in creating a study-specific scope and procedure.[236] Further, methods have been developed for specific application studies in certain industry sectors. Regardless, the general goal of LCC is to "ensure that all the costs of a product or system incurred over its entire life cycle are integrated into the decision-making process" in the early stages of development.[237]

There are three classifications of LCC: conventional, societal and economical. Conventional LCC was developed first to assess the real, internal costs that are expenses for either the producer or user of the product. However, this approach may not always address the entire lifecycle of the product if use and disposal phases are not the financial responsibility of the producer. Additionally, conventional LCC does not address other sustainability aspects such as environmental and social, as it focuses more on the cost for an individual. Thus, environmental LCC was developed to improve conventional LCC by including all life cycle phases and anticipated costs while linked to LCA. Moreover, societal LCC assesses costs covered by anyone within society throughout the product life cycle. Societal LCC builds on environmental LCC while including an assessment of external costs. Societal LCC focuses on society overall and on all people in society affected, including those in the future.[237] As this review is focused on LCA of natural fibre composites, the environmental LCC approach will be presented in more detail.

The main purpose of environmental LCC is to utilize an assessment of both environmental and economic performance to guide product development and create an optimized weighting between environmental and economic concerns.[237] Although environmental LCC closely follows an LCA study, the economic system will not follow the exact goals and boundaries of the LCA product system. Instead, the studies must be done in conjunction through the life cycle of the product while setting individual and equivalent system boundaries. An element that is not significant in LCA can still be included in the LCC if it is of economic interest.[238] Although cradle-to-gate studies are often used for LCA of a product, a partial life cycle for cost is an inaccurate method for determining the economic impact of a product. The product has a monetary value that is increased and decreased throughout all phases of its life cycle.[239] Hence, the framework for environmental LCC follows five stages: R&D, material production, manufacturing, use and maintenance, and end-of-life.[237] R&D stages are usually not included in LCA because this phase does not significantly contribute to environmental impact. However, in LCC, the R&D phase is often included since costs are required to develop the product. If the LCC is performed following an LCA, the LCI can be used. LCI lists and quantifies all the flows of resources into and out of the system. By multiplying the LCI flows by the specific company cost or market price, the costs of the flows can be found.[238] Then, only the phases excluded in the LCA must be determined separately for the LCC. Caution must be taken when performing LCC due to the danger of double counting costs. LCA includes upstream processes, where materials are extracted and compiled. In LCC however,

when a raw material is extracted/harvested and then is used to make another material, the cost for the raw material can be counted twice. For example, if steel is required, the cost of the iron used in the steel may be counted, but that cost is also included in the total cost of the steel. So, if both the costs of the steel and the iron are counted, the iron is double counted. The upstream costs for purchasing a good or service during one stage should be summarized in the price of that good or service, instead of separately counting all the individual inputs.[239] Finally, an important aspect of LCC scope that must be addressed and carefully considered is the perspective from which the study is performed. Unlike LCA, the values of each stage depend on which perspective is considered, such as the manufacturer or user. The manufacturer is focused on the costs of production and the price of selling the product, whereas the user may only be concerned with the cost of the product, the maintenance required during product use and the disposal costs. [238,239] These decisions depend on the goal of the LCC study and whether it follows an LCA.

7.4 Durability and Life Prediction

In recent times, scientists and engineers are being encouraged to explore green alternatives in engineering processes and material use to reduce their collective ecological footprint.[233] One area of innovation emerging to meet this objective is natural composites made from environmentally friendly renewable materials. Widespread availability, low cost of production, biodegradability and similar specific stiffness to glass fibres are some of the advantages of natural fibres and composites.[229,231,233] However, certain limitations of the durability of natural fibres exist when compared to synthetic fibres. When evaluating the overall environmental impact of a composite, its durability within its use phase is an important factor to consider. The durability of a composite material is defined as “the ability of resistance to damage developed during the service life or utilization periods”.[230] The main environmental parameters affecting the durability and lifespan of a composite which will be considered are moisture absorption, UV absorption, biodegradation and weathering and climate effects. Furthermore, material parameters such as fibre volume fraction and the type of fibre and matrix used within a composite material can also influence a composites durability under certain environmental conditions. The time-dependent degradation of composites poses challenges to engineers when choosing the correct material for long-term applications, as it

is often accompanied by significant reductions in mechanical properties which can lead to material failure.[229–233]

One method of integrating the effects of durability on environmental impact is by using an LCA.[229,240,241] Multiple environmental impact categories can be utilized to quantify the ecological effects of composite durability. Furthermore, comparing the LCAs of a composite material with and without considering the consequences of durability demonstrates the importance of this variable in conducting a comprehensive analysis.[229] Most studies including weathering effects on composites prefer using artificial accelerated weathering inside ageing chambers instead of natural weathering for organisational and economical reasons. Since artificial weathering's regularity of cycles, duration, intensity and exposure conditions often cannot perfectly reproduce natural environments' more unpredictable qualities, these studies cannot be directly correlated with natural weathering processes. Instead, they serve to provide basic understanding on composite degradation mechanisms under predetermined exposure cycles.[233]

7.4.1 Moisture Absorption

Moisture uptake is an important variable in determining a given composite's durability. Moisture absorption is particularly important in the context of composites made of natural fibres, as these fibres tend to be hydrophilic and more readily sorb water than synthetic fibres.[229–231,233] The presence of hemicellulose, a structural component in natural fibres, is the main source of this hydrophilic tendency.[233] Moisture uptake inside the composite also causes intermolecular hydrogen bonding between the water and fibres, which reduces interfacial fibre-matrix adhesion.[233] Furthermore, swelling of the fibres via moisture uptake induces stress at the fibre-matrix interface, causing microcracking within the matrix promoting capillarity. Water soluble substances then leach from the fibres, furthering debonding between the fibre and matrix.[230,233] Finally, water due to humidity can significantly alter the mechanical properties of some polymers due to the hydrolysis or plasticizing effect of water on the polymer chains and molecules.[242]

The net effect of moisture absorption within natural fibres is considerably lower mechanical properties and compromised long-term durability.[229–233] Water absorption tests conducted by Dhakal et al.[243] tested the change in mechanical properties of composites composed of hemp fibres and an unsaturated polyester matrix. Multiple composite samples of different fibre volume

fractions were dried in an oven before being immersed in deionized water for 888 hours. Tensile and flexure tests were conducted before and after immersion to measure mechanical property deterioration. The results indicated that lower maximum flexural stresses were endured by the wetted samples, as expected. Higher failure strain values were recorded for all the wetted samples, which is likely a consequence of plasticization of the fibres or the fiber-matrix interfaces caused by moisture absorption. However, tensile test results varied between test samples of different volume fibre fractions, as one wetted sample with higher fibre content had a higher tensile strength than when it was dry. The paper suggested that crosslinking or some "other mechanism" could explain this deviation. Another similar study by Maslinda et al.[244] observed the effects of water absorption on the mechanical properties of hybrid composites consisting of interwoven kenaf/jute and kenaf/hemp yarns combined with an epoxy matrix. The composites were tested while dry and after reaching water saturation following submersion for 1400 hours in a container filled with tap water at room temperature. The tensile strength and modulus of the water-saturated composites were found to decrease by up to 67-75% and 74-83%, respectively, compared to when they were dried. Furthermore, the flexural strength and modulus reduced by 57-73% and 68-78%, respectively, when comparing the dry and wetted samples. Higher tensile and flexural strains experienced by the wetted samples are suggested by the authors of the study to be a plasticization effect induced by lower cellulose content during water ingress. Accordingly, natural fibre hydrophilicity necessitates measures to inhibit moisture absorption to improve green composite performance.

Several methods can be employed to mitigate the negative effects of moisture absorption on natural fibre composite properties. Fibre volume fraction in natural composites, consisting of natural fibres and synthetic matrices, directly influences composite longevity and environmental impact.[229] The longevity of a composite can be increased by reducing its fibre volume fraction, and vice versa, as the hydrophilic nature of natural fibres ensures increased moisture absorption which leads to accelerated degradation.[229,233] However, the use of lower fibre contents, which consequently increases the synthetic polymer matrix content, has a negative environmental effect as synthetic matrices are less biodegradable.[229] Fibre treatments with chemical compounds is another method utilized to minimize moisture absorption. Modifying fibres with specific compounds through an alkalization process decreases the hydrogen bonding capabilities of cellulose and dissolves the hydrophilic hemicellulose within natural fibres. The result is fibres with

reduced hydrophilicity, improved fibre/matrix bonding and overall improved moisture durability.[233]

7.4.2 Ultraviolet Absorption

Long-term exposure of both natural and synthetic composites to ultraviolet radiation (UVR) reduce their durability and longevity. Due to their organic compositions, photodegradation effects from UVR exposure are significant in natural composites. Covalent bonds within organic polymers are broken upon exposure to UVR, consequently inducing yellowing, colour fading, surface roughening, embrittlement and overall mechanical property deterioration.[230,233] UV absorption weakens the polymer matrix through shorter chain scission, embrittling the matrix material and reducing the tensile strength of fibre-reinforced polymer composites.[230] Furthermore, photo-oxidation of the polymer's surface promoted by UVR uses up surrounding oxygen before it can diffuse into the center of the matrix. Subsequently, degradation is concentrated at the surface of the polymer, and an oxygen gradient is generated. The oxygen gradient results in a density gradient, which in conjunction with shorter polymer chains from chain scission initiates and propagates cracks which deteriorate mechanical properties.[233]

Several studies from literature have investigated the affects of UVR on composite material degradation and their mechanical properties. A weathering study conducted by Joseph et al.[245] exposed sisal/polypropylene (PP) composites of various fibre weight fractions to UVR inside of a controlled weatherometer for 12 weeks. Afterwards, tensile tests on the samples were conducted using an Instron machine. The neat (pure) PP samples had a 92.57% reduction in tensile strength, the largest drop of any of the samples. Samples with 10, 20 and 30% fibre weight fractions experienced drops in their tensile strength of 58, 37 and 23%, respectively, suggesting that increasing fibre weight fractions within the composite correlates to an increase in the retention of tensile properties after UV exposure due to the photodegradation effects endured by the polymer. Research conducted by da Silva et al.[246] tested hybrid composites made of carua-aramid reinforcement combined with unsaturated polyester resin under UVR and gamma radiation. The samples irradiated with UV light were placed inside an aging chamber for exposure times of 300 and 600 hours. Three-point bending tests was performed on the samples after irradiation. As expected, the samples irradiated for 300 hours showed degradation and a reduction in flexural strength and modulus of 30% and 41%, respectively, when compared to the non-irradiated

samples. Interestingly, the samples irradiated for 600 hours only show a decrease in flexural strength and modulus of just 1.5% and 14%, respectively, in comparison to the non-irradiated samples. It is suggested that longer UV exposure times allowed free radicals generated from UV exposure to recombine, causing greater cross-linking between neighbouring particles from both fibre and resin and ultimately increasing the mechanical properties of the composite from their previous degraded state. These studies indicate a strong correlation between UVR exposure and material degradation, while also suggesting at additional complex mechanisms responsible for inhibiting deterioration in certain composites. Developments from research have found solutions to minimize UVR damage on composite materials.

Recommended methods of engineering UV degradation resistance within natural composites include the hybridization of the reinforcement material within natural composites and the use of synthetic plastics as the matrix.[231,247] Including plastics combined with photostabilizers and UV inhibitors as the matrix material reinforced with natural fibres may help to reduce UV damage to the fibres, with the added benefit of increased water absorption resistance.[231] An investigation by Fiore et al. concerning the use of hybrid jute-basalt laminate with an epoxy resin found that a "sandwich" like structure of the laminates with basalt laminas situated near the outer layers of the structure and jute laminas near the center exhibit greater resistance to weathering effects including UVR exposure when compared to pure jute laminates.[247] Efforts by Yu et al.[248] to understand the complex interactions between UV light and textiles lead to the development of an optical model, verified by experimental results, to understand the effects of fibre parameters on UV protection. The findings show that shorter diameter fibres are ideal for UV protection as their transmittance of UVR is low. Furthermore, materials with high refractive indices absorbed less UVR, and fibres with low porosity proved to provide more UV protection as well. These parameters should be considered when designing composites for UV intense environments.

7.4.3 Biodegradation

Biodegradation is a key factor in determining the service span and methods for end-of-life disposal for composite materials. Microorganisms including fungi, bacteria and actinomycetes utilize enzymes to break down organic polymers. Enzymatic reactions are specific and only take place under defined environmental conditions. Natural products in particular are more susceptible

to enzyme degradation. Cellulose is biodegraded by bacteria and fungi in a wide range of temperatures (up to 85 °C) and pH (up to 9). Different materials can have vastly different biodegradation mechanics because of the specificity of enzymes. Some of the important factors in determining degradation rate are molecular weight, crosslinking, crystallinity, environmental conditions and structure porosity.[249]

Biodegradation reduces mechanical properties of composites during their service time. The degree of degradation incurred after a given period can be estimated by the weight loss percentage of the tested composite.[232,250] Takagi and Ochi[250] conducted testing of green composite samples with unidirectional hemp reinforcement and a starch-based biodegradable resin to examine changes in mechanical properties after biodegradation had taken place. These samples were placed in a home-use garbage processing machine filled with compost to undergo degradation for 20 days, during which samples were tested on days 0-5, 10, 15 and 20 for tensile strength and weight loss. The tensile strength of the composite fell from about 250 MPa initially to just 50 MPa after the full 20 days, with the biggest drop in strength observed during days 2-5. Under the same 20-day duration, the composite's degree of degradation was just over 15%, with the rate of degradation rapidly increasing after 15 days. Another study by Peterson et al.[232] examined the biodegradation of Biopol™, alongside woodfibre-Biopol™ composites. Samples of pure Biopol™ and woodfibre-Biopol™ composites of fibre weight fractions of 15, 20 and 25% were placed in sludge oil for five weeks, after which they were cleaned, and their masses measured. The composites samples degraded significantly faster than the pure Biopol™ samples, with maximum degradation experienced by the 15% fibre weight fraction sample. It was proposed that the woodfibres act as conduits for bacteria, thereby accelerating the degradation process in comparison to pure Biopol™.

Depending on the intended service life and use of the composite, biodegradation may be intended as an environmentally friendly end-of-life disposal method. Research conducted by Ji et al.[251] tested starch-sisal green composites combined with both organic and inorganic fillers for their mechanical properties, moisture absorption and rates of biodegradation to see if the fillers had any effect. The inorganic fillers included talcum powder (TP) and $CACO_3$ (CC), while the organic filler used was eggshell powder (EP) with the control group having no filler (NF). The fillers were mixed with the starch matrix and fibre using a blender, with the resulting slurry being hot-pressed to create the final composite. Biodegradation was conducted via soil burial for 30 days, after which the samples were recovered, and their initial and final masses compared.

Biodegradation of the NF-composite was the highest at 71% weight loss, followed by 67, 61 and 60% for the EP-, CC- and TP-composites, respectively, with the masses of the fillers being excluded from the calculations for better comparison. The NF-composite had the largest degradation rate as the filler samples tightly combined with the matrix, preventing microorganisms from decomposing them. Water absorption experiments as well as tensile and compressive tests showed superior mechanical properties and water resistance from the EP-composite in comparison to the other three. Considering the results, biofillers are a feasible, inexpensive method to produce high-performance, biodegradable green composites.

If the intention is to reduce biodegradability of a composite material to reduce degradation within its service life, the usage of biocides should be considered. Biocides are a broad group of chemical additives widely used in industry to protect materials by killing microorganisms responsible for biodegradation. Multiple blended biocides provide a larger scope of protection from microbial attack. Other properties of biocides, such as toxicity, working pH, temperature and UV stability, water solubility and cost effectiveness should also be considered within the scope of a particular application and environment to maximize its potency and minimize any ecological damage.[249]

7.4.4 Weathering, Temperature and Climate Effects

Combinations of moisture absorption, UV absorption and biodegradation on material samples are often carried out by weathering studies in literature. Natural weathering involves a material being aged "by natural elements, weathering or the action of the environment in which the material is subjected to conditions of use.".[233] Although natural weathering studies can accurately mimic the conditions a material undergoes throughout its lifecycle, these studies are often impractical due to the amount of time they require to collect years worth of data. Regardless, multiple natural weathering studies confirm the degradation of material and subsequent loss of mechanical properties following material exposure to natural environments.[233,248]

Accelerated or artificial weathering is a process occurring in ageing chambers which attempts to "simulate a natural environment and the damaging effects of long-term outdoor exposure by exposing test samples to ultraviolet radiation, moisture and heat in a controlled manner".[233] Different UV, moisture and temperature conditions can be cycled through in steps to reproduce

environmental ageing.[247] However, results from accelerated weathering have no exact correlation with real conditions due to the regularity of cycles, duration, intensity and exposure conditions.[233] A study conducted by Fibiyi et al. compared the effects of natural and accelerated weathering of a wood plastic composite (WPC) with formulations based on high density polyethylene and polypropylene.[252] Their results indicated WPC degradation from the 2-year natural test (17,520 hours) to be greater than that of 400 hours of accelerated ageing, but less than that of 2000 hours of aging. Like natural weathering tests, accelerated weathering tests reduce mechanical properties, degrade material and show color fading.[233,252] Despite their limitations, the fast, convenient and reproducible nature of accelerated aging makes them the preferred weathering method in most modern research.[233]

Varying climate conditions and temperatures subsequently result in differing durability of composite materials. Miller et al.[229] performed durability analysis on eleven WPCs with formulations of varying wood fibre weight fractions, different polymer matrices, different carbon feedstock sources and the addition of maleic anhydride for improved water resistance. By utilizing a stochastic degradation model developed earlier by Srubar et al.[240], these WPCs were considered for outdoor decking applications. The degradation model exposed these samples under the environmental conditions of three different American cities: Phoenix, Arizona (dry climate), Seattle, Washington (marine climate) and Lihue, Hawaii (humid climate). Finite element implementation simulated fluctuations in temperature, relative humidity and wet-day statistics for all three cities using data from the National Weather Service. Moisture absorption, property degradation and deflection were considered to determine exceedance of defined service-lifespan limit states, with a maximum lifespan of 20 years. Composites exposed to higher moisture levels, such as rain in Seattle or humidity in Lihue, displayed considerably shorter service lives than the composites from the more arid climate conditions of Phoenix. The most common failure mode resulted from strength reduction exceeding the allowable limit because of moisture absorption. High temperature environments exacerbate the effect of humidity on material lifespan, as demonstrated by the relatively short service life of the WPCs tested in the high-temperature, high-humidity environment of Lihue. Moisture uptake is accelerated at higher temperatures as high-temperature, humid environments allow for microcracks to form within the surface and bulk of the composite, thereby inducing non-Fickian water absorption behaviour and increasing the material's permeability coefficient.[233,243]

7.4.5 Durability Considerations Within Life Cycle Assessment

Studies investigating the environmental impacts of bio-based composites and bioplastics often adopt a cradle-to-grate analysis, overlooking the use-phase of the material within its lifespan.[229] Limitations on knowledge of in-service behaviour and deterioration properties, especially for novel materials such as green composites, pose barriers into assessing the environmental implications of material service life.[229,240] Material behaviour and maintenance through its use phase can increase its overall environmental impact, and in some cases exceed that of its production phase. Thus, service life performance should be integrated into LCAs and material design procedures to provide a more complete assessment of environmental impact.[229]

From the aforementioned weathering study, Miller et al. integrated durability-based service life predictions within LCAs of all the WPCs tested.[229] The LCIA categories considered in the study included "resource consumption during cultivation of wood and carbon feedstock for polymers; energy and material flows during biosynthesized or synthetic polymerization; refinement processes resulting in the wood by-product and the polymer; manufacturing of composites; and end-of-life disposal" and the LCIs considered were developed to represent 1 kg of material for each of the eleven WPCs. The functional unit considered in the study was "*based on the volumetric amount of material required to safely resist structural design loads*", though additional LCAs were also made based on the volume of material needed to meet the serviceability design criteria assuming material replacement occurred once the defined service-lifespan limit states were exceeded. Life cycle models were developed using Monte Carlo simulations which incorporated the quantities of material, processing and transportation distance required for each of the WPCs. Four different categories were assigned to assess environmental impacts: global warming potential (GWP) in kg of CO_2, fossil fuel demand (FFD) in megajoule surplus, acidification (H+ moles equivalent) and eutrophication (g of N equivalent). Environmental impacts were drastically different between the LCAs that included and excluded material degradation with replacement for most of the WPCs. Composites with 40% fibre weight fractions, which deteriorated more rapidly within the degradation model, had far greater GWP, FFD and acidification than composites with 20% fibre weight fractions when deterioration and replacement were accounted for. In contrast, these three categories for the 40% fibre weight fraction composites were only slightly higher than those with just 20% when degradation was not considered. Furthermore, smaller differences in all four environmental categories between the LCAs including and excluding deterioration were

observed for WPCs tested under the dry conditions of Phoenix Arizona, as less material replacement was required in this environment. Thus, the study concluded that service conditions have the potential to influence a given material's environmental impact, hence necessitating use-phase durability integration within the scope of an LCA.

A study done by Dufluo et al.[241] compared the LCAs of flax fibre and glass fibre composites with polypropylene (PP) matrices using a cradle-to-grave approach. The functional unit chosen was that of a gasoline car with a total travel distance over its entire lifetime of 200,000 km. Flax composite stiffness and strength were a function of flax fibre volume fraction, and two glass fibre composites with fibre volume fractions of 10% and 20% were tested. Hydrophilicity within flax fibres limits their durability and deteriorates their mechanical properties over time. However, it was concluded even with high frequencies of replacement, flax fibre-PP composites still had lower global warming impacts than their glass fibre-PP counterparts for compression moulded parts under bending loads with equal stiffness criterion between the two composites. In contrast, flax fibre-PP composites had a higher global warming impact than the glass fibre-PP composites when an equal strength design criterion was applied, due to the relatively low tensile and bending strengths of flax fibres. Accordingly, manufacturing green composite components with different design criteria affects their durability, resulting in different environmental impacts. Engineers should consider the effects of their design criteria and relevant weather conditions at their product's site of application on material durability when pursuing environmentally friendly alternatives for industrial use.

7.5 Choosing Constituent Materials

When choosing natural fibres for engineering applications, some important factors to consider include fibre cultivation requirements, locality, mechanical properties and cost.[253–273] Knowledge of fibre plant usability across many regions worldwide aids in utilization of plant by-products to reduce waste.[274–278] Alongside cultivation requirements, economic and industrial factors influence the type of fibres grown in certain countries or regions.[213,257] For the authors, flax and hemp are strong candidates for natural fibre cultivation due to Alberta, Canada's favorable geo-climactic conditions, recent harvesting regulation changes for hemp and market demand from multiple market channels.[278–281] Selection of biopolymers for industrial purposes is highly dependant on

application-specific criteria. For composite materials, favourable biopolymer attributes include high strength, weather resistance, biodegradability, biocompatibility and hydrophobicity.[209,282,283]

7.5.1 Requirements for Fibre Cultivation

Natural fibres have a diverse range of environmental and climactic requirements to obtain optimal growth. Some plant fibres such as jute only grow within tropical and subtropical environments, whereas hemp fibres can be cultivated within various environments around the world.[259,263] Cultivation conditions and typical cultivation regions for some common natural fibres are summarized in Table 7.1.

TABLE 7.1: CULTIVATION CONDITIONS AND REGIONS FOR SOME COMMON NATURAL FIBRES

Fibre type	Cultivation conditions	Cultivation regions	Reference
Jute	Hot, humid climate during wet summer seasons. 24-27 °C is ideal with annual pre-monsoon rainfall of 1000-2000 mm at sowing time.	Equatorial, tropical and subtropical zones. Cultivated in India, Bangladesh, China, Vietnam, Myanmar, Thailand and Brazil	259
Ramie	Humid climates with moderate temperature. Relative humidity of 25% with temperatures of 20-31 °C are optimal. Requires uniformly distributed rainfall of 1500-3000 mm annually.	Most production occurs in China. Also cultivated in India, Indonesia, Korea, Taiwan, Brazil, Japan and the Philippines.	260
Kenaf	Production fits well around the world with high ecological adaptability. Requires soil temperature of about 15 °C for germination and growth.	Can be cultivated between 30°S and 45°N. Typical production regions include India, China and Pakistan.	261
Flax	High relative humidity with temperatures ideally in the 18-20 °C range. Optimum soil conditions include fertile soils with loose aggregate structure for air access and a pH of 6.5-6.9.	Popular areas of cultivation include Canada, Argentina, India, USA, Ukraine, Kazakhstan, Egypt and the Czech Republic.	262
Hemp	Grows between 5.6-27.5 °C, with 14 °C being optimal for growth. Requires 4-5 months free of frost to produce harvestable crops. Optimum yields require 500-700 mm of precipitation. Ideal soil pH is suggested to be 6.0	Adapted to grow in various regions worldwide, including temperate, tropical and sub-tropical zones. Most hemp production is located within Canada, China and the European Union (EU).	263

		France, the Netherlands and Romania are the biggest producers in the EU.	
Abaca	Typically grows within tropical climates. Optimal development of fibres occurs at 28-30 °C with good relative humidity and 2000-2500 mm of water annually. The first fibre takes approximately two years to produce, with subsequent harvests occurring every two to three months.	Commercialization and production of abaca is led by the Philippines at 60% market share, followed by Ecuador with 35% market share.	[264]
Bamboo	Grows within many unique climates, from jungles to mountainsides. Supported best with soils possessing high moisture content and good water-holding capabilities. Snowfall should be avoided, and annual rainfall should be more than 1000 mm.	Almost all bamboo production takes place throughout the Asia-Pacific region. The largest producers of bamboo are China, India and Brazil.	[265,266]
Sisal	Grows in tropical or subtropical countries in well-drained soil anywhere between sea level and frost line. Requires a moist atmosphere with high temperature. Sisal feeds on lime, magnesia, potash and phosphoric acid.	Presumed to be native to Central America. Most production occurs in Brazil and Tanzania, though China and Kenya are also major cultivators.	[267,268]

7.5.2 Fibre Properties Requirements for Application

Different natural fibres possess distinct mechanical properties, thereby warranting their use in various engineering applications. Often, designing composite materials requires knowledge of constituent properties to predict their combined properties using tools such as the rule of mixtures.[255] Table 7.2 presents the mechanical properties of some common natural fibres as well as conventional synthetic fibres for comparison purposes. Higher mechanical properties are exhibited by bast fibres (hemp, kenaf, flax, jute and ramie) which possess higher amounts of cellulose with more cellulose microfibrils oriented in the fibre direction.[257] Large variances within reported values of natural fibre mechanical properties arise from factors inherent to fibres, including plant maturity, age, location, source, fibre extraction methods and microstructure.[255] Growing and extraction conditions also impact natural fibre strength, as previous studies have shown strength reductions of 15% by waiting five days after the optimum harvest time to extract the fibres. Furthermore, flax fibres were found to have 20% higher tensile strength when harvested manually rather than mechanically.[257] Different testing methods conducted on natural fibres within literature often add to reported mechanical property variabilities as well.[256] Using unconventional fibre cross-sectional area measurements may help to mitigate mechanical property variability within natural fibres.

TABLE 7.2: MECHANICAL PROPERTIES OF COMMONLY USED NATURAL AND SYNTHETIC FIBRES

Fibre	Tensile Strength (MPa)	Young's Modulus (GPa)	Failure Strain (%)	Density (g/cm^3)	Reference
Abaca	400-813	12-33.6	2.9	1.5	[253,256]
Bagasse	96.24-290	8.5-17	4.03	1.25	[253,256]
Bamboo	140-230	11-17	1.3	0.6-1.1	[253,256]
Flax	345-1500	27.6-100	1.2-3.2	1.5	[253,255,256]

Hemp	550-900	68.9-70	1.6-4	1.47-1.48	[253,255,256]
Jute	200-800	13-55	1.16-3	1.3-1.49	[253–256]
Kenaf	930	53	1.6	1.45	[253,256]
Sisal	511-710	9.4-22	2-3	1.34-1.5	[253,256]
Ramie	400-938	24.5-128	2.5-3.8	1.5	[253,256]
Oil palm	206-248	3.2-3.567	4-25	0.7-1.55	[253,256]
Pineapple	170-1627	1.44-82	2.4-14.5	0.8-1.6	[253,256]
Coir	130-1150	4-6.2	15-40	1.2	[253,255,256]
Curaua	500-1150	11.8	3.7-4.3	1.4	[256]
E-glass	3400	73	2.5	2.55	[284]
Kevlar	3000	60	2.5-3.7	1.44	[284]
Carbon	3400[a]-4800[b]	240[b]-425[a]	1.4-1.8	1.78	[284]

[a]Ultra-high modulus carbon fibres

[b]Ultra-high tenacity carbon fibres

Several limitations exist when reporting the mechanical properties of natural fibres as opposed to synthetic ones. Standard simplifying engineering assumptions assume fibres have a circular cross-sectional area (CSA) that is constant throughout its length. Such assumptions rarely hold for natural fibres. An investigation into natural fibre CSA variability conducted by Thomason et al.[258] measured the CSAs of flax and sisal fibres. Four different locations along the fibres' longitudinal

axis were used to measure the average CSAs of the fibres with conventional circular area calculations using average diameter estimations made from microscopic images. Then, separate fibre micrographs were taken and traced to find the fibres' true average CSA. The study found that the conventional method overestimated the CSAs by a factor of two or more, with these differences translating directly into tensile strength and modulus differences of the same magnitude. Furthermore, using additional measurements along the direction of the fibre, the average deviations from the mean CSA were about 11% and 14% for sisal and flax fibres, respectively. However, a model developed in the study that treated each fibre as having short cylinder constituents connected in series indicated that these deviations would result in at most a 3% error in the experimental modulus calculation, thereby eliminating cross-section variation as a major source of variability for fibre modulus measurements. The errors in CSA calculations associated with conventional measurements were found to scale with larger diameter measurements, thus providing a plausible explanation for the inverse relationship between fibre strength and modulus and fibre diameter found in literature. Separate studies have also shown relationships between clamping length during testing, fibre length and mechanical properties. Since fibre breakage is expected to occur at the weakest point of the fibre, longer fibres have a higher probability of having a weak section within them, consequently reducing their strength and strain to failure. For similar reasons, clamping length exhibits an inversely proportional relationship with fibre strength as larger clamping lengths introduce more defects that weaken the fibre.[255]

7.5.3 Local Fibres and Usability

Natural fibre selection for natural composites depends heavily on geographic availability. Flax fibres are popular within Europe, whereas jute, kenaf, hemp, ramie and sisal fibres are favored in Asia. In New Zealand, Harakeke fibres (commonly known as New Zealand flax) are being considered for structural applications by virtue of their high mechanical properties and local availability.[257] Industrial chains connected to natural fibres impart considerable influence upon global economies, and vice-versa. World natural fibre production is estimated to be 33 million tonnes with a total farm value of US$60 billion in 2013. In the European Union (EU), approximately 10,000 companies from 14 countries are involved in planting, harvesting, scutching, spinning, weaving, knitting, finishing and trading to produce finished fabrics made from linen

(flax). Rapid growth in Brazil following the end of the Second World War propelled the country into becoming the largest producer and exporter of sisal today. Hemp production takes place predominantly in China, Canada and the EU, with their main fibre usage being channeled towards specialty pulp and paper, insulation material and biocomposites for automotive applications . India and Bangladesh account for 97% of worldwide jute and kenaf production in 2013/14, with their labour-intensive cultivation and processing requirements providing a livelihood and food security for many families across Asia. National laws requiring jute usage in packaging material prompted India to become the largest consumers of jute as well. When considering the full value chain of jute including agriculture, marketing, transportation and manufacturing, 25 million people in Bangladesh (or about one-fifth of its population) are dependent on jute. Overall, a reasonable estimate of total employment in natural fibre industries is about 300 million people globally, roughly 4% of the world population.[285] Even with the importance of natural fibres in the global economy, plants containing usable fibres often see many other uses as well.

Typically, only a small fraction of a plant is fit for fibre production, with the rest being used for industrial, medicinal and culinary applications.[274–278,286,287] Only 4% by weight of sisal fibres are extracted from sisal leaves, with the remaining weight being attributed to plant cuticle, dry matter and water.[274] Ramie plants produce even lower fibre yields between 2-4% by weight of the plant, with jute plant fibre yields falling between 4-6%.[286,287] However, other parts of these plants can still be utilized as by-products for a variety of other purposes, thereby reducing waste. Oil extracted from kenaf seeds are known to have extensive medicinal uses. Furthermore, kenaf seed oil has found industrial usage as an alternative to mineral oils for lubricant applications resulting from its inexpensive, renewable nature.[275] Roots and leaves from Ramie, one of the oldest crops in China, see frequent therapeutic use in traditional Chinese medicine.[276] Bamboo leaves possess medicinal properties as well, with bamboo shoots having culinary value as sources of high protein, vitamins and minerals.[277] Hemp is a versatile crop with multiple industrial uses. Other than fibre usage from the stalk of the plant, hemp leaves are used to create pulps and building materials including insulation, cement and stucco. Oils, isolates and distillates are extracted from hemp flowers for medicinal and recreational purposes. Moreover, hempseed oil is an ingredient in hygiene products such as soaps and lotions, as well as in industrial products including paints, solvents and printing inks.[278]

In pursuit of a domestic source of natural fibre, hemp is a commercial crop of interest in Alberta, Canada. As a short season crop which thrives in long hours of sunshine, hemp is well suited towards Alberta's geo-climatic conditions. Well-developed fibrous root systems grant hemp better resiliency against dry conditions in the Canadian Prairies than most crops, although the plant is not as compatible with saturated soils by the same token. In Canada, the optimum time of sowing is mid- to late-May, as the risk of hard frost has passed by this time.[278] In recent years, overall hemp production acreage has trended upwards for both Alberta and Canada as a whole, with these trends largely driven by the hemp grain market. Alberta's share of Canadian hemp production area rose from 2% in 1998 to 32% in 2011.[288] High versatility regarding plant part utilization allows for the generation of multiple revenue streams corresponding to each part of the hemp plant. Increasing demand exists for hemp protein in both human and pet food markets, with growing demand for food markets for certified organic hemp production. High mechanical properties make hemp fibres a viable product within biocomposites in the aerospace, automotive and packaging industries. Additionally, textile, paper and building markets express interest in hemp fibres for specialty applications by virtue of its durable, anti-microbial, acoustic and aesthetic properties. The Albertan government collaborates with the hemp fibre industry "to advance product development and commercialization as well as facilitate supply chain development" . Efforts by the government to meet this end include investment in a fibre processing pilot plant for the decortication of hemp stalk in 2009. Prior to 2018, harvesting of hemp chaff (flowers, leaves and stems) was forbidden as these parts contained bioactives, primarily cannabidiol (CBD), which were restricted by regulations. Changes in these regulations brought about by the *Cannabis Act* authorized bioactive extraction from the chaff by licensed processors, thereby triggering a market surge by allowing for the creation of cosmetics, natural health products and pharmaceuticals with bioactive ingredients.[278] Favorable geo-climactic conditions for growth, a high degree of usability and increasing market demand have propelled hemp to become a strong contender for natural fibre cultivation in Alberta.

A comparative cradle-to-manufacture LCA study conducted by la Rosa et al.[228] on hemp and glass fibres demonstrates the disparities between the two materials' environmental impacts. The functional unit in the study was defined as an eco-sandwich panel made of natural material including a cork core sandwiched by bio-based epoxy resin reinforced with hemp mats. For comparison, a traditional sandwich composite consisting of a polyurethane core with petroleum-

based epoxy resin and glass fibre reinforcement was also studied. By using data for energy, materials, processes and transportation from European sources, 11 different impact categories were created to compare the environmental effects of 1 kg of hemp mat and glass fibre production. Some common categories used include global warming, eutrophication and acidification potential, though other rarer categories such as human toxicity and terrestrial ecotoxicity potential were also used. All impact categories were considerably higher for the glass fibres, except for land occupation since hemp production required over 20 times as much land usage. Typically, renewable materials score worse than petrochemical polymers in the ecotoxicity and eutrophication categories, though the choice of using organic hemp grown without fertilization and pesticides in the LCA reduced these impacts for the hemp mats.

Alongside hemp, flax is another available crop in Alberta with encouraging prospects for cultivation and use. Geo-climactic conditions including a narrow temperate climate band across Western Canada with long hours of daylight in the summer and low to freezing temperatures in the fall are suitable for flax cultivation in northern Alberta.[279] Sensitivity to spring frosts requires flax seeding to be delayed until the risk of frost is reduced.[280] The flax industry contributes about $300 million annually to the Canadian economy, though only 9% of Canadian flax production occurs in Alberta. Flax production and acreage have expanded in Alberta as markets have shifted from Europe to China, with China being the largest export market.[279] Flax cultivars are selected for either fibre (fibre flax) or oil (oilseed flax) production, with most flax cultivated in North America being grown for the oil. Locations of production between these two types of flax differ, as fibre flax is adapted to wet fall climates which aid in postharvest fibre processing . Until recently, straw was considered an impediment for oilseed production and was burned. However, uses for industrial fibres in composites, paper and nonwoven fibre have increased whole plant utilization potential.[280] Considerable interest has been shown towards flaxseed oil as a functional food ingredient with many health benefits. In industrial applications, flaxseed oil (often referred to as linseed oil) is used extensively to produce paints, printer ink, varnishes and linoleum flooring.[280,281] Multipurpose utilization across several industries, increasing foreign market demand and desirable climate conditions in Alberta highlight the feasibility of flax as a local source of natural fibre within the province.

To highlight the significance of material production location on environmental impacts, Deng and Tian[289] conducted a consequential LCA (CLCA) study on flax fibre reinforced composites.

The focus of the CLCA was on the "marginal environmental impact changes due to a shift from glass fibres to flax fibres for composite reinforcement from a macro-economic perspective", with the functional unit for both types of fibres being interior car panels with equal stiffness serving a driving distance of 200,000 km. Unlike using a regular LCA, the CLCA used here addresses environmental impact changes associated with marginal production, use and disposal changes, while also incorporating the global flax fibre market in the analysis. Since most fibre flax production occurs in China and France, flax supply ratios of 70% and 30% were used for each country, respectively, based on global market data. Using this supply mix, environmental impacts such as climate change, fossil depletion and many others, were found to be higher in the production and end-of-life stages of the flax composite when compared to the glass composite. The high impact of the flax composite was attributed to inferior flax cultivars producing lower flax yield efficiencies in China compared to France, as well as China's heavy dependence on coal as a source for electricity. Inclusion of the use phase benefits of the flax composites negated many of its production and end-of-life impacts, with positive environmental impacts being observed in 10 of the 17 environmental impact categories when compared to the glass composites for a full life cycle. Further, consideration of an alternate scenario where 100% of flax fibres were sourced from France resulted in significant impact reductions in most of the impact categories. Accordingly, geographic location can have substantial effects on environmental impacts for products in their production and end-of-life stages, thereby entailing its careful reflection within LCA studies.

7.5.4 Fibre Material Cost

An attractive feature of natural fibres in engineering applications are their relatively low costs in comparison to synthetic fibres. In many cases, natural fibres meet engineering design criteria while still being inexpensive. Although synthetic fibres tend to have superior mechanical properties when density is not accounted for, the specific strength and modulus of natural fibres are comparable to those of synthetic ones.[269] Table 7.3 shows the average prices of some natural and synthetic fibres.

TABLE 7.3: AVERAGE PRICES OF NATURAL AND SYNTHETIC FIBRES PER KILOGRAM IN 2017 AS REPORTED BY VÄISÄNEN ET AL.[269]. THESE PRICES ARE LIKELY TO HAVE CHANGED DUE TO THE GLOBAL COVID-19 PANDEMIC, AND ACCORDINGLY SHOULD BE VIEWED RELATIVE TO EACH OTHER.

Fibre	Price (US$/kg)

Wood	0.3-0.6
Flax	2.1-4.2
Hemp	1.0-2.1
Jute	0.4-1.5
Coir	0.3-0.5
Cotton	2.1-4.2
Sisal	0.6-0.7
Kenaf	0.3-0.5
Bamboo	0.5
Wool	1.6-2.4
Feather	1.1-2.0
Silk	2.6-40.0
Glass	2.0
Carbon	22.0-27.0

Both natural and glass fibre price variations depend heavily on sources of geographic area.[273] Low densities found in natural fibres correspond to lower transportation costs, thereby reducing the cost of natural fibres.[270] Use-phase cost savings of natural fibres emerge in the automobile industry through weight reductions of composite parts, allowing for higher fuel efficiency.[234]

Reduced energy demands are required for natural fibre production as well.[272] Lower costs of natural fibres imply lower costs for composites reinforced with natural fibres instead of synthetic fibres, meaning the overall cost of the composite can be reduced by varying the amount of natural fibre loading if the cost of the fibre and matrix material differ.[270] On the contrary, implementing natural fibres as a substitute for glass fibres was a costly alternative within the European automotive industry in 2002. Retooling injection moulding processes within the industry already geared towards glass fibres would have been expensive, so glass fibres remained the standard.[271] Thus, although their raw material costs may be lower, other costs of production must also be considered for a more complete approach in bolstering the cost-efficiency of natural fibres within industrial settings.

7.5.5 Biopolymer Matrices

As an alternative to petroleum-derived synthetic polymers, biopolymers made of renewable resources have garnered increased interest recently from scientific and industrial fields.[282] Environmental concerns related to petrochemical plastics including global warming, limited fossil fuel availability, low biodegradability and accelerated landfill deposits have shifted research interests towards biopolymers to mitigate these effects.[209] Two different criteria are used in in defining the term "biopolymer": the source of the raw materials and the polymer's biodegradability. From this definition, biodegradable polymers made from renewable resources (biobased), non-biodegradable polymers made from sustainable crude polymers (biobased) and biodegradable polymers made from fossil fuels all classify as biopolymers. Biobased biopolymers are produced either by biological systems (plants, animals and microorganisms) or by chemical synthesis of natural starting materials such as starch, sugar and corn.[282] Further, natural polymers can be divided into three main classes based on their structure: polysaccharides, polynucleotides and polypeptides.[209]

Most bio-based biopolymers today are sourced from first-generation feedstock, including edible biomass (starch, sugar, plant oils, etc.) as well as non-consumable sources like natural rubber. Cellulose, a polysaccharide found in plant cell walls, is the most abundant biopolymer in the world. Plants produce over 10^{11} tons of cellulose annually, though other living organisms like bacteria and fungi can produce cellulose as well. Starch is another abundant plant-based biopolymer, stored in plants as an energy reserve. As a natural carbohydrate polymer, starch can be extracted from

many diverse sources in nature, including rice, wheat, potato and corn. Biopolymer matrices sourced from renewable materials like soy, starch and cellulosic plastics can be used in biocomposite applications. Polylactic acid (PLA) is a common biopolymer produced by the polymerization of lactic acid from renewable resources such as corn starch or sugar canes. Collagen is the most abundant animal-based biopolymer, with its most important sources being pig skin, bovine hide and pork and cattle bones. Polyhydroxyalkanoates (PHAs) are a family of microbially produced biopolymers mainly synthesized from renewable materials through fermentation.[282] Polycaprolactone (PCL), a synthetic polyester, is easily biodegraded by enzymes and fungi despite its fossil fuel-based origins.[290] Different types of biopolymers provide a variety of attributes useful for industrial applications.

Selection criteria for biopolymers vary drastically between different industrial applications. Biopolymer characteristics to consider include pH, density, refractive index, diffusion coefficients, melting temperature, rheological properties, fracturability, durability and many others. For example, polysaccharides such as chitosan are chosen to coat fruits and vegetables owing to their low toxicity, high biodegradability, antifungal, antioxidant and film-forming capabilities.[209] Regarding composite materials, high biodegradability and weather resistance enables PLA to be a suitable green matrix material.[282] Composites based on biopolymers like hyaluronic acid have been used in medical applications for drug delivery, as they possess excellent biocompatibility, biodegradability and nontoxicity characteristics.[209] In the automotive industry, Mitsubishi Motors used PLA and polybutylene succinate (PBS) reinforced with bamboo fibre to prepare high strength car floor mats. For composite durability, composites manufactured with hydrophilic biopolymers like cellulose and starch absorbed more moisture compared to composites prepared with hydrophobic biopolymers like PHB and PHBV (both types of PHAs).[283] On account of the different benefits and attributes available across their numerous varieties, biopolymer matrices for composites should primarily be chosen based on application-specific criteria.

7.6 Conclusion

From the findings of this review, green composites have proven to be a viable alternative to synthetic composites in many applications. Low production costs, widespread availability, reduced environmental impacts and high specific strength and stiffness are just a few benefits of green

composites over traditional glass, carbon, Kevlar and other man-made composites. As an analytical tool, LCA can aid in quantifying the environmental impacts of a product through its production, use and end-of-life phases. LCAs can be applied/used on a variety of products from different areas and industries, meaning guidelines for conducting LCAs are unable to outline the procedure for conducting every step of the analysis. However, ISO has established general protocols to complete an LCA. When analyzing the short- and long-term economic costs and benefits of a product or system, an LCC study should be employed. Like LCA, LCC is a broad analysis tool without concrete steps for how to conduct all analyses, though it instead aims to integrate the costs that a product or system incurs throughout its life cycle into the decision-making process in early stages of development. Both LCA and LCC studies should be utilized when determining the economic and environmental impacts of the use or advancement of green composites.

Use phase durability of green composites should ideally be included within LCA studies but is rarely done so in practice due to limited knowledge of material deterioration processes. Regardless, four different mechanisms were identified in compromising the mechanical properties of green composites: moisture absorption, UVR exposure, biodegradation and temperature and weather effects. The hydrophilic nature of natural fibres encourages moisture absorption, thereby causing swelling of the fibres and compromising the structural integrity of the composite. UVR weakens composites by breaking covalent bonds within polymer matrices and promoting photo-oxidation at the polymer's surface. Biodegradation occurs when microorganisms break down organic polymers via enzymatic reactions, though biodegradation is often viewed favourably as a means of environmentally friendly end-of-life disposal. Combinations of these three mechanisms are studied in both natural and accelerated weathering studies, with added temperature effects amplifying moisture induced degradation.

When choosing natural fibres as reinforcement in green composites, their cultivation conditions and locality, mechanical properties, usability and cost are some parameters to consider. Different fibres have varying requirements for optimal temperatures, rainfall and soil conditions. Geographic availability of certain fibre types can also limit which fibres can be utilized in a specific region. Knowledge of the mechanical properties of natural fibres may help in choosing the right type of fibre for a particular application, though considerable variance exists in reported mechanical properties of natural fibres due to inconsistent testing methods and measurements between studies in literature. Ideally, natural fibres should be sourced from plants with usable by-products from its

non-fibre counterparts to minimize plant waste. Costs of different types of natural fibres vary, though most are significantly cheaper than their traditional synthetic alternatives. Within Alberta and Canada, hemp and flax are viable crops for fibre cultivation o to Alberta's suitable climate conditions, market demands from multiple products and channels and from recent relaxation of hemp cultivation regulations. Biopolymer matrices within green composites are another feasible substitute to synthetic polymers to support sustainable development. Considering the wide range of biopolymers available with each possessing unique characteristics, their selection criteria for green composites are heavily dependent on usage requirements such as weather and moisture resistance, biocompatibility, biodegradability and many others.

Although extensive research has been conducted regarding the durability, life cycle analyses and mechanical properties of green composites, work from these categories as they relate to green braided composites are sparse. Unlusoy and Melenka[185] demonstrated the effects of area moment of inertia, braiding angle and void content on the flexural properties of cellulose-based braided composites. Rajesh and Pitchaimani[291] discovered that braided architectures of jute-based composites have enhanced mechanical properties when compared to the conventional woven fabric architecture. Bruni-Bossio et al.[292] studied the significance of braid angle, resin type and curing method on the porosity of braided green composites. Further studies into green composite mechanical properties should investigate the effects of varying several composite parameters including linear yarn density, a wide range of braiding angles, fibre volume fraction and different fibre-matrix compositions for proper composite characterisation. Little to no information is available for life cycle analyses of green braided composites. LCA and LCC studies must be performed on these composites to assess their ability to meet environmental impact and cost constraints, especially in contrast to synthetic composites with traditional structures. Durability considerations must also be included within these analyses to estimate environmental impacts with greater accuracy. Weathering studies should be conducted on green braided composites to predict their use-phase durability and longevity alongside biodegradation tests to develop procedures for end-of-life disposal.

In this chapter, we present the viability of green composites in terms of their environmental impact. As shown, in all stages of the life cycle of composites, including procurement, use and recycling, green composites have a smaller environmental impact than synthetic composites. Although limited studies have characterized the tensile, compressive, fatigue and thermal

properties of green braided composites, this chapter suggests that green composites have a future in composite research and applications.

CHAPTER 8 – Overall Discussion, Conclusions and Future Work

2D Tubular Braided Composites (TBCs) are materials that are formed by interlacing yarns into a braided pattern on a cylindrical mandrel. The resulting preform is impregnated with matrix to form the final TBC. Due to the tailorability of the manufacturing process and the ability to manufacture near net shape composites, TBCs can be manufactured and designed to have diverse mechanical and physical properties. This has encouraged extensive research into these materials for various applications including construction, sports, medicine, automotive and aerospace. The current state of research conducted identified gaps in the thermal properties of TBCs, the variability in tensile properties of TBCs and a lack of exploration into green fibres and matrices as constituent materials in TBC characterization. These gaps were addressed in this thesis. In chapter 3, a review of the literature on the thermal expansion coefficient was conducted to further specify the gaps in thermal TBC research. The longitudinal CTE gaps identified in chapter 3 were experimentally and analytically investigated in chapter 4. The variability in TBC tensile properties was addressed in chapter 5 and chapter 6. In chapter 5, an experimental investigation of the influence of tensile testing displacement rate was conducted. In chapter 6, an experimental investigation of the influence of stress-free aging time was conducted. Finally, the future of composites in terms of their mechanical and thermal properties was investigated with regards to material selection in chapter 7. A life cycle analysis literature review was conducted to address the final gap and encourage further characterization of the mechanical and thermal of TBCs. Through addressing these various gaps in the material selection, characterization and testing of 2D TBCs, we have shown the guaranteed future of braided composite materials in terms of their applications and areas of research. In this chapter, an overall discussion of the work conducted, a summary of conclusions and suggestions for areas of future research with regards to 2D TBCs.

8.1 Overall Discussion

In chapter 2, we presented the general background pertaining to this work in terms of the existing literature on TBCs and areas of further research needed to use these advanced materials in their intended applications. The objectives of this thesis can be summarised as:

I. Identify gaps in thermal research pertaining to 2D TBCs through a literature review of textile composites.
II. Develop a non-contact experimental method for measuring the longitudinal coefficient of thermal expansion of 2D TBCs.
III. Develop an analytical model based in classical laminate plate theory that can predict the longitudinal coefficient of thermal expansion of 2D Kevlar®/epoxy TBCs.
IV. Conduct an experimental study on the influence of displacement rate on the tensile properties of 2D Kevlar®/epoxy TBCs and their variation.
V. Investigate the relationship between stress-free aging and the tensile properties of 2D Kevlar®/epoxy TBCs.
VI. Conduct a life cycle analysis-based literature review to investigate the environmental impact of using green TBCs as a potential alternative to typical synthetic TBCs.

We addressed objective in chapter 3. A review of literature was conducted to present the extent of research conducted investigating the thermal expansion behaviour of textile composites. Journal articles were found through Google Scholar and Scopus and limited through keywords pertaining to thermal expansion only. Objectives II and III were addressed in chapter 4. A non-contact experimental method based in digital image correlation was developed to measure the longitudinal CTE of Tubular Braided Composites. The experimental method was tested on TBCs manufactured at three braid angles (35-, 45- and 55-degrees) heated to 150^{o}C, with images taken every five minutes. Collected images were used to measure strain and plot strain against temperature and CTE against temperature. Braid angles were limited to the three tested due to the ability of these angles to show a suitable range of thermal expansion behaviour of TBCs. To address objective III, the experimental work was supplemented with an analytical model developed using classical laminate late theory. The developed model was compared to the limited available experimental data to confirm its ability to predict the properties of composites. The model was then used to predict the properties of Kevlar®/epoxy TBCs and compare to the experimental data.

We address the objectives related to the mechanical variability seen in TBC samples in chapters 5 and 6. In chapter 5, a brief review of literature showed the relevance of displacement rate on the properties of polymers, often changing the measured mechanical properties. ASTM standards do not specify displacement rate for tensile testing, further suggesting the importance of studying the

influence of displacement rate on the measured mechanical properties. Three braid angles (35-, 45- and 55-degrees) Kevlar®/epoxy TBCs were tested at three different displacement rates, (1 mm/min, 2 mm/min and 6 mm/min). Stress-strain curves were used to calculate the elastic modulus and identify the influence of displacement rate on the variation in the properties of TBCs. In chapter 6, the influence of strain-free aging time on the tensile properties of TBCs was investigated. Kevlar®/epoxy TBCs were manufactured at three different braid angles (35-, 45- and 55-degrees) and three different aging times (0 weeks, 2 weeks and 6 weeks). Stress-strain curves were used to calculate the elastic modulus and strength of TBCs.

With the results from chapters 3 through 6, one final research hurdle to address was the materials selected for further future investigation into the properties of TBCs. To address the final objective, a review of literature was conducted through the lens of a life cycle analysis to identify the viability of green composites as having lower environmental impact then traditional synthetic. The life cycle analysis looks at constituents of composites including reinforcement fibres and matrices and their viability from procurement, use and recycling perspectives.

8.2 Summary of Conclusions

The results and discussions presented in this dissertation can be summarized into the following points considering the original objectives of the work:

- A literature review of the investigation into the thermal expansion behaviour of textile composites indicates that although studies have investigated the CTE behaviour of laminate and woven composites, little research has looked into the CTE of 2D braided composites.
- A new non-contact method was developed to measure the CTE of 2D TBCs. Although capable of measuring the thermal strains developed in the samples, experimental results indicate the sensitivity of CTE to braid angle.
- Experimental CTE results show a non-linear relationship between the braid angle and the CTE. Due to the negative longitudinal CTE and the large positive transverse CTE of the Kevlar® fibres, increasing the braid angles causes the CTE of 2D TBCs to become more positive as yarns align in the transverse direction. Average CTE of the 35-degree, 45-degree and 55-degree TBCs were -60.5 μm/m^{o}C, -38.3 μm/m^{o}C and 7.08 μm/m^{o}C.

- The CLPT-based model developed in this work can accurately predict the thermal expansion behaviour of Kevlar®/epoxy unidirectional laminae, Kevlar®/epoxy bidirectional symmetric balanced laminates and Kevlar®/epoxy 2D TBCs. The current model in conjunction with the experimental data suggests that the CTE of Kevlar® fibres is less than the values typically reported in literature. This different CTE of fibres is hypothesized to be a consequence of fibre damage and filament misalignment.
- An experimental investigation into the influence of tensile displacement rate during testing of TBCs suggested that tensile displacement rate must be considered for stiffness-sensitive applications of TBCs. From the three different displacement rates tested (1 mm/min, 2 mm/min and 6 mm/min) and the three braid angles considered (35-, 45- and 55-degrees), higher displacement rates were associated with larger spread of elastic moduli values for the larger braid angles. Due to the larger contribution of the matrix to the longitudinal properties at higher braid angles, the viscoelastic nature of the polymers affects the stiffness properties measured. This is one potential reason to explain the 5-10% variation in documented tensile properties between different studies.
- An experimental investigation into the influence of post-cure stress-free aging on the elastic modulus and strength of 2D TBCs suggests that stress-free aging does not play a significant role in these measured properties. Three different aging times (0, 2 and 6 weeks) and three different braid angles (35-, 45- and 55-degree) TBCs were considered. Results indicate that although stress-free aging might have an influence on stiffness for larger braid angles, this influence is not significant for lower braid angles. At higher braid angles, larger aging times (2 and 6 weeks) were associated with increased strength and modulus. This result provides a potential explanation of the variation in tensile properties seen within samples tested in a study.
- In terms of an LCA, green materials present an environmentally preferable alternative to synthetic polymers. More research must be conducted, however, to fully understand the tensile, compressive, thermal, hygral, creep and fatigue properties of green fibres and green TBCs.

8.3 Future Work

For TBCs to be used in their potential applications, further work needs to be conducted to fully understand the behaviour of these materials. Potential avenues for future work are:

- In light of the global climate crisis, more investigation must be conducted on the use of green fibres and natural polymer matrices for composite applications. These studies can further identify the suitability of green materials for the various applications of TBCs in construction, medicine, sports and aerospace.
- In addition to investigating the thermal expansion behaviour of Kevlar®/epoxy TBCs in elevated temperatures, investigating the behaviour in sub-zero temperatures in necessary for the use of TBCs in construction and aerospace. For these applications, temperatures can fall to -80 °C, necessitating materials that do not exhibit strains in these conditions.
- Further verification of the accuracy and precision of using DIC to measure the thermal strain of polymer fibre reinforced composites is necessary. The limited experimental standards on the measurement of thermal strain data presents an obstacle to testing and using FRPCs, including TBCs.
- Testing a wider range of braid angles to fully understand the thermal expansion behaviour is necessary. These include angles below 35-degrees and larger than 55-degrees and angles in between the range selected for this work.
- Applying the CLPT-based model to measure the thermal expansion behaviour of a wider group of materials is necessary. Experimental verification of these materials can further help improve the accuracy of the model.

Bibliography

1. Carey JP. Introduction to braided composites. *Handbook of Advances in Braided Composite Materials: Theory, Production, Testing and Applications* 2017; 1–21.
2. NASA. Global Climate Change , https://climate.nasa.gov/ (accessed 8 October 2023).
3. Butler CD. Climate Change, Health and Existential Risks to Civilization: A Comprehensive Review (1989–2013). *Int J Environ Res Public Health*; 15.
4. Goff JR. The Geometry of Tubular braided Structures. *Thesis* 1976; 1–145.
5. Du GW, Popper P. Analysis of a circular braiding process for complex shapes. *Journal of the Textile Institute* 1994; 85: 316–337.
6. Zhang Q, Beale D, Broughton RM. Analysis of circular braiding process, part 1: Theoretical investigation of kinematics of the circular braiding process. *Journal of Manufacturing Science and Engineering, Transactions of the ASME* 1999; 121: 345–350.
7. Zhang Q, Beale D, Broughton RM, et al. Analysis of circular braiding process, part 2: Mechanics analysis of the circular braiding process and experiment. *Journal of Manufacturing Science and Engineering, Transactions of the ASME* 1999; 121: 351–359.
8. Carey J, Munro M, Fahim A. Longitudinal Elastic Modulus Prediction of a 2-D Braided Fiber Composite. *Journal of Reinforced Composites and Plastics* 2003; 22: 813–831.
9. Ayranci C, Carey JP. Predicting the longitudinal elastic modulus of braided tubular composites using a curved unit-cell geometry. *Compos B Eng* 2010; 41: 229–235.
10. Ayranci C, Carey J. 2D braided composites: A review for stiffness critical applications. *Compos Struct* 2008; 85: 43–58.
11. Melenka GW, Carey JP. Experimental analysis of diamond and regular tubular braided composites using three-dimensional digital image correlation: *https://doi.org/101177/0021998317695418* 2017; 51: 3887–3907.
12. Ead AS, Ayranci C, Carey JP. An Experimental Study of the Creep Behavior of Braided Composites. In: *SAMPE 2019*. Charlotte: SAMPE, 2019.

13. Bruni-bossio B, Ayranci C, Carey JP, et al. Experimental testing of the tensile elastic properties of cellulose braided composites. *Composites Part B* 2019; 166: 542–548.

14. Yan Y. A study of two dimensional braided composites.

15. Kaw K. *Mechanics of Composite Materials*. Second. CRC Press, 2006.

16. Haresceugh RI. Aircraft and aerospace applications of composites. *Concise Encyclopedia of Composite Materials* 2003; 1–7.

17. Beardman P. Automotive Components: Fabriciation. *Concise Encyclopedia of Composite Materials* 1989; 24–31.

18. Bowen DH. Applications of Composites: an overview. *Concise Encyclopedia of Composite Materials1* 1989; 7–15.

19. Mouritz AP, Bannister MK, Falzon PJ, et al. Review of applications for advanced three-dimensional fibre textile composites. *Compos Part A Appl Sci Manuf* 1999; 30: 1445–1461.

20. Ishmael N, Fernando A, Andrew S, et al. Textile technologies for the manufacture of three-dimensional textile preforms. *Research Journal of Textile and Apparel* 2017; 21: 342–362.

21. Scardino F. Introduction to textile structures. In: *Textile Structural Composites*. El Sevier, 1989.

22. Fukuta K, Aoki E. 3D fabrics for structural composties. In: *Proceedings of the 15th Textile Research Symposium*. Philadelphia, PA, 1986.

23. Smith CS. *Design of Marine Structures in Composite Materials*. London: Elsevier Applied Science, 1990.

24. Haresceugh RI. Aircraft and aerospace applications of composites. In: Kelly A (ed) *Concise Encyclopedia of composite materials*. Oxford: Pergamon Press, 1989, pp. 1–7.

25. Niu MCY. *Composite airframe structures*. Hong Kong: Conmilit Press, 1992.

26. Beardman P. Automotive components: Fabrication. In: Kelly A (ed) *Concise Encyclopedia of composite materials*. Oxford: Pergamon Press, 1989, pp. 24–31.

27. Bowen DH. Applications of composites: an overview. In: Kelly A (ed) *Concise encyclopedia of composite materials*. Oxford: Pergamon Press, 1989, p. 715.

28. Carey JP. *Handbook of Advances in Braided Composite Materials: Theory, Production,Testing and Applications*. 2017.

29. Croon C. Braided Fabrics: Properties and Applications. In: *Engineering with Composites, the Third Technology Conference*. 1983, pp. 20.1-20.15.

30. Soebroto HB, Ko F. 3-DIMENSIONALLY BRAIDED CARBON/POLYSULFONE COMPOSITE FOR BONE FIXATION. In: *Bioengineering, Proceedings of the Northeast Conference*. 1987, pp. 198–201.

31. Wan YZ, Wang YL, Cheng GX, et al. Three-dimensionally braided carbon fiber-epoxy composites, a new type of material for osteosynthesis devices. I. Mechanical properties and moisture absorption behavior. *J Appl Polym Sci* 2002; 85: 1031–1039.

32. Sainsburg-Carter JB. BRAIDED COMPOSITE TUBES. 1987, pp. 193–197.

33. Brookstein D. Structural applications of advanced braided composites. In: *Proceedings SPE/APC '88. Advanced Polymer Composites for Structural Applications. Los Angeles, 14-17 November*. 1988, pp. 415–424.

34. Pastore CM, Ko FK. Near net shape manufacturing of composite engine components By 3-D fiber architecture. *Proceedings of the ASME Turbo Expo*; 2. Epub ahead of print 1989. DOI: 10.1115/89-GT-315.

35. Krebs NE, Rahnenfuehrer EW. Aerospace application of braided structures. *Journal of the American Helicopter Society* 1989; 34: 69–74.

36. Colton J, Lyons J, Lukasik B, et al. On-orbit fabrication of space station structures. In: *International SAMPE Symposium and Exhibition (Proceedings)*. 1989, pp. 810–816.

37. Antonio BK. *Material and Mechanical Characterizations for Braided Composite Vessels*, https://apps.dtic.mil/sti/citations/ADA226640 (1990).

38. Stinton DP, Lowden RA, Besmann TM. Fiber-reinforced composites for gas turbine applications. In: *ASME 1992 International Gas Turbine and Aeroengine Congress and Exposition, GT 1992*, https://www.scopus.com/record/display.uri?eid=2-s2.0-84925967765&origin=resultslist&sort=plf-t&src=s&nlo=&nlr=&nls=&sid=c13147063078eb7308cca2b2cf4f34eb&sot=b&sdt=b&sl

=46&s=TITLE-ABS-KEY%28applications+braided+composites%29&relpos=61&citeCnt=0&searchTerm= (1992, accessed 3 November 2021).

39. Smith S, Romanyk D, Major P, et al. An Investigation on the Preparation and Mechanical Properties of Three-dimensional Braided Composite Orthodontic Archwires. *Journal of International Oral Health* 2016; 8: 554–559.

40. Kin B, Cheung O. *Benjamin Kin On Cheung*. 2019.

41. Cheung BKO, Carey JP. Characterizing and modeling of low twist yarn mechanics. *J Eng Fiber Fabr*; 14. Epub ahead of print 2019. DOI: 10.1177/1558925019866945.

42. Allen SR, Farris RJ. Complications of cylindrical anisotropy on the properties of fibres. *Polymer (Guildf)* 1990; 31: 1467–1472.

43. Lacks DJ. Molecular simulation of compressive failure in poly(p-phenylene teraphthalamide) crystals. *J Mater Sci* 1996; 31: 5885–5889.

44. Weinberg A, Schwartz P. Twist effects on the mechanical behaviour of Kevlar 29/epoxy strands. *J Mater Sci Lett* 1987; 6: 832–834.

45. Naik NK, Madhavan V. Twisted impregnated yarns: elastic properties. *Journal of Strain Analysis for Engineering Design* 2000; 35: 83–91.

46. Gegauff C. Strength and elasticity of cotton threads. *Bull Soc Ind Mulhouse*.

47. Rao Y, Farris RJ. Modeling and experimental study of the influence of twist on the mechanical properties of high-performance fiber yarns. *J Appl Polym Sci* 2000; 77: 1938–1949.

48. Shah DU, Schubel PJ, Clifford MJ. Modelling the effect of yarn twist on the tensile strength of unidirectional plant fibre yarn composites. *J Compos Mater* 2013; 47: 425–436.

49. Mertová I, Moučková E, Neckář B, et al. Influence of Twist on Selected Properties of Multifilament Yarn. *Autex Research Journal* 2018; 18: 110–120.

50. Peirce FT. *5—The geometry of cloth structure*. 1937. Epub ahead of print 1937. DOI: 10.1080/19447023708658809.

51. Du Z, Xu B, Yu W. Theoretical study on the bending rigidity of filament yarns with an elliptical cross-section using energy method. I. Theoretical modeling. *Fibers and Polymers* 2010; 11: 883–890.

52. Jeon BS. A study on the structural properties of plain fabrics using the lenticular model. *Fibers and Polymers* 2013; 14: 1927–1932.

53. Cheung BKO, Carey JP. Improving two-dimensional braided composite tensile properties by including low angle yarn twist: Production, experimental verification, and modeling. *J Eng Fiber Fabr*; 15. Epub ahead of print 2020. DOI: 10.1177/1558925020946449.

54. Yu G, Shang-Li D, Song H, et al. Characterization of stress distribution and thermal expansion behavior for M40J/AG-80 composites experienced vacuum thermo-cycling. *Journal of Reinforced Plastics and Composites* 2006; 25: 1647–1657.

55. Bowles DE, Tompkins SS. Prediction of Coefficients of Thermal Expansion for Unidirectional Composites. *J Compos Mater* 1989; 23: 370–388.

56. ASTM International. *Standard Test Method for Linear Thermal Expansion of Solid Materials by Thermomechanical Analysis*. Epub ahead of print 2018. DOI: 10.1520/E0831-19.

57. ASTM International. *Standard Test Method for Linear Thermal Expansion of Solid Materials With a Push-Rod Dilatometer*. Epub ahead of print 2022. DOI: 10.1520/E0228-22.

58. Pastore CM. *OPPORTUNITIES AND CHALLENGES FOR TEXTILE REINFORCED COMPOSITES*. 2000.

59. Dixit A, Mali HS. Modeling techniques for predicting the mechanical properties of woven-fabric textile composites: A Review. *Mechanics of Composite Materials* 2013; 49: 1–20.

60. Carey JP, Melenka GW, Hunt AJ, et al. Introduction to braided composite material behavior. In: *Handbook of Advances in Braided Composite Materials: Theory, Production, Testing and Applications*. Elsevier Inc., 2017, pp. 207–237.

61. Lomov S, Verpoest I. Manufacturing and internal geometry of textiles. In: *Design and Manufacture of Textiles Composites*. 2005, pp. 1–61.

62. Lord PR, Mohamed MH. *Weaving: Conversion of yarn to fabric*. 1982.

63. Ko F, Head A, Pastore C. *Handbook of Industrial Braiding*. Covington, Kentucky: Atkins and Pearce, 1989.

64. Mouritz AP, Bannister MK, Falzon PJ, et al. Review of applications for advanced three-dimensional fibre textile composites. *Composites: Part A*.

65. Bobet J-L, Lamonf J. *THERMAL RESIDUAL STRESSES IN CERAMIC MATRIX COMPOSITES-I. AXISYMMETRICAL MODEL AND FINITE ELEMENT ANALYSIS*. 1995.

66. Agrawal P, Conlon K, Bowman KJ, et al. Thermal residual stresses in co-continuous composites. *Acta Mater* 2003; 51: 1143–1156.

67. Choo H, Bourke MAM, Daymond MR. A finite-element analysis of the inelastic relaxation of thermal residual stress in continuous-fiber-reinforced composites. *Composite Science and Technology* 2001; 1757–1772.

68. Lu C, Chen P, Yu Q, et al. Thermal residual stress distribution in carbon fiber/novel thermal plastic composite. *Applied Composite Materials* 2008; 15: 157–169.

69. Jia Y, Li K, Xue L, et al. Electromagnetic interference shielding effectiveness of carbon fiber reinforced multilayered (PyC–SiC)n matrix composites. *Ceram Int* 2016; 42: 986–988.

70. Daghyani HR, Ye L, Mai Y-W. Effect of thermal residual stress on the crack path in adhesively bonded joints. *Journal of Material Science* 1996; 31: 2523–2529.

71. Chamis CC, Sendeckyj GP. Critique on Theories Predicting Thermoelastic Properties of Fibrous Composites. *J Compos Mater* 1968; 2: 332.

72. L. B. Greszczuk. Thermoelastic Properties of Filamentary Composites. In: *AIAA 6th Str. and Mater. Conference*. Palm Springs, California, 1965, p. 285.

73. Turner PS. Thermal-Expansion Stresses in Reinforced Plastics. *J Res Natl Bur Stand (1934)* 1946; 37: 239–250.

74. Van Fo Fy GA. Elastic constants and thermal expansion of certain bodies with inhomogenous regular structure [in Russian]. *Soviet Physics*.

75. Van Fo Fy GA. Thermal strains and stress in glass fiber reinforced media. *Prikl Mekh Teor Fiz* 1965; 101 [in Russian].

76. Van Fo Fy GA, Savin GN. Fundementals of the theory of non-fabric glass reinforced plastics . *Fundementals of the theory of non-fabric glass reinforced plastics* 1965; 1-151 [in Russian].

77. Levin VM. On the Coefficients of Thermal Expansion of Heterogeneous materials. *Mekhanika Tverdogo Tela* 1967; 88 [in Russian].

78. Schapery RA. Thermal Expansion Coefficients of Composite Materials Based on Energy Principles. *J Compos Mater* 1968; 2: 380–404.

79. Haplin JC. *Primer on Composite Material Analysis*. 1st ed. 1969.

80. Rosen BW, Hashin Z. Effective thermal expansion coefficients and specific heats of composite materials. *Int J Eng Sci* 1970; 8: 157–173.

81. Holliday L, Robinson J. Review: The thermal expansion of composites based on polymers. *Journal of Material Science* 1973; 8: 301–311.

82. Wakashima K, Otsuka M, Umekawa S. Thermal Expansions of Heterogeneous Solids Containing Aligned Ellipsoidal Inclusions. *J Compos Mater*; 8.

83. Craft WJ, Christensen RM. Coefficient of Thermal Expansion for Composites with Randomly Oriented Fibers. *J Compos Mater* 1981; 15: 2–20.

84. Yalvac S, Tastistcheff EM. An Analytical Model for Estimating the Coefficient of Thermal Expansion of Random Fiber Reinforced Composites. *Journal of Reinforced Plastics and Composites* 1989; 8: 472–483.

85. Chamis CC. *Simplified Composite Micromechanics Equations for Hygral, Thermal and Mechanical Properties*. 1983.

86. Ishikawa T, Koyama K, Higeo Kobayashi S. Thermal Expansion Coefficients of Unidirectional Composites. *J Compos Mater* 1978; 153–168.

87. Johnson RR, Kural MH, Mackey GB. *THERMAL EXPANSION PROPERTIES OF COMPOSITE MATERIALS*, https://ntrs.nasa.gov/search.jsp?R=19810023033 (1981).

88. Titomanlio G, Piccarolo S. Thermal expansion behaviour of laminated composites: Evaluation of superficial deviation from lamination theory.

89. Pagano NJ, Pipes RB. Some Observations on the Interlaminar Strength of Composite Materials. *International Journal of Mechanical Science* 1973; 15: 679–68.

90. Sideridis E. Thermal expansion coefficients of fiber composites defined by the concept of the interphase. *Compos Sci Technol* 1994; 51: 301–317.

91. Ran Z, Yan Y, Li J, et al. Determination of thermal expansion coefficients for unidirectional fiber-reinforced composites. *Chinese Journal of Aeronautics* 2014; 27: 1180–1187.

92. Ishikawa T, Chou TW. In-Plane Thermal Expansion and Thermal Bending Coefficients of Fabric Composites. *J Compos Mater* 1983; 17: 92–104.

93. Naik NK, Ganesh VK. Prediction of thermal expansion coefficients of plain weave fabric composites. *Compos Struct* 1993; 26: 139–154.

94. Naik NK, Ganesh VK. *Prediction of on-axes elastic properties of plain weave fabric composites*. 1992.

95. Sankar B V, Marrey R V. Analytical Method for Micromechanics of Textile Composites. *Compos Sci Technol* 1997; 703–713.

96. Powell RE, Yeh HY. Mechanical Characterization of Hybridized Braided Composite Structures. *Journal of Reinforced Plastics and Composites* 1995; 14: 164–194.

97. Naik RA. *Analysis of Woven and Braided Fabric-Reinforced Composites*. American Society for Testing and Materials, www.astm.org (1996).

98. ASTM INTERNATIONAL. *D3039/D3039M-08: Standard Test Method for Tensile Properties of Polymer Matrix Composite Materials*, https://compass.astm.org/document/?contentCode=ASTM%7CD3039_D3039M-08%7Cen-US&proxycl=https%3A%2F%2Fsecure.astm.org&fromLogin=true (2014, accessed 9 February 2022).

99. Fahmy AA, Ragai AN. Thermal expansion of graphite-epoxy composites. *J Appl Phys* 1970; 41: 5112–5115.

100. Freeman WT, Campbell MD. *Thermal Expansion Characteristics of Graphite Reinforced Composite Materials*, www.astm.org (1972).

101. Yates B, Overy MJ, Sargent JP, et al. *The thermal expansion of carbon fibre-reinforced plastics Part 2 The influence of fibre volume fraction*. 1978.

102. Strife JR, Prewo KM. The Thermal Expansion Behavior of Unidirectional and Bidirectional Kevlar/Epoxy Composites. *J Compos Mater* 1979; 13: 264–277.

103. Adams RD. Compositional Effects of Fiber Reinforced Composites on the Coefficient of Thermal Expansion. In: *Materials Characterization by Thermomechanical Analysis*. 1991, pp. 150–160.

104. Raghava RS. Prediction of thermal and mechanical properties of glass-epoxy composite laminates. *Polym Compos* 1984; 5: 173–178.

105. Chamberlain NJ. *Derivation of Expansion Coefficients For a Fiber Reinforced Composite*. 1968.

106. Raghava RS, Valentich J, Nathenson RD. *Thermoelastic Behavior of Thick Glass/Epoxy Composite Laminates*. 1984.

107. Akay M, Mun SKA, Stanley A. Influence of moisture on the thermal and mechanical properties of autoclaved and oven-cured Kevlar-49/epoxy laminates. *Compos Sci Technol* 1997; 57: 565–571.

108. Tezvergil A, Lassila LVJ, Vallittu PK. The effect of fiber orientation on the thermal expansion coefficients of fiber-reinforced composites. *Dental Materials* 2003; 19: 471–477.

109. Rupnowski P, Gentz M, Sutter JK, et al. An evaluation of the elastic properties and thermal expansion coefficients of medium and high modulus graphite fibers. *Compos Part A Appl Sci Manuf* 2005; 36: 327–338.

110. Mori T, Tanaka K. Average stress in matrix and average elastic energy of materials with misfitting inclusions. *Acta Metallurgica* 1973; 21: 571–574.

111. Rogers KF, Kingston-Lee DM, Phillips LN, et al. *The thermal expansion of carbon-fibre reinforced plastics Part 6 The influence of fibre weave in fabric reinforcement*. 1981.

112. Liao X, Li H, Xu W, et al. Study on the thermal expansion properties of C/C composites. *J Mater Sci* 2007; 42: 3435–3439.

113. Zhang Q, Cheng L, Zhang L, et al. Thermal expansion behavior of carbon fiber reinforced chemical-vapor-infiltrated silicon carbide composites from room temperature to 1400 °C. *Mater Lett* 2006; 60: 3245–3247.

114. Zhang D, Cao Y, Liu R, et al. Effect of 3d-braided structure on thermal expansion of PIP-Cf/SiC composites. *Powder Metallurgy and Metal Ceramics* 2014; 52: 722–726.

115. Furusho N, Komatsu T, Nakagawa T. A study of the thermal degradation of several halogen containing polymers by torsional braid analysis. *Bull Chem Soc Jpn* 1974; 47: 1573–1577.

116. Mackowski MJ, West KE, Samsel DA, et al. Expansion coefficients of some epoxies in the temperature range 4-300 K. *Cryogenics (Guildf)* 1976; 16: 45–47.

117. Adamson MJ. Thermal expansion and swelling of cured epoxy resin used in graphite/epoxy composite materials. *J Mater Sci* 1980; 15: 1736–1745.

118. Joshi OK. The effect of moisture on the shear properties of carbon fibre composites. *Composites* 1983; 14: 196–200.

119. Bowles DE. *Finite Element Composite Analysis Program (FECAP) for a microcomputer*. 1 July 1988.

120. Liu ST, Cheng GD. [in Mandarin]. *Acta Mater Compos Sinica*; 14.

121. Islam R, Sjölind SG, Pramila A. Finite element analysis of linear thermal expansion coefficients of unidirectional cracked composites. *J Compos Mater* 2001; 35: 1762–1776.

122. Karadeniz ZH, Kumlutas D. A numerical study on the coefficients of thermal expansion of fiber reinforced composite materials. *Compos Struct* 2007; 78: 1–10.

123. Raju IS, Craft WJ, Avva VS. Thermal Expansion Characteristics of Woven Fabric Composites. In: *Advances in Structural Testing, Analysis and Design*. 1990.

124. Hahn HT, Pandey R. A Micromechanics Model for Thermoplastic Properties of Plain Weave Fabric Composites. *J Eng Mater Technol*, http://asmedigitalcollection.asme.org/materialstechnology/article-pdf/116/4/517/5549408/517_1.pdf (1994).

125. Dasgupta A, Agarwal RK, Bhandarkar SM. THREE-DIMENSIONAL MODELING OF WOVEN-FABRIC COMPOSITES FOR EFFECTIVE THERMO-MECHANICAL AND THERMAL PROPERTIES. *Compos Sci Technol* 1996; 56: 209–223.

126. Whitcomb JD. *THREE-DIMENSIONAL STRESS ANALYSIS OF PLAIN WEAVE COMPOSITES*. 1989.

127. Marrey R V, Sankar B V. *Micromechanical Models for Textile Structural Composites*. Gainesville, Florida, 1995.

128. Ishikawa T, Watanabe N, Bansaku K, et al. Closed Form Predictions of Macroscopic Thermomechanical Properties of Orthogonal 3-D Woven Fabric Composites. In: *Proceedings of ICCM-11*. 1997, p. 189.

129. Tan P, Tong L, Steven GP. A three-dimensional modelling technique for predicting the linear elastic property of opened-packing woven fabric unit cells. *Compos Struct* 1997; 38: 261–271.

130. Tan P, Tong L, Steven GP. Models for Predicting Thermomechanical Properties of Three-dimensional Orthogonal Woven Composites. *Journal of Reinforced Plastics and Composites* 1999; 18: 151–185.

131. Chen ZR, Zhu DC, Lu M, et al. A homogenisation scheme and its application to evaluation of elastic properties of three-dimensional braided composites. *Composites: Part B* 2001; 32: 67–86.

132. Sun CT, Vaidya RS. PREDICTION OF COMPOSITE PROPERTIES FROM A REPRESENTATIVE VOLUME ELEMENT. *Compos Sci Technol* 1996; 56: 171–179.

133. Naik NK, Shembekar PS. Elastic Behavior of Woven Fabric Composites: I—Lamina Analysis. *J Compos Mater* 1992; 26: 2196–2225.

134. Shembekar PS, Naik NK. Elastic Behavior of Woven Fabric Composites: II—Laminate Analysis. *J Compos Mater* 1992; 26: 2226–2246.

135. Wang Y-Q, Wang ASD. *MICROSTRUCTURE/PROPERTY RELATIONSHIPS IN THREE-DIMENSIONALLY BRAIDED FIBER COMPOSITES*. 1995.

136. Mohajerjasbi S. Predictions for coefficients of thermal expansion of three-dimensional braided composites. *AIAA Journal* 1997; 35: 141–144.

137. Mohajerjasbi S. Predictions for coefficients of thermal expansion of 3-D braided composites. In: *37th AIAA/ASME/ASCE/AHS/ASC Structure, Structural Dynamics and Materials Conference*. 1996. Epub ahead of print 1996. DOI: 10.2514/6.1996-1531.

138. Xu Y, Zhang W. Numerical prediction of the effective coefficient of thermal expansion of 3D braided C/SiC composite. *Int J Simul Multidisci Des Optim* 2009; 3: 443–448.

139. Liang J, Du SY, Chen XF. Thermal Expansion Coefficients of 3D braided composites with penny-shaped microcracks. *Acta Mater Compos Sin* 1998; 15: 103–107.

140. Li KZ, Li HJ. Thermal Expansion Property of C/C Composite. *Trans Mater Heat Treat* 2006; 27: 1–4.

141. Cheng L. Thermal Expansion Coefficients of carbon/epoxy braided composites [in Mandarin]. *Journal of Solid Rocket Technology* 2010; 33: 108–111.

142. Yao XF, Yang G, Yao ZH, et al. Experimental study of thermal expansion behaviour on braided structure composite. *Acta Mater Compos Sin* 2000; 17: 20–25.

143. Lu Z, Wang C, Xia B, et al. Effect of interfacial properties on the thermophysical properties of 3D braided composites: 3D multiscale finite element study. *Polym Compos* 2014; 35: 1690–1700.

144. Jiang LL, Xu GD, Cheng S, et al. Finite element analysis of thermo-mechanical properties of 3D braided composites. *Applied Composite Materials* 2014; 21: 325–340.

145. Hu CX, Li HJ, Zhang SY, et al. Numerical simulation on thermal expansion coefficient of 3D braided C/C composites. *Rare Metals* 2014; 33: 99–106.

146. Jiang L li, Xu G dong, Cheng S, et al. Predicting the thermal conductivity and temperature distribution in 3D braided composites. *Compos Struct* 2014; 108: 578–583.

147. Pan Z, Gu B, Sun B. Numerical analyses of thermo-mechanical behaviors of 3-D rectangular braided composite under different temperatures. *Journal of the Textile Institute* 2015; 106: 173–186.

148. Wang H, Cao M, Siddique A, et al. Numerical analysis of thermal expansion behaviors and interfacial thermal stress of 3D braided composite materials. *Comput Mater Sci* 2017; 138: 77–91.

149. Zhai J, Zeng T, Xu G dong, et al. A multi-scale finite element method for failure analysis of three-dimensional braided composite structures. *Compos B Eng* 2017; 110: 476–486.

150. Zhai J, Cheng S, Zeng T, et al. Thermo-mechanical behavior analysis of 3D braided composites by multiscale finite element method. *Compos Struct* 2017; 176: 664–672.

151. Ead AS, Ayranci C, Carey JP. An Experimental Study of the Creep Behavior of Braided Composites. Charlotte: SAMPE, 2019. Epub ahead of print 2019. DOI: 10.33599/nasampe/s.19.1408.

152. Cai Y, Sun H. Thermo-viscoelastic analysis of three-dimensionally braided composites. *Compos Struct*; 98. Epub ahead of print 2013. DOI: 10.1016/j.compstruct.2012.11.012.

153. Tsai SW, Hahn HThomas. *Introduction to composite materials*. Technomic Pub, 1980.

154. Melenka GW, Hunt AJ, van Ravenhorst JH, et al. Manufacturing processes for braided composite materials. *Handbook of Advances in Braided Composite Materials: Theory, Production, Testing and Applications* 2017; 47–153.

155. Brookstein D. Structural applications of advanced braided composites. In: *Proceedings SPE/APC '88. Advanced Polymer Composites for Structural Applications. Los Angeles, 14-17 November*. 1988, pp. 415–424.

156. Carey J, Munro M, Fahim A. Regression-based model for elastic constants of 2D braided/woven open mesh angle-ply composites. *Polym Compos* 2005; 26: 152–164.

157. Carey J, Munro M, Fahim A. Longitudinal elastic modulus prediction of a 2-D braided fiber composite. *Journal of Reinforced Plastics and Composites* 2003; 22: 813–831.

158. Brunnschweiler D. The structure and tensile properties of braids. *Journal of the Textile Institute Transactions* 1954; 45: T55–T77.

159. Falzod PJ, Herszbergb I. MECHANICAL PERFORMANCE OF 2-D BRAIDED CARBON / EPOXY COMPOSITES *. 1998; 3538: 253–265.

160. Ayranci C, Carey JP. Effect of diameter in predicting the elastic properties of 2D braided tubular composites. *J Compos Mater* 2010; 44: 2031–2044.

161. Melenka, G.W. Nobes, D.S. Carey JP. 3D DIC Measurement of Tubular Braided. *The 19th International Conference on Composite Materials* 2012; 1–12.

162. Ayranci C, Carey J, Romanyk D. Elastic Properties of Large-Open-Mesh 2D Braided Composites: Model Predictions and Initial Experimental Findings. *Polym Compos* 2010; 2017–2024.

163. Carey J, Fahim A, Munro M. Design of Braided Composite Cardiovascular Catheters Based on Required Axial , Flexural , and Torsional Rigidities. 2004; 73–81.

164. Cichosz J, Wehrkamp-Richter T, Koerber H, et al. Failure and damage characterization of (±30°) biaxial braided composites under multiaxial stress states. *Compos Part A Appl Sci Manuf* 2016; 90: 748–759.

165. Yang Y, Ahmed K, Zhang R, et al. A study on the energy absorption capacity of braided rod composites. *Compos Struct* 2018; 206: 933–940.

166. Tong Y, Xu Y. Improvement of crash energy absorption of 2D braided composite tubes through an innovative chamfer external triggers. *Int J Impact Eng* 2018; 111: 11–20.

167. Tate JS, Kelkar AD, Whitcomb JD. Effect of braid angle on fatigue performance of biaxial braided composites. *Int J Fatigue* 2006; 28: 1239–1247.

168. Tate JS, Kelkar AD. Stiffness degradation model for biaxial braided composites under fatigue loading. *Compos B Eng* 2008; 39: 548–555.

169. James JD, Spittle JA, Brown SGR, et al. *A review of measurement techniques for the thermal expansion coefficient of metals and alloys at elevated temperatures*, www.iop.org/Journals/mt (2001).

170. Hunt AJ, Carey JP. A machine vision system for the braid angle measurement of tubular braided structures. *Textile Research Journal* 2019; 89: 2919–2937.

171. Aldrich DR. *Design and Development of a New Model for Predicting the Mechanical Properties of Three-Dimensional Braided Composite Materials*, https://era.library.ualberta.ca/items/09999b5a-9f7d-495e-9814-2d00b88f7872 (2018).

172. Bigger R, Blaysat B, Boo C, et al. *A Good Practices Guide for Digital Image Correlation*. Epub ahead of print 24 October 2018. DOI: 10.32720/idics/gpg.ed1/print.format.

173. Affdl JCH, Kardos JL. The Halpin-Tsai equations: A review. *Polymer Engineering & Science* 1976; 16: 344–352.

174. Chou T, Ishikawa T. Elastic Behavior of Woven Hybrid Composites. *J Compos Mater*; 16.

175. Ishikawa T, Chou TW. In-Plane Thermal Expansion and Thermal Bending Coefficients of Fabric Composites. *J Compos Mater* 1983; 17: 92–104.

176. Hexion. *Epoxy Resin System 826 862 LS-81K*.

177. Akay M, Mun SKA, Stanley A. Influence of moisture on the thermal and mechanical properties of autoclaved and oven-cured Kevlar-49/epoxy laminates. *Compos Sci Technol* 1997; 57: 565–571.

178. Van Ravenhorst JH, Akkerman R. A yarn interaction model for circular braiding. *Compos Part A Appl Sci Manuf* 2016; 81: 254–263.

179. Van Ravenhorst JH, Akkerman R. Circular braiding take-up speed generation using inverse kinematics. *Compos Part A Appl Sci Manuf* 2014; 64: 147–158.

180. Kessels JFA, Akkerman R. Prediction of the yarn trajectories on complex braided preforms. *Compos Part A Appl Sci Manuf* 2002; 33: 1073–1081.

181. Cornelissen B, de Rooij MB, Rietman B, et al. Frictional behaviour of high performance fibrous tows: A contact mechanics model of tow-metal friction. *Wear* 2013; 305: 78–88.

182. Howell HG. Inter-fibre friction. *Journal of the Textile Institute Transactions* 1951; 42: T521–T533.

183. Howell HG, Mazur J. Amontons' law and fibre friction. *Journal of the Textile Institute Transactions* 1953; 44: T59–T69.

184. Ben Boubaker B, Haussy B, Ganghoffer JF. Discrete woven structure model: yarn-on-yarn friction. *Comptes Rendus - Mecanique* 2007; 335: 150–158.

185. Unlusoy C, Melenka GW. Flexural testing of cellulose fiber braided composites using three dimensional digital image correlation. *Compos Struct* 2019; 230: 111538.

186. Bruni-Bossio BM, Melenka GW, Ayranci C, et al. Micro-computed tomography analysis of natural fiber and bio-matrix tubular-braided composites. *J Compos Mater* 2019; 53: 4003–4013.

187. Li J, Yang H, Kou C. Fatigue properties of three dimensional braiding composites. *Fuhe Cailiao Xuebao/Acta Materiae Compositae Sinica* 2005; 22: 172–176.

188. Wolfahrt M, Grosser J, Fleischmann M, et al. Characterization of the mechanical and fatigue behavior of braided composites made of twisted yarns. *Materials Science Forum* 2015; 825–826: 876–882.

189. Carvelli V, Pazmino J, Lomov S V., et al. Quasi-static and fatigue tensile behavior of a 3D rotary braided carbon/epoxy composite. *J Compos Mater* 2013; 47: 3195–3209.

190. ASTM standard. D3039M-08 (2008) Standard test method for tensile properties of polymer matrix composite materials. *Annual Book of ASTM Standards* 2013; 1–13.

191. May M, Kilchert S. The effect of loading rate on the in-plane shear strength of tri-axial braided composites. *J Compos Mater* 2022; 56: 421–426.

192. Böhm R. "Experimental Investigation of the Strain Rate Dependent Behaviour of 2D Biaxially and Triaxially Reinforced Braided Composites. *Applied Composite Materials* 2014; 21: 285–299.

193. Jiang L, Xiao S, Jiang W, et al. Effect of stacking configuration on dynamic tensile properties of braided carbon fibre composites under medium-low strain rates. *Compos Sci Technol*; 213.

194. Hou JP, Ruiz C. *Measurement of the properties of woven CFRP T300/914 at di€erent strain rates*, www.elsevier.com/locate/compscitech.

195. Naresh K, Shankar K, Rao BS, et al. Effect of high strain rate on glass/carbon/hybrid fiber reinforced epoxy laminated composites. *Compos B Eng* 2016; 100: 125–135.

196. Gilat A, Goldberg RK, Roberts GD. *Experimental study of strain-rate-dependent behavior of carbon/epoxy composite*, www.elsevier.com/locate/compscitech.

197. Al-Zuaidy H, Zhao X-L, Al-Mahaidi R. Mechanical characterisation of the dynamic tensile properties of CFRP sheet and adhesive at medium strain rates. *Compos Struct* 2013; 96: 153–164.

198. Hexion. *Technical Data Sheet for Epoxy Resin System 826 862 LS-81K*, https://www.hexion.com/en-US/product/sf-8017-epoxy-resin-system-826-862-ls-81k (2022, accessed 9 February 2022).

199. Brunnschweiler D. Braids and braiding. *Journal of the Textile Institute* 1953; 44: 666–686.

200. Bruni-bossio BM, Melenka GW, Ayranci C, et al. Micro-computed tomography analysis of natural fiber and bio-matrix tubular-braided composites. Epub ahead of print 2019. DOI: 10.1177/0021998319853023.

201. Si J, Wang J, Yu X, et al. Influence of thermal-oxidative aging on the mechanical performance and structure of cold-mixed epoxy asphalt. *J Clean Prod*; 337. Epub ahead of print 20 February 2022. DOI: 10.1016/J.JCLEPRO.2022.130482.

202. Kong ES, Wilkes GL, McGrath JE, et al. Physical aging of linear and network epoxy resins. *Polym Eng Sci* 1981; 21: 943–950.

203. Chiao TT, Moore RL, H T. No-Stress Aging of Aramid / Epoxy Composites. 2019; 98–100.

204. Odegard GM, Bandyopadhyay A. Physical aging of epoxy polymers and their composites. *J Polym Sci B Polym Phys* 2011; 49: 1695–1716.

205. Lepp EA, Carey JP. An examination of initial structural degradation in tubular braided composites through region-by-region strain analysis: *https://doi.org/101177/1558925020978325*; 15. Epub ahead of print 4 December 2020. DOI: 10.1177/1558925020978325.

206. ASTM INTERNATIONAL. *E111-17: Standard Test Method for Young's Modulus, Tangent Modulus , and Chord Modulus*. 2010. Epub ahead of print 2010. DOI: 10.1520/E0111-04R10.

207. Curran MA. Life Cycle Assessment. *Kirk-Othmer Encyclopedia of Chemical Technology* 2016; 1–28.

208. Gupta A, Kumar A. Composites Materials: Addressing the Climate Change. *Asia Pacific Business Review* 2010; 6: 78–89.

209. Thankachen RU, Nair A, Raj J, et al. Methodologies for selecting biopolymers and their characteristic features for industrial applications. In: *Biopolymers and their Industrial Applications*. Elsevier, 2021, pp. 81–103.

210. Netravali AN, Chabba S. Composites get greener. *Materials Today* 2003; 6: 22–29.

211. Tukker A. Life cycle assessment as a tool in environmental impact assessment. *Environ Impact Assess Rev* 2000; 20: 435–456.

212. La Rosa AD, Cozzo G, Latteri A, et al. Life cycle assessment of a novel hybrid glass-hemp/thermoset composite. *J Clean Prod* 2013; 44: 69–76.

213. Rebitzer G, Ekvall T, Frischknecht R, et al. Life cycle assessment Part 1: Framework, goal and scope definition, inventory analysis, and applications. *Environment International* 2004; 30: 701–720.

214. ISO. *Environmental management — Life cycle assessment — Principles and framework*. Geneva, 2006.

215. ISO. *Environmental management — Life cycle assessment — Requirements and guidelines*. Geneva, 2006.

216. Mansor MR, Salit MS, Zainudin ES, et al. Life cycle assessment of natural fiber polymer composites. In: *Agricultural Biomass Based Potential Materials*. Springer International Publishing, 2015, pp. 121–141.

217. Mansor MR, Mastura MT, Sapuan SM, et al. The environmental impact of natural fiber composites through life cycle assessment analysis. In: *Durability and Life Prediction in Biocomposites, Fibre-Reinforced Composites and Hybrid Composites*. Elsevier, 2018, pp. 257–285.

218. Pegoretti TDS, Mathieux F, Evrard D, et al. Use of recycled natural fibres in industrial products: A comparative LCA case study on acoustic components in the Brazilian automotive sector. *Resour Conserv Recycl* 2014; 84: 1–14.

219. Ramesh M, Deepa C, Kumar LR, et al. Life-cycle and environmental impact assessments on processing of plant fibres and its bio-composites: A critical review. *Journal of Industrial Textiles*. Epub ahead of print 21 May 2020. DOI: 10.1177/1528083720924730.

220. Leejarkpai T, Mungcharoen T, Suwanmanee U. Comparative assessment of global warming impact and eco-efficiency of PS (polystyrene), PET (polyethylene terephthalate) and PLA (polylactic acid) boxes. *J Clean Prod* 2016; 125: 95–107.

221. Pennington DW, Potting J, Finnveden G, et al. Life cycle assessment Part 2: Current impact assessment practice. *Environment International* 2004; 30: 721–739.

222. Yates MR, Barlow CY. Life cycle assessments of biodegradable, commercial biopolymers - A critical review. *Resources, Conservation and Recycling* 2013; 78: 54–66.

223. Baum R, Bieńkowski J. Eco-efficiency in measuring the sustainable production of agricultural crops. *Sustainability (Switzerland)*; 12. Epub ahead of print 1 February 2020. DOI: 10.3390/su12041418.

224. Brentrup F, Küsters J, Lammel J, et al. Environmental impact assessment of agricultural production systems using the life cycle assessment (LCA) methodology II. The application to N fertilizer use in winter wheat production systems. *European Journal of Agronomy* 2004; 20: 265–279.

225. Nair AB, Sivasubramanian P, Balakrishnan P, et al. Environmental Effects, Biodegradation, and Life Cycle Analysis of Fully Biodegradable 'Green' Composites. In: *Polymer Composites, Biocomposites*. Wiley Blackwell, 2013, pp. 515–568.

226. Mukhopadhyay S. Environment-Related Issues. In: *Natural Fiber Composites*. CRC Press, 2015, pp. 199–220.

227. Zampori L, Dotelli G, Vernelli V. Life cycle assessment of hemp cultivation and use of hemp-based thermal insulator materials in buildings. *Environ Sci Technol* 2013; 47: 7413–7420.

228. La Rosa AD, Recca G, Summerscales J, et al. Bio-based versus traditional polymer composites. A life cycle assessment perspective. *J Clean Prod* 2014; 74: 135–144.

229. Miller SA, Srubar W V., Billington SL, et al. Integrating durability-based service-life predictions with environmental impact assessments of natural fiber-reinforced composite materials. *Resour Conserv Recycl* 2015; 99: 72–83.

230. Mayandi K, Rajini N, Manojprabhakar M, et al. Recent studies on durability of natural/synthetic fiber reinforced hybrid polymer composites. In: *Durability and Life Prediction in Biocomposites, Fibre-Reinforced Composites and Hybrid Composites*. Elsevier, 2018, pp. 1–13.

231. Bari E, Morrell JJ, Sistani A. Durability of natural/synthetic/biomass fiber-based polymeric composites: Laboratory and field tests. In: *Durability and Life Prediction in Biocomposites, Fibre-Reinforced Composites and Hybrid Composites*. Elsevier, 2018, pp. 15–26.

232. Peterson S, Jayaraman K, Bhattacharyya D. Forming performance and biodegradability of woodfibre-Biopol™ composites. *Compos Part A Appl Sci Manuf* 2002; 33: 1123–1134.

233. Azwa ZN, Yousif BF, Manalo AC, et al. A review on the degradability of polymeric composites based on natural fibres. *Materials and Design* 2013; 47: 424–442.

234. Joshi S V., Drzal LT, Mohanty AK, et al. Are natural fiber composites environmentally superior to glass fiber reinforced composites? In: *Composites Part A: Applied Science and Manufacturing*. Elsevier, 2004, pp. 371–376.

235. Shogren R, Wood D, Orts W, et al. Plant-based materials and transitioning to a circular economy. *Sustainable Production and Consumption* 2019; 19: 194–215.

236. Miah JH, Koh SCL, Stone D. A hybridised framework combining integrated methods for environmental Life Cycle Assessment and Life Cycle Costing. *Journal of Cleaner Production* 2017; 168: 846–866.

237. Hunkeler D, Lichtenvort K, Rebitzer G. Introduction: History of Life Cycle Costing, Its Categorization, and Its Basic Framework. In: *Environmental Life Cycle Costing*. CRC Press, 2020, pp. 35–50.

238. Hunkeler D, Lichtenvort K, Rebitzer G. *Environmental life cycle costing*. CRC Press, 2008. Epub ahead of print 1 January 2008. DOI: 10.1201/9781420054736.

239. Heijungs R, Settanni E, Guinée J. Toward a computational structure for life cycle sustainability analysis: Unifying LCA and LCC. *International Journal of Life Cycle Assessment* 2013; 18: 1722–1733.

240. Srubar W V., Miller SA, Lepech MD, et al. Incorporating spatiotemporal effects and moisture diffusivity into a multi-criteria materials selection methodology for wood-polymer composites. *Constr Build Mater* 2014; 71: 589–601.

241. Duflou JR, Yelin D, Van Acker K, et al. Comparative impact assessment for flax fibre versus conventional glass fibre reinforced composites: Are bio-based reinforcement materials the way to go? *CIRP Ann Manuf Technol* 2014; 63: 45–48.

242. Holm VK, Ndoni S, Risbo J. The stability of poly(lactic acid) packaging films as influenced by humidity and temperature. *J Food Sci* 2006; 71: E40–E44.

243. Dhakal HN, Zhang ZY, Richardson MOW. Effect of water absorption on the mechanical properties of hemp fibre reinforced unsaturated polyester composites. *Compos Sci Technol* 2007; 67: 1674–1683.

244. Maslinda AB, Abdul Majid MS, Ridzuan MJM, et al. Effect of water absorption on the mechanical properties of hybrid interwoven cellulosic-cellulosic fibre reinforced epoxy composites. *Compos Struct* 2017; 167: 227–237.

245. Joseph P V., Rabello MS, Mattoso LHC, et al. Environmental effects on the degradation behaviour of sisal fibre reinforced polypropylene composites. *Compos Sci Technol* 2002; 62: 1357–1372.

246. Da Silva AO, Monsores KGDC, De Sant'Ana Oliveira S, et al. Influence of gamma and ultraviolet radiation on the mechanical behavior of a hybrid polyester composite reinforced with curaua mat and aramid fabric. *Journal of Materials Research and Technology* 2020; 9: 394–403.

247. Fiore V, Scalici T, Badagliacco D, et al. Aging resistance of bio-epoxy jute-basalt hybrid composites as novel multilayer structures for cladding. *Compos Struct* 2017; 160: 1319–1328.

248. Yu Y, Hurren C, Millington KR, et al. Effects of fibre parameters on the ultraviolet protection of fibre assemblies. *Journal of the Textile Institute* 2016; 107: 614–624.

249. Wypych G. *Handbook of Material Weathering*. Elsevier, 2013. Epub ahead of print 2013. DOI: 10.1016/C2012-0-07343-7.

250. Takagi H, Ochi & S. *Mechanical properties and biodegradation behavior of high-strength 'green' composites*. WIT Press, 12 May 2004.

251. Ji M, Li F, Li J, et al. Enhanced mechanical properties, water resistance, thermal stability, and biodegradation of the starch-sisal fibre composites with various fillers. *Mater Des* 2021; 198: 109373.

252. Fabiyi JS, McDonald AG, Wolcott MP, et al. Wood plastic composites weathering: Visual appearance and chemical changes. *Polym Degrad Stab* 2008; 93: 1405–1414.

253. Lakshmi Narayana V, Bhaskara Rao L. A brief review on the effect of alkali treatment on mechanical properties of various natural fiber reinforced polymer composites. *Mater Today Proc* 2021; 44: 1988–1994.

254. Pujari S. Comparison of Jute and Banana Fiber Composites: A Review. *International Journal of Current Engineering and Technology* 2013; 2: 121–126.

255. Everitt NM, Aboulkhair NT, Clifford MJ. Looking for Links between Natural Fibres' Structures and Their Physical Properties. *Conference Papers in Materials Science* 2013; 2013: 1–10.

256. Faruk O, Bledzki AK, Fink HP, et al. Biocomposites reinforced with natural fibers: 2000-2010. *Progress in Polymer Science* 2012; 37: 1552–1596.

257. Pickering KL, Efendy MGA, Le TM. A review of recent developments in natural fibre composites and their mechanical performance. *Composites Part A: Applied Science and Manufacturing* 2016; 83: 98–112.

258. Thomason JL, Carruthers J, Kelly J, et al. Fibre cross-section determination and variability in sisal and flax and its effects on fibre performance characterisation. *Compos Sci Technol* 2011; 71: 1008–1015.

259. Roy S, Lutfar LB. Bast Fibres: Jute. In: *Handbook of Natural Fibres*. 2020, pp. 47–55.

260. Roy S, Lutfar LB. Bast Fibres: Ramie. In: *Handbook of Natural Fibres*. 2020, pp. 24–46.

261. Roy S, Lutfar LB. Bast Fibres: Kenaf. In: *Handbook of Natural Fibres*. 2020, pp. 71–92.

262. Kozasowski RM, Mackiewicz-Talarczyk M, Allam AM. Bast fibres: Flax. In: *Handbook of Natural Fibres*. 2020, pp. 56–113.

263. Horne MRL. Bast fibres: hemp cultivation and production. In: *Handbook of Natural Fibres*. 2020, pp. 114–145.

264. Simbaña EA, Ordóñez PE, Ordóñez YF, et al. Abaca: cultivation, obtaining fibre and potential uses. In: *Handbook of Natural Fibres*. 2020, pp. 197–218.

265. Prakash C. Bamboo fibre. In: *Handbook of Natural Fibres*. 2020, pp. 219–229.

266. Etsuzo U. Bamboo Cultivation. In: *Bamboo research in Asia : proceedings of a workshop held in Singapore, 28-30 May 1980*. 1980, pp. 151–160.

267. Ramesh M. Hemp, jute, banana, kenaf, ramie, sisal fibers. In: *Handbook of Properties of Textile and Technical Fibres*. 2018, pp. 301–325.

268. Conter FE. *The Cultivation of Sisal in Hawaii*. Honolulu, Hawaii: Hawaii Agricultural Experiment Station, University of Hawaii, 1903.

269. Väisänen T, Das O, Tomppo L. A review on new bio-based constituents for natural fiber-polymer composites. *Journal of Cleaner Production* 2017; 149: 582–596.

270. Shahinur S, Hasan M. Natural Fiber and Synthetic Fiber Composites: Comparison of Properties, Performance, Cost and Environmental Benefits. In: *Encyclopedia of Renewable and Sustainable Materials*. Elsevier, 2020, pp. 794–802.

271. Karus M, Kaup M. Natural fibres in the european automotive industry. *Journal of Industrial Hemp* 2002; 7: 119–131.

272. Song YS, Youn JR, Gutowski TG. Life cycle energy analysis of fiber-reinforced composites. *Compos Part A Appl Sci Manuf* 2009; 40: 1257–1265.

273. Faruk O, Bledzki AK, Fink HP, et al. Progress report on natural fiber reinforced composites. *Macromol Mater Eng* 2014; 299: 9–26.

274. Sanjay MR, Arpitha GR, Naik LL, et al. Applications of Natural Fibers and Its Composites: An Overview. *Natural Resources* 2016; 07: 108–114.

275. Cheng WY, Haque Akanda JM, Nyam KL. Kenaf seed oil: A potential new source of edible oil. *Trends Food Sci Technol* 2016; 52: 57–65.

276. Hao DC, Gu X-J, Xiao PG. High-throughput sequencing in medicinal plant transcriptome studies. In: *Medicinal Plants*. Elsevier, 2015, pp. 49–96.

277. Yuming Y, Kanglin W, Shengji P, et al. Bamboo Diversity and Traditional Uses in Yunnan, China. *Mt Res Dev* 2004; 24: 157–165.

278. of Alberta - Agriculture G. *Growing Hemp in Alberta*. 2020.

279. Government of Alberta - Agriculture. *Industrial Hemp & Flax*. 2017.

280. Hall LM, Booker H, Siloto RMP, et al. Flax (Linum usitatissimum L.). In: *Industrial Oil Crops*. 2016, pp. 157–194.

281. Jhala AJ, Hall LM. Flax (Linum usitatissimum L.): Current Uses and Future Applications. *Aust J Basic Appl Sci* 2010; 4: 4304–4312.

282. Abhilash M, Thomas D. Biopolymers for Biocomposites and Chemical Sensor Applications. In: *Biopolymer Composites in Electronics*. Elsevier Inc., 2017, pp. 405–435.

283. Aaliya B, Sunooj KV, Lackner M. Biopolymer composites: a review. *International Journal of Biobased Plastics* 2021; 3: 40–84.

284. Shahzad A, Nasir SU. Mechanical properties of natural fiber/synthetic fiber reinforced polymer hybrid composites. *Green Energy and Technology* 2017; 0: 355–396.

285. Townsend T, Sette J. Natural fibres and the world economy. In: *RILEM Bookseries*. Kluwer Academic Publishers, 2016, pp. 381–390.

286. Jose S, Rajna S, Ghosh P. Ramie Fibre Processing and Value Addition. *Asian Journal of Textile* 2016; 7: 1–9.

287. Mittal S. Jute Fibre, Tossa Jute Fibre, White Jute Fibre, https://www.technicaltextile.net/articles/application-of-jute-fibres-3329 (accessed 7 May 2021).

288. Government of Alberta - Agriculture. *Industrial Hemp Enterprise* . 2017.

289. Deng Y, Tian Y. Assessing the environmental impact of flax fibre reinforced polymer composite from a consequential life cycle assessment perspective. *Sustainability (Switzerland)* 2015; 7: 11462–11483.

290. Vroman I, Tighzert L. Biodegradable polymers. *Materials* 2009; 2: 307–344.

291. Rajesh M, Pitchaimani J. Mechanical Properties of Natural Fiber Braided Yarn Woven Composite: Comparison with Conventional Yarn Woven Composite. *J Bionic Eng* 2017; 14: 141–150.

292. Bruni-Bossio BM, Melenka GW, Ayranci C, et al. Micro-computed tomography analysis of natural fiber and bio-matrix tubular-braided composites. *J Compos Mater* 2019; 53: 4003–4013.